



Università  
Ca' Foscari  
Venezia



THE UNIVERSITY OF  
**SYDNEY**

**Scuola Dottorale di Ateneo  
Graduate School**

**Dottorato di ricerca  
in Scienze Chimiche  
Ciclo XXVI  
Anno di discussione 2013**

**GREEN PROCEDURES FOR THE SELECTIVE  
AQUEOUS-PHASE HYDROGENATION OF  
BIOMASS-DERIVED LEVULINIC ACID TO  $\gamma$ -  
VALEROLACTONE. INNOVATIVE DESIGN FOR  
CATALYTIC RECYCLE AND REGENERATION**

Tesi in co-tutela con l'Università di Sidney, Australia

**SETTORE SCIENTIFICO DISCIPLINARE DI AFFERENZA: CHIM/06  
Tesi di dottorato di Marina Gottardo, matricola 955839**

**Coordinatore del Dottorato**

**Prof. Maurizio Selva**

**Tutore del Dottorando**

**Prof. Maurizio Selva (Ca' Foscari)  
Prof Thomas Maschmeyer (USyd)**

*To my family*

## Abstract

This Thesis work was aimed at studying the catalytic upgrading of an important biomass derived platform chemical such as levulinic acid (LA). In particular, the hydrogenation/dehydration of levulinic acid (LA) to  $\gamma$ -valerolactone (GVL) was considered with a major focus on the implementation of original methods for the recovery and recycle of catalysts, both heterogeneous and homogeneous ones. Research activities were carried out within a cotutelle agreement between the University of Ca' Foscari Venezia (Italy) and The University of Sydney (Australia).

In Venice, a liquid triphase system made by an aqueous phase, an organic phase, and an ionic liquid was designed and applied for the conversion of LA to GVL. It was demonstrated that, operating at 100–150°C and 35 atm of H<sub>2</sub>, in the presence of either Ru/C or RuCl<sub>3</sub> as catalysts, the use of the triphase system designed to match the investigated reaction allowed: *i*) to obtain up to quantitative conversions and 100% selectivity toward the desired product; *ii*) to recover the product by simple phase separation; and *iii*) to preserve the catalyst activity for *in situ* recycles without any loss of metal. Overall, the study proved the concept that a multiphasic catalytic system could remarkably improve the global sustainability of the investigated hydrogenation reaction, where a key step was the catalyst segregation in an IL phase and its recycle.

In Sydney, the behavior of iron as a hydrogenation promoter of model organic compounds was explored. In particular, the recovery and recycle of iron was examined through electrochemical methods including both cyclic voltammetry and controlled potential electrolysis (CPE). The deposition of Fe<sup>0</sup> was carried out in acidic aqueous solutions (pH ~3) of FeSO<sub>4</sub>. Under such conditions, at 25 - 50°C, the aqueous phase hydrogenation of both cyclohexanone and LA in the presence of Fe<sup>0</sup> and diluted acid was performed selectively to produce the expected products (cyclohexanol and GVL, respectively) on a practical laboratory scale (0.4 mmol, ~50 mg). Though, conversions must be further optimized. Based on the gravimetric analyses of deposits of Fe<sup>0</sup>, the measurement of the net Q charge involved in CPE experiments, and the GC-MS analysis of reaction mixture, preliminary results suggested that Fe<sup>0</sup> acted as promoter/catalyst for the hydrogenation of the cyclohexanone and of the levulinic acid. Globally, although the investigation was far from being exhaustive, it was proved that the hydrogenation of carbonyl derivatives including the target of this study (*i.e.* LA), was feasible in aqueous solutions through an iron-based clean procedure.

# Contents

<b>1 Introduction.....</b>	<b>1</b>
<b>1.1 Green Chemistry .....</b>	<b>1</b>
<b>1.2 Alternative feedstocks: renewable resources .....</b>	<b>4</b>
<b>1.3 Biomass and Biorefineries .....</b>	<b>7</b>
1.3.1 Lignocellulose as a biorefinery feedstock .....	10
1.3.2 Routes for the transformation of monosaccharides into chemicals.....	15
<b>1.4 Levulinic acid.....</b>	<b>18</b>
1.4.1 Production of LA.....	19
1.4.2 LA: reactivity and derivatives .....	23
1.4.2.1 Derivatives .....	23
1.4.2.2 Reactivity.....	24
<b>1.5 <math>\gamma</math>-Valerolactone .....</b>	<b>27</b>
1.5.1 Production of GVL via LA hydrogenation.....	28
<b>1.6 Aim and Summary of the Thesis.....</b>	<b>31</b>
<b>1.7 References .....</b>	<b>34</b>
<b>2 Upgrading of Biomass-Derived Levulinic Acid via Ru-Catalyzed Hydrogenation to <math>\gamma</math>-Valerolactone in Aqueous-Organic-Ionic Liquids Multiphasic Systems .....</b>	<b>38</b>
<b>2.1 Introduction .....</b>	<b>38</b>
2.1.1 Ionic Liquids (ILs).....	39
2.1.2 Multiphasic systems based on ILs .....	41
2.1.3 Formic acid as hydrogen source .....	44
2.1.4 Aim and brief summary of the research .....	46
<b>2.2 Results .....</b>	<b>47</b>
2.2.1 Reaction conditions .....	47
2.2.2 Setup of the multiphasic system.....	48
2.2.3 Inverse Multiphasic hydrogenations of LA in the presence of Ru/C .....	50
2.2.3.1 The amount of $[N_{8,8,8,1}][Cl]$ .....	50
2.2.3.2 Best IL .....	51
2.2.3.3 Comparison with and without IL.....	54
2.2.3.4 Recycle and metal leaching.....	55

---

2.2.4	Homogeneous Catalyst: RuCl <sub>3</sub> .....	56
2.2.4.1	<i>The use of a homogeneous catalyst in the multiphasic system.....</i>	<i>56</i>
2.2.5	The Reaction of Levulinic Acid in Mixtures of Levulinic and Formic Acid	60
<b>2.3</b>	<b>Discussion.....</b>	<b>65</b>
<b>2.4</b>	<b>Conclusions .....</b>	<b>72</b>
<b>2.5</b>	<b>Experimental section.....</b>	<b>73</b>
2.5.1	Materials and chemicals .....	73
2.5.2	Synthesis of ionic liquids .....	74
2.5.3	The Ru/C-catalyzed hydrogenation of LA in organic solvents .....	76
2.5.4	The Ru/C-catalyzed hydrogenation of LA in triphasic systems.....	76
2.5.5	The triphasic hydrogenation of LA in the presence of RuCl <sub>3</sub> .....	77
2.5.6	The Ru/C-catalyzed hydrogenation of LA in the presence of formic acid ...	77
2.5.7	Analysis of the reaction mixtures .....	77
2.5.8	Isolation of the product GVL .....	78
2.5.9	Characterization of IL1-7 .....	79
2.5.10	Preparation of Ru metallic mirrors .....	93
2.5.11	Characterization of Ru-nanoparticles and Ru mirror .....	93
<b>2.6</b>	<b>References .....</b>	<b>95</b>
<b>3</b>	<b>The Bio-Inspired Reduction of Cyclohexanone and Levulinic Acid using an Iron/Acid System Coupled to the Electrocatalytic Regeneration of Active Iron Species .....</b>	<b>98</b>
<b>3.1</b>	<b>Foreword.....</b>	<b>98</b>
<b>3.2</b>	<b>Introduction.....</b>	<b>99</b>
3.2.1	Iron .....	99
3.2.2	Electrochemical studies .....	100
3.2.3	Aim of the research .....	101
<b>3.3</b>	<b>Cyclic voltammetric studies .....</b>	<b>103</b>
3.3.1	Cyclic voltammetry experiments.....	103
3.3.1.1	<i>Preliminary experiments .....</i>	<i>104</i>
3.3.1.2	<i>Electrochemical characterization of FeSO<sub>4</sub> systems .....</i>	<i>108</i>
<b>3.4</b>	<b>Linear sweep - anodic stripping voltammetric studies .....</b>	<b>117</b>
<b>3.5</b>	<b>Discussion.....</b>	<b>120</b>
<b>3.6</b>	<b>Controlled potential bulk electrolysis.....</b>	<b>124</b>

3.6.1	Results .....	125
3.6.1.1	<i>The setup of the bulk electrolysis cell</i> .....	125
3.6.1.2	<i>Single-step CPE</i> .....	126
3.6.1.3	<i>Multistep CPE</i> .....	127
3.6.1.4	<i>Multistep CPE in the presence of organic substrates</i> .....	131
3.6.2	Discussion .....	133
<b>3.7</b>	<b>Conclusions .....</b>	<b>136</b>
<b>3.8</b>	<b>Experimental section.....</b>	<b>137</b>
3.8.1	Preparation of aqueous solutions for CV and ASV experiments .....	137
3.8.2	Instrumentation and procedures for voltammetry .....	138
3.8.3	Instrumentation and procedures for bulk electrolysis .....	140
3.8.4	Characterization of Fe <sup>0</sup> deposits.....	141
<b>3.9</b>	<b>Appendix .....</b>	<b>141</b>
<b>3.10</b>	<b>References .....</b>	<b>143</b>
<b>4</b>	<b>Concluding remarks .....</b>	<b>145</b>
4.1	Paper originated from this thesis.....	146
4.2	Acknowledgements.....	147

---

# 1 Introduction

---

## 1.1 Green Chemistry

The first description of sustainable development probably dates back to 1987 on the Brundtland report of the World Commission on Environmental and Development<sup>1</sup> which introduced the following definition: “*Meeting the needs of the present generation without compromising the ability of future generations to meet their own needs*”. Nowadays, this concept has become an aspirational cornerstone for the development of modern industry and society. Focusing on this direction, a new idea of designing human activity has been developed and the term “*green*” has been used to qualify everything that is characterized by an environmental protection orientation.

In particular, Green Chemistry<sup>2</sup> is the branch of chemistry that seeks to reduce the impact of chemical technology on human health and environment. Its objective is to prevent, or at least decrease, pollution derived from the use or generation of hazardous substances in the design, manufacture and application of chemical products, improving the greenness of industrial chemical production and spreading, at the same time, a culture linked to the sustainability of resources. Green Chemistry acts both on existing chemical processes, improving them, and on the development of new procedures, focusing on the choice of reagents, process conditions and the use of catalysts. The important government environmental agencies, industry and the world of chemistry in general, in response to this trend, are developing and adopting codes of conduct aimed at identifying specific strategies to prevent pollution. These strategies are summarized in the well known 12 Principles of Green Chemistry, which are encapsulated in the mnemonic acronym PRODUCTIVELY:<sup>3</sup>

*Prevent wastes*

*Renewable Materials*

*Omit derivatization steps*

*Degradable Chemical Products*

*Use safe synthetic methods*

*Catalytic reagents*

*Temperature, Pressure ambient*

*In Process monitoring*

*Very few auxiliary substances*

*E-factor, maximize feed in product*

*Low toxicity of chemical products*

*Yes, it is safe*

The guiding principles of this discipline, introduced in the early 90s, are useful to set the general behavior and the theoretical approach that chemists should adopt to develop more environmentally friendly processes, products, and technologies. In addition, a set of mathematical parameters, named *green chemistry metrics*, have also been defined to give a practical and quantitative evaluation of a chemical process. Some examples of the more widely used metrics are reported in Table 1.1. Among them, AE (atom economy)<sup>4</sup> and E (Environmental) factor<sup>5</sup> are probably the best parameters for quickly assessing the environmental and economic impact of a chemical process. They express respectively: the efficiency of a process, according to the percentage by molecular weight of reactants converted into products and the amount (by mass) of waste produced per unit of product obtained.

**Table 1.1.**  
Summary of the most used green chemistry metrics

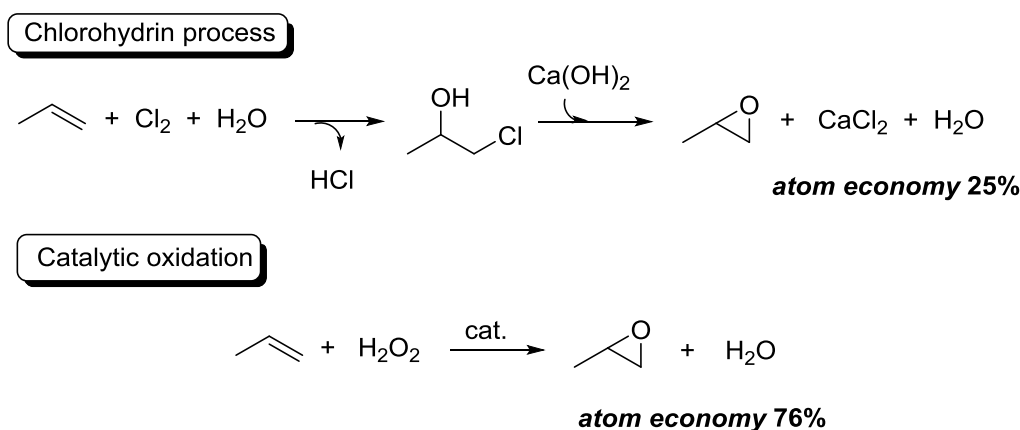
<b>Metric</b>	<b>Acronym</b>	<b>Formula</b>
Environmental factor	<b>E</b>	$E = \frac{\text{total waste [kg]}}{\text{product [kg]}}$
Atom economy	<b>AE</b>	$AE = \frac{\text{m.w. product}}{\sum \text{m.w. reagents}} \times 100$
Reaction mass efficiency	<b>RME</b>	$RME = \frac{\text{mass of product [kg]}}{\sum \text{mass reagents [kg]}} \times 100$
Carbon efficiency	<b>CE</b>	$CE = \frac{\text{carbon mass in product [kg]}}{\sum \text{carbon masses in reagents [kg]}} \times 100$
Mass index	<b>S<sup>-1</sup></b>	$S^{-1} = \frac{\sum \text{reagents + catalysts + solvents [kg]}}{\text{product [kg]}}$
Cost index	<b>CI</b>	$CI = \text{€ / kg of product}$

Other metrics such RME, CE, S<sup>-1</sup> contribute to the definition of the different levels of greenness of a process. Last, but not least is the cost index (CI) that expresses how the green virtues of a synthetic method become irrelevant if it (the method) cannot survive economically. From a strictly economic standpoint, costs include not just those related to equipment, reagents,



energy and labour, but also everything that is related to the separation and disposal of waste and co-products. It follows that the processes defined as "smart" until a few decades ago, today are unacceptable because of the mark up that the operations of separation and disposal have on the final price of the product.

The synthesis of propylene oxide from propene is a good example of an historical process successfully converted into a greener version with a tripling in atomic efficiency (Scheme 1.1).



**Scheme 1.1** Propylene oxide production via stoichiometric process with  $\text{Cl}_2$  and  $\text{Ca}(\text{OH})_2$  (**top**), and via catalytic process with hydrogen peroxide (**bottom**).

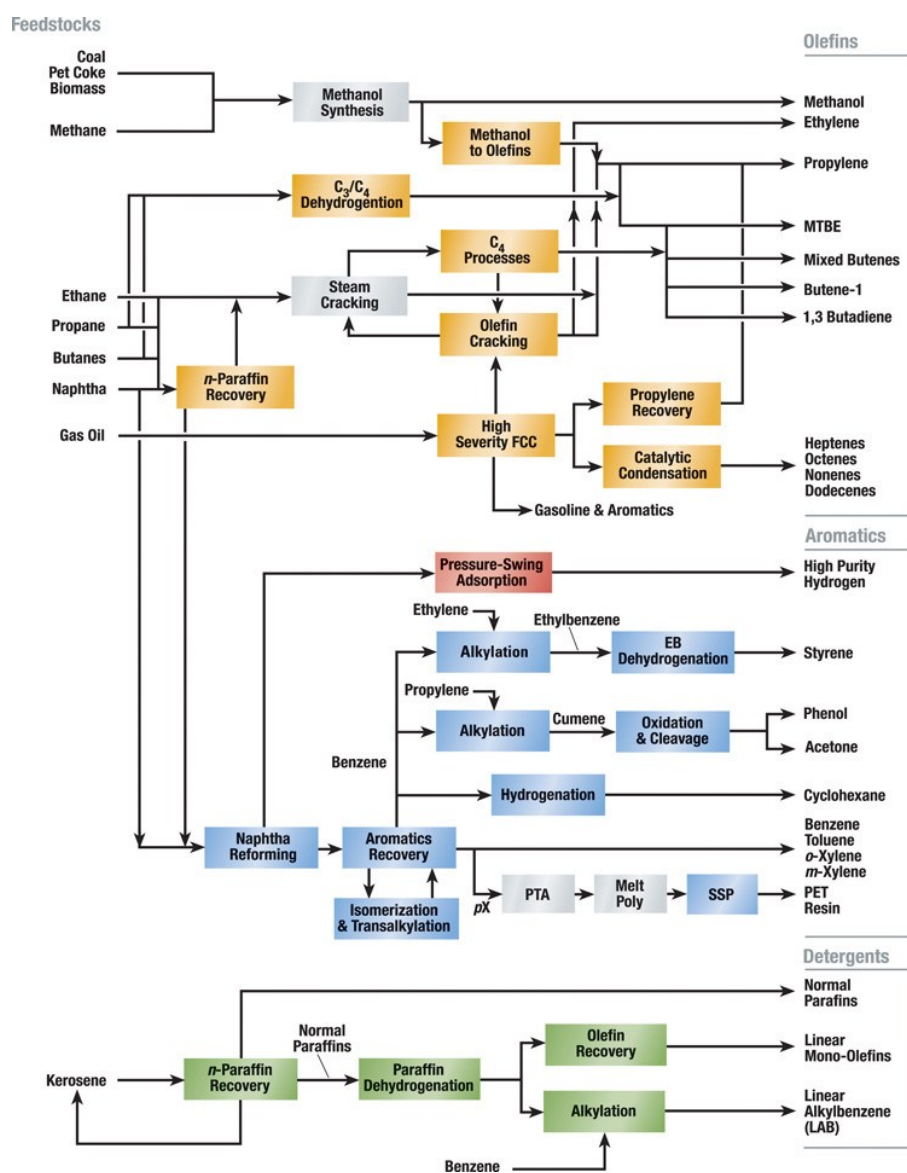
The reaction of propene with aqueous chlorine via the chlorohydrin process (Scheme 1.1, **top**) gave the corresponding chlorohydrin, which in turn was treated with lime to isolate the desired epoxide. Overall, the atom economy that characterized this process was of only 25% and sizable amounts of byproducts including HCl and  $\text{CaCl}_2$  were formed. An innovative and by far greener route was invented by using  $\text{H}_2\text{O}_2$  as an oxidizing agent with propene (Scheme 1.1, **bottom**). Under such conditions, a single catalytic step with an atom economy as high as 76% occurred producing only water as a byproduct. Not only the quantity of waste per Kg of product in the catalytic process was considerably lower, but also the cost of disposal of the waste was reduced.<sup>5</sup>

However, it would be a gross mistake to leave a discussion on metrics at the point of considering only mass implications. Clearly, wasted resources may have significant cost implications, but also hazardous processes could cause costs to rise. As an example, given a process characterised by very high atom economy and a very low amount of by produced waste, if the same process uses a very toxic reagent, or a very hazardous material (pyrophoric substances or extremely flammable gas), it would not be considered "green" at all. This reasoning leads to the proposition that the ideal green synthesis should respect all of the twelve green chemistry principles and pass the test of green chemistry metrics. A very tough goal,

indeed. Therefore, the solutions/tools proposed by chemists for green chemistry have, one by one, been influenced by the principles/aspects selected as the most relevant. Among them, the substitution of fossil resources (oil, coal and natural gas) by renewable raw materials has aroused a strong interest in the chemical fraternity to address green chemistry and sustainability issues.

## 1.2 Alternative feedstocks: renewable resources

Most of the energy and materials that we use today come from non-renewable sources (petroleum, natural gas and coal, Scheme 1.2), which by definition are finite and will be depleted at some point. Furthermore, the combustion of non-renewable fossil fuels for the production of heat and power, is associated with a net increase in greenhouse gas levels worldwide.<sup>6</sup>



Scheme 1.2 Petrochemicals flow scheme<sup>7</sup>

Both these issues have been well recognized since the beginning of the Green Chemistry movement:<sup>8</sup> in fact, the 7<sup>th</sup> principle of Green Chemistry “A raw material or feedstock should be renewable rather than depleting whenever technically and economically practicable” was enunciated to make chemists and engineers conscious of the urgent need to provide modern society with materials and energy obtained through alternative ways able to reverse the current trend. The response to this stimulus however, has been and is a hard task. Major reasons are both technical and economic. Although the petrochemical industry did not start out being an efficient operation, it has developed and evolved over the course of more than 100 years. Due to the tremendous expertise acquired, petrochemical industry is today assisted by mature technologies that allow highly effective transformations with E-factors (as small as 0.1 kg of wastes/Kg product) among the lowest available for syntheses scaled on millions of tons per year.<sup>5</sup> In addition, the exploitation of oil still involves great profits for major petrochemical companies and conflicts in areas where oil is extracted imply a very frequent increase/variation of the price of oil barrels, which raises even further the economic interests into play.

On the other hand, nowadays, environmental statutes and regulations, especially in Europe, are proliferating very quickly. For example, according to EU's Climate Change Package, new directives lay down mandatory national targets to be achieved by the Member States through promoting the use of renewable energy in the electricity, heating and cooling, and transport sectors in order to ensure that by 2020 renewable energy makes up at least 20% of the EU's total energy consumption. In particular, targets to be achieved by 2020 are: *i*) 20% reduction in greenhouse gas emissions, *ii*) 20% improvement in energy efficiency, *iii*) 20% share for renewable in the EU energy mix.<sup>9</sup>

These regulations also aim at encouraging petrochemical industries to invest resources and money for the development of new processes that utilize sustainable resources rather than oil, as raw materials. In this sense, a significant recent example has been offered by the Italian ENI which stopped an old conventional refinery at Porto Marghera (Italy) and turned it into a new biorefinery plant for the production of green diesel.<sup>10</sup>

Renewable resources offer an appealing alternative to derive energy and materials, which have the potential to be replenished indefinitely. This however, poses two fundamental issues and challenges: *i*) chemists have to replicate derived petroleum-based supply chain that took 100 years to optimize using a completely different type of feedstock (renewable resources); *ii*) chemists must invent innovative paradigms to transform and use renewables in a short time frame and without major environmental damage to preserve Earth's biodiversity and large human and nonhuman populations. In other words, the rate of consumption of bio-feedstocks

must be less than that at which they can be replenished without providing additional stress to the environment.

Production systems should therefore operate closer to the way that nature works, in a cyclical manner, where materials and energy can be utilized while minimizing waste. In an ideal system, the exploitation of renewable sources should be conceived to re-assimilate all products, at the end of their useful life, as inputs for closed-loop industrial cycles. Figure 1.1 simply compares the biorefinery cycle (see also later on this chapter) with the conventional refinery production and shows how re-growth and combustion of biomass derivatives can mitigate the release of greenhouse gas (mainly  $\text{CO}_2$ ) emissions.

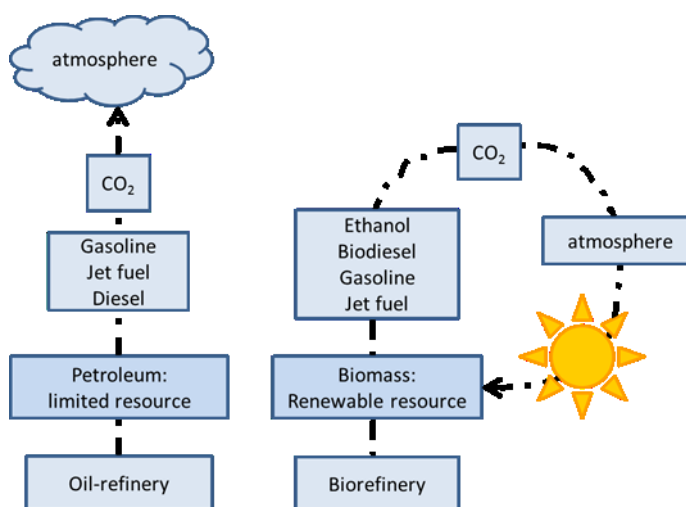


Figure 1.1  $\text{CO}_2$  cycles for petroleum- and biomass-derived fuels

This direction has taken remarkable steps forward in the energy sector, where alternatives such as solar, wind and hydro, hydrogen-based technology, the new generation of nuclear power, and biofuels are becoming more and more competitive every day. Therefore, given these potential benefits and the pivotal role of renewable resources in achieving greater sustainability, the United States and the European Union have set targets to increase the use of renewable resources for fuels and energy, as shown in Table 1.2.

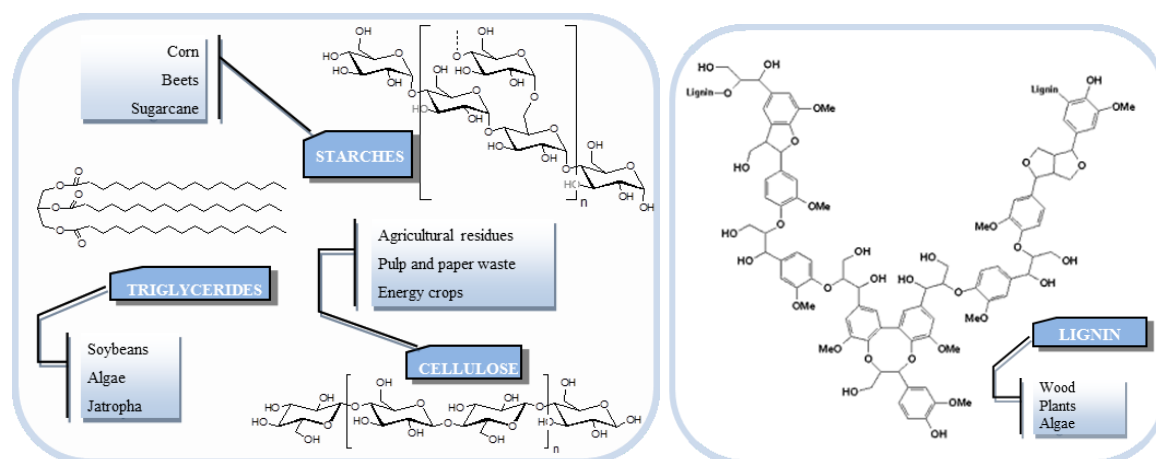
**Table 1.2**  
U.S. and European Union goals for the use of renewable resources in energy generation, transportation fuels, and products (%)<sup>11</sup>

Renewable Resource	United States				European Union			
	2001	2010	2020	2030	2001	2005	2010	2020-2050
Bioenergy: share of electricity and heat demands	2.8	4	5	5	7.5	-	12.5	26 (2030)
Biofuels: share of demand for transportation	0.5	4	10	20	1.4	2.8	5.8	20 (2020)

On the other hand, the upgrading of renewable resources in high-added value chemicals and materials has attracted interest only in recent years.<sup>11b, 12</sup> This area still appears as a largely unexplored one and it could greatly benefit from innovation. Due to the relevance of this subject to the work presented in this Thesis, the following paragraphs will summarize the state of the art on major strategies and perspectives in the exploitation of biomass for chemical production.

### 1.3 Biomass and Biorefineries

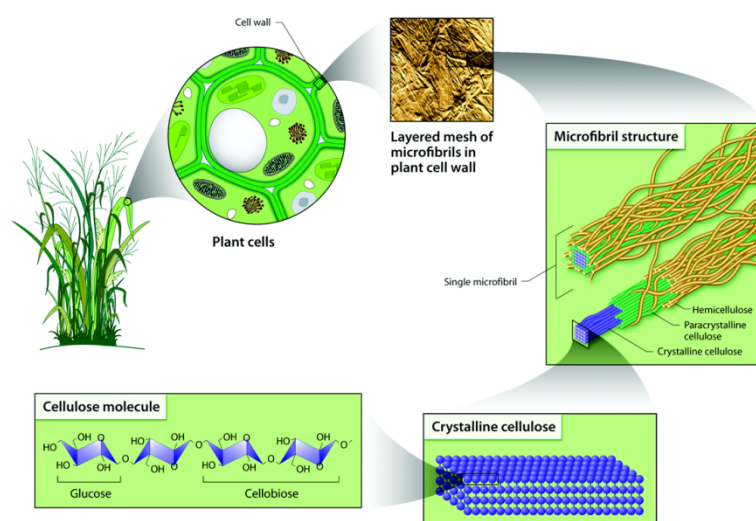
Biomass is a general term to refer to all organic material of renewable origin, including the "energy crops" (cultures grown at low cost and low maintenance, used for the production of biofuels or as fuels to produce other types of energy), trees, agricultural residues, aquatic plants, wood and wood residues, animal wastes and others. Biomass is the only renewable source of fixed carbon (generated from CO<sub>2</sub> and H<sub>2</sub>O using sunlight as the energy source, producing O<sub>2</sub> as a coproduct), which can be used for the production of fuels and chemicals as an alternative to the refining of fossil resources. From biomass it is possible to derive three general classes of feedstocks: 75% is carbohydrate, mainly in the form of cellulose, starch and saccharose, 20% is lignin and only 5% is other natural compounds, such as fats (oils), triglycerides, proteins and various substances.<sup>11a</sup> In Scheme 1.3, the representative chemical structures of the predominant component of biomass, the cellulose and lignin, are compared to those of starches and triglycerides.



**Scheme 1.3** The chemical structure of the major components of biomass

Starchy feedstocks are those composed of glucose polysaccharides joined by  $\alpha$ -glycosidic linkages, which are easily hydrolyzed into the constituent sugar monomers. Triglyceride feedstocks are those comprised of fatty acids and glycerol derived from both plant and animal sources.

Lignocellulose is the principal class of biomass that contributes to the structural integrity of plants. It consists of three polymeric components, the percentages of which vary according to the species of origin. Cellulose, the most abundant biopolymer on the planet, is made up exclusively of glucose linked unbranched chains (between 38 and 50% of dry weight). Hemicellulose (between 23-32% of dry weight) is composed of different sugars (C5 and C6) and surrounds the cellulose interacting through hydrogen bonds. Lignin is formed by substituted phenolic units, and serves as the adhesive and coating for the two polysaccharides, conferring structural rigidity and making them resistant to enzymatic digestion (15-25%) (Scheme 1.4).<sup>13</sup>

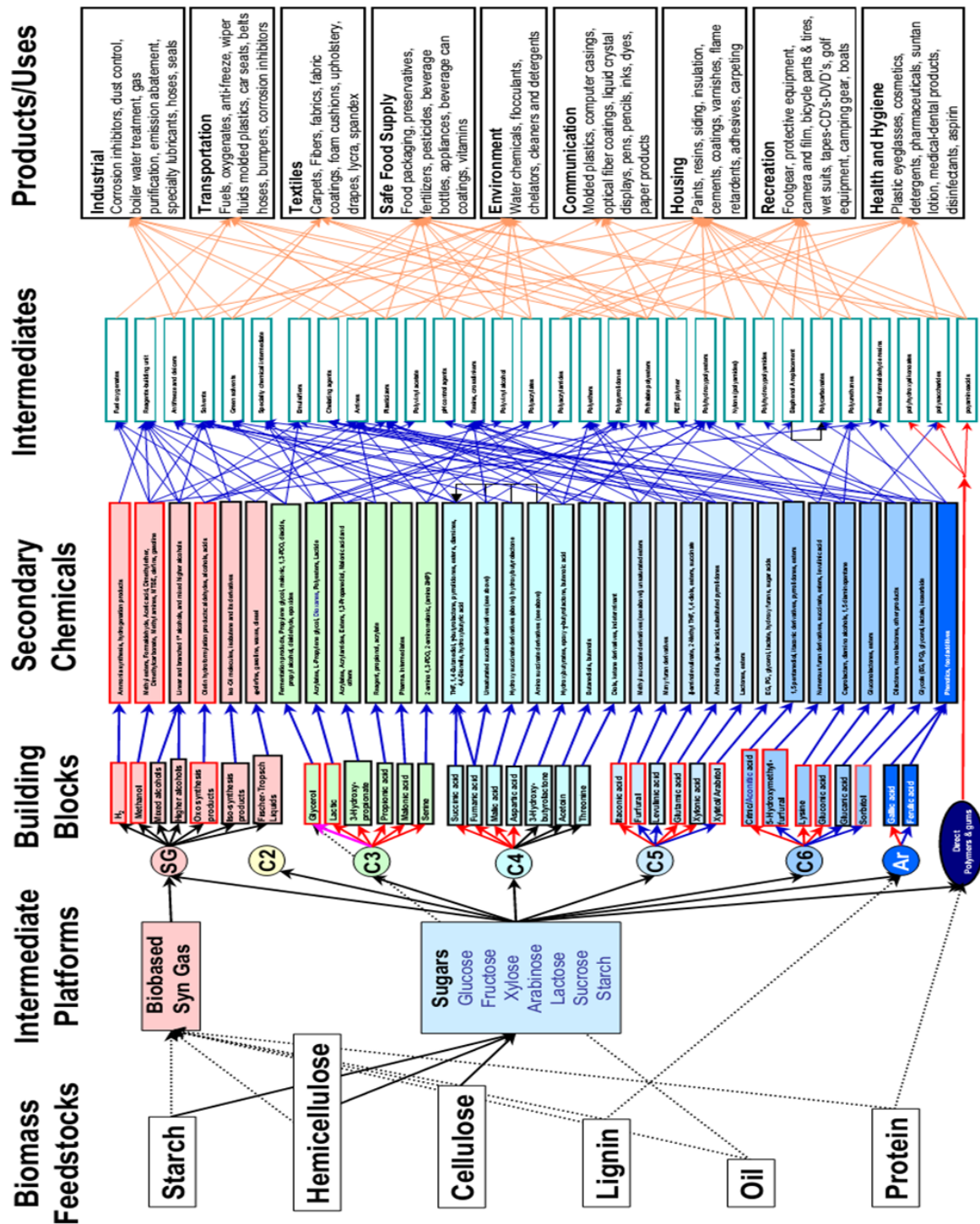


**Scheme 1.4.** Lignocellulosic biomass at various length scales<sup>14</sup>

The investigation and implementation of energy- and mass-efficient processes able to exploit biomass for the production of chemicals and materials (and energy as well), gave birth to the concept of the biorefinery.<sup>11a, 15</sup> By analogy to the well-established notion of a petrochemical plant, the simplest form of a fully integrated biorefinery produces a variety of products from different bio-based feedstocks through a combination of technologies and processing methodologies. The output of such a facility also includes the energy to operate the plant and the use of by-products for internal power generation or cogeneration. In addition, the products of a biorefinery comprise oxygenated building blocks such as succinic acid, which can be otherwise obtained only through energy intensive oxidations of petroleum feedstocks (e.g. from butane through maleic anhydride).<sup>16</sup>

Scheme 1.5 details the massive potential of an integrated biorefinery in terms of feedstocks and raw materials (intermediate platforms), and different types, scales, and final uses in the market of the products (building blocks, secondary chemicals and intermediates).





Scheme 1.5 A flow scheme of a biorefinery<sup>17</sup>

The biorefinery concept is still evolving, but there have been recent attempts to describe the potential types of such plants systematically. Three different types, named *phase I*, *II* and *III* biorefineries, have been defined.<sup>11-12</sup> A *phase I* biorefinery has specific process capabilities and uses biomass to produce a fixed amount of products with almost no flexibility in processing. One example of this type of facility is a dry mill ethanol plant. A *phase II* biorefinery also uses grain feedstocks but has the additional capability of varying production processes to make a range of

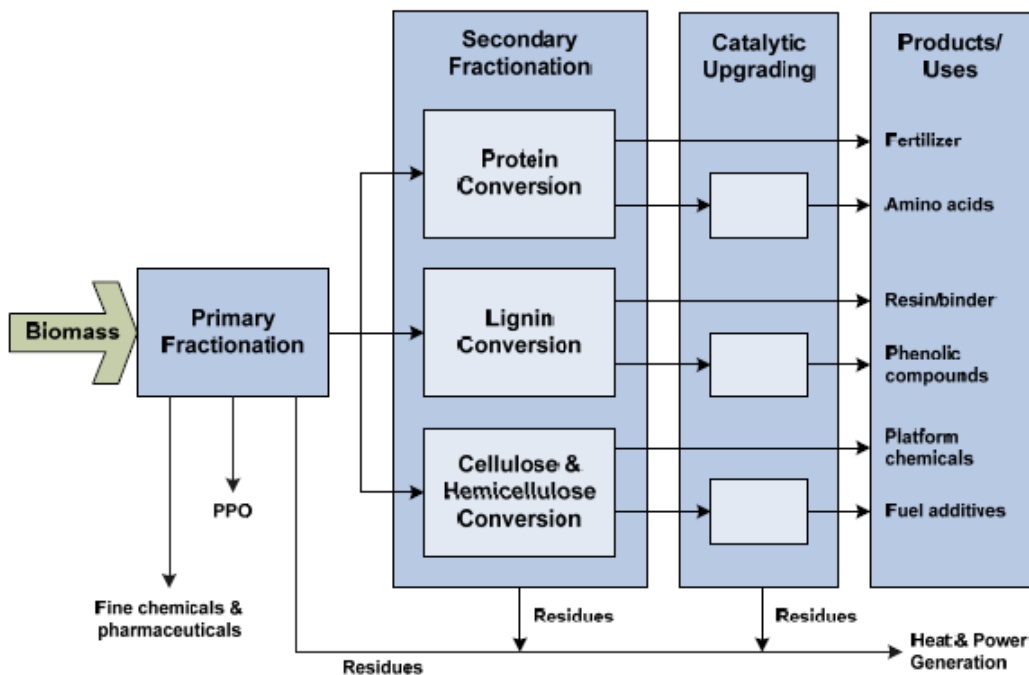
products, depending on product demand. Facilities of this type include for instance, corn wet millers that produce ethanol and a few other chemicals such as starch, high fructose corn syrup, corn oil and corn gluten feed and meal.<sup>18</sup> Finally, a *phase III* biorefinery, is a fully developed and integrated chemical manufacturing complex that utilizes a mix of bio-based feedstocks to produce a number of chemicals and materials through different technologies. Such a facility has the capability to produce a mix of higher-value compounds along with biofuels and other lower-value chemicals, in a fashion similar to a petroleum refinery.<sup>19</sup>

Currently, most of the carbohydrates (sugars) used as carbon sources in fermentation processes come from starches (*e.g.* corn, soy), and their use in biorefineries may give rise to a competition with their use as food sources. Depending on the geographical site of production of such biomass, the overall situation may not only results in an increase of food prices, but raises ethical issues in respect to malnourished populations. Therefore, lignocellulosic materials from non-edible biomass appear as a more sustainable alternative. These feedstocks can be processed in a *phase III* biorefinery.

### **1.3.1 Lignocellulose as a biorefinery feedstock**

Among the potential large-scale industrial biorefinery types, the lignocellulose-feedstock (LCF) biorefinery will most probably be pushed through with highest success. On the one hand, the raw material situation is optimal since lignocellulose (LC) coming from straw, reed, grass, wood, paper-waste, etc., is a very cheap source of carbon; on the other hand, conversion products have a good position within both the traditional petrochemical and the future biobased product markets.<sup>11a</sup> It should be noted however, that technologies for the treatment of biomass and of its primary derivatives are far from being mature. In particular, the development of methods to fractionate and separate the fermentable sugars at a competitive cost is highly desirable.





**Scheme 1.6** A biorefinery fed by lignocellulose-feedstock (LCF): major operation/units

Scheme 1.6 summarizes the three main stages occurring in a biorefinery fed by lignocellulose-feedstock (LCF), and, in addition to Scheme 1.7 (see later on this paragraph), it highlights the most important chemicals (and some of its applications) obtained from LC. The following key biorefinery operations/units can be recognised.

1. Pretreatments to enhance digestibility of lignocellulosic biomass (Figure 1.2).<sup>20</sup>

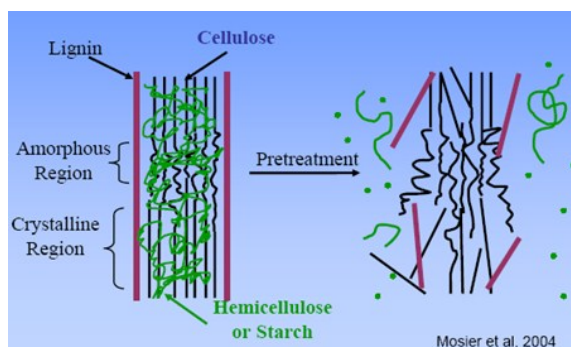


**Figure 1.2** Goals of pretreatments of lignocellulosic material<sup>21</sup>

The biodegradability of LC biomass is limited by several factors like crystallinity of cellulose, available surface area, and lignin and hemicellulose content. Pretreatments are physical and/or chemical methods that improve its digestibility, acting on one or more of these aspects. The methods that occur in a first separation unit (Scheme 1.6) are different.

- *Mechanical pretreatments*, including comminution and milling. The objective of these procedure is a reduction of particle size leads to an increase of available specific surface and a reduction of the degree of polymerization. They also cause shearing of the biomass.<sup>22</sup>
- *Thermal pretreatments*, such as steam pretreatment (ST), steam explosion (SE), and liquid hot water (LHW) pretreatment. During these thermal processes the LC biomass is heated, in order to solubilise the hemicellulose, to make the cellulose better accessible for further treatment, and to avoid the formation of inhibitors.<sup>23</sup>
- *Acid pretreatments*. Pretreatment of LC with acids ( $H_2SO_4$  is the most common) at ambient temperature is done to enhance the anaerobic digestibility. The objective is to solubilize the hemicellulose, and so make the cellulose more accessible.<sup>24</sup>
- *Alkaline pretreatments*. During these processes (NaOH is the most commonly used base) solvation and saponification take place to swell the biomass and make it more accessible for enzymes and bacteria.<sup>24</sup>
- *Oxidative pretreatments*. These involve the addition of an oxidizing compound, like hydrogen peroxide or peracetic acid, to the biomass suspended in water. The objective is to remove the hemicellulose and lignin to increase the accessibility of the cellulose.<sup>25</sup>
- *Green solvent pretreatments*. Processing of lignocellulosic biomass with ionic liquids (ILs) and other solvents has gained importance in the last decade due to the tunability of the solvent chemistry and hence the ability to dissolve a wide variety of biomass types. For example, many IL have been discovered to dissolve cellulose with no degradation by-products.<sup>26</sup>
- *Supercritical Fluid (SCF) Pretreatments*. Due to high diffusivity and low viscosity, some SCFs have the ability to penetrate the crystalline structure of lignocellulosic biomass thus overcoming mass transfer limitations encountered in other pretreatments. Supercritical carbon dioxide ( $CO_2$ ) with a critical temperature ( $T_c$ ) of 31 °C and a critical pressure ( $P_c$ ) of 7.4 MPa, has excellent potential for biomass pretreatment.<sup>27</sup>

Each of these pretreatments can affect differently the biodegradability of biomass, as showed in **Table 1.3**.

**Table 1.3**  
Effects of the different pretreatments on the physical/chemical composition of structure of lignocellulose<sup>20b</sup>

	<b>Increase accessible surface area</b>	<b>Decrystallization cellulose</b>	<b>Solubilization hemicellulose</b>	<b>Solubilization lignin</b>	<b>Alteration ligninstructure</b>
Mechanical	+	+			
ST/SE	+		+	-	+
LHW (batch)	+	ND	+	-	-
Acid	+		+	-	+
Alkaline	+		-	+/-	+
Oxidative	+	ND		+/-	+
ILs	+	+	-	+/-	-
SCF	+	+	+		-

+ = major effect. - = minor effect. ND = not determined.

2. Conversion of intermediate fractions into final products of value (e.g. biofuels) and chemical intermediates.<sup>28</sup>

The latter compounds include several types of alcohols, phenols, and carboxylic acids, some of which are platform chemicals of particular interest: for example, levulinic acid, lactic acid, and phenol-derived aromatics such as guaiacol and cresols, belong to this class (Scheme 1.7). This second process is usually carried out by thermo-chemical and biochemical treatments. Emerging thermo-chemical techniques include:

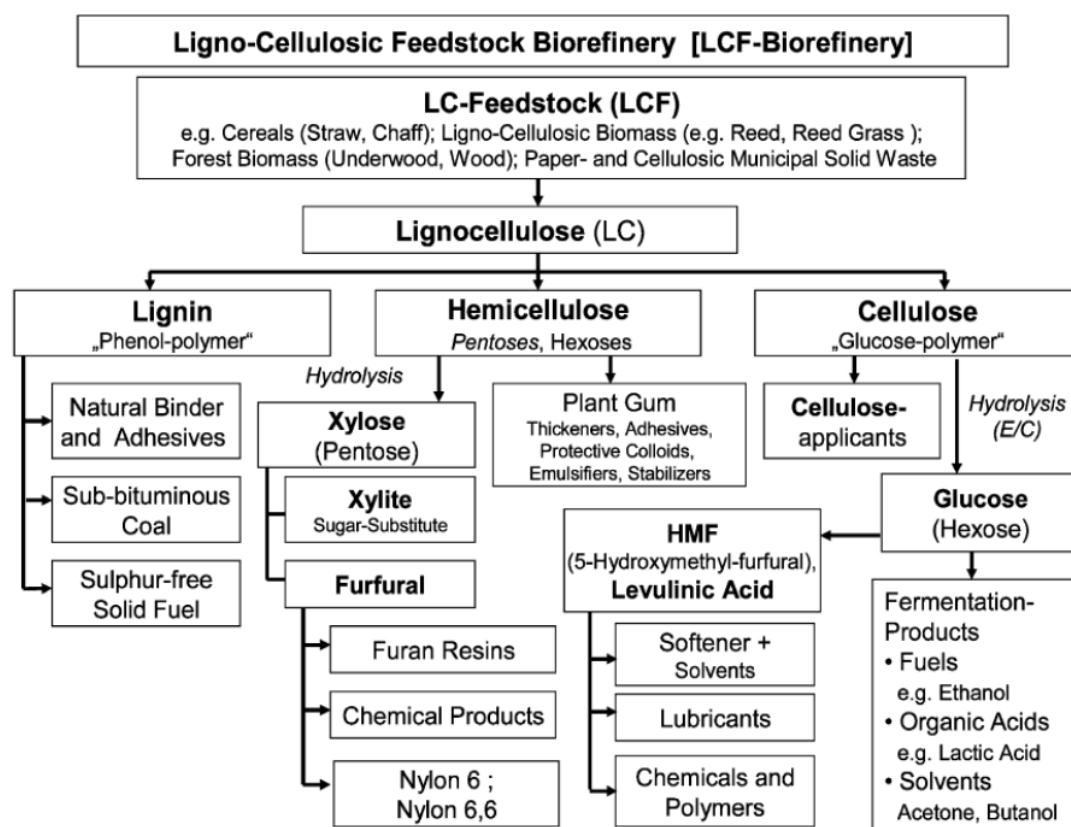
- *Direct combustion*, which occurs in the presence of air to convert the chemical energy to power, both heat and mechanical;<sup>29</sup>
- *Pyrolysis*, which is thermal decomposition occurring in the absence of oxygen. Relatively low temperature are employed (500 - 800 °C) and three products are usually produced: gas, pyrolysis oil and charcoal;<sup>30</sup>
- *Gasification*, which takes place at high temperature (600 - 1,000 °C) in the presence of an oxidizing agent (typically air, steam, nitrogen, carbon dioxide, oxygen or a combination of these). In the presence of an oxidizing agent at high temperature, the large polymeric molecules of biomass decompose into lighter molecules and eventually to permanent gases (CO, H<sub>2</sub>, CH<sub>4</sub> and lighter hydrocarbons), ash, char, tar and minor contaminants.<sup>31</sup>
- *Liquefaction*, which is generally carried out at 280 - 370 °C and between 10 - 25 MPa. Under these conditions water is still in a liquid state, though it exhibits peculiar acidic properties. In hydrothermal liquefaction water simultaneously acts as, reactant and catalyst.<sup>32</sup>

On the other hand, biochemical conversion is the process by which biomass is converted to gas (CO<sub>2</sub>/CH<sub>4</sub>), waste (compost or fertilizer) and water or ethanol by using microorganisms. The biochemical processes refer mainly to:

- *Aerobic fermentation*, which produces compost, carbon dioxide and water;

- *Anaerobic fermentation*, which produces fertilizer and gas ( $\text{CH}_4/\text{CO}_2$ );
- *Alcoholic fermentation*, which produces ethanol,  $\text{CO}_2$  and waste.<sup>33</sup>

3. Additional processes for the transformation of intermediates into a large variety of useful compounds. These include chemical transformations for the selective removal of functionalities and adjustment of the molecular weight of the final product. An example is the decrease of the oxygen content in sugars and polyols through combined catalytic processes of reforming and de-oxygenation yielding mono-functional chemical intermediates.<sup>34</sup>

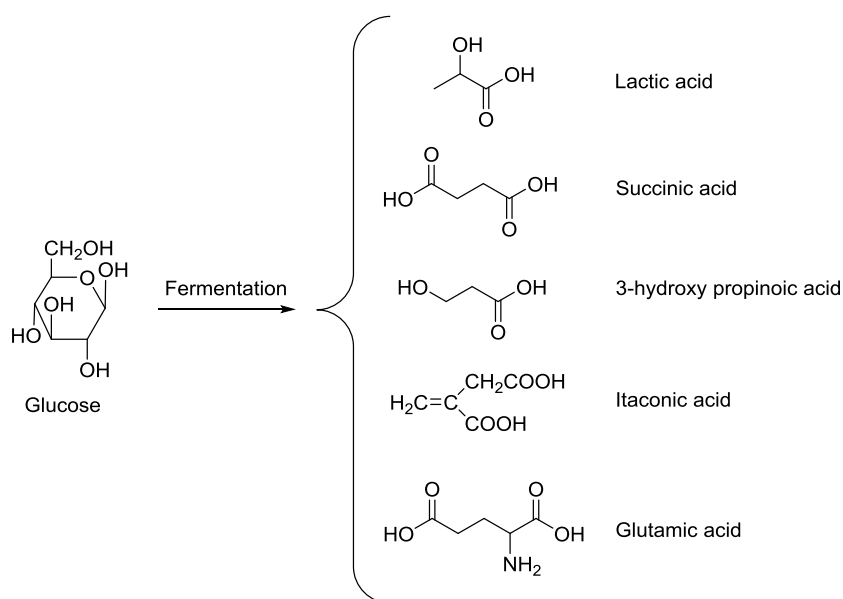


**Scheme 1.7** A biorefinery fed by lignocellulose-feedstock (LCF): major products.

The vast literature available on this subject does not allow an exhaustive analysis within the limits of this chapter. Therefore, the remaining paragraphs will focus on some specific methods for the transformation of monosaccharides (from LC) with a view to producing a chemicals platform, since this strategy has underpinned the work reported in this Thesis. In particular, the case of levulinic acid (LA) and of its derivative  $\gamma$ -valerolactone (GVL) will be detailed.

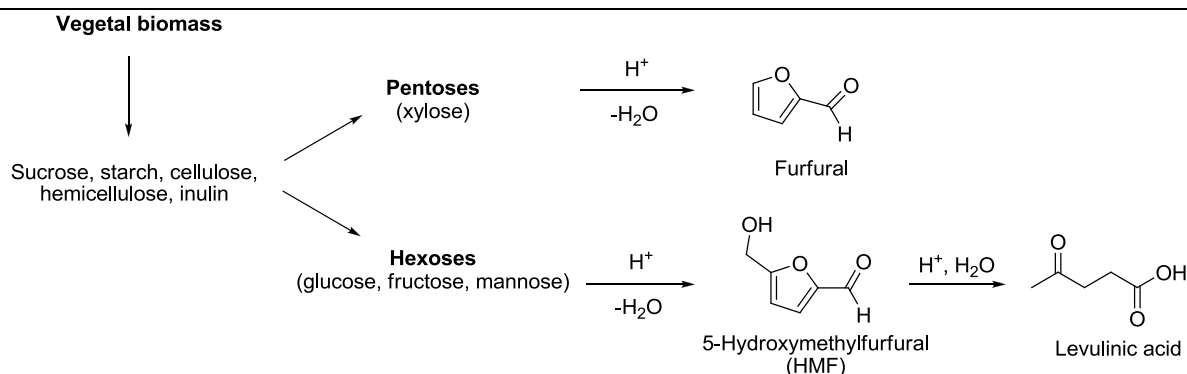
### 1.3.2 Routes for the transformation of monosaccharides into chemicals

The transformation of sugars into bio-derived products can be carried out either via fermentation processes or via chemical methods. Fermentative procedures are mainly applied to glucose (the most abundant sugar), which in turn, is mostly obtained by the enzymatic hydrolysis of starch corn.<sup>35</sup> The glucose fermentation, thanks to a wide range of micro-organisms available, allows the isolation of some important platform chemicals,<sup>36</sup> the structures of some of which are shown in Scheme 1.8:



**Scheme 1.8** Some platform chemicals from the fermentation of glucose

Chemical methods for the conversion of sugars are generally suitable for both C5 and C6 substrates coming from lignocelluloses. Among the common procedures, the thermal dehydration of pentoses and hexoses in acidic media is perhaps the most used one. The reaction leads to the formation of several chemicals. Three of the major compounds are furfural (2-furancarboxaldehyde, from pentoses), 5-hydroxymethylfurfural (HMF, from hexoses), which is considered one of the most promising sustainable substitutes for petroleum-based building blocks, and levulinic acid arising from the hydration of HMF (Scheme 1.9).



**Scheme 1.9** Products obtained by dehydration of monosaccharides

Many types of catalysts have been used for the dehydration of hexoses. According to Cottier,<sup>37</sup> such catalytic systems could be divided into five groups: organic and inorganic (mineral) acids,<sup>38</sup> organic and inorganic salts,<sup>39</sup> Lewis acids,<sup>40</sup> and others (ion-exchange resins and zeolites). Some examples are shown in Table 1.4.

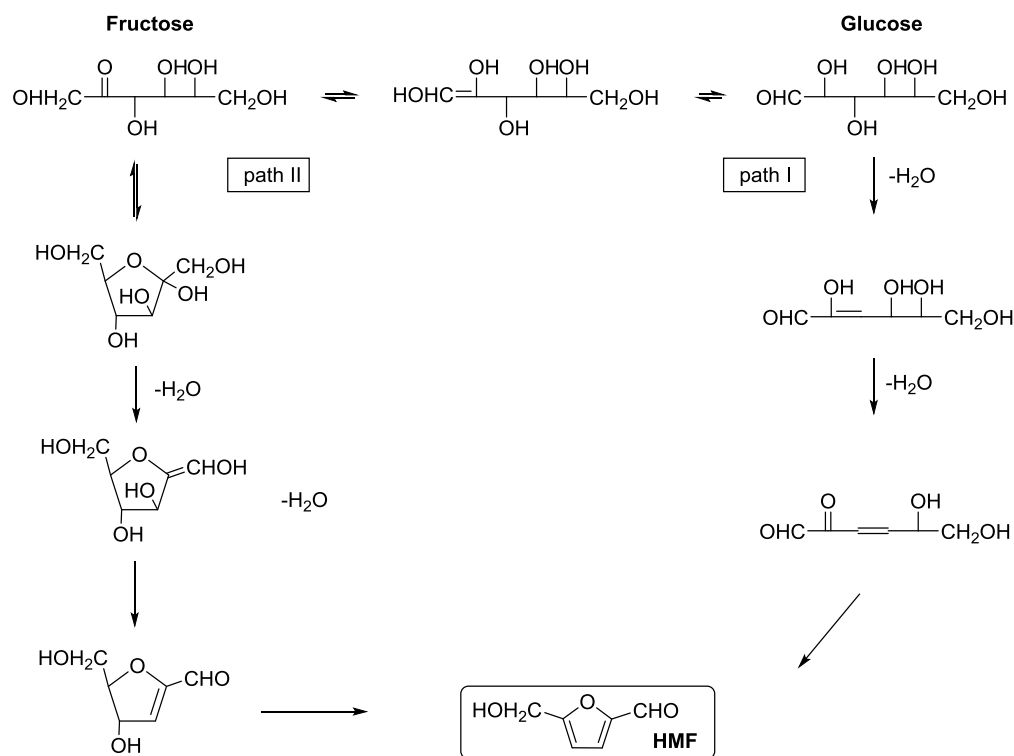
**Table 1.4**  
Examples of catalysts for the dehydration of hexoses

Catalyst groups	Catalysts
Organic acids	oxalic acid; levulinic acid; maleic acid; <i>p</i> -toluenesulfonic
Inorganic acids	phosphoric acid; sulfuric acid; hydrochloric acid; iodine or hydroiodic acid generated in situ
Salts	(NH <sub>4</sub> ) <sub>2</sub> SO <sub>4</sub> /SO <sub>3</sub> ; pyridine/PO <sub>4</sub> <sup>3-</sup> ; pyridine/HCl; aluminum salts; Th and Zr ions; zirconium phosphate; Cr; Al, Ti, Ca, In ions; ZrOCl <sub>2</sub> ; VO(SO <sub>4</sub> ) <sub>2</sub> , TiO <sub>2</sub> ; V, Zr, Cr, Tiporphyrins
Lewis acid	ZnCl <sub>2</sub> ; AlCl <sub>3</sub> ; BF <sub>3</sub>
Others	Ion exchange resins; zeolites

More recently, the dehydration of hexoses for the selective formation of HMF has been reviewed.<sup>41</sup> These reviews not only confirmed that nearly one hundred inorganic and organic acidic compounds have been positively identified as catalysts for the synthesis of 5-HMF, but they also described several reaction conditions to improve the HMF yield, that included the use of solvents such as pure water, aprotic organic media [dimethylsulfoxide (DMSO), N,N-dimethylformamide, and N-methyl pyrrolidone], ionic liquids (*e.g.* [BMIM]BF<sub>4</sub>, [BMIM]PF<sub>6</sub>, and [EMIM]Cl) combined organic media (*e.g.* acetone/DMSO) or aq./organic mixtures (*e.g.* H<sub>2</sub>O/DMSO), and biphasic systems [*e.g.* water/methylisobutylketone (MIBK)], and a range of different temperatures from 150 up to 250 °C, even in the presence of microwave irradiation. Also, numerous mechanistic proposals have been formulated for the synthesis of HMF from

hexoses. Among the first hypotheses were those of van Dam *et al.*,<sup>42</sup> Antal,<sup>43</sup> and Kuster,<sup>38a</sup> which assumed that the formation of HMF took place through an acid-catalyzed triple dehydration of hexoses (mainly glucose and fructose) *via* two possible pathways (

**Scheme 1.10**): the first route was based on acyclic compounds (path I), while the second one involved the transformation of 5-membered cyclic systems (path II).



**Scheme 1.10** Pathways for the dehydration of hexoses

More recent results have confirmed that the production of 5-HMF from hexoses involves many different reactions including isomerization, dehydration, fragmentation, reversion, and condensation steps, and they have indicated that 5-HMF may form through an open-chain 1,2-enediol mechanism or a fructofuranosyl intermediate.<sup>44</sup>

From the commercial standpoint, the multi-functional 5-HMF has generated considerable interest as an intermediate in the syntheses of precursors of pharmaceuticals, thermoresistant polymers, macrocyclic compounds, dialdehydes, ethers, amino alcohols, and other organic intermediates. In particular, as mentioned above, 5-HMF also serves as the major source for bio-based levulinic acid.

## 1.4 Levulinic acid

Levulinic acid (LA) is a ketoacid, more specifically a C5 linear carboxylic acid in which a ketone carbonyl group is present at position 4 (4-oxopentanoic acid, Scheme 1.9). The properties, the general chemistry and the utilization of LA have been excellently reviewed over the years and these reviews highlighted major applications of LA as a solvent, a food flavoring agent, and a starting compound for the preparation of a variety of products of both pharmaceutical and large-scale uses (Table 1.5).<sup>45</sup>

**Table 1.5**  
Some selected levulinic acid applications<sup>46</sup>

Applications
Chiral reagents
Biologically active materials
Polyhydroxyalkanoates
Polymers
Polymerization initiators
Antifouling compounds
Personal care products
Lubricants
Adsorbents
Printing/inks
Coatings
Electronics
Photography
Batteries
Drug delivery
Corrosioninhibitors

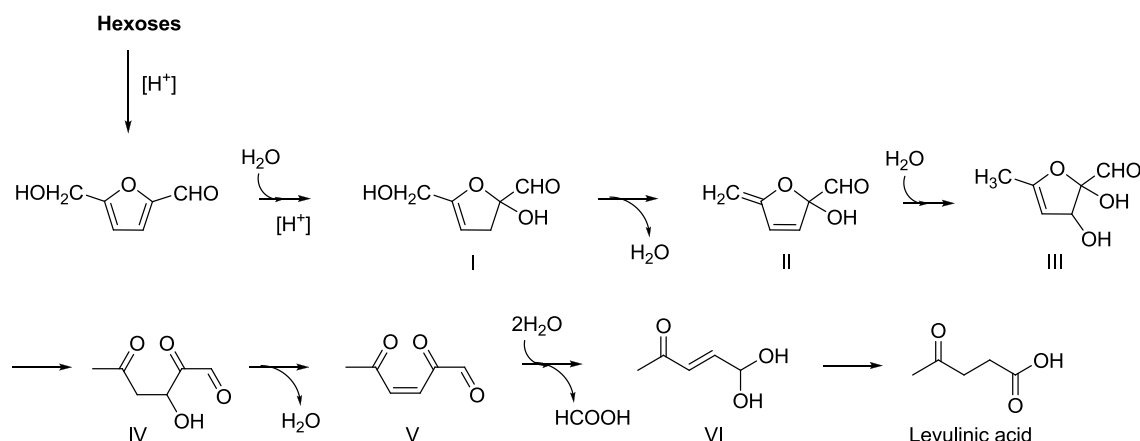
In particular, during the past decade, the emerging potential of LA as a resin/plasticizer and coating material, as well as a component for animal feed, has fuelled an intensive research activity, which is expected to grow in the near future. This has also been largely recognized by the Department of Energy of the United States that in 2004, which has classified LA among the 12 most attractive platform chemicals that can be produced from wood-based feedstock.<sup>17</sup> Along with the intriguing chemical reactivity, another driver to the exploitation of LA as a renewable C5-source is based on the above mentioned method of preparation by multiple acid-catalyzed reactions of 6- and 5-carbon monosaccharides mostly derived from cellulose wastes, such as paper mill sludge, urban waste paper, agricultural residues, and cellulose fines of papermaking.<sup>46-47</sup> Available technologies for the treatment of these biomass sources allow promising cost effective estimations even for large scale productions of LA (ton/day).<sup>48</sup> According to a recent evaluation, LA might be obtained at the price of 0.09–0.22 USD/kg.<sup>49</sup> At



this stage however, further considerations are necessary to analyze the technical and economic viability of the commercial use of LA.

### 1.4.1 Production of LA

In the past, LA was never available in significant volumes. Historical reasons plausibly accounted for this fact: most of the research activity on the production of LA was performed in the early 1940s, when both the raw materials (cane sugar and hydrochloric acid) and the equipments for separation and purification of the product were expensive, and final yields were moderate-to low.<sup>50</sup> Today however, advances in science and technology and the use of considerably cheaper raw materials give good reason to reconsider the industrial potential of levulinic acid and to make this product pass the most practical test of market viability, *i.e.* its availability at a low enough cost. The most used approach to the synthesis of LA is based on the acid catalyzed hydration reaction of 5-HMF, the mechanism of which is outlined in Scheme 1.11 according to the original proposal formulated by Horvat et al.<sup>51</sup>



**Scheme 1.11** Mechanism of the acid-catalyzed hydration 5-HMF to levulinic acid

The overall reaction involves 6 different intermediates (I-VI) and it starts with the acid-catalyzed hydration of the furan ring, more precisely, of the ring portion adjacent to the aldehyde group, to produce I. Then, compounds II-III form by the subsequent loss and addition of water: the ring finally opens to form the tri-carbonyl intermediate IV. This unstable compound readily decomposes (again by loss and addition of water) and, after the release of formic acid, the formation of stable levulinic acid is observed. The general balance consists in the addition of two molecules of water to one of HMF, with the formation of one mole of levulinic acid and formic acid. The formation of the side-product generally defined as humine is not shown. Humine is a

mixture of fulvic and humic acids characterized by the presence of several carboxylic groups and phenol substituents, in a wide range of molecular weights.<sup>52</sup>

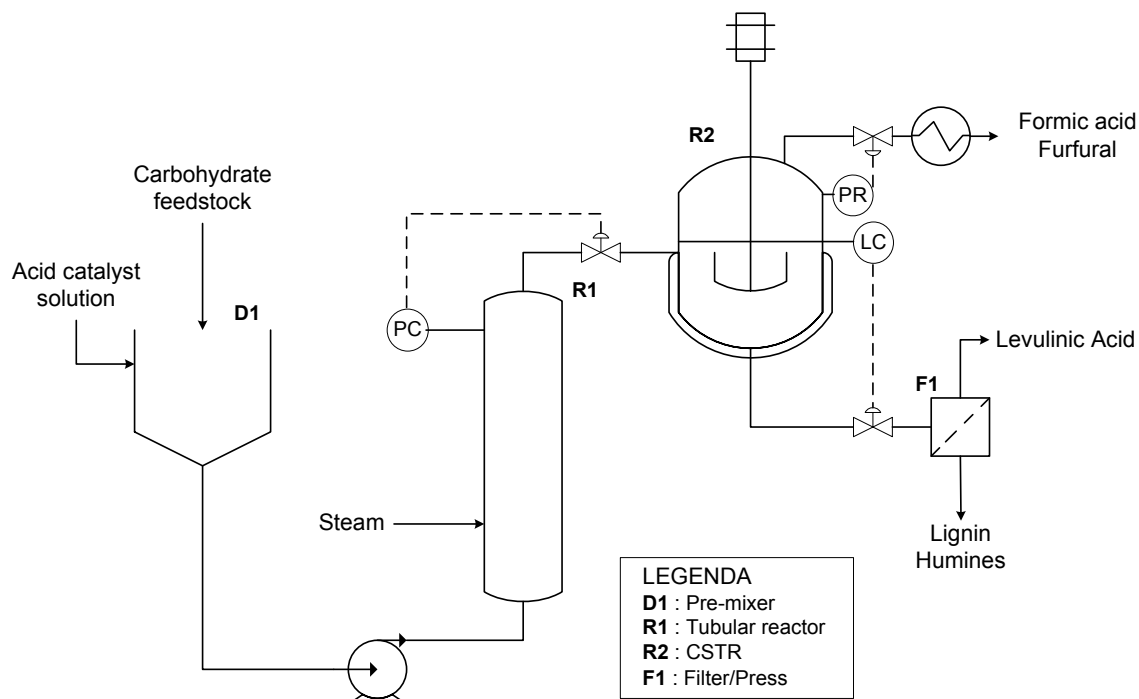
Since the reaction is not difficult, a number of solutions has been proposed over the years including several patents that claim the production of levulinic acid from different materials containing carbohydrates, from the simplest, such as starch, to the more complex, such as the lignocelluloses.

One of the first processes designed to be fed with different sources of hexoses, was proposed in 1957 by Dulop and Wells.<sup>53</sup> In the original configuration, the raw material was processed at atmospheric pressure in a mixture of water and an acid catalyst (sulfuric acid, phosphoric acid, sodium acid sulfate) that passed continuously into a high temperature reactor operating at 150-200 °C. Typical residence times were of 2-3 hours. Outgoing heavy products (humine) were filtered from the liquid, and the resulting aqueous solution of levulinic acid and catalyst was mixed in a column with a hydrophobic solvent, in which levulinic acid was solubilized. However, due to sizeable amounts of by-products, isolated yields of LA were rather moderate: they did not exceed 20% on the dry weight of the feedstock.

30 years later, in 1997, a process developed by Biofine Corporation claimed one of the best ever reported solutions for the synthesis of LA by acid degradation of biomass.<sup>54</sup> In this procedure, the continuous production of levulinic acid and furfural was carried out through the acid hydrolysis of carbon sugars, while at the same time, the minimization of side product formation was achieved by significantly improving the traditional engineering of the LA production process through a novel, two reactor system (Scheme **1.12**). The biomass feedstock was mixed with sulfuric acid (1.5-3%) and first introduced into a plug-flow reactor where the hydrolysis of the carbohydrates took place at 210-230 °C and 25 bar with a short residence time (12 s). This produced different intermediates, mainly 5-HMF, and minimized the formation of degradation products. Subsequently, in a second reactor, intermediate compounds were converted to LA and formic acid at 195-215 °C and 14 bar, with a residence time close to 20 min. LA was continuously removed as a liquid from the bottom of the reactor. The conditions of the second reactor were chosen so that formic acid and the co-product furfural were removed as vapor and externally condensed.

The Biofine Process, due to its efficient reactor system and the use of polymerisation inhibitors that reduced excessive char formation, achieved (from cellulose) LA yields of 70-80% of the theoretical maximum. This meant the conversion of approximately 50% of the mass of 6-carbon sugars to LA, with 20% being converted to formic acid and 30% to tars.<sup>47b</sup> Moreover, another remarkable advantage was that the process used a wholly chemical-based technology

without any form of micro-organisms to degrade the biomass. It should be noted that biological agents are not only often responsible for poor yields, but they also limit the heterogeneity of lignocellulosic feedstocks to be utilised, including for example, those deriving from (cellulosic) municipal solid waste and sewage that contain contaminants able to inhibit fermentation.



**Scheme 1.12** Continuous production of levulinic acid according to technology "Biofine"<sup>47b</sup>

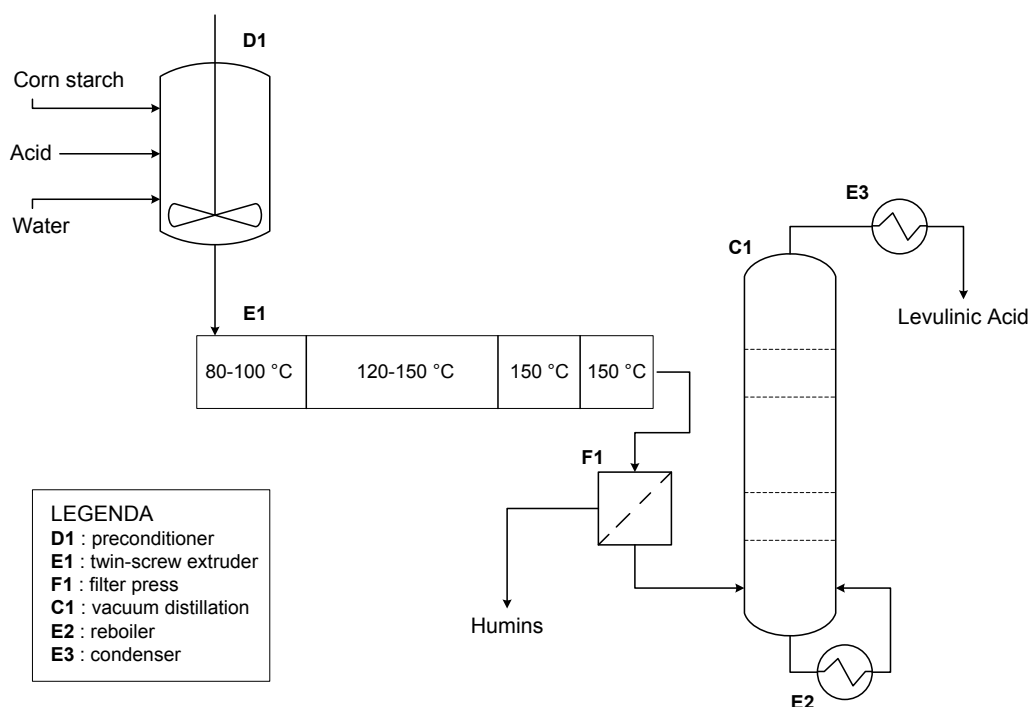
The viability of the Biofine technology was initially examined on a pilot plant built in 1996 in Glens Falls, in the state of New York. This was put into operation for many trial periods, processing one ton per day of dry raw material. Remarkably, the use of paper industry waste as a feedstock yielded from 0.42 to 0.595 kg of levulinic acid per kg of cellulose (between 59 and 83% of the maximum theoretical yield).<sup>47b</sup> After these tests, a commercial plant able to process 50 dry tonnes of feedstock (mainly paper sludge, agricultural residue and waste paper) per day was constructed in Caserta (Italy) with joint funding from the EU and private investment (Figure 1.3). However, although this plant was expected to be operational in 2005, private legal problems did not allow its start. The Biofine process is presently not yet commercially exploited.



**Figure 1.3** Plant in Caserta (Italy) for the production of levulinic acid and ethyl levulinate. Storage tanks (top left); exterior of the building (bottom left); mixing tank (top center), the second reactor (bottom center) aerial view (right).

It should also be noted that almost at the same time of the development of the Biofine process, other relevant solutions were proposed for the synthesis of LA from biomass. Among them, the work of Ghorpade and Hanna should be mentioned.<sup>55</sup> In this configuration, starch was the feedstock, and the preparation of LA took place in a continuous mode via a reactive extrusion process. The extruder was fed by an aqueous mixture of starch and acid catalyst and worked at a variable temperature (initial: 80-100 °C; middle: 120-150 °C; final: 150 °C) to optimize not only of the hydrolysis process, but also the separation of the products. Outgoing humine was filtered away and the levulinic acid was purified by distillation under vacuum. The feeding of 820 kg $\times$ h<sup>-1</sup> of corn starch, 40 kg $\times$ h<sup>-1</sup> of sulfuric acid and 290 kg $\times$ h<sup>-1</sup> of water resulted in an overall yield of levulinic acid of 48% by weight, one of the best ever reported from starch. A simplified scheme of the process is shown in Scheme 1.13.

One last mention goes also to the work of Farone *et al.* that proposed a simple, though efficient method for the treatment of biomass containing both cellulose and hemicellulose components.<sup>56</sup> Advantages of the procedure included: *i*) the possibility of using a mixed C6-C5 acid stream without the need for separating the sugars; *ii*) the use of a relatively high concentration of sulfuric acid that under specific conditions, was discovered to act as a dehydration catalyst thus minimizing by-products; *iii*) the recycle and reuse of all streams. For example, starting from a mixture of papers (predominantly newspaper with a cellulose content of 85%) as the raw material, this technology claimed the production of levulinic acid in up to 59.8% of the theoretical yield (from the quantity of cellulose in the paper).



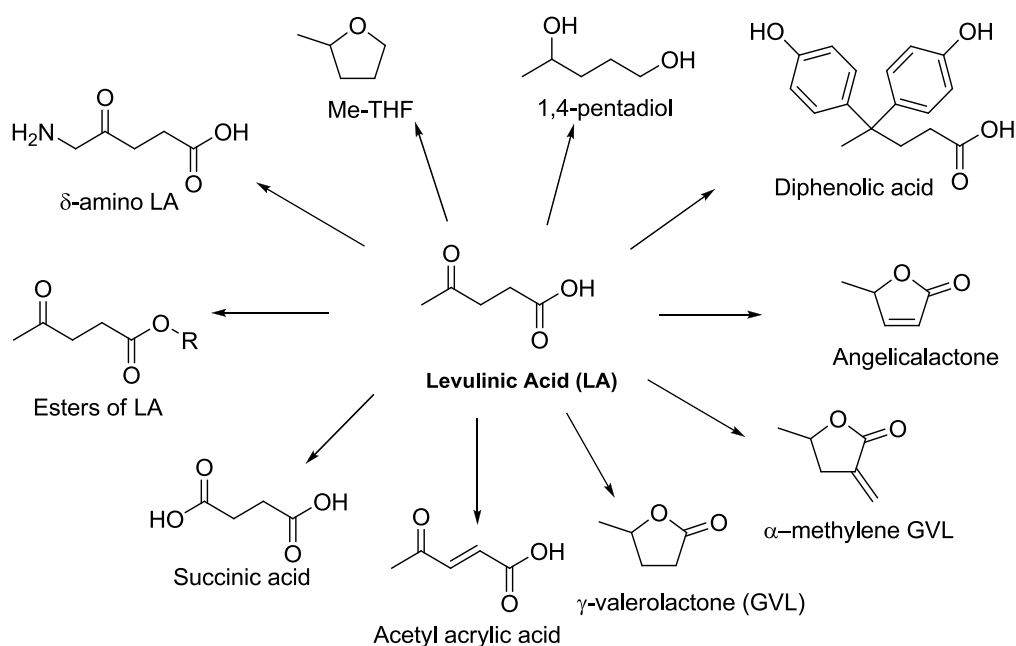
**Scheme 1.13** Continuous production of levulinic acid from starch, via reactive extrusion

To conclude this paragraph, one should note that cost-effective procedures already exist to convert complex raw materials from renewable sources into rather inexpensive LA. However, as all the technologies that try to stimulate the transition from a hydrocarbon- to a carbohydrate-based economy (at least where local self-sustainability is possible), also the green technology for the LA synthesis meets difficulties to make its way mostly for political/legal barriers rather than for technical/economical ones. In the future, the extent to which this potentially sustainable “bio-recycling” productions are realized will largely depend also on the size and applications of the market for LA especially in material (plastics), food, and fuel sectors.

## 1.4.2 LA: reactivity and derivatives

### 1.4.2.1 Derivatives

Among bio-based platform chemicals, levulinic acid offers one of the largest families of derivatives of potential industrial interest, including fuel additives, monomers for plastics and textiles, and chemicals. The most important ones are shown in Scheme 1.14:



**Scheme 1.14** Derivatives of Levulinic Acid (LA)

The conversion of LA to methyltetrahydrofuran (Me-THF) and various levulinate esters (top left) addresses the fuel markets as gasoline and biodiesel additives, respectively.<sup>6a, 57</sup>  $\delta$ -Aminolevulinic acid is a herbicide<sup>46, 58</sup> and  $\alpha$ -methylene- $\gamma$ -valerolactone can be used in the production of new acrylate polymers.<sup>59</sup> Diphenolic acid is of particular interest as a replacement for bisphenol A in the production of polycarbonates.<sup>46, 60</sup> Lactones (middle and bottom right: Angelicalactone,  $\gamma$ -valerolactone, and  $\alpha$ -methylene, $\gamma$ -valerolactone) have interest as solvents.<sup>46, 61</sup> In this context, a remarkable possibility is also the conversion of lactones into the analogous substituted N-methylpyrrolidone, a valuable polar aprotic media. Controlled hydrogenation of LA may lead to 1,4-pentenediol, which is useful in the production of polyesters.<sup>62</sup> Finally, LA is also a potential starting material for the synthesis of succinic acid via oxidative processes.<sup>63</sup>

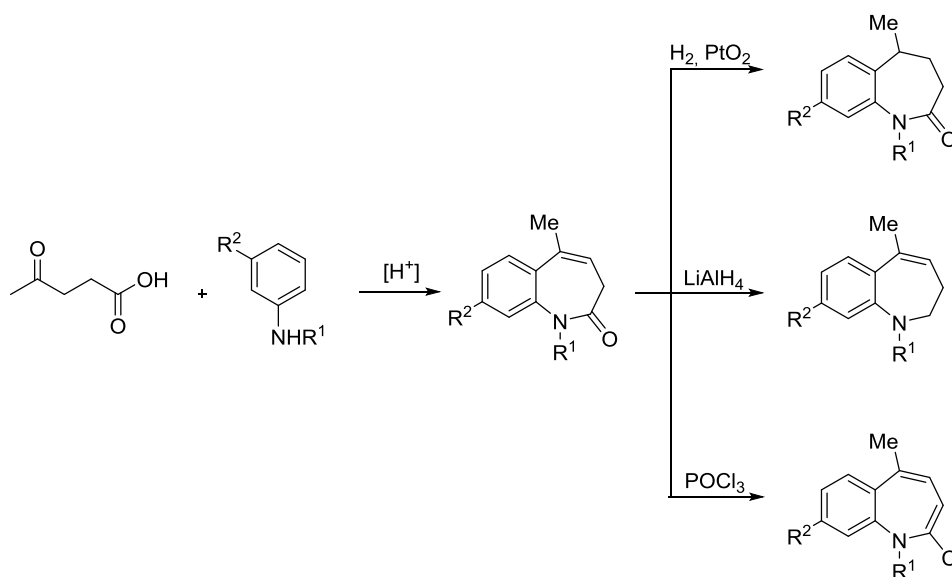
#### 1.4.2.2 Reactivity

LA is the simplest member of gamma-keto acids. Several authors have explored possible chemical transformations of levulinic acid and a general consensus has emerged on the fact that synthetic potentialities of this molecule are far from being exhausted.<sup>45b, 64</sup>

As expected, the co-presence of both a carbonyl and a carboxylic acid group in the LA molecule, allows it to react as a ketone and as a fatty acid. Several reactions of LA have been described accordingly.

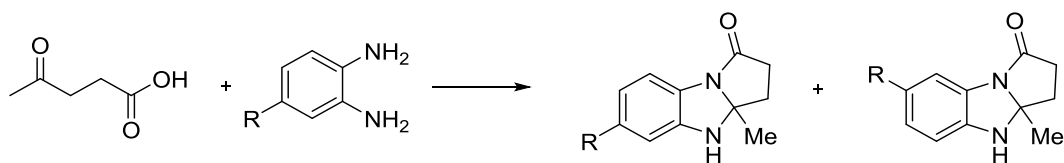
Among the transformations at the carboxyl function, the most common are esterification processes of LA with alcohols. These produce a number of levulinate esters which beside the above mentioned use as additives in fuels, find applications as flavoring, solvents, and plasticizers.<sup>6a, 57a</sup> Esterifications are easy reactions that usually take place at ordinary (or slightly higher) temperatures and with simple catalysts such as sulfuric acid<sup>64a</sup> and polyphosphoric acid.<sup>65</sup> The use of anion-exchange resins and molecular sieves supported by sulfated titania ( $\text{TiO}_2/\text{SO}_4^{2-}$ ) also gives very good results.<sup>35a</sup> Although less frequent, electrolytic decarboxylations and cross-decarboxylations<sup>66</sup> as well as additions of alkoxyacetylenes<sup>67</sup> have also been reported as transformations at the carboxyl function of LA. These reactions produce unsaturated ketones and diacids, respectively.

Nucleophilic additions are by far the most usual processes occurring at the carbonyl function of LA. In the presence of N-nucleophiles, the addition step is often followed by a rearrangement which is mediated by the carboxylic group of LA.<sup>45b</sup> The formation of heterocyclic products takes place. An example is the reaction of LA with anilines in acidic medium leading to bicyclic derivatives (Scheme 1.15). These compounds can be hydrogenated to different lactames or cyclic amines, or dehydrogenated (with, e.g.,  $\text{POCl}_3$ ) to produce benzodiazepine-like derivatives.<sup>45b, 68</sup>



**Scheme 1.15** Reaction of anilines with LA

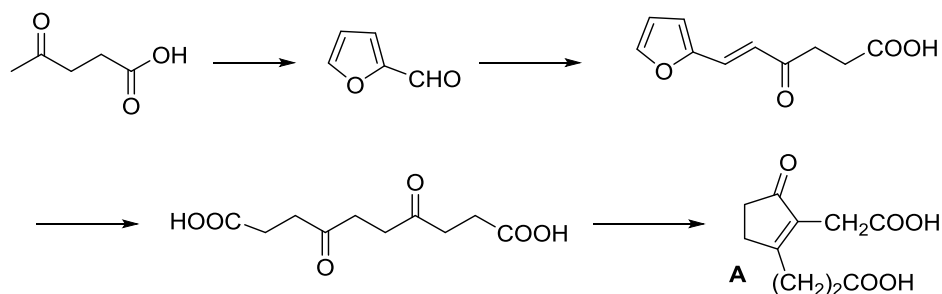
In a similar way, the reaction of LA with *o*-phenylenediamine derivatives gives rise to isomeric pyrrolobenzoimidazolones (Scheme 1.16).<sup>69</sup>



Scheme 1.16. Reaction of *o*-phenylenediamine derivatives with LA

The behavior of the reaction of LA with O- and S-nucleophiles such as alcohols and thiols, is analogous to that observed in the addition of the N-homologues: in these cases, the formation of heterocyclic products including dialkylacetals and dialkyldithioacetals, is observed.<sup>45b</sup>

Another reactive site of the LA molecule is the  $\alpha$ -position to the carbonyl group. Accordingly, aldol condensations of LA with non enolizable aromatic and heterocyclic aldehydes have been reported to produce the expected  $\alpha,\beta$ -unsaturated carbonyl compounds. A remarkable example is the reaction of LA with furfural, which gives different furancarboxylic acids.<sup>70</sup> In particular, 5-furfurylidenelevulinic acid serves as a precursor for intermediates useful in the synthesis of prostaglandins (Scheme 1.17).<sup>71</sup>

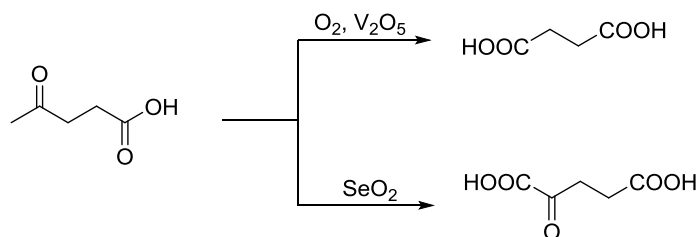


Scheme 1.17 Reaction of furfural with LA

Other reactions involving C-positions neighboring to the carbonyl or the carboxyl groups of LA include chlorination and bromination processes. These transformations are promoted by the temperature or acid and base catalysis, and produce organic halides as valuable building blocks.<sup>45b</sup>

Oxidations of LA have also been reported over different catalysts. For example, in the presence of oxygen and  $V_2O_5$ , LA can be converted to succinic acid,<sup>63</sup> while, the oxidation of LA mediated by selenium dioxide produces 2-oxo-glutaric acid (Scheme 1.18).<sup>45b, 72</sup>

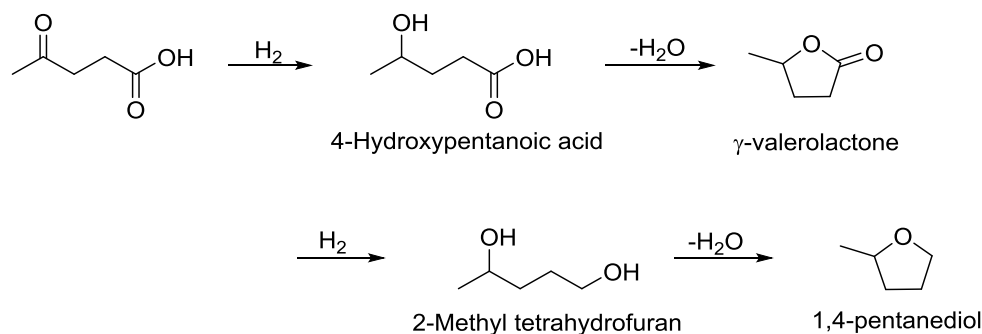




**Scheme 1.18** Oxidation reactions of LA

A recent synthesis of another valuable chemical, methyl vinyl ketone (MVK), has been proposed by the oxidation of levulinic acid over supported copper oxide catalysts.<sup>73</sup> At a high temperature (300 °C), CuO has also been used to catalyze the oxidative decarboxylation of LA to 2-butanone.<sup>74</sup>

Catalytic reduction reactions represent the majority of transformations of LA reported in the literature.<sup>64d, 75</sup> The catalytic system and reaction conditions steer the hydrogenation of LA towards the formation of different products. The general reaction pathway is illustrated in Scheme 1.19. LA can be initially reduced to 4-hydroxypentanoic acid which, even spontaneously, is able to dehydrate to  $\gamma$ -valerolactone (GVL). GVL may be further hydrogenated to 1,4-pentanediol (PDO), which dehydrates to 2-methyltetrahydrofuran (MTHF).<sup>76</sup>



**Scheme 1.19** Different products from the hydrogenation of LA.

Due to the interest for GVL in this Thesis, details on this compound are described in the next paragraph.

## 1.5 $\gamma$ -Valerolactone

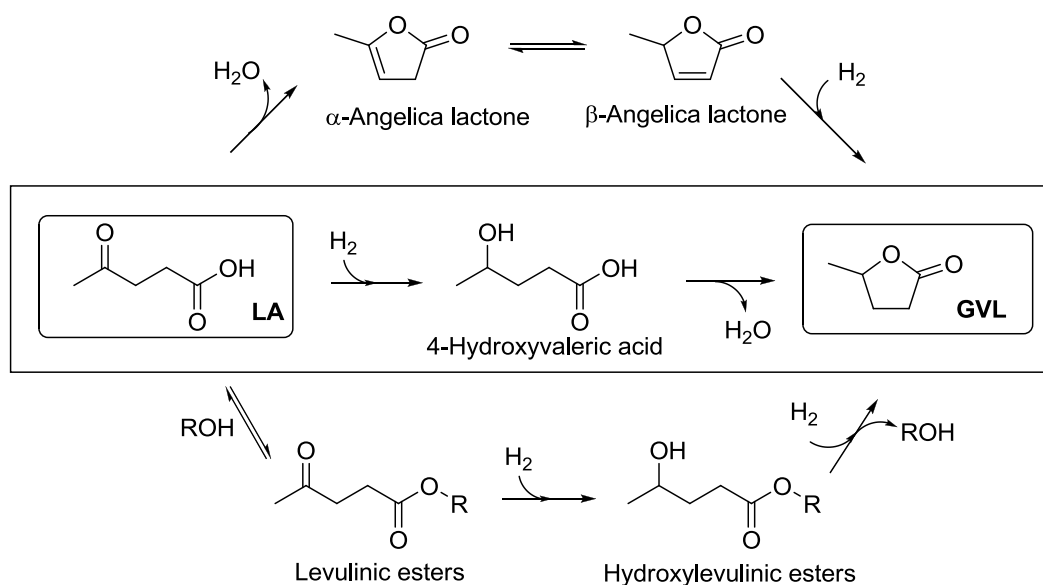
$\gamma$ -Valerolactone (GVL) is a 5 carbon cyclic ester stable at normal conditions as a colorless liquid. GVL has a sweet, herbaceous odor, which makes it suitable for the production of perfumes and food additives.<sup>77</sup> Some properties of GVL are listed in Table 1.6. The compound is reactive enough to produce a variety of derivatives including butane, valeric acid and 5-nonanone.<sup>64d, 78</sup> However, GVL is also stable enough to be used as a biomass derived solvent.<sup>61,77</sup>

**Table 1.6**  
Main properties of GVL<sup>77, 79</sup>

Properties	Value
CAS-No	108-29-2
Formula	C <sub>5</sub> H <sub>8</sub> O <sub>2</sub>
MW (g mol <sup>-1</sup> )	100.112
Refractive index (n <sub>20</sub> /D)	1.432
Density (g mL <sup>-1</sup> )	1.05
Flash point (°C)	96
Melting point (°C)	-31
Boiling point (°C)	201-208
Solubility in water (%)	100
$\Delta H_{\text{vap}}$ (kJ mol <sup>-1</sup> )	54.8
$\Delta_c H_{\text{liquid}}^0$ (kJ mol <sup>-1</sup> )	-2649.6

### 1.5.1 Production of GVL via LA hydrogenation

Among different strategies to produce GVL, the most efficient synthesis is the above mentioned hydrogenation of LA.<sup>64d, 75-76</sup> Two possible mechanisms have been reported for the reaction. In the first one, the hydrogenation of LA follows the pattern of Scheme 1.15, where the initial formation of  $\gamma$ -hydroxyvaleric acid, an unstable intermediate, is followed by an intramolecular esterification with the spontaneous loss of a water molecule. In the second pathway, the reaction starts with the dehydration of LA to form the angelica lactone which is then hydrogenated to produce GVL (Scheme 1.20, top).<sup>80</sup> This alternative, less frequent route, requires an added acid, and typically leads to lower yields due to some coke formation by a side acid-catalyzed decomposition of the angelica lactone.<sup>81</sup> The hydrogenation of esters of levulinic acid also leads to the formation of GVL. The reaction proceeds similarly to that of LA. First, the ester is hydrogenated to a hydroxyl levulinic ester, which then undergoes an intramolecular transesterification to produce GVL and the corresponding alcohol.<sup>82</sup> (Scheme 1.20, bottom). If water is present, the ester may be first hydrolyzed to LA and an alcohol. Then, LA is hydrogenated according to the scheme above described above.



**Scheme 1.20** Different hydrogenation reactions to produce GVL

Several methods have been recently proposed to conduct the hydrogenation of LA in the presence of different catalysts. Some of the most interesting ones are described below.

In 2004, Manzer has proposed two procedures. The first involved the reaction of LA (50% in dioxane) in an autoclave at a temperature of 150 °C for 4 hours, using a hydrogen pressure of 3.4 MPa and a Ru/C (5%) as a catalyst. A quantitative conversion and a selectivity of 97% towards GVL were achieved.<sup>83</sup> The second method, patented together with Hutchenson, described a continuous flow hydrogenation of LA (once again dissolved in dioxane) in supercritical  $\text{CO}_2$  ( $\text{scCO}_2$ ) as a carrier. The reaction was carried out in a tubular reactor at 200 °C and 20 MPa ( $\text{H}_2$  gas was equimolar to LA), over a catalytic bed of Ru/ $\text{Al}_2\text{O}_3$  (1%). Conversion and selectivity towards GVL were 98% and 100%, respectively.<sup>84</sup>

In 2007, Bourne *et al.*<sup>85</sup> proposed another method for the continuous hydrogenation of LA in supercritical carbon dioxide: in this case, water was a co-solvent (LA:  $\text{H}_2\text{O}$ , 75% w/w; ~1:2 mol/mol), and  $\text{H}_2$  (10 MPa) was used in a 3 molar excess on LA. The reaction temperature was 200 °C and the catalyst was of Ru/ $\text{SiO}_2$ (5%). Conversion and selectivity were almost quantitative ( $\geq 99\%$ ). The main advantage of this configuration was the solubility of GVL in the combined water/ $\text{scCO}_2$  mixture (of note, under the reported conditions of T and P, LA was not water soluble). The authors therefore proposed a reactor system that in addition to the LA hydrogenation, allowed the continuous separation of pure GVL without extra energy input: since GVL was liquid even at high pressures, the complete depressurization of  $\text{CO}_2$  was not required to isolate the product.

In 2009, an innovative methodology was reported for the exploitation of formic acid, a co-product in the synthesis of LA by dehydration of biomass, as a source of H<sub>2</sub> for the reduction of LA itself.<sup>86</sup> The method had the double advantage of avoiding both the use of external sources of H<sub>2</sub> and the separation of LA from formic acid in the aqueous stream recovered after the biomass treatment. It was demonstrated that, using a mixture of RuCl<sub>3</sub> (0.1 mol%) and PPh<sub>3</sub> (0.3 mol%) as catalyst and ligand, and pyridine as a base, an aqueous solution of LA and formic acid (1:1 mol:mol) was converted into GVL with an overall yield of 88%. Co-products were water and CO<sub>2</sub>, the latter was supposed to have a positive effect on the catalyst. In a model experiment starting directly with glucose as a source of both LA and FA, GVL was produced in a final yield of 48%.

In 2010, Lange et al.<sup>78c</sup> evaluated the stability of about 50 catalysts for the hydrogenation of LA. At 200 °C and 40 bar H<sub>2</sub> pressure, best performances were reported for Pt supported on TiO<sub>2</sub> or ZrO<sub>2</sub>, that allowed a very high hydrogenation productivity ( $\sim 10 \text{ g}_{\text{GVL}}\text{g}_{\text{CAT}}^{-1} \text{ h}^{-1}$ ), an excellent selectivity towards GVL (> 95 mol%), and a marginal deactivation after 100 h.

In 2012, an original method was patented to obtain GVL along with LA and furfural, starting directly from cellulose (and/or other C<sub>6</sub> carbohydrates) or xylose (and/or other C<sub>5</sub> carbohydrates) or combinations thereof.<sup>87</sup> The procedure used either a monophasic medium comprising GVL and an acid, or a biphasic system comprising an organic layer of GVL and a substantially immiscible aqueous layer. During the process, carried out at 180 °C and 35 bar H<sub>2</sub> pressure, LA was converted into GVL using different hydrogenation catalysts, with preference for ruthenium and tin supported systems. A remarkable novelty of this process was that the product GVL also acted as a reaction solvent.

The above discussed list along with references cited in the previous paragraphs (albeit not exhaustive) help the reader to go through most convenient reaction conditions and catalysts for the LA hydrogenation, and to appreciate the evolution of such hydrogenation methods over the past decade. However, one may note that aspects which have been only marginally considered throughout the literature available on this subject, are the recovery and recycle of (precious) metal catalysts as well as the exploitation of reusable catalytic systems based on cheaper metals. In the context of the growing need for innovative solutions to upgrade biomass derivatives, issues on the catalyst recycle in the hydrogenation of LA have inspired the present Thesis.

## 1.6 Aim and Summary of the Thesis

The research reported in this Thesis was aimed at investigating methods for the catalytic upgrading of levulinic acid (LA) as a biomass derived platform chemical. The Thesis project was focused on hydrogenation reactions of LA, and it was developed within a cotutelle agreement between the University of Ca' Foscari Venezia (Italy) and the University of Sydney (Australia), under the supervision of Prof. Maurizio Selva (Department of Molecular Sciences and Nanosystems, Centre for Sustainable Technologies, Venezia) and Prof. Thomas Maschmeyer (Laboratory for Advanced Catalysis and Sustainability, School of Chemistry, Sydney). For convenience, the aim and the summary of activities carried out in Venezia and in Sydney will be presented separately.

*Venezia.* In the past fifteen years, at Ca' Foscari University, an original multiphase technique was implemented for the investigation of a number of hydrogenation processes. The multiphase systems used in these studies were composed of a couple of immiscible solvents (mostly water and an organic medium), a hydrogenation heterogeneous metal catalyst, and an ionic liquid (full details and references are given later in Chapter 2). It was demonstrated that such multiphase configurations had several advantages: they were not only suitable to control the activity of the metal catalyst and to tune the selectivity of the investigated hydrogenation reactions, but they also improved the isolation of the desired products and allowed an efficient recycle of the catalyst.

In the light of these results, the first fifteen months of this Thesis work in Venezia were devoted at exploring the feasibility of the hydrogenation of LA under multiphase conditions. After a screening of the most appropriate solvents, catalysts, and ionic liquids, it was discovered that new “unconventional” multiphase conditions were necessary for the reaction to proceed. In particular, contrarily to all multiphase arrangements previously used, an inverse configuration was developed where the substrate and the product (LA and  $\gamma$ -valerolactone, GVL) were converted and recovered in an aqueous phase, respectively. Accordingly, at 100 °C, in the presence of Ru/C (5%) and gaseous H<sub>2</sub> at 35 bar, substantially quantitative conversion and selectivity towards GVL were achieved. Even most important, the metal catalyst remained perfectly segregated in the ionic liquid phase and it could be recycled several times with no loss in its performance. Tests also demonstrated that no leaching of the metal occurred in the aqueous phase, while an hydrocarbon solvent (isooctane) was a necessary component of the multiphase system to secure the phase separation and the recovery of both the product and the catalyst.

Multiphase conditions also proved to be suitable for the use of homogeneous catalysts. In particular, RuCl<sub>3</sub> was employed. It was noticed that during the hydrogenation trials, the original

water soluble catalyst was progressively transformed into Ru nanoparticles (NPs) which were excellently confined and stabilized by the ionic liquid phase used. Moreover, metal NPs were even more active than the starting Ru salt in the hydrogenation of LA and they could be easily recycled.

Attempts to apply the investigated multiphase systems to the hydrogenation of aqueous mixtures of LA and formic acid (of composition similar to those obtained after the acid hydrolytic treatment of cellulosic biomass) were not successful. Formic acid could not be used as a hydrogen source. Under such conditions, reactions were sluggish or did not proceed at all even in the presence of an additional pressure of  $H_2$ . Tests demonstrated that the results were not due to a change of pH of the reacting mixture, nor to a modification of the partitioning of LA between aqueous and organic phases. A hypothesis for this lack of reactivity was formulated on a plausible H-bond interaction between FA and LA in the aqueous phase, which might reduce the availability of LA for the hydrogenation.

*Sydney.* A recent work carried out at the University of Sydney, demonstrated that an iron-based system, by far cheaper than conventional catalysts used for the hydrogenation of LA, was active to promote the use of FA as a hydrogen source for the selective reduction of LA to GVL. However, the overall process needed a stoichiometric amount of iron, and therefore, it was not only difficult to apply but also, not economically viable. (Details and references are given later on Chapter 3)

A method must be devised to recover the iron promoter and make the reaction a catalytic transformation. This was the aim of the second part of this Thesis work carried out at the University of Sydney. The general idea was to recover and re-use iron in aqueous solutions by electrolytical methods capable to allow the reduction of  $Fe^{2+}$  ions produced during the hydrogenation of LA, back to  $Fe^0$ . The investigated reaction was the cathodic deposition  $Fe^{2+} + 2e^- \rightarrow Fe^0$  performed under different conditions compatible to an environment where the LA hydrogenation was possible. In particular,  $Fe^{2+}$  aqueous acidic solutions containing either  $H_2SO_4$  or  $HCOOH$  were considered.

The initial investigation of the feasibility of the metal (iron) deposition on a glassy carbon electrode was conducted through voltammetric techniques. The influence of major parameters such as the concentration of  $Fe^{2+}$ , pH, the temperature and the co-presence of organic compounds (reagents or products of hydrogenation reactions). was also explored. These experiments were necessary to select conditions to provide a basis for longer time scale experiments of bulk electrolysis, *i.e.* exhaustive electrolysis. A two-step CPE experiments proved to be suitable for the iron electrodeposition: when two different potentials were applied to an acidic aq. solution of

FeSO<sub>4</sub>, the first nucleation of the metal occurred at -1.30/-1.25 V (for 60 sec), while the further growth of the iron layers took place at -1.15 V (for 940 sec).

The geometry of iron deposits seemed to be sensitive to the composition/nature of the system. In particular, a thin and compact homogeneous iron layer was obtained using formic acid solutions, while a relatively disordered morphology of Fe<sup>0</sup> depositions was observed in the presence of sulfuric acid.

Once the initial concept was proved, *i.e.* the possibility to regenerate the metallic iron in acid aqueous solutions of Fe<sup>2+</sup> was demonstrated, then, the most interesting results of CPE experiments were considered to implement an iron-based technique for the hydrogenation of organic compounds on a practical lab. scale (0.4 mmol, ~50 mg). Bulk electrolysis experiments were carried out using Fe<sup>0</sup> as a reaction promoter, and levulinic acid and cyclohexanone as model reactants. Under such conditions, cyclohexanone was hydrogenated to the expected  $\gamma$ -cyclohexanol with relatively moderate conversions (3-17 %); no conclusive results were obtained for levulinic acid, although the formation of the expected product (GVL) was detected. Overall, the investigation was promising, but it certainly required a more in-depth analysis to optimize the technique. This aspect will be the object of future investigations.

## 1.7 References

1. World Commission on Environmental and, D., Our Common Future. 27 April 1987 ed.; Oxford University Press: Oxford (UK), 1987; p 416.
2. Anastas, P. T.; Warner, J. C., *Green Chemistry: Theory and Practice*. Oxford University Press: Oxford, 2000; p 148.
3. Tang, S. L. Y.; Smith, R. L.; Poliakoff, M., *Green Chem.* **2005**, *7*, 761-762.
4. Trost, B., *Science* **1991**, *254*, 1471-1477.
5. Sheldon, R. A., *Chem. Commun.* **2008**, 3352-3365.
6. (a) Huber, G. W.; Iborra, S.; Corma, A., *Chem. Rev.* **2006**, *106*, 4044-4098; (b) Zhang, Y. H. P., *J. Ind. Microbiol. Biotechnol.* **2008**, *35*, 367-375.
7. <http://www.uop.com/petrochemicals-flow-scheme/>.
8. Anastas Paul, T., "Benign by Design Chemistry" in *Benign by Design*, American Chemical Society: 1994; Vol. 577, pp 2-22.
9. [http://ec.europa.eu/energy/energy2020/index\\_en.htm](http://ec.europa.eu/energy/energy2020/index_en.htm) (accessed 30/10/13)
10. (a) [http://www.eni.com/it\\_IT/home.html](http://www.eni.com/it_IT/home.html) (accessed 30/10/13); (b) <http://www.ogj.com/articles/2012/09/enis-venice-refinery-to-be-biorefinery.html> (accessed 30/10/13);
11. (a) Kamm, B.; Kamm, M., *Appl. Microbiol. Biotechnol.* **2004**, *64*, 137-145; (b) Jiménez-González, C.; Constable, D. J. C., *Green Chemistry and Engineering: a Practical Design Approach*. John Wiley & Sons, Inc.: Hoboken, 2011.
12. Clark, J. H.; Deswarte, F. E. I., "The Biorefinery Concept—An Integrated Approach" in *Introduction to Chemicals from Biomass*, John Wiley & Sons, Ltd: 2008; pp 1-20.
13. Alonso, D. M.; Bond, J. Q.; Dumesic, J. A., *Green Chem.* **2010**, *12*, 1493-1513.
14. <https://public.ornl.gov/site/gallery/detail.cfm?id=181&topic=&citation=&general=cellulose&restsection=all>.
15. Kamm, B.; Gruber, P. R.; Kamm, M., *Biorefineries - Industrial Processes and Products*. Wiley: Weinheim, 2010.
16. Cornils, B.; Lappe, P., "Dicarboxylic Acids, Aliphatic" in *Ullmann's Encyclopedia of Industrial Chemistry*, Wiley-VCH: Verlag, 2000.
17. Werpy, T. P., G. *Top Value Added Chemicals from Biomass*; U.S. Department of Energy Laboratory, Pacific Northwest National Laboratory, National Renewable Energy Laboratory, Office of Biomass Program: Richland, WA, 2004.
18. Nonato, R.; Mantelatto, P.; Rossell, C., *Appl. Microbiol. Biotechnol.* **2001**, *57*, 1-5.
19. Fernando, S.; Adhikari, S.; Chandrapal, C.; Murali, N., *Energy Fuels* **2006**, *20*, 1727-1737.
20. (a) Hendriks, A. T. W. M.; Zeeman, G., *Bioresour. Technol.* **2009**, *100*, 10-18; (b) Mosier, N.; Wyman, C.; Dale, B.; Elander, R.; Lee, Y. Y.; Holtzapple, M.; Ladisch, M., *Bioresour. Technol.* **2005**, *96*, 673-686; (c) Brodeur, G. Y., E.; Badal, K.; Collier, J.; Ramachandran, K. B.; Ramakrishnan, S., *Enzyme Res.* **2011**, *2011*, 17.
21. <https://nararenewables.org/feature/newsletter-2>
22. (a) Millett Merrill, A.; Effland Marilyn, J.; Caulfield Daniel, F., "Influence of Fine Grinding on the Hydrolysis of Cellulosic Materials? Acid Vs. Enzymatic" in *Hydrolysis of Cellulose: Mechanisms of Enzymatic and Acid Catalysis*, AMERICAN CHEMICAL SOCIETY: 1979; Vol. 181, pp 71-89; (b) Palmowski, L. M. M., J. A., *Water Sci. Technol.* **2000**, *41*, 155-162.
23. Bobleter, O., *Prog. Polym. Sci.* **1994**, *19*, 797-841.
24. Fengel, D.; Wegener, G., *Wood: chemistry, ultrastructure, reactions*. De Gruyter: 1983.



25. Hon, D. N. S.; Shiraishi, N., *Wood and Cellulosic Chemistry, Second Edition, Revised, and Expanded*. Taylor & Francis: 2000.
26. (a) da Costa Lopes, A. M.; João, K. G.; Rubik, D. F.; Bogel-Lukasik, E.; Duarte, L. C.; Andreus, J.; Bogel-Lukasik, R., *Bioresour. Technol.* **2013**, *142*, 198-208; (b) Moniruzzaman, M.; Ono, T., *Bioresour. Technol.* **2013**, *127*, 132-137.
27. (a) Demirbaş, A., *Energy Convers. Manage.* **2001**, *42*, 279-294; (b) Arai, K.; Smith Jr, R. L.; Aida, T. M., *J. Supercrit. Fluids.* **2009**, *47*, 628-636.
28. (a) Arshadi, M.; Sellstedt, A., "Production of Energy from Biomass" in *Introduction to Chemicals from Biomass*, John Wiley & Sons, Ltd: 2008; pp 143-178; (b) Küçük, M. M.; Demirbaş, A., *Energy Convers. Manage.* **1997**, *38*, 151-165.
29. Demirbas, A., *Prog. Energy Combust. Sci.* **2004**, *30*, 219-230.
30. (a) Bridgwater, A. V., *Biomass Bioenergy* **2012**, *38*, 68-94; (b) Zhang, Q.; Chang, J.; Wang, T.; Xu, Y., *Energy Convers. Manage.* **2007**, *48*, 87-92.
31. (a) Kumar, A.; Jones, D.; Hanna, M., *Energies* **2009**, *2*, 556-581; (b) Kirubakaran, V.; Sivaramakrishnan, V.; Nalini, R.; Sekar, T.; Premalatha, M.; Subramanian, P., *Renewable Sustainable Energy Rev.* **2009**, *13*, 179-186.
32. (a) Behrendt, F.; Neubauer, Y.; Oevermann, M.; Wilmes, B.; Zobel, N., *Chem. Eng. Technol.* **2008**, *31*, 667-677; (b) Toor, S. S.; Rosendahl, L.; Rudolf, A., *Energy* **2011**, *36*, 2328-2342.
33. (a) Saxena, R. C.; Adhikari, D. K.; Goyal, H. B., *Renewable Sustainable Energy Rev.* **2009**, *13*, 167-178; (b) Olsson, L.; Hahn-Hägerdal, B., *Enzyme Microb. Technol.* **1996**, *18*, 312-331.
34. (a) West, R. M.; Kunkes, E. L.; Simonetti, D. A.; Dumesic, J. A., *Catal. Today* **2009**, *147*, 115-125; (b) Kunkes, E. L.; Simonetti, D. A.; West, R. M.; Serrano-Ruiz, J. C.; Gärtner, C. A.; Dumesic, J. A., *Science* **2008**, *322*, 417-421.
35. (a) Corma, A.; Iborra, S.; Velty, A., *Chem. Rev.* **2007**, *107*, 2411-2502; (b) Lichtenthaler, F. W., *Carbohydr. Res.* **1998**, *313*, 69-89; (c) Saha Badal, C.; Bothast Rodney, J., "Enzymes in Lignocellulosic Biomass Conversion" in *Fuels and Chemicals from Biomass*, American Chemical Society: 1997; Vol. 666, pp 46-56.
36. (a) Louwrier, A., *Biotechnol. Appl. Biochem.* **1998**, *27*, 1-8; (b) Varadarajan, S.; Miller, D. J., *Biotechnol. Progr.* **1999**, *15*, 845-854.
37. Cottier, L. D., G., *Trends Heterocycl Chem* **1991**, *2*.
38. (a) Kuster, B. F. M., *Starch - Stärke* **1990**, *42*, 314-321; (b) Kuster, B. F. M., *Carbohydr. Res.* **1977**, *54*, 177-183; (c) Kuster, B. F. M.; S. van der Baan, H., *Carbohydr. Res.* **1977**, *54*, 165-176.
39. (a) Fayet, C.; Gelas, J., *Carbohydr. Res.* **1983**, *122*, 59-68; (b) Tyrlik, S. K.; Szerszeń, D.; Olejnik, M.; Danikiewicz, W., *Carbohydr. Res.* **1999**, *315*, 268-272; (c) Mednick, M. L., *J. Org. Chem.* **1962**, *27*, 398-403.
40. Hales, R. A.; Le Maistre, J. W.; Orth, G. O. US 3071599, 1963.
41. (a) Chheda, J. N.; Roman-Leshkov, Y.; Dumesic, J. A., *Green Chem.* **2007**, *9*, 342-350; (b) Tong, X.; Ma, Y.; Li, Y., *Appl. Cat. A: Gen.* **2010**, *385*, 1-13; (c) Hansen, T. S.; Mielby, J.; Riisager, A., *Green Chem.* **2011**, *13*, 109-114.
42. van Dam, H. E.; Kieboom, A. P. G.; van Bekkum, H., *Starch - Stärke* **1986**, *38*, 95-101.
43. Antal Jr, M. J.; Mok, W. S. L.; Richards, G. N., *Carbohydr. Res.* **1990**, *199*, 91-109.
44. Qian, X.; Nimlos, M. R.; Davis, M.; Johnson, D. K.; Himmel, M. E., *Carbohydr. Res.* **2005**, *340*, 2319-2327.
45. (a) Ghorpade, V. M. H., M. A. 1996; (b) V. Timokhin, B.; A. Baransky, V.; D. Eliseeva, G., *Russ. Chem. Rev.* **1999**, *68*, 73-84.
46. Bozell, J. J.; Moens, L.; Elliott, D. C.; Wang, Y.; Neuenschwander, G. G.; Fitzpatrick, S. W.; Bilski, R. J.; Jarnefeld, J. L., *Resour. Conserv. Recy.* **2000**, *28*, 227-239.

47. (a) Ragauskas, A. J.; Williams, C. K.; Davison, B. H.; Britovsek, G.; Cairney, J.; Eckert, C. A.; Frederick, W. J.; Hallett, J. P.; Leak, D. J.; Liotta, C. L.; Mielenz, J. R.; Murphy, R.; Templer, R.; Tschaplinski, T., *Science* **2006**, *311*, 484-489; (b) Hayes, D. J.; Fitzpatrick, S.; Hayes, M. H. B.; Ross, J. R. H., "The Biofine Process – Production of Levulinic Acid, Furfural, and Formic Acid from Lignocellulosic Feedstocks" in *Biorefineries-Industrial Processes and Products*, Wiley-VCH Verlag GmbH: 2008; pp 139-164.
48. Centi, G.; Lanzafame, P.; Perathoner, S., *Catal. Today* **2011**, *167*, 14-30.
49. Patel, A. D.; Serrano-Ruiz, J. C.; Dumesic, J. A.; Anex, R. P., *Chem. Eng. J.* **2010**, *160*, 311-321.
50. (a) McKenzie, B. F., *Org. Synth.* **1929**, *9*; (b) Leonard, R. H., *Ind. Eng. Chem.* **1956**, *48*, 1330-1341.
51. Horvat, J.; Klaić, B.; Metelko, B.; Šunjić, V., *Tetrahedron Lett.* **1985**, *26*, 2111-2114.
52. Rice, J. A.; MacCarthy, P., *Sci. Total Environ.* **1992**, *117-118*, 83-88.
53. Dunlop, A. P.; Wells, J. P. A. US2813900, 1957.
54. (a) Fitzpatrick, S. W. WO8910362 1989; (b) Fitzpatrick, S. W. WO9640609 1996.
55. Ghorpade, V. M.; Hanna, M. A. US5859263, 1999.
56. Farone, W. A.; Cuzens, J. E. US6054611, 2000.
57. (a) Shu, C.-K.; Lawrence, B. M., *J. Agric. Food. Chem.* **1995**, *43*, 782-784; (b) Olson Edwin, S.; Kjelden Michelle, R.; Schlag Adam, J.; Sharma Ramesh, K., "Levulinate Esters from Biomass Wastes" in *Chemicals and Materials from Renewable Resources*, American Chemical Society: 2001; Vol. 784, pp 51-63.
58. Takeuchi, Y.; S., F. US2010317527 2010.
59. Martin, J.; Watts, P. C.; Johnson, F., *J. Chem. Soc. D, Chem. Commun.* **1970**, 27-27.
60. Yu, X.; Guo, Y.; Li, K.; Yang, X.; Xu, L.; Guo, Y.; Hu, J., *J. Mol. Catal. A: Chem.* **2008**, *290*, 44-53.
61. Fegyverneki, D.; Orha, L.; Láng, G.; Horváth, I. T., *Tetrahedron* **2010**, *66*, 1078-1081.
62. Elliott, D. C.; Frye, J. G. US5883266 1999.
63. Dunlop, A. P. S. S. US2676186 (A), 1954.
64. (a) Bart, H. J.; Reidetschlager, J.; Schatka, K.; Lehmann, A., *Ind. Eng. Chem. Res.* **1994**, *33*, 21-25; (b) Stájer, G.; Szabó, Angela E.; Csámpai, A.; Sohár, P., *Eur. J. Org. Chem.* **2004**, *2004*, 1318-1322; (c) Guo, Y.; Li, K.; Clark, J. H., *Green Chem.* **2007**, *9*, 839-841; (d) Serrano-Ruiz, J. C.; Wang, D.; Dumesic, J. A., *Green Chem.* **2010**, *12*, 574-577.
65. Bader, A. R.; Kontowicz, A. D., *J. Am. Chem. Soc.* **1953**, *75*, 5416-5417.
66. (a) Buchta, E.; Burger, K., *Justus Liebigs Ann. Chem.* **1953**, *580*, 125-131; (b) Knolle, J.; Schäfer, H. J., *Angew. Chem.* **1975**, *87*, 777-777; (c) Toubiana, R. A. J., *c. R. Herbd. Seances Acad. Sci.* **1960**, *251*, 884.
67. Cohen, D.; Pattenden, G. E., *J. Chem. Soc. C, Org.* **1967**, *0*, 2314-2316.
68. (a) Bertho, A., *Chem. Ber.* **1957**, *90*, 29-43; (b) Bowie, J.; Hayes, R.; Mitkas, S.; Prager, R.; Raftery, M.; Skelton, B.; Stringer, M.; White, A., *Aust. J. Chem.* **1986**, *39*, 529-539.
69. Chimirri, A.; Grasso, S.; Monforte, P.; Romeo, G.; Zappalà, M., *Il Farmaco* **1988**, *27*.
70. Bockstahler, T. US2753358, 1958.
71. Fetizon, M. M., M.; Rens, J., *J. Chem. Res. (S)* **1982**, *9*.
72. Riley, H. L.; Morley, J. F.; Friend, N. A. C., *J. Chem. Soc.* **1932**, *0*, 1875-1883.
73. Gong, Y.; Lin, L.; Zhang, B., *Chin. J. Chem.* **2012**, *30*, 327-332.
74. Gong, Y.; Lin, L.; Shi, J.; Liu, S., *Molecules* **2010**, *15*, 7946-7960.
75. (a) Yan, Z.-p.; Lin, L.; Liu, S., *Energy Fuels* **2009**, *23*, 3853-3858; (b) Upare, P. P.; Lee, J.-M.; Hwang, D. W.; Halligudi, S. B.; Hwang, Y. K.; Chang, J.-S., *J. Ind. Eng. Chem.* **2011**, *17*, 287-292; (c) Wettstein, S. G.; Bond, J. Q.; Alonso, D. M.; Pham, H. N.; Datye, A. K.; Dumesic, J. A., *Appl. Cat. B: Environ.* **2012**, *117-118*, 321-329; (d) Hengne, A. M.; Rode, C. V., *Green Chem.* **2012**, *14*, 1064-1072; (e) Galletti, A. M. R.; Antonetti, C.; De Luise, V.; Martinelli, M.,

- Green Chem.* **2012**, *14*, 688-694; (f) Tukacs, J. M.; Kiraly, D.; Stradi, A.; Novodarszki, G.; Eke, Z.; Dibo, G.; Kegl, T.; Mika, L. T., *Green Chem.* **2012**, *14*, 2057-2065.
76. Dunlop, A. P. M., J. W. US2786852 (A), 1957.
77. Horvath, I. T.; Mehdi, H.; Fabos, V.; Boda, L.; Mika, L. T., *Green Chem.* **2008**, *10*, 238-242.
78. (a) Bond, J. Q.; Alonso, D. M.; Wang, D.; West, R. M.; Dumesic, J. A., *Science* **2010**, *327*, 1110-1114; (b) Palkovits, R., *Angew. Chem. Int. Ed.* **2010**, *49*, 4336-4338; (c) Lange, J.-P.; Price, R.; Ayoub, P. M.; Louis, J.; Petrus, L.; Clarke, L.; Gosselink, H., *Angew. Chem. Int. Ed.* **2010**, *49*, 4479-4483.
79. <http://www.sigmaaldrich.com>.
80. Morrison, R. T.; Boyd, R. N., *Organic Chemistry*. Allyn and Bacon: 1983.
81. Serrano-Ruiz, J. C.; West, R. M.; Dumesic, J. A., *Annu. Rev. Chem. Biomol. Eng.* **2010**, *1*, 79-100.
82. (a) Starodubtseva, E. V.; Turova, O. V.; Vinogradov, M. G.; Gorshkova, L. S.; Ferapontov, V. A., *Russ. Chem. Bull.* **2005**, *54*, 2374-2378; (b) Gürbüz, E. I.; Alonso, D. M.; Bond, J. Q.; Dumesic, J. A., *ChemSusChem* **2011**, *4*, 357-361.
83. Manzer, L. E. US6617464, 2003.
84. Manzer, L. E.; Hutchenson, W. W. US6946563 2005.
85. Bourne, R. A.; Stevens, J. G.; Ke, J.; Poliakoff, M., *Chem. Commun.* **2007**, *0*, 4632-4634.
86. Deng, L.; Li, J.; Lai, D.-M.; Fu, Y.; Guo, Q.-X., *Angew. Chem. Int. Ed.* **2009**, *48*, 6529-6532.
87. Dumesic, J. A.; Alonso, D. M.; Gürbüz, E. J.; Wettstein, S. G. US20120302767, 2012.

## 2 Upgrading of Biomass-Derived Levulinic Acid via Ru-Catalyzed Hydrogenation to $\gamma$ -Valerolactone in Aqueous-Organic-Ionic Liquids Multiphasic Systems

---

### 2.1 Introduction

*The catalytic hydrogenation of LA.* As was already described in the introduction, the catalytic hydrogenation of LA has been known for a long time.<sup>1</sup> Earlier papers reported that under batch conditions, the reaction occurred in a liquid phase over several types of catalysts. For example, in the presence of Raney nickel or platinum oxide catalysts, LA hydrogenation results in almost quantitative yield of GVL (87-94%) at low to moderate hydrogen pressures (3-48 bar) and temperatures up to 220 °C.<sup>1a,1b</sup> The use of other catalysts such as copper chromite, and harsher conditions (250 °C, 202 bar of H<sub>2</sub>), resulted in the conversion of LA in a complex mixture of products among which GVL and 1,4-pentanediol (PDO) were obtained in 11% and 44% yields, respectively.<sup>1b</sup>

More recently, in 2004, Manzer reported a screening of the LA hydrogenation in the solvent dioxane in the presence of a series of catalysts containing Group 8 metals supported on carbon with a metal loading of 5% (Ir, Rh, Pd, Ru, Pt, Re and Ni): in this study Ru was clearly the most selective metal, giving a conversion of 100% with GVL selectivity >97%. Relatively mild conditions (150 °C, 55 bar of H<sub>2</sub>) were used.<sup>2</sup> Different studies on the hydrogenation of LA were also performed in supercritical CO<sub>2</sub> in the presence of supported Pd, Ru, Re and Pt: also in these cases, the best results were achieved with Ru dispersed on both alumina and silica, though a high hydrogen pressure (200 bar) was necessary.<sup>3</sup> Even more recently, the liquid phase hydrogenation of LA was explored over 5% Ru/C in a batch reactor with methanol as a solvent: at 130 °C and 12 bar of H<sub>2</sub>, the conversion of LA was 92%, and the selectivity to GVL was 99%.<sup>4</sup> At the same time, Guo *et al.* developed a route to convert a 1:1 aqueous mixture of LA and formic acid into GVL in high yields using a RuCl<sub>3</sub>/PPh<sub>3</sub>/pyridine catalyst system: formic acid was used as hydrogen source and no external H<sub>2</sub> supply was needed.<sup>5</sup> Leitner *et al.* also reported the quantitative conversion of LA into GVL through the use of molecular ruthenium

phosphine catalysts,<sup>6</sup> while Horváth *et al.* proposed the LA hydrogenation by using a water-soluble ruthenium catalyst prepared from  $\text{Ru}(\text{acac})_3$  and  $\text{P}(\text{m-C}_6\text{H}_4\text{SO}_3\text{Na})_3$  in water.<sup>7</sup>

Overall, these recent systematic investigations have demonstrated that a selective conversion of LA to GVL was most efficiently performed on Ru-based catalysts, as either heterogeneous C-supported solids or homogeneous complexes. Procedures for the use of these catalytic systems as such, or in combination with co-catalysts or ligands, have been optimized to the point that quantitative yields of GVL were achieved also by hydrogenating LA in aqueous solutions. This was an essential finding for the upgrading of bio-derived LA, which is often available as aqueous feed.

Further improvement of the process sustainability has involved the optimization of the catalyst support and the selection of acid co-catalysts as well as the use of milder experimental conditions.<sup>8</sup> For example, in a system composed of Ru/C (5%) and an acid ion exchanged resin (Amberlyst A70) as a co-catalyst, a quantitative yield of GVL (99 mol%) was achieved after 3 hours at 70 °C under 0.5 MPa of  $\text{H}_2$ .

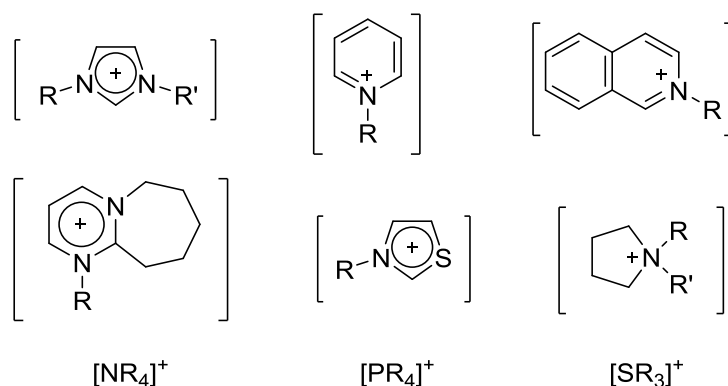
Notwithstanding the value of such methods, a general drawback lies in the practical recovery and recycle of the (precious) metal catalyst, particularly from water-based matrices where a loss of catalytic activity was observed. This largely unexplored issue was crucial in view of practical applications of any of these catalytic hydrogenation methods. In the work described in the thesis, multiphase systems based on ionic liquids (ILs) were investigated to devise efficient recycling operations.

### 2.1.1 Ionic Liquids (ILs)

Ionic liquids (ILs) represent today one of the most fascinating areas of research towards alternative eco-friendly synthetic methodologies. ILs have been known for a long time: the first observation of these compounds is historically dated 1914, when Paul Walden reported the physical properties of ethylammonium nitrate  $[\text{EtNH}_3][\text{NO}_3]$ .<sup>9</sup> However, syntheses and applications of ILs have shown an exponential growth only in the last 15 years.<sup>10</sup>

As their name suggests, ILs are materials composed entirely of cations and anions that, by definition, melt in the proximity of the ambient temperature. The former description of ionic liquids was restricted to salts that were liquid at room temperature; today, all salts which have a melting point  $\leq 100$  °C are defined as ionic liquids. In this category, a large number of these compounds are known and are commercially available either as organic salts or mixtures consisting of at least one organic component. Scheme 2.1 reports the most common cations used

to obtain ionic liquids. N,N-dialkylimidazolium, N-alkylpyridinium, alkylammonium and alkylphosphonium are the most conventional organic cations. The formation of these cations may be performed either via protonation with a free acid, or by quaternization of an amine, phosphine or sulfide, most commonly using a haloalkane or dialkylsulfates.



**Scheme 2.1.** Examples of cations commonly used for the formation of ionic liquids

The intriguing physical-chemical properties of ILs account for their large interests in green chemistry.<sup>11</sup> First of all, ILs have a negligible vapour pressure at near ambient conditions: many of them do not distill below the temperature of their thermal decomposition, and for a long time, it was believed that ionic liquids could not evaporate at all.<sup>12</sup> This feature allows minimization of the risks of atmospheric contamination and it remarkably reduces associated health and environmental concerns. Accordingly, ILs have been named “green solvents” and they can efficiently replace conventional volatile organic media in developing new synthetic methodologies, although toxicity may be an issue and must be assessed.

Secondly, ILs display properties such as the dissolution power, polarity and hydro/lipophilicity, which are rather peculiar and different to those of conventional organic liquids. These features depend on the nature of the cation and the anion that compose the ionic liquid: in a first very crude approximation, cations are responsible for the physical properties (density, viscosity, melting and boiling points, etc.), whereas anions control chemical properties and reactivity.<sup>13</sup> For this reason, ILs have been named “designer solvents”, as either the cation or the anion can be changed in order to tune their behaviour as solvents for chemical reactions. Ionic liquids can in principle, be designed to optimize the relative solubilities of reactants and products, the reactions kinetics, the liquid range of the solvent and even the intrinsic catalytic behavior of the media and the air-stability of the system.<sup>14</sup> A lot of studies have been conducted to determine correlations between the chemical structures of both cations and anions and the properties of ILs, in order to predict those properties already at the stage of ionic liquid design.

Even if general quantitative methods are still not available, some general trends have been observed. The melting point of ionic liquids is affected by both the asymmetry and the size of cations,<sup>15</sup> as well as by the occurrence of hydrogen bonds between cations and anions.<sup>16</sup> Also, the ability of ions to act as hydrogen-bond donors and/or acceptors influences the polarity of ionic liquids, while the increase of the chain length of alkyl substituents on both cations and anions leads to a greater lipophilicity of these materials. This scenario offers plausible explanations for the good solvent capabilities of ILs towards a wide range of both inorganic and organic compounds: unusual combinations of reagents/catalyst can be brought into the same phase by using ILs. In addition, thanks to the immiscibility of ILs with polar or nonpolar solvents, innovative two-phase or multiphasic systems can be originated to facilitate either the recovery of final reaction products or of the catalyst.

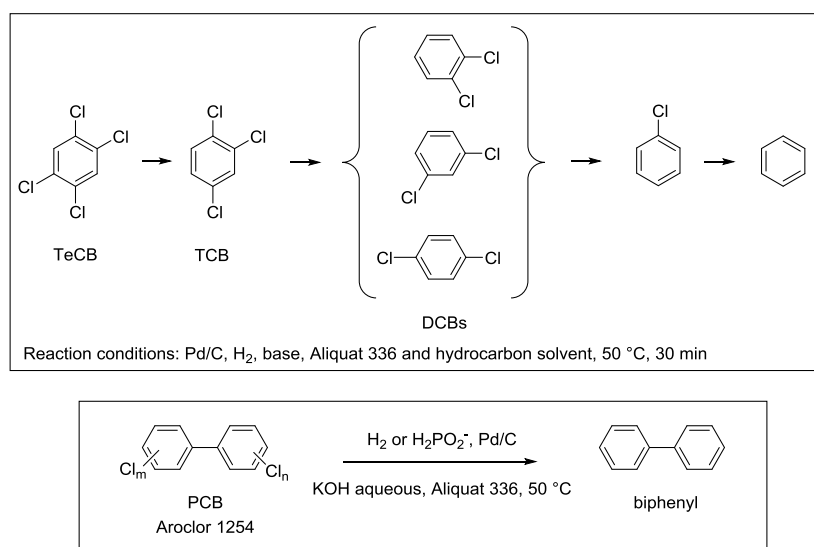
### 2.1.2 Multiphasic systems based on ILs

ILs can form multiphasic systems with organic compounds and have the ability to retain catalytic metal species.<sup>17</sup> Two main advantages of the multiphasic configuration are that the catalysts reside in a different liquid phase with respect to the reagents and products, making for easy recovery by phase separation, and that the metal catalyst is often stabilized by the IL. In addition, catalyst efficiency can sometimes be tuned by choosing an appropriate IL phase to segregate the catalyst itself.

A multiphasic system for a chemical reaction can be constituted by any combination of gaseous, liquid and solid phases. If a metal catalyst is present, it can be homogeneous or heterogeneous, thereby adding further phases to the system. Multiphasic systems described in this chapter are liquid tri-phasic ones constituted by mutually immiscible components including an alkane, water, and an ionic liquid, more often an onium salt. To this ensemble, a metal catalyst is also added.

A number of such multiphasic systems have been reported to accomplish very different reactions. Remarkable examples of such processes were developed also by our group over the past 20 years: they include hydrodehalogenations, hydrogenations, hydroformylations, and C-C bond formation reactions.<sup>17d, 18</sup>

Hydrodehalogenation reactions were initially investigated to implement an efficient and mild catalytic methodology for the chemical degradation of organic micropollutants such as poly-chloro and -bromo biphenyls (PCB and PBB, respectively), and dioxins (Scheme 2.2).<sup>19</sup>

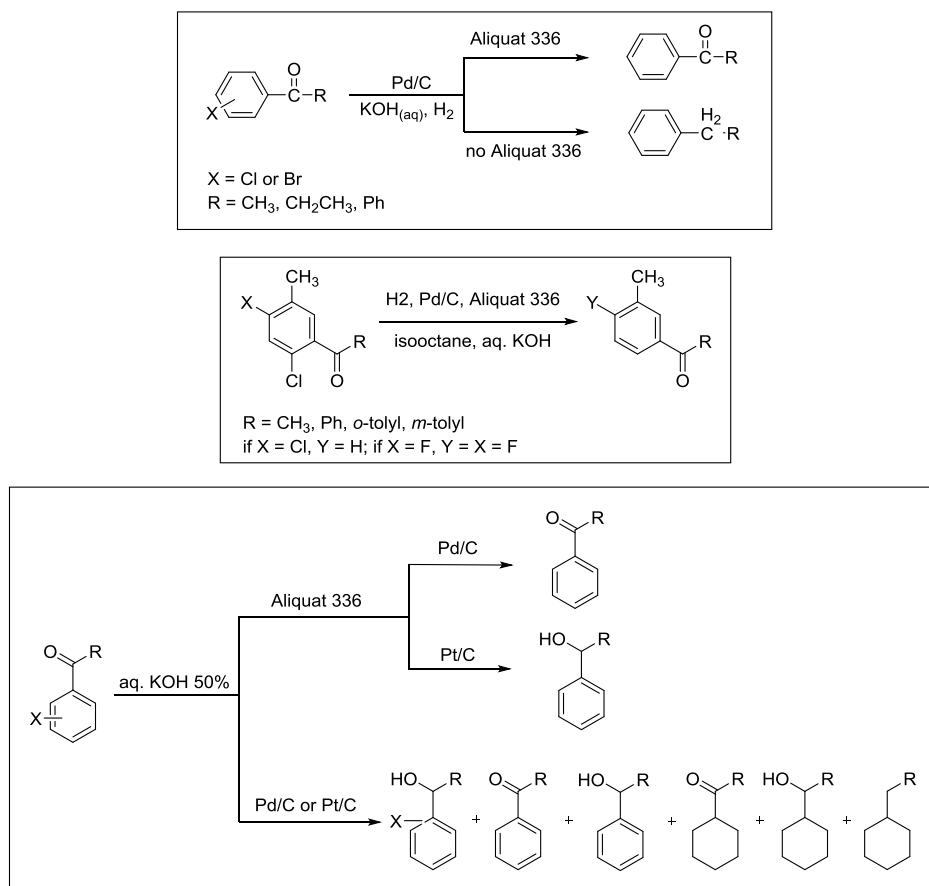


**Scheme 2.2** Multiphasic hydrodehalogenations of some model haloaromatics

In the presence of gaseous hydrogen at ambient pressure, the use of multiphasic systems composed of a hydrocarbon, an alkaline aq. phase, an ionic liquid (an onium salt), and a hydrogenation catalyst (Pd/C, Pt/C, and Raney-Ni) allowed not only substantially quantitative reactions, but also the separation of organic products (biphenyls and dibenzodioxanes), which were solubilised in the hydrocarbon solvent, from halides which were confined as alkaline metal salts in the aq. solution. Moreover, the metal catalyst was segregated in the ionic liquid (catalyst-phylic) phase.

Further investigations of similar multiphasic arrangements proved the critical role of the ionic liquid phase: the nature of the onium salt could have a direct impact on the performance of the metal catalyst. For example, highly chemoselective multiphasic transformations could be achieved for organic substrates bearing two or more functional groups able to undergo hydrodehalogenation, hydrogenation and hydroformylation reactions. Scheme 2.3 summarizes some of the most salient results:<sup>20</sup>





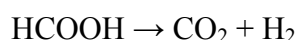
**Scheme 2.3.** Examples of chemoselective transformations of organic substrates achieved by using a multiphasic system

Both the reaction rate and the product distribution could be improved and tuned by the use of appropriate onium salts. In the majority of cases, Aliquat 336<sup>®</sup> (tricapryl-methylammonium chloride,  $(\text{C}_8\text{H}_{17})_3\text{N}^+\text{CH}_3\text{Cl}^-$ : A336) was the IL of choice to produce the catalyst-phylic phase: this salt in fact, was a well-known phase transfer agent, liquid at room temperature, cheap and commercially available, and last but not least, it had excellent properties to induce the formation of immiscible liquid phase systems with alkanes and water. Nonetheless, many other onium salts were devised and considered for their applications in multiphasic reaction systems.<sup>17d, 18c</sup> These investigations allowed our group to consolidate an expertise in the engineering of such arrangements for cleaner catalytic procedures. Under such (multiphasic) conditions, experiments have shown that the occurrence of phase separation and catalyst segregation (often made possible by common ionic liquids) provided unique environments to control the reaction outcome and also to allow a simple and efficient recovery of (precious) metal catalysts. Both these aspects inspired the first part of the present thesis work which was dedicated to the selective hydrogenation of levulinic acid in the presence of gaseous hydrogen and/or other

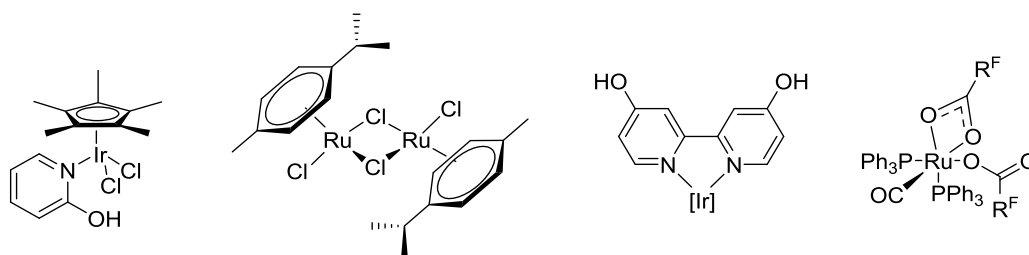
hydrogen donors such as formic acid (FA). Due to this specific interest, the next paragraph will briefly review some of the common and recent uses of FA as a hydrogenation reagent.

### 2.1.3 Formic acid as hydrogen source

Formic acid is the simplest carboxylic acids available on a commercial scale from the hydrolysis of methyl formate or the reduction of  $\text{CO}_2$  with  $\text{H}_2$ .<sup>21</sup> FA is a non-toxic liquid<sup>22</sup> that, along with its conjugated base, the formate anion, have been widely used to promote transfer hydrogenation reactions.<sup>23</sup> In fact, FA may decompose to produce  $\text{H}_2$  and  $\text{CO}_2$  according to a simple equation which is the exact reverse of the above mentioned  $\text{CO}_2$  hydrogenation process:<sup>24</sup>



Although this reaction may be complicated by the formation of CO and water as side-products [ $\text{HCOOH} \rightarrow \text{CO} + \text{H}_2\text{O}$ ], recent investigations reported that several transition-metal complexes could act as catalysts to improve the selectivity for  $\text{H}_2$ .<sup>25a-d, 25e, Johnson, 2010 #2223</sup> Scheme 2.4 illustrates some of these catalytic systems.



**Scheme 2.4.** Examples of transition-metal complexes commonly used for the decomposition of formic acid to  $\text{H}_2$  and  $\text{CO}_2$

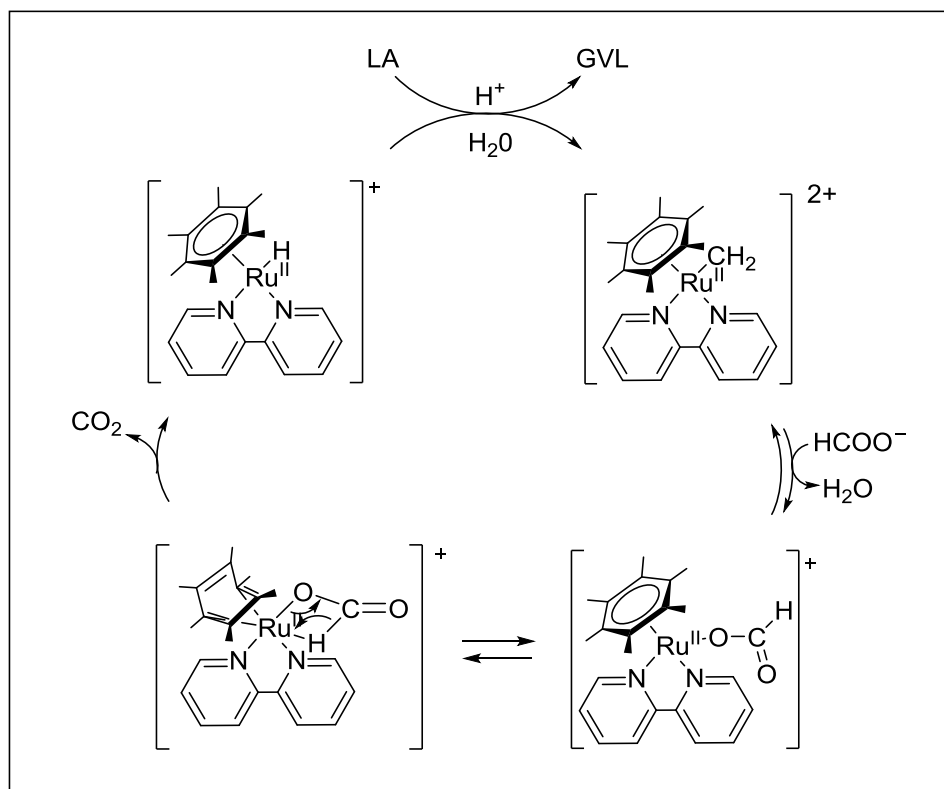
An interesting reaction mechanism was proposed for the decomposition of FA in aqueous solutions catalyzed by both Ru-aquo complexes such as  $[\text{Ru}(\text{H}_2\text{O})_6]^{2+}$ ,  $[\text{Ru}(\text{H}_2\text{O})_6]^{3+}$ , and salts as  $\text{RuCl}_3$  in the presence of *m*-trisulfonated triphenylphosphine. Accordingly, the metal complex was initially activated by the substitution of a water ligand with a formate moiety. This process was favored by the presence of a base in solution. Then, the generation of a monohydride complex took place, which allowed the catalytic cycle to close with the generation of  $\text{H}_2$ . A formatodihydrogen intermediate was likely formed in this step.<sup>26</sup> The overall reaction occurred under mild conditions and over a large range of pressure.

The same Ru-aquo complexes and salts were also reported as catalysts for the decomposition of  $\text{HCOOH}$  in aq. mixtures of  $\text{HCOOH}$  and  $\text{HCOONa}$  (9:1).<sup>25c</sup>

Studies by Beller and co-workers demonstrated that the catalytic decomposition of formic acid could take advantage of the presence of amines (*i.e.* triethylamine, *N,N*-dimethylhexylamine,

*N,N*-dimethylaminoethanol). Under such conditions, the reaction was observed even at room temperature over Ru-based catalysts including  $\{\text{RuCl}_2(\text{p-cymene})\}_2$  and  $\{\text{RuCl}_2(\text{Benzene})\}_2/(\text{PPh}_3)_3$ ; though, a good catalytic activity was achieved only on condition that a high ratio of organic amine to formic acid was used (typically, a 2:5 molar ratio).<sup>25a</sup> In general, homogeneous transition-metal catalysts allowed a higher selectivity in the decomposition of FA,<sup>26-27</sup> heterogeneous catalysts such as Ru/C could however be used.

For the specific case of the transfer hydrogenation of LA using formic acid or its derivatives as hydrogen sources, several examples have been reported with both homogeneous and heterogeneous catalysts. Among the first methods, the gas phase hydrogenation of LA or ethyllevulinate to GVL was claimed by Haanet *al.* that used formic acid as a hydrogen donor with a variety of heterogeneous catalysts (*e.g.* Ni/Pt on silica, Re/Pt on silica, Ni)<sup>28</sup>. The reactions was typically performed at 200-350 °C and pressures between 1-10 bar. A subsequent, more interesting procedure was based on a homogeneous Ru catalyst  $[(\eta^6\text{-C}_6\text{Me}_6)\text{Ru}(\text{bpy})(\text{H}_2\text{O})][\text{SO}_4]$  able to promote the transfer hydrogenation of LA with  $\text{HCOONa}$  (37 molar equivs) in liquid water solutions. Both GVL and 1,4-pentanediol were obtained in 25% yield. Scheme 2.5 depicts a plausible mechanism for such a reaction.<sup>7a,29</sup>



**Scheme 2.5.** Mechanism for the transfer hydrogenation of LA using  $[(\eta^6\text{-C}_6\text{Me}_6)\text{Ru}(\text{bpy})(\text{H}_2\text{O})][\text{SO}_4]$  as a catalyst precursor in water

The potential of this method was immediately obvious to process crude LA available in aq. mixtures with formic acid, that came directly from the hydrolytic processing of biomass carbohydrate feedstocks.<sup>2,7,30</sup>

In an analogous context, other examples were developed: Heeres *et al.* demonstrated that a one-pot catalytic synthesis of GVL could be achieved from the treatments of aq. streams of C6-sugars by the combined use of an acid catalyst such as trifluoroacetic acid, a hydrogenation catalyst (Ru/C), and formic acid as the hydrogen donor.<sup>31</sup> One last method reported the selective conversion of aq. LA to GVL through Ru-based homogeneous catalysts (*i.e.*  $\text{RuCl}_3 \cdot 3\text{H}_2\text{O}$ ) coupled to bases and phosphine ligands.<sup>5, 32</sup> Best results were achieved using pyridine, which gave stable adducts with formic acid, and  $\text{PPh}_3$ . The latter, even though it was not a water-soluble ligand, improved the stability of the catalytic active specie.<sup>25a,26</sup>

Whatever the method, the use of formic acid as a  $\text{H}_2$  donor for the reduction of aqueous solutions of LA certainly represents a breakthrough in terms of process intensification and cost minimization.<sup>6,33</sup>

#### 2.1.4 Aim and brief summary of the research

The aim of this study has been the design of multiphasic systems whereby, through the choice of readily available ILs belonging to the class of onium salts as, an efficient hydrogenation/dehydration of LA to  $\gamma$ -valerolactone can be performed in aqueous solutions in the presence of either a heterogeneous supported Ru catalyst (Ru/C) or a homogeneous Ru precursor ( $\text{RuCl}_3$ ). Under such conditions, the major advantage with respect to known methods, has been the perfect confinement of the metal catalyst in the IL phase that allows not only an easy isolation of the product in quantitative yields, but also an *in situ* re-use of the catalysts. In the development of the multiphasic system, molecular hydrogen has been successfully used, while any attempts to exploit formic acid as an alternative hydrogen source has proven of no practical interest.

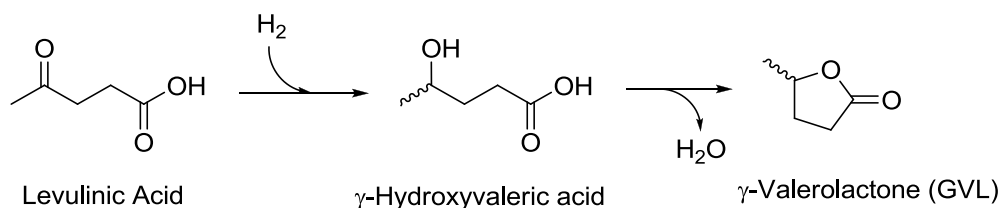


**Figure 2.1.** Hydrogenation/dehydration of LA to GVL

## 2.2 Results

### 2.2.1 Reaction conditions

The initial screening methodology for the hydrogenation of LA to  $\gamma$ -valerolactone was developed based on existing literature. In particular, the work described by Manzer *et al.* was considered for the choice of the catalyst and solvent, which were Ru/C (5%) and dioxane, respectively (Figure 1.2).<sup>2</sup>

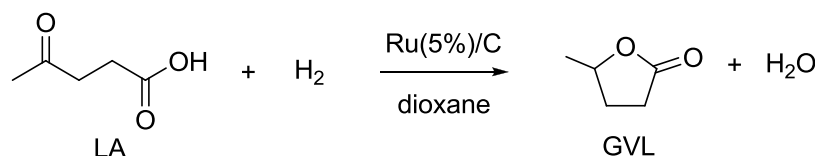


Figure 2.2. LA hydrogenation in the presence of H<sub>2</sub> in dioxane

The hydrogenation of LA was then performed in an autoclave charged with mixture of LA (915 mg, 7.88 mmol), Ru/C (0.15 mol%; 0.0124 mmol of Ru), and dioxane (4.4 mL). (further details are in the experimental section). In order to establish base-line for the reaction, the effects of temperature, time, and H<sub>2</sub> pressure were investigated. Tests were performed under three sets of conditions:

- at 80-150 °C, over a H<sub>2</sub> pressure of 35 bar and for 16 hours;
- at 100 °C, over a H<sub>2</sub> pressure of 35 bar, and for 4-16 hours;
- at 100 °C, over a H<sub>2</sub> pressure of 20-60 bar, and for 4 hours.

At the end of each test, the progress of the reaction was evaluated by GC/MS. Figure 2.3 summarizes the results.

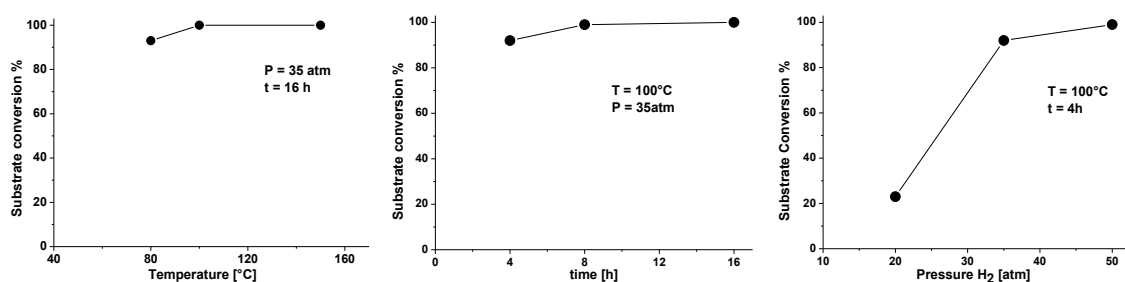


Figure 2.3. Conversion of LA to GVL as a function of the temperature (**left**), reaction time (**middle**) and pressure (**right**) in dioxane with 5% Ru/C [LA:915 g (7.88 mmol); Ru/C: 0.15 mol% (0.0124 mmol of Ru), dioxane = 4.4 mL]

Except for when the reaction was performed at 20 bar of H<sub>2</sub>, the conversion of LA was always satisfactory ( $\geq 90\%$ ). In analogy to literature results,<sup>34</sup> up to two products,  $\gamma$ -hydroxyvaleric acid and  $\gamma$ -valerolactone, were detected. Notably,  $\gamma$ -hydroxyvaleric acid

underwent a spontaneous dehydrative cyclization to GVL, simply on standing at room temperature (Figure 2.1).<sup>35</sup>

This analysis allowed to conclude that the hydrogenation of LA to GVL could be conveniently performed at 100 °C and 35 atm of H<sub>2</sub> (the H<sub>2</sub> pressure was chosen also in agreement to previous literature results<sup>2, 36</sup>). Under such conditions, the conversion of LA was 97% in 4 hours. This result was used for the subsequent phase of the work, the objective of which was to extend and test the same reaction in a multiphasic system.

## 2.2.2 Setup of the multiphasic system

A multiphasic system analogous to those described in paragraph 2.1.1 was considered for the hydrogenation of LA. The first issue with such an arrangement was the choice of the organic solvent. Dioxane, which was used for the preliminary screening of the reaction, was obviously not suitable to build-up a multiphasic system since it (dioxane) was fully miscible with water. Likewise, LA was water-soluble as well. Only organic solvents immiscible with water and with the ability to dissolve the substrate LA and the product GVL were suitable.

Six different solvents were selected based on their availability as well as favourable cost and toxicological profiles (Table 2.1). Apolar isooctane and cyclohexane, which are immiscible with water, were not able, however, to dissolve the substrate or the product. At the other extreme, polar ethyl lactate and acetonitrile both dissolved the reactant and the product, but were also soluble with water, preventing formation of a triphasic system. Toluene satisfied both requirements, but was ruled out because it was easily hydrogenated to methylcyclohexane. Ethyl acetate (EA) was finally selected.

**Table 2.1**  
Solubility properties of solvents tested for the triphasic system

Solvent	LA solubility	GVL solubility	Solubility in water at 20°C
Iso-octane	No	No	Immiscible
Cyclohexane	No	No	Immiscible
Toluene	Yes	Yes	0.52 g/L
Ethyl acetate	Yes	Yes	0.83 g/L
Ethyl lactate	Yes	Yes	Miscible
Acetonitrile	Yes	Yes	Miscible
water	Yes	Yes	Miscible

Methyltrioctyl ammonium chloride ([N<sub>8,8,8,1</sub>][Cl], **IL1**) was initially used as the third component of the multiphasic system. This choice was based on previous works of our group,<sup>18a, 18c</sup> and motivated by the need of a room-temperature ionic liquid bearing a sufficiently lipophilic cation.<sup>37</sup>

The investigation of the multiphasic hydrogenation of LA was then started. Preliminary experiments were aimed at exploring the effect of variable amounts of the ionic liquid. A mixture of commercial 5% Ru/C (0.15 mol %, 0.0124 mmol of Ru), EA (4.4 mL), water (4.4 mL), LA (810  $\mu$ L), was set to react in an autoclave at 100 °C, under 35 atm of H<sub>2</sub>, in the presence of [N<sub>8,8,8,1</sub>][Cl] (143-884 mg). An additional test was also performed in the absence of the IL. In both cases, reacting mixtures were magnetically stirred throughout the experiments (further details are in the experimental section). All reactions were stopped after 4 h.

GC/MS and <sup>1</sup>H NMR analyses of the reaction mixture showed that the product, GVL, was present in both the organic and aqueous phases. This behaviour was in analogy to a literature result reporting that GVL was able to partition between EA and water in approximately a 3 to 1 ratio.<sup>33a</sup> In order to measure the conversion and the selectivity, the aqueous phase recovered at the end of each experiment was carefully extracted with ethyl acetate (3 x 5 mL) until GVL was completely removed. Then, organic extracts were combined to the EA phase used for the reaction, and the resulting mixture was analysed by <sup>1</sup>H NMR.

The results are summarized in Table 2.2. In the absence of IL (run 1), the reaction was extremely efficient, while increasing amounts of [N<sub>8,8,8,1</sub>][Cl] seemed to depress the conversion and yield (entries 2 and 3). In all cases, however, the partitioning of GVL between aqueous and organic phases made the quantitative recovery of the product hardly practicable, unless an extraction and a considerable amount of additional EA were used. This was a crucial drawback that prompted us to abandon the system EA/water/[N<sub>8,8,8,1</sub>][Cl].

**Table 2.2**  
Conversion of LA to GVL in an EA/water/[N<sub>8,8,8,1</sub>][Cl] triphasic system.<sup>a</sup>

[N <sub>8,8,8,1</sub> ][Cl]:Cat [wt:wt]	LA Conv.	GVL Yield
-	100%	91% <sup>b</sup>
5.7	56%	55% <sup>b</sup>
35.4	11%	11% <sup>b</sup>

<sup>a</sup> Conditions: Ru/C (0.15 mol%, 0.0124 mmol of Ru), 100 °C, 35 atm of H<sub>2</sub>, 4 h. GVL partitioned between EA and H<sub>2</sub>O in a 3:1 molar ratio, respectively

A different multiphasic arrangement was then conceived based on the observation that both the reagent and the product (LA and GVL, respectively) were water soluble, while, on the contrary, they were not at all dissolved by light hydrocarbons. The new system for the hydrogenation of LA was composed of an aqueous solution of levulinic acid (1.8 M; 4.4 mL), isooctane (*i*-oct, 4.4 mL) as the hydrocarbon component, 5% Ru/C (25 mg, 0.0124 mmol of Ru), and different amounts of [N<sub>8,8,8,1</sub>][Cl] (33–315 mg) as the ionic liquid phase. Initial tests showed

promising behaviour. Once the mixture was placed in a test tube, vigorously stirred for 1 h at room temperature, and allowed to stand, a neat phase separation was observed: regardless of the amount of  $[N_{8,8,8,1}][Cl]$  used, the IL always appeared as a liquid phase in between the top organic and the bottom aqueous phases. Moreover, the heterogeneous Ru/C catalyst was perfectly segregated in the middle IL phase, while LA remained totally dissolved in water. Figure 2.4 left offers a picture of such a system. By contrast, if no IL was present, Ru/C was dispersed among the phases (Figure 2.4 right).

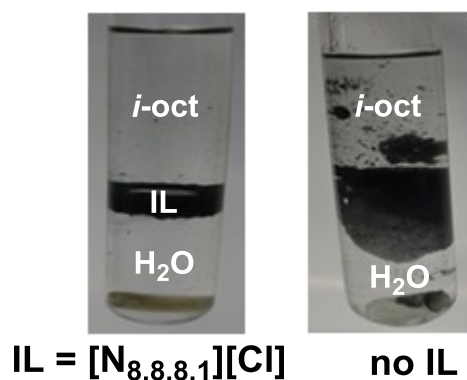


**Figure 2.4.** Pictures of aqueous solutions of levulinic acid (1.8 M; 4.4 mL), *iso*-octane (4.4mL), 5% Ru/C (25 mg, 0.0124 mmol of Ru): without IL (**right**), and with  $[N_{8,8,8,1}][Cl]$  (138 mg, 0.34 mmol) (**left**)

It should be noted that, while *i*-octane had no an apparent role as a solvent for the chemical species, it was necessary, however, to obtain good phase separation and catalyst segregation. This new setup was named an “inverse” multiphasic system because, contrary to all multiphasic arrangements previously reported<sup>18a, 18c</sup>, the organic reactant LA and product GVL, both highly polar compounds, remained dissolved in the aqueous solution and not in the organic phase.

### 2.2.3 Inverse Multiphasic hydrogenations of LA in the presence of Ru/C

#### 2.2.3.1 The amount of $[N_{8,8,8,1}][Cl]$

With the aim of establishing the optimal composition of the multiphasic system, the effect of varying of the IL phase was initially investigated. Accordingly, the mixture described above (aq. levulinic acid 1.8 M, 4.4 mL; isooctane, 4.4 mL; and 5% Ru/C, 25 mg, 0.0124 mmol of Ru), was charged in autoclave in the presence of increasing quantities of  $[N_{8,8,8,1}][Cl]$  (from 35 to 315 mg; 0.087–0.78 mmol). A series of hydrogenation reactions were then run at 100 °C, 35 atm of  $H_2$ , and for 4 h. Conversion and selectivity were measured by  $^1H$  NMR (further details are available in the experimental section). The results are summarized in Figure 2.5.



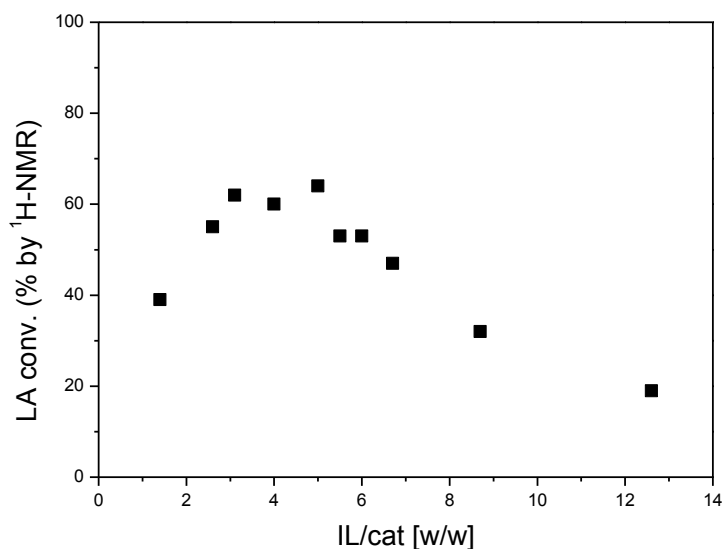


**Figure 2.5** Conversion of LA to GVL as a function of the amount of IL in the *i*-octane-water-[N<sub>8,8,8,1</sub>][Cl] triphasic system with 5% Ru/C after 4 h (Conditions: 100°C, p[H<sub>2</sub>] = 35 bar, Ru 0.15 mol% (0.0124 mmol of Ru), water = *i*-octane = 4.4 mL, [N<sub>8,8,8,1</sub>][Cl] = 35 to 316 mg)

In the presence of the IL, a third liquid phase between the aqueous and hydrocarbon solvents was observed both at the start and at the end of the hydrogenation tests. In this third phase, the Ru/C catalyst was always perfectly confined. The profile of Figure 2.5 indicates that an optimal amount of IL could be found to favour the LA conversion: in particular, this increased up to 60–65% when the IL/Cat (w/w) ratio was in the interval between 3 and 6. In all cases, the reaction proceeded with the exclusive formation of GVL.

### 2.2.3.2 Best IL

Although the [N<sub>8,8,8,1</sub>][Cl] did form three separate phases, it was discovered that this salt was partially soluble in the aqueous phase as well. NMR analyses showed that some 2-3% of [N<sub>8,8,8,1</sub>][Cl] (by weight) was lost in water after each hydrogenation test. Therefore a less water-soluble IL was sought by modifying the anion. To this end, more lipophilic ILs such as [N<sub>8,8,8,1</sub>][NTf<sub>2</sub>] (**IL2**) and [P<sub>8,8,8,1</sub>][NTf<sub>2</sub>] (**IL3**) were prepared. Also, two more salts of intermediate lipophilicity, [N<sub>8,8,8,1</sub>][CF<sub>3</sub>COO] (**IL4**) and [P<sub>8,8,8,1</sub>][NO<sub>3</sub>] (**IL5**) were considered.

Salts **IL2-5** were synthesized by adjusting a procedure recently reported by our group.<sup>37</sup> The synthesis proceeded through a two step sequence: i) at first, dimethyl carbonate (DMC, 30.0 mL, 32.1 g, 356 mmol) was used as green methylating agent of both trioctylamine (24.5 mL, 19.8 g, 0.056 mol) and trioctylphosphine (25.0 mL, 20.8 g, 0.056 mol). The reaction was performed in an autoclave at 140 °C, in the presence of MeOH (30 mL) as a cosolvent. The corresponding ammonium and phosphonium methylcarbonate salts (**IL6**: [N<sub>8,8,8,1</sub>][MeOCO<sub>2</sub>], and

**IL7**: [ $P_{8,8,8,1}$ ][MeOCO<sub>2</sub>], respectively) were obtained in quantitative yields; ii) in the second step, at 50 °C, these onium salts were set to react with either Brønsted acids (H-A, A=CF<sub>3</sub>CO<sub>2</sub>, NO<sub>3</sub>; the molar ratio **IL**:HA was 1) or lithium salt of bis(trifluoromethanesulfonyl) amine (Li<sup>+</sup>[NTf<sub>2</sub>]<sup>-</sup>). An ion exchange reaction occurred, replacing the methylcarbonate anion (MeOCO<sub>2</sub><sup>-</sup>) with both A<sup>-</sup> and NTf<sub>2</sub><sup>-</sup> anions. This allowed the isolation of compounds **IL4**, **IL5** ([ $N_{8,8,8,1}$ ][CF<sub>3</sub>COO] and [ $P_{8,8,8,1}$ ][NO<sub>3</sub>]), **IL2** and **IL3**( $N_{8,8,8,1}$ [NTf<sub>2</sub>] and  $P_{8,8,8,1}$ [NTf<sub>2</sub>]), respectively. (Further details on the preparation/characterization of such compounds are available in both the discussion and the experimental sections).

In the presence of **IL2-IL5**, the hydrogenation of LA was then performed under the conditions of Figure 2.5 (IL/Cat =10, wt/wt). Table 2.3 reports the results which include, for comparison, also those obtained with [ $N_{8,8,8,1}$ ][Cl] (**IL1**).

**Table 2.3**  
Conversion of LA to GVL in different *i*-octane/water/IL triphasic systems<sup>a</sup>

	<b>IL</b> [ <b>IL</b> :Cat=10, wt/wt]	<b>LA Conversion</b> (%, <sup>1</sup> H NMR)	<b>Solubility of IL in H<sub>2</sub>O</b> (%, wt)
<b>1</b>	[ $N_{8,8,8,1}$ ][Cl], <b>IL1</b>	32	2-3
<b>2</b>	[ $N_{8,8,8,1}$ ][NTf <sub>2</sub> ], <b>IL2</b>	100	not measurable
<b>3</b>	[ $P_{8,8,8,1}$ ][NTf <sub>2</sub> ], <b>IL3</b>	100	not measurable
<b>4</b>	[ $N_{8,8,8,1}$ ][TFA], <b>IL4</b>	100	41
<b>5</b>	[ $P_{8,8,8,1}$ ][NO <sub>3</sub> ], <b>IL5</b>	100	17

<sup>a</sup> Conditions: Ru/C (0.15 mol%, 0.0124 mmol of Ru), 100 °C, 35 atm of H<sub>2</sub>, 4h  
250 mg of each IL were used: **IL2** (0.38 mmol); **IL3** (0.37 mmol); **IL4** (0.50 mmol); **IL5** (0.56 mmol)

Unlike the reaction with [ $N_{8,8,8,1}$ ][Cl] that reached 32% conversion, all the hydrogenations with salts **IL2-IL5** achieved complete conversion in 4 h. The less lipophilic **IL4** and **IL5**, however, were significantly soluble in water: <sup>1</sup>H NMR analyses allowed to estimate that the weight loss in water was of 41 and 17%, for **IL4** and **IL5**, respectively (entries 4 and 5). Therefore, such compounds were abandoned. The triflamide ammonium and phosphonium **IL2** and **IL3** salts instead prompted 100% conversion after 4 h without partitioning into the aqueous phase and with perfect segregation of Ru/C (entries 2 and 3).

At the end of the reactions performed in the presence of **IL2** and **IL3** (entries 2 and 3), the final aqueous solutions of GVL were carefully extracted with ethyl acetate, dried over Na<sub>2</sub>SO<sub>4</sub>, and filtered. After solvent removal under vacuum, crude GVL was isolated in quantitative yields (780 mg, 99%). This confirmed the accuracy of NMR analyses for the evaluation of conversion and selectivity as well as the overall reaction mass balance.

Under the conditions of Figure 1.5, additional LA hydrogenation experiments were performed with both **IL2** and **IL3**, by varying the IL/Cat ratio (wt/wt) between 0 and 27. In all cases, the tests proved that the conversion remained quantitative after 4 h (Figure 2.6). With

respect to  $[N_{8,8,8,1}][Cl]$ , these results highlighted a remarkable difference and advantage of triflamide salts **IL2** and **IL3**: the amount of such salts did not substantially affect the reaction outcome. **IL2** and **IL3** were, therefore, the most suitable ILs to set up an “inverse” multiphase system. Because of the higher thermal stability of phosphonium versus ammonium salts,<sup>38</sup>  $[P_{8,8,8,1}][NTf_2]$  (**IL3**) was chosen to proceed with the investigation.

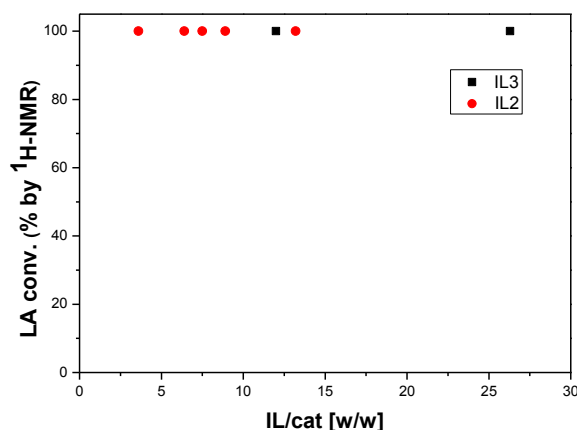


**Figure 2.6.** Conversion of LA to GVL with **IL2**(●), with **IL3**(■) and 5% Ru/C as a function of the amount of IL after 4 h. Conditions: 100 °C,  $p[H_2] = 35$  bar, Ru 0.15 mol %, water = *i*-oct = 4.4 mL, **IL2** = 89-609 mg = 0.14-0.93 mmol; **IL3** = 300-658 mg = 0.45-0.99 mmol

In the presence of **IL3**, further tests were performed to investigate the effect of the reaction time and of the IL/Cat ratio to achieve a quantitative Ru/C confinement. Conditions for the temperature and volumes/concentrations of aqueous/*i*-octane phases were those reported in Table 2.3. Three sets of reactions were performed at 0.5, 1, and 2 h, respectively. Within each set, the **IL3**/Cat molar ratio ranged between 6 and 25. The results are shown in Figure 2.7.

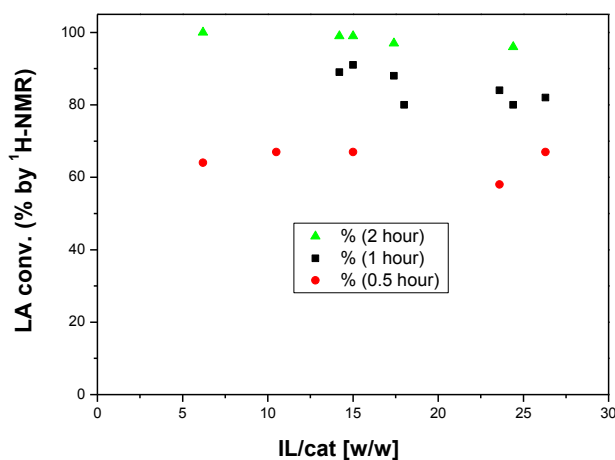


**Figure 2.7** Conversion of LA to GVL with **IL3** and 5% Ru/C as a function of the amount of IL after 0.5, 1, and 2 h (red, black, and green dots, respectively). Conditions: 100 °C,  $p[H_2] = 35$  bar, Ru 0.15 mol %, water = *i*-oct = 4.4 mL,  $[P_{8,8,8,1}][NTf_2] = 355-657$  mg = 0.53-0.99 mmol

The screening demonstrated that the **IL3** amount had little (if any) effect on the LA conversion: this increased from ~65% up to a quantitative value by increasing the reaction time from 0.5 to 2 h, but it (conversion) remained rather constant in each set of experiments (~65%, ~85%, and >97% at 0.5, 1, and 2 h, respectively). However, the use of a **IL3**/Cat ratio below 6 was not practicable, because only partial recovery of Ru/C catalyst in the IL phase was possible.

Overall, an **IL3**/Cat ratio around 15 (~360 mg of IL3) corresponded to a good compromise between a satisfactory LA conversion and a high reaction rate (92% after 1 h) with the full isolation of Ru/C in the IL phase. The last condition (Ru/C confinement) was mandatory in order to achieve efficient recycle of the catalyst.

### 2.2.3.3 Comparison with and without IL

Once the triphasic system was optimized, the next objective was to compare its efficiency to the biphasic aqueous–isooctane system without IL. Accordingly, two sets of hydrogenation/dehydration reactions of LA were conducted. In the first reaction, conditions were those used in Figure 2.5 and Table 2.3, except for the fact that no IL was present ( $\Delta$ , blank experiments): in particular, a multiphasic mixture of 5% Ru/C (25 mg; Ru = 0.0124 mmol), a 1.8 M solution of LA in water (4.4 mL) and *i*-octane (4.4 mL) was set to react in an autoclave under 35 atm of H<sub>2</sub>. In the second set, with the same LA/Cat ratio and with the same volumes/concentrations of aqueous/*i*-octane ratios, **IL3** was added in a **IL3**/Cat ratio of 23 (576 mg of **IL3**). In both sets of reactions, the temperature was varied from 30 to 100 °C, and mixtures were analyzed by <sup>1</sup>H NMR after 0.5 h. The results are summarized in Figure 2.8.

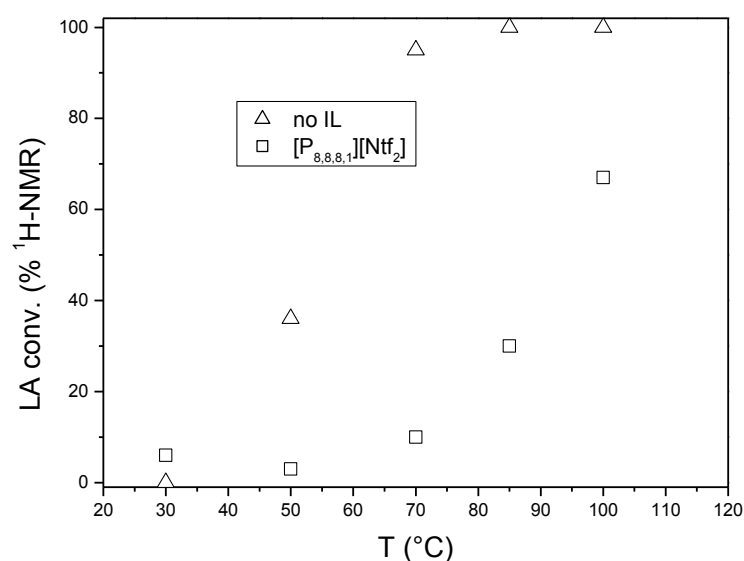


**Figure 2.8.** Conversion of LA to GVL in the multiphasic system with 5% Ru/C as a function of temperature after 30 min: ( $\Delta$ ) without the IL third phase; ( $\square$ ) with a third phase made by [P<sub>8,8,8,1</sub>][NTf<sub>2</sub>]. (Conditions: p[H<sub>2</sub>] = 35 bar, Ru 0.15 mol%, water = *i*-oct = 8.8 mL, [P<sub>8,8,8,1</sub>][NTf<sub>2</sub>] = 576 mg, 0.87 mmol)

At temperatures between 50 and 90 °C, the reaction was faster in the biphasic system without the IL ( $\Delta$ , blank tests), but Ru/C was always dispersed throughout the final mixture. The situation was analogue to that described in Figure 2.4 right. This meant that any recover/recycle of the metal catalyst by phase separation was out of the question. The kinetics in the triphasic system became competitive at 100 °C, where the conversion of LA went up to 67%; under such conditions, Ru/C remained confined in the IL, with clean phase separation. In both sets of experiments, the temperature had no effect on the reaction selectivity, which was always 100% toward the formation of GVL.

#### 2.2.3.4 Recycle and metal leaching

The perfect segregation of Ru/C in the **IL3**-phase was exploited to set up a very simple protocol for the re-use of the catalyst: under the conditions of Figure 2.7 (**IL3**/cat = 24, 1 h), once the first reaction was complete, the lower aqueous phase containing the product GVL was removed and a fresh aqueous layer containing LA was added. The recycling procedure was repeated eight times. The results are illustrated in Figure 2.9.

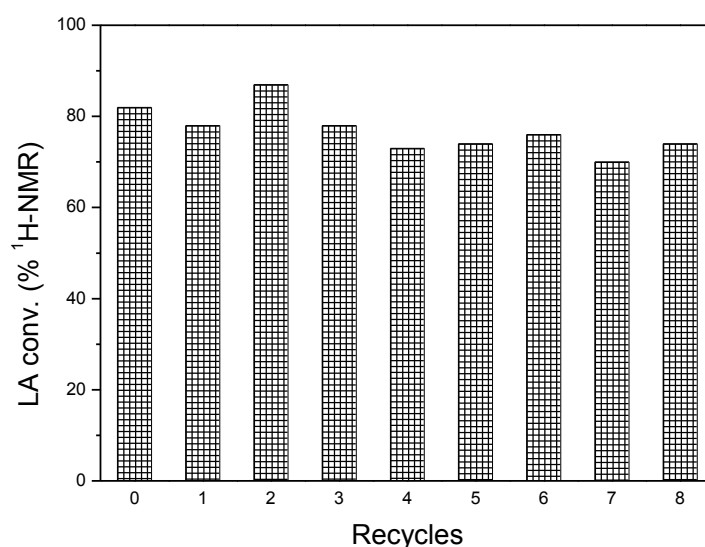


**Figure 2.9.** Conversion of LA to GVL: recycling of the Ru/C catalyst system. (Conditions: 1 h, 100 °C,  $p[\text{H}_2] = 35$  bar, Ru 0.15 mol% (Ru 0.0124 mmol), water = *i*-octane = 4.4 mL,  $[\text{P}_{8,8,8,1}][\text{NTf}_2] = 610$  mg, 0.92 mmol)

Conversion was substantially constant, in the range of 75–80%, over 8 subsequent runs. Selectivity was always 100% on GVL. These results were verified on a second set of eight recycles. Overall, this trend proved one of the major advantages of the procedure: the inverse multiphasic LA hydrogenation engineered via the IL addition, allowed an efficient recycle of the catalyst hitherto not possible with other methods.

Supplementary tests also made it possible to rule out leaching of metal active species in the water phase. In particular, at the end of a reaction performed under the conditions of Figure 2.9, the aqueous GVL-containing phase was recovered. Then, the water phase was added with fresh LA (810  $\mu$ L, 7.88 mmol), and re-set to react at 100 °C and 35 atm of H<sub>2</sub>, for 1 h. Once the experiment was complete, <sup>1</sup>H NMR analyses proved that the ratio LA/GVL of the aq. mixture was not varied: further hydrogenation of LA did not take place due to the total absence of the metal catalyst.

### 2.2.4 Homogeneous Catalyst: RuCl<sub>3</sub>

The investigation continued by switching to homogeneous RuCl<sub>3</sub> as a catalyst for the multiphasic reduction/dehydration of LA to GVL. Rationale for using such a metal salt was based on two aspects: *i*) previous reports showed that this compound was an active catalytic species for the investigated reaction<sup>5-7, 30</sup>; *ii*) a previous work of our group demonstrating that in a multiphasic organic/IL/water arrangement similar to those above described (figure 1.4), an effective partitioning of homogeneous catalysts was possible in the IL phase<sup>18d</sup>.

As for the case of heterogeneous Ru/C, a number of multiphasic conditions were explored aimed at segregating the metal catalyst in the IL phase.

#### 2.2.4.1 The use of a homogeneous catalyst in the multiphasic system

*LA Hydrogenations.* A multiphasic system analogue to those previously described in paragraph 1.1.3 was also considered for out the hydrogenation of LA. The first issue with such an arrangement was the replacement of the heterogeneous catalyst with the metal salt RuCl<sub>3</sub> (4 mg, 0.0193 mmol). Contrary to the behaviour observed in the presence of Ru/C (Figure 2.4 left), the mixture of isooctane, water, and [N<sub>8,8,8,1</sub>][NTf<sub>2</sub>] did not allow the segregation of RuCl<sub>3</sub> in the IL phase. Before the reaction, the metal salt was visibly dissolved in the aqueous phase; while, after different hydrogenation tests performed at 100-150 °C, 35 atm of H<sub>2</sub>, and for 16 h, part of the catalyst appeared as a black wet powder stuck to the inner glass wall of the reactor (the residual RuCl<sub>3</sub> was still in the aqueous solution). Under such conditions, although a quantitative conversion the LA was achieved, the multiphasic configuration failed in the attempt to recover and reuse the active metal.

A screening was therefore performed to investigate the segregation of RuCl<sub>3</sub> in each of the ionic liquids previously tested with Ru/C. This work (for brevity, details are omitted) led to conclude that [N<sub>8,8,8,1</sub>][Cl] was the most suitable to build up the desired multiphasic system: although [N<sub>8,8,8,1</sub>][Cl] gave a (minor) leaching in the water phase (see Table 2.3), it showed a

superior capability for the confinement of Ru salt. Accordingly, LA hydrogenation tests were performed in an autoclave under the following set of conditions: 150 °C, 16 h, 35 atm of H<sub>2</sub>, RuCl<sub>3</sub> (20 mg, 0.0964 mmol), LA (810  $\mu$ L, 7.875 mmol), H<sub>2</sub>O/*i*-octane = 1:1 (4.4 mL), and a IL/catalyst ratio  $\geq 7$ . Experiments showed that the conversion of LA increased by increasing the IL/catalyst ratio up to 7; though, it (conversion) levelled off to a maximum of  $\sim$ 65% (Figure 1.10).

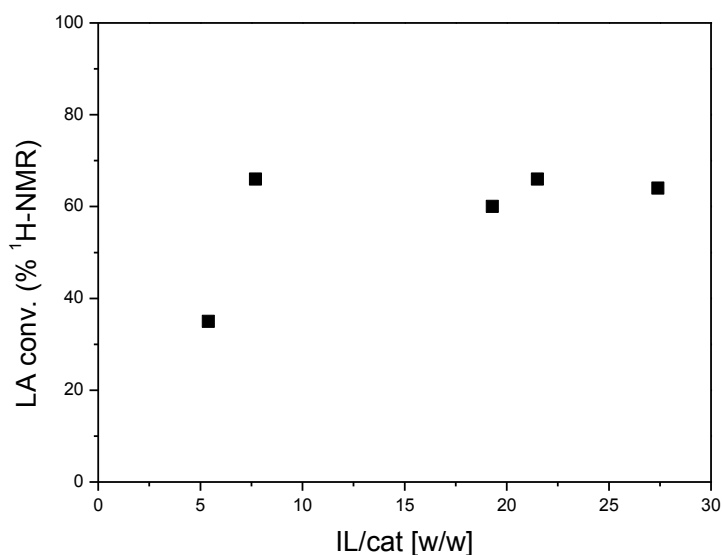


**Figure 2.10** Conversion of LA to GVL as a function of the IL/cat ratio in the *i*-octane-water-[N<sub>8,8,8,1</sub>][Cl] triphasic system with RuCl<sub>3</sub> after 16 h {Conditions 150°C, p[H<sub>2</sub>] = 35 bar, RuCl<sub>3</sub> (20mg, 0.0964 mmol), LA (810  $\mu$ L, 7.875 mmol), H<sub>2</sub>O = *i*-octane = 4.4 mL}.

However, two salient features of such system were observed:

*i*) the multiphasic mixture underwent a physical change after the reaction. The starting mixture of *i*-octane, water, and [N<sub>8,8,8,1</sub>][Cl] with RuCl<sub>3</sub> appeared biphasic initially, but it became triphasic, once subjected for 16 h to the reaction conditions (Figure 2.11).

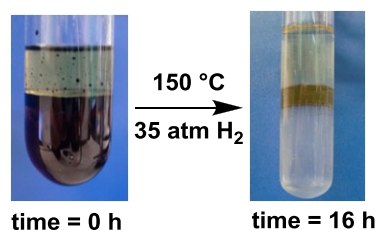


**Figure 2.11** Conversion of LA to GVL with RuCl<sub>3</sub> in the multiphasic system: formation of the triphasic system after 16 hours reaction

*ii*) once the triphasic mixture formed, if the water phase was removed and replaced with fresh aq. LA (810  $\mu$ L in 4.4 mL of H<sub>2</sub>O), then not only the catalyst could be reused, but it (catalyst) became even more active. Rewardingly, under the same conditions above described (150°C, p[H<sub>2</sub>] = 35 bar), just one recycle was sufficient to boost conversion of LA from  $\sim$ 65% to 99%,

with total selectivity toward GVL. Analogous quantitative conversion and selectivity were achieved in five subsequent recycles of the system that were further performed (Figure 2.12).

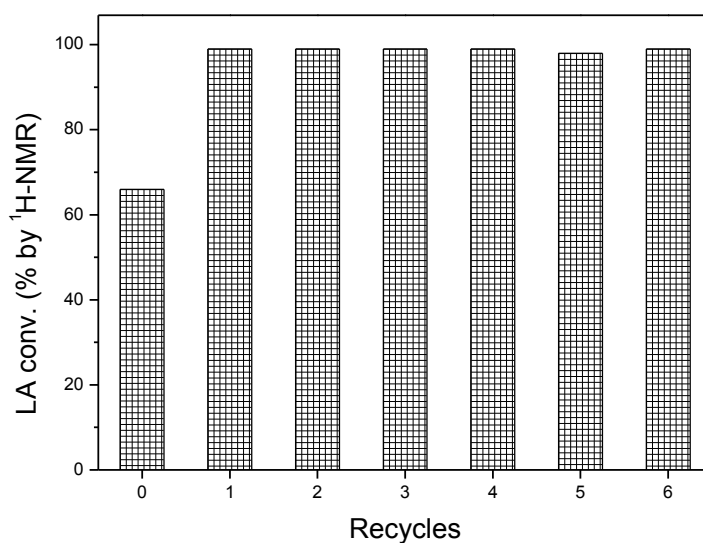


**Figure 2.12.** Conversion of LA to GVL: recycling of the  $\text{RuCl}_3$  catalyst system. Conditions: 16 h, 150 °C,  $p[\text{H}_2] = 35$  bar,  $\text{RuCl}_3$  (20 mg, 0.0964 mmol; Ru = 1.22 mol%), LA (810  $\mu\text{L}$ , 7.875 mmol,  $\text{H}_2\text{O} = i$ -octane= 4.4 mL,  $[\text{N}_{8,8,8,1}][\text{Cl}]$  (399 mg, 0.99 mmol)

The remarkable increase of the LA conversion from the initial test with  $\text{RuCl}_3$  (60%) and the subsequent experiments (100%) of Figure 2.12 suggested that the recycled catalyst might be operating very close to its maximum activity. Both the visual observation of the reaction mixture (Figure 2.11) and the trend of Figure 2.12 provided evidence for the modification of  $\text{RuCl}_3$  into a more active catalytic species. An analogous behaviour was observed on previous investigation of Rh- and Pd-multiphasic systems by our group:<sup>18a, 18d</sup> under such conditions, it was proved that the metal segregated in the IL-phase was present in the form of nanoparticles (Pd-NPs and Rh-NPs, respectively). Such nanoparticles were responsible for an efficient catalytic activity in the multiphasic hydrodehalogenation of aromatic halides (Pd-NPs) and in the multiphasic hydroformylation of olefins (Rh-NPs). In the light of this finding, the occurrence of Ru-nanoparticles confined in the  $[\text{N}_{8,8,8,1}][\text{Cl}]$  phase, was also hypothesised to account for the results of Figure 2.12 and Figure 2.13. The Ru-containing IL-phase recovered at the end of the reaction was therefore analysed by TEM. This confirmed the presence of Ru nanoparticles of average size between 2 and 3 nm (Figure 2.13).



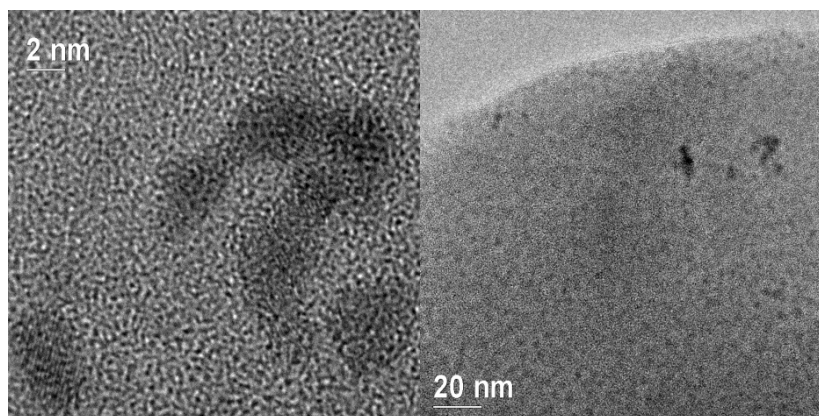


**Figure 2.13** TEM images of Ru nanoparticles formed in the ionic liquid phase under the reaction conditions

These nanoparticles were stabilized by the presence of the IL and enabled an excellent recycle of the system. Under such conditions, leaching tests for the metal were also performed as follows: the aqueous layer was removed, fresh LA was added (810  $\mu$ L, 7.875 mmol), and the mixture was stirred for 16 h, at 150  $^{\circ}$ C and 35 atm  $H_2$ . NMR and GC/MS analyses proved that no reaction took place and, therefore, that no residual Ru was present in water. This is analogous to the behavior of multiphase LA hydrogenations on Ru/C.

*Ru mirrors.* As was mentioned at the beginning of this paragraph, multiphase LA hydrogenations performed in the presence of  $RuCl_3$  and  $[N_{8,8,8,1}][NTf_2]$  (35 atm of  $H_2$  and 100-150  $^{\circ}$ C) did not allow any metal segregation. Once the reaction was complete, part of the catalyst was still dissolved in the aqueous phase, while the residual portion was strongly stuck (as a black powder) to the inner wall of the glass reactor used for the experiments. This required a cleaning of the apparatus in hot aqua regia (60  $^{\circ}$ C, overnight) to remove any trace of the metal. Curiously, after this quite severe acid treatment, if the reactor was used to repeat hydrogenation experiments under the usual conditions ( $RuCl_3$ ,  $[N_{8,8,8,1}][NTf_2]$ , 35 atm of  $H_2$  and 100-150  $^{\circ}$ C), the formation of metallic Ru was observed as a uniform and brilliant thin deposit adhered to the glass reactor.

Metallic Ru appeared as a mirror similar to that achieved by the classical Tollens reaction on  $Ag(NO_3)$ . This unexpected result was obtained every time a multiphase LA hydrogenation experiment was performed on glassware freshly cleaned in aqua regia.

A portion of a Ru mirror on glass was gently cut out from the reactor and analyzed by TEM. This confirmed the presence of a ruthenium film made up of nanoparticles, the size of which ranged from 2 to 8 nm. HREM images and SAD diffraction also proved that the film was constituted by an hexagonal phase of the Ru metal (Figure 2.14).

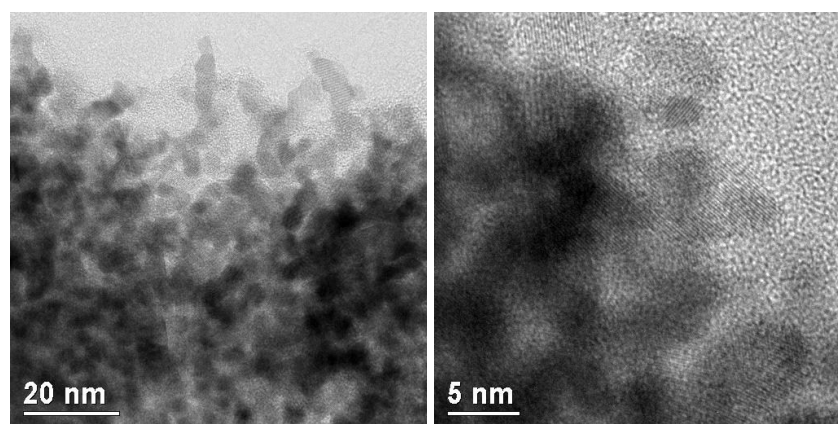


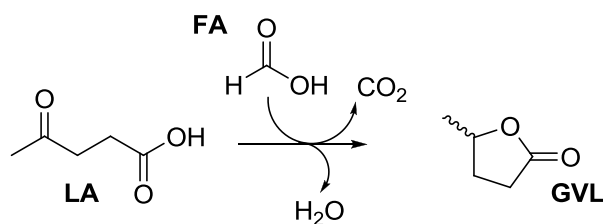
**Figure 2.14.** TEM images of a ruthenium mirror deposited on a glass surface via the multiphase conditions

No further investigations of this intriguing result were performed since they were beyond the scope and the project of this Thesis work. It should be noted however, that the deposition of Ru mirrors was already reported on fused silica (D. Q. Li, D. C. Smith, B. I. Swanson, J. D. Farr, M. T. Paffett, M. E. Hawley, *Chem. Mater.* 1992,4, 1047-1053): these procedures required the functionalization of the silica surface with alkoxy silanes, such as N-[3-(trimethoxysilyl)propyl]ethylenediaminetriacetate (TMPEDETA), able to form monolayers onto which the growth of thin metal films was possible. A comparable result was achieved under considerably simpler experimental conditions here used: the combination of a strong acid (aqua regia) treatment that apparently activated the glass surface, with the above described multiphase system allowed the formation of Ru mirrors composed of size-controlled metal nanoparticles.

This finding certainly deserves future studies that may open new perspectives in the application of the investigated multiphase systems.

### 2.2.5 The Reaction of Levulinic Acid in Mixtures of Levulinic and Formic Acid

The common route to produce biomass-derived LA is the acid-catalyzed hydrolytic treatment of cellulose. By this method however, LA acid is not obtained in a pure form, but rather in aqueous mixtures of LA and formic acid (FA)<sup>5</sup>. This result along with the known capability of FA (and its derivatives) to act as a hydrogen source,<sup>39</sup> has fueled investigations for intensified processes able to upgrade LA to GVL by the use of FA as an *in situ* hydrogenating agent (Scheme 2.6).<sup>5-6, 33a</sup>



**Scheme 2.6.** Hydrogenation/dehydration of LA to GVL using FA as hydrogen source

In analogy to these approaches, we decided to explore our inverse multiphasic system for the use of FA as a hydrogen donor in the conversion of LA to GVL. With respect to the previous investigated multiphasic arrangements, this meant that the aq. LA must be replaced with aqueous solutions containing both LA and FA.

Preliminary experiments were performed by using an aq. solution (total volume: 4.4 mL) of FA/LA in a 3.5:1 molar ratio, respectively (LA: 7.9 mmol). This choice was in agreement to the indications reported by Heeres et al.<sup>31</sup>. Additional components of the reacting mixture were the catalyst 5% Ru/C (0.15 mol %, 0.0124 mmol of Ru), *i*-octane (4.4 mL) and  $[\text{P}_{8,8,8,1}][\text{Ntf}_2]$  (450 mg; IL/Cat = 18, wt/wt) as the hydrocarbon and the IL phases, respectively. Before each test, the reactor (autoclave) was pressurized with  $\text{N}_2$  (35 bar) in order to prevent a massive boiling of aqueous and organic phases from at the reaction temperature. Under such conditions, no reaction took place: at 150 °C, LA was recovered unaltered after 16 h. Not even traces of any product were observed also at 180 °C, after 16 h.

Further experiments were then performed to evaluate if a transfer hydrogenation of LA could take place under simplified conditions, *i.e.* in the absence of both the IL and hydrocarbon phases. At 180 °C, an aq. mixture of FA/LA (3.5:1 molar ratio, 4.4 mL; 7.9 mmol of LA) and the catalyst 5% Ru/C (0.15 mol %, 0.0124 mmol of Ru) was set to react in an autoclave pressurized with  $\text{N}_2$  (35 bar). The formation of GVL was detected in this case, but a very moderate LA conversion of 9 and 18% was achieved after 16 and 48 hours, respectively. Although no specific analyses were performed to evaluate the amount of FA after the hydrogenation tests, results suggested that the decomposition of FA took place to a minor extent in water, while it did not occur at all during multiphasic tests. Despite the harsh conditions used, FA could not be used as a hydrogen donor in the investigated system.

A different approach was therefore considered: the reaction of LA in aq. LA/FA mixtures was investigated under  $\text{H}_2$  pressure. Once again, in order to understand the effect of FA, initial experiments were performed in a simplified environment, *i.e.* in water solutions without any IL or hydrocarbon phases added. Experimental conditions, in particular the  $\text{H}_2$  pressure, were

chosen according to our previous results and to a procedure recently reported by Dumesic and co-workers<sup>33a</sup>. Accordingly, an aqueous solution of LA (810  $\mu$ L, 7.9 mmol) and FA (950  $\mu$ L, 27.7) in a 3.5:1 molar ratio (total volume: 4.4 mL), 5% Ru/C (0.15 mol %, 0.0124 mmol of Ru) was set to react in an autoclave at different temperatures of 100-180  $^{\circ}$ C, under 35 bar of H<sub>2</sub>, and for 16-48 hours.

The results are shown in Figure 2.15. Data confirmed that the presence of FA had a remarkable detrimental effect on the reaction outcome (compare for example, Table 1.2 which refers to similar conditions in the absence of FA). Nonetheless, under H<sub>2</sub> pressure, a reasonable good conversion of LA in GVL could be achieved: it (conversion) rose from 9% (100  $^{\circ}$ C, 16 h) up to 68% after 48 h at 180  $^{\circ}$ C.

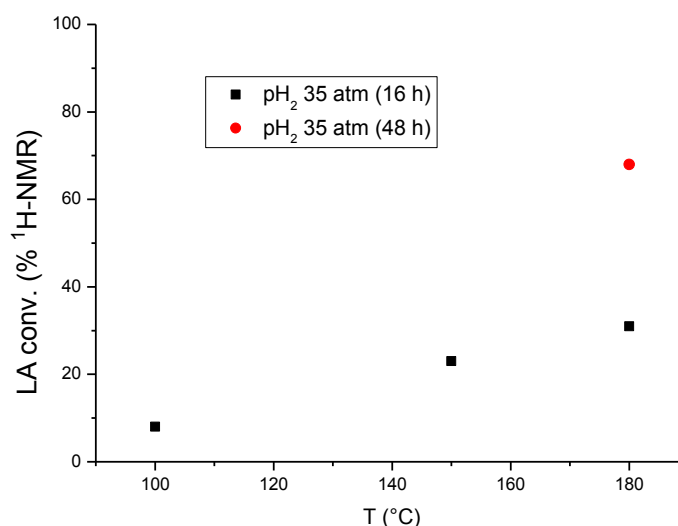


**Figure 2.15.** Effects of temperature and reaction time in the conversion of LA to GVL in aqueous LA/FA solutions. Conditions: 5% Ru/C (0.15 mol %); LA (810  $\mu$ L, 7.9 mmol), FA (950  $\mu$ L, 27.7), molar ratio FA/LA = 3.5; H<sub>2</sub>O = 4.4 mL; p[H<sub>2</sub>] = 35 bar; 100-180  $^{\circ}$ C; 16-48 h

A series of hydrogenation reactions were then performed to explore whether the FA/LA molar ratio could be varied to improve the LA conversion. Experiments were run under the following set of conditions: 5% Ru/C: 0.15 mol %; 35 bar of H<sub>2</sub>, 150  $^{\circ}$ C; 16 h; FA/LA molar ratio of the aq. solution (4.4 mL) in the range of 3.5-1. Results are reported in Figure 2.16. As the FA/LA molar ratio was decreased from 3.5 to 1, the conversion of LA showed a remarkable increase from 23% to 77%, respectively.

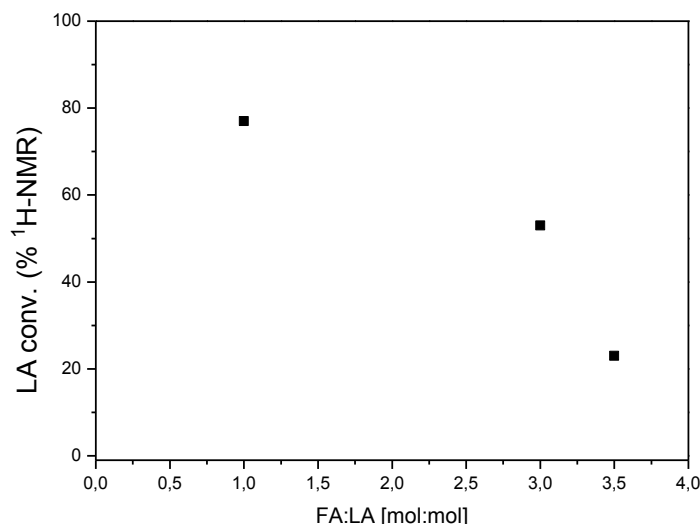


**Figure 2.16** Effect of FA/LA molar ratio in the conversion of LA to GVL in aqueous solutions. Conditions: 150 °C,  $p[\text{H}_2] = 35$  bar, 5% Ru (0.15 mol %), LA (810  $\mu\text{L}$ , 7.875 mmol),  $\text{H}_2\text{O} = 4.4$  mL; molar ratio FA/LA from 3.5 to 1; 16 h.

A more detailed profile of the LA-conversion *vs* time was also obtained for the reaction performed by using a molar ratio FA/LA=1 (Figure 2.17).

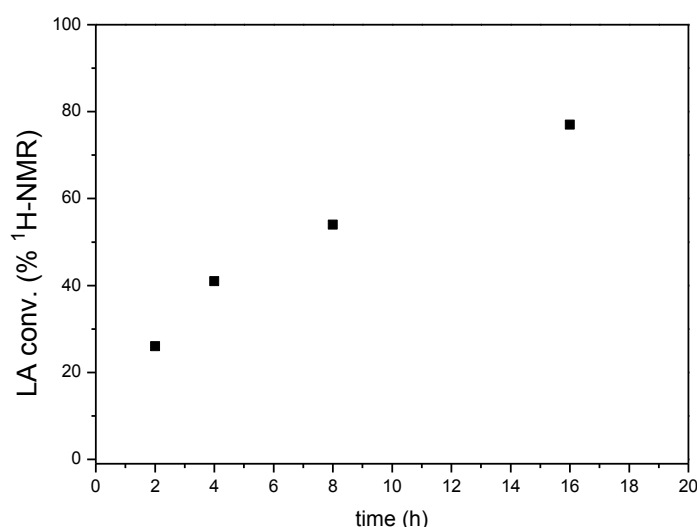


**Figure 2.17** Conversion of LA to GVL as a function of the reaction time. Conditions: 150°C;  $p[\text{H}_2] = 35$  bar; 5% Ru (0.15 mol %); LA (810  $\mu\text{L}$ , 7.875 mmol), FA (300  $\mu\text{L}$ , 7.875), molar ratio FA/LA = 1;  $\text{H}_2\text{O} = 4.4$  mL.

Trends of both **Figure 2.15** and **Figure 2.16** further substantiated the described observations above and they left few doubts about the negative consequences of the presence of FA in the kinetics of the aqueous phase hydrogenation of LA.

In order to explore whether the effects of FA could be due to pH changes of the aqueous phase, a new series of hydrogenation tests were performed in the presence of an additional base such as NaOH. Under the conditions of **Figure 2.17** (5% Ru/C: 0.15 mol %; 35 bar of  $\text{H}_2$ , 150 °C; 16 h; molar ratio FA/LA=1), different amounts of NaOH (0-725 mg, 0-18 mmol) were added

to control the acidity of the environment: in particular, three reactions were performed at initial pH of 4.1, 5.4, and 12.3, respectively. Results are reported in Table 2.4. For a convenient comparison, also the outcome of the reaction run in the absence of the base is indicated. In that case, initial pH was 1.6.

**Table 2.4**  
Effect of NaOH/FA molar ratio on the conversion of LA to GVL in aqueous solutions.

	NaOH/FA [mol:mol]	pH	LA Conversion (%, $^1\text{H NMR}$ )
1	0	1.6	77
2	1	4.1	5
3	1.8	5.4	10
4	2.3	12.8	27

Conditions: 150°C;  $p[\text{H}_2] = 35$  bar; 5% Ru (0.15 mol %); LA (810  $\mu\text{L}$ , 7.875 mmol), FA (300  $\mu\text{L}$ , 7.875 mmol), molar ratio FA/LA = 1;  $\text{H}_2\text{O} = 4.4$  mL; molar ratio NaOH/FA from 0 to 2.3.

A remarkable decrease of the conversion (5-10%) was observed at pH in the range of 4-5 (entries 2-3). Although an increase of pH up to 12 favored the conversion (27%, entry 4), the progress of the hydrogenation was clearly not helped by the presence of NaOH (compare to entry 1). Apparently, the pH or the nature of the added base could have important effects: however, these did not improve the reaction outcome.

Although these results were not particularly encouraging, the investigation proceeded to examine if, under  $\text{H}_2$  pressure, multiphasic conditions could be applied for the recovery of the metal catalyst after the treatment of aq. FA/LA mixtures. In the light of data of Figures 1.15-16, an equimolar aq. solution (4.4 mL) of FA and LA (LA and FA: 7.9 mmol) was set react at 150 °C and 35 bar of  $\text{H}_2$ , in the presence of 5% Ru/C (0.15% mol, 0.0124 mmol of Ru), *i*-octane (4.4 mL) and  $[\text{P}_{8,8,8,1}][\text{Ntf}_2]$  (450 mg; IL/Cat = 18, wt/wt).

The results are reported in Table 2.5. The reaction of the LA/FA mixture, that in water afforded GVL in yields up to 77% (entry 1, 16 h), was depressed down to 42% (entry 2, 16 h) in the biphasic system formed upon addition of *i*-octane. Further introduction of  $[\text{P}_{8,8,8,1}][\text{NTf}_2]$  to give a triphasic system resulted in even lower amounts of GVL (9%, entry 3), after a prolonged reaction time (32 h). On the basis of literature reports on transfer hydrogenations with FA promoted by a catalytic amounts of amines,<sup>40</sup> trioctylamine (TOA) was tested in the triphasic system made by water/*i*octane/ $[\text{P}_{8,8,8,1}][\text{NTf}_2]$ . This reaction reached a 21% yield (run 4). Analogous experiments performed in a triphasic system made by water/*i*-octane/ $[\text{N}_{8,8,8,1}][\text{Cl}]$  with added TOA and  $\text{RuCl}_3$  as the catalyst gave a maximum 13% conversion of the LA/FA mixture to GVL (run 5).

**Table 2.5.**  
The reaction of aq. LA/FA mixtures under multiphasic conditions.<sup>a</sup>

H <sub>2</sub> O (mL)	<i>i</i> -octane (mL)	Catalyst	IL	Base <sup>b</sup> (TOA:FA mol:mol)	LA Conversion, <sup>c</sup> %, (time, h)
4.4	0	Ru/C	-	-	77 (16)
4.4	4.4	Ru/C	-	-	42 (16)
4.4	4.4	Ru/C	[P <sub>8,8,8,1</sub> ][NTf <sub>2</sub> ]	-	9 (32)
4.4	4.4	Ru/C	[P <sub>8,8,8,1</sub> ][NTf <sub>2</sub> ]	TOA (10:31)	21 (16)
4.4	4.4	RuCl <sub>3</sub>	[N <sub>8,8,8,1</sub> ][Cl]	TOA (5:31)	13 (16)

<sup>a</sup> Conditions: LA (810  $\mu$ L, 7.9 mmol), FA (300  $\mu$ L, 7.9 mmol), 150°C, p[H<sub>2</sub>] = 35 bar; entries 1-4: Ru/C = 0.15% mol (0.0124 mmol of Ru); entries 3-4: [P<sub>8,8,8,1</sub>][NTf<sub>2</sub>] (450 mg, IL:cat = 18, wt/wt); entry 5: RuCl<sub>3</sub> = 1.22% mol (20 mg of Ru), [N<sub>8,8,8,1</sub>][Cl] (360 mg, IL:cat = 18). <sup>b</sup> TOA: trioctyl amine; entries 4 and 5: 2.5 and 1.27 mmol. <sup>c</sup> Conversions were measured by <sup>1</sup>H NMR.

Overall, multiphasic conditions were very efficient for the hydrogenation of aq. LA, but they were not suitable for aq. LA/FA mixtures, in other words, they could not be applied in the perspective of using crude mixtures coming from aqueous cellulose streams.

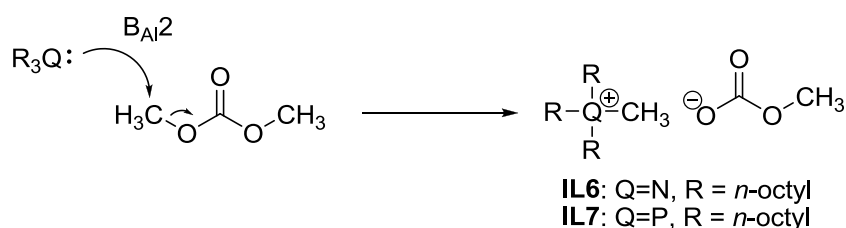
### 2.3 Discussion

*Solvents, ionic liquids and metal catalysts for multiphasic systems.* A first “design and test” phase was required to set up a multiphasic system for the catalytic conversion of LA to GVL (Figure 2.1) with built-in catalyst separation. The objective was 2-fold: not only the identification of an efficient multiphasic catalytic procedure but, even more importantly, the possibility to confine/isolate and recycle the (precious) metal catalyst. On the basis of previous results,<sup>17d, 18a, 18c, 18d, 41</sup> the investigation was initially focused on triphasic systems composed by *i*) an organic solvent able to dissolve the LA reagent and GVL product; *ii*) an ionic liquid (catalyst-philic) phase able to segregate the metal catalyst; and *iii*) an aqueous phase necessary to generate the phase separation. The screening of six readily available organic solvents including hydrocarbons (*i*-octane, toluene, and cyclohexane), esters (ethyl lactate and acetate), and acetonitrile proved that none of them was suitable to our purpose: in the presence of [N<sub>8,8,8,1</sub>][Cl] as a model IL, some (esters and acetonitrile) were good solvents for reagents and products but also partitioned in the water phase and partially dissolved the IL, whereas some others (hydrocarbons) gave excellent phase separation but were not able to act as solvents.

The triphasic arrangement that was successful for several previously reported reactions, was apparently not effective for the LA hydrogenation. A different configuration was therefore considered: in the system made by *i*-octane–water–IL, the highly polar LA and GVL were reacted and recovered in/from the aqueous phase, respectively, rather than in the organic phase.

This kind of solvent system represented an atypical solution for multiphasic reactions for which the name inverse multiphasic system was coined. It is important to underline that the role of a third-apparently “inactive”- phase of *i*-octane was justified precisely by the good phase separation that was able to induce. The design of such multiphasic arrangement also included the preparation, characterization, and use of five ionic liquids with different hydro-/lipo-phylic properties.

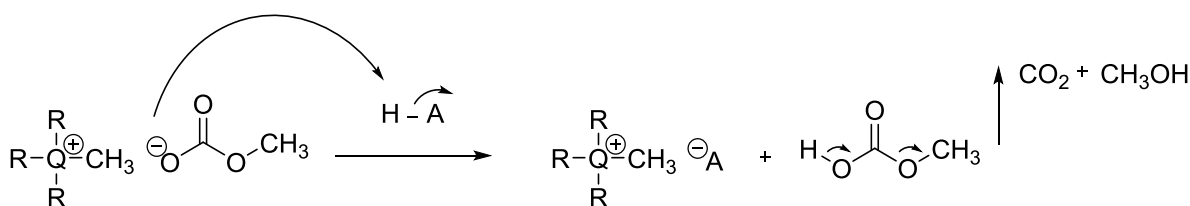
These ILs were obtained through a two-step green synthesis: i) an initial quaternarisation reaction of trioctylamine and trioctylphosphine was performed with non-toxic dimethyl carbonate (DMC) as a methylating agent. The reaction plausibly occurred via a direct nucleophilic attack of the amine or phosphine to the methyl group of DMC by a  $B_{Al2}$  mechanism (Scheme 2.7).<sup>42</sup>



**Scheme 2.7.**  $B_{Al2}$  mechanism for amine and phosphine quaternarisation with dimethylcarbonate

This enabled the preparation of ammonium and phosphonium methylcarbonate salts (**IL6** and **IL7**). Products were clear and colourless, and they were isolated quantitatively simply by distilling the excess of DMC and the co-solvent methanol used in the reaction.

ii) in the second step methylcarbonate onium salts were anion exchanged with Brønsted acids ( $H-A$ ,  $A=CF_3CO_2$ ,  $NO_3$  Scheme 2.8) to replace the methylcarbonate ( $MeOCO_2^-$ ) with an  $A^-$  anion. The reaction co-product was methylhydrogencarbonate (*i.e.* the half-ester of carbonic acid), an unstable compound<sup>43</sup> that immediately decomposed to form methanol and  $CO_2$ , thus providing its built-in removal. This exchange procedure involved mixing the precursor ionic liquid with the acid under air, slight warming ( $50\text{ }^\circ\text{C}$ ), and finally stripping methanol and  $CO_2$  under vacuum to yield the pure products. It proved simple, rapid, clean, and free of any workup steps.



**Scheme 2.8** Reaction products of oniummethylcarbonates with Brønsted acids



Accordingly, compounds **IL4** and **IL5** ( $[\text{N}_{8,8,8,1}][\text{CF}_3\text{COO}]$  and  $[\text{P}_{8,8,8,1}][\text{NO}_3]$ , respectively) were prepared. By analogy with the Brønsted acid addition procedure, the syntheses of bistriflamide onium salts (**IL2**: $\text{N}_{8,8,8,1}[\text{NTf}_2]$ , and **IL3**: $\text{P}_{8,8,8,1}[\text{NTf}_2]$ , respectively) could be obtained by the treatment of the methylcarbonate onium salts with bis(trifluoromethanesulfonyl)amine ( $\text{HN}(\text{SO}_2\text{CF}_3)_2$ ), which is a very strong acid<sup>44</sup>. However, this was a very expensive and difficult to handle material. On the contrary the lithium salt of the conjugated base ( $\text{Li}^+[\text{NTf}_2]^-$ ) is cheaper and appears like a stable white solid. Thanks to the lipophilic character of the  $\text{NTf}_2$  anion, the desired ionic liquids (**IL2** and **IL3**) could be precipitated out of an aqueous solution of  $\text{P}_{8,8,8,1}[\text{CH}_3\text{OCOO}]$  and  $\text{N}_{8,8,8,1}[\text{CH}_3\text{OCOO}]$  simply by addition of  $\text{LiNTf}_2$ .

The first IL to be tested in the inverse multiphase system was  $[\text{N}_{8,8,8,1}][\text{Cl}]$  (**IL1**). In the presence of **IL1**, a third liquid phase between the aqueous and hydrocarbon solvents was observed both at the start and at the end of the hydrogenation tests. The profile of the LA conversion vs the weight ratio IL:Cat showed that the presence of the salt always reduced the reaction rate, but a bell-shaped curve was obtained: in the middle range of IL/Cat (3-5, conversion up to 60–65%), the detrimental kinetic effect was by far, poorer than that observed when lower or higher amounts of the salt were added. This suggesting a peculiar mechanism of adsorption (coverage) of **IL1** over the C-support. A similar behavior was reported by us also for multiphase hydrodehalogenations of aromatics.<sup>45</sup>

However, this onium salt was shelved because the conversion after 4 h reaction was incomplete and a modest leaching in the aqueous phase occurred: NMR analyses showed that 2-3% (by weigh) of the initial amount of the salt was swept away by water.

Then, a less water-soluble IL was sought by modifying the anion. In the presence of 5% Ru/C as a catalyst, a series of LA hydrogenation experiments allowed optimization of the IL phase, the IL/Cat ratio, and general experimental conditions (T, P, time) in order to combine high LA conversion and GVL selectivity with phase separation and acceptable reaction times. These included the triphasic system made by *i*-octane–water– $[\text{P}_{8,8,8,1}][\text{NTf}_2]$  at 100 °C with 35 atm  $\text{H}_2$ , 1 h, IL/Cat = 14–16 (w/w), Ru/C = 0.0124 mmol (Ru = 0.15 mol %), *i*-octane = 4.4 mL, and LA aq. solution (1.8 M, 4.4 mL). Ru/C was chosen from specific literature data reporting its superior performance for the hydrogenation/dehydration of LA; meanwhile, among the available ILs,  $[\text{P}_{8,8,8,1}][\text{NTf}_2]$  was devised for the lipophilic properties of the triflamidecounteranion able to avoid any partitioning of such an ionic liquid in the water phase. Also,  $[\text{P}_{8,8,8,1}][\text{NTf}_2]$  turned out to be an outstanding segregating phase for the metal catalyst.

Notwithstanding the inconfutable empirical evidence proving the capabilities of ILs to induce unique phase separations as well as to act as metal phyllic-phases, reasons on the origin of

complex multiphase environments such as those investigated in this work, are still somewhat unclear. The observed phase separation is made possible (or largely improved) by the presence of a hydrocarbon that except for this function, plays no other roles as a solvent or a reactant. A network of weak (Van Der Waals and H-bond) and strong (polar/ionic) interactions operating at the interphases might plausibly account for the establishment of these systems. However, the energy balance for such an equilibrium of forces is far to be rationalized. As per the catalytic-phylicity of IL phases with respect to C-supported metals (*i.e.* Pd/C or Ru/C), one hypothesis has considered the presence of carboxylic groups that usually reside over the surface of activated charcoals. These acid functionalities could act as anchoring points for onium salts which therefore, would be favored to stick and penetrate the C-support generating a sort of surface membrane.<sup>41b, 41c</sup>

As a general comment, taking into account that regio-, chemo-selectivity or the rate of certain multiphase reactions changed according to the nature of the IL,<sup>41d, 45</sup> a molecular-scale mode of action of the IL present on the catalyst active sites should be considered to alter the processes of adsorption of the reagents or their reaction on the active sites.<sup>41b, 41c</sup>

In view of the objective to design a system that would allow simple recycle of the catalytic phase, the optimized conditions were applied to a series of recycling experiments; the whole process is illustrated by Figure 2.18. Once the hydrogenation reaction of LA was complete, the recycling procedure proceeded through the simple removal of the aqueous GVL-containing phase (A), and its replacement with fresh aqueous LA (B); then, the resulting multiphasic mixture was resubjected to the reaction conditions (C). Up to 8 recycles indicated that the system was stable and reusable.

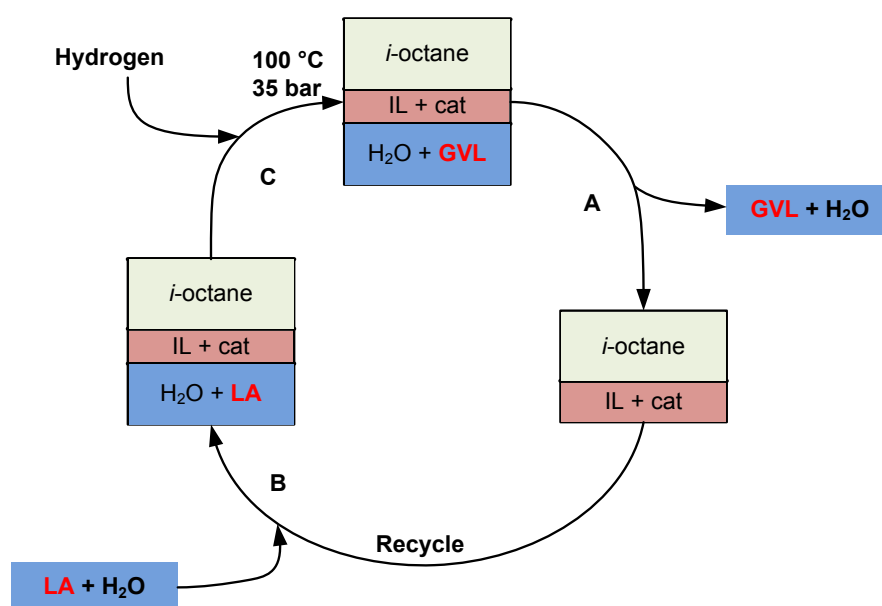


Figure 2.18 Multiphase conversion of LA to GVL: recycling procedure.

Leaching tests proved the absence of the metal catalyst in the aq. phase, while GC-MS analyses of the organic solvent did not show any loss of reagent or product in this phase. The overall mass balance was confirmed also by the isolation of the product: at the end of hydrogenation tests, GVL was separated from the water solution in substantially quantitative yields ( $\geq 99\%$ ). Although the reaction in the absence of IL was always faster than in the multiphase system, this limitation was largely offset by the ease with which the catalytic system could be recycled.

For comparison, a recent paper of the same reaction that was focused on optimizing conditions<sup>8</sup> indicated that, with 5% Ru/C as catalyst in water as solvent, at 70 °C and 30 atm H<sub>2</sub> after 3 h, only 23% yield of GVL was obtained, whereas at 70 °C and 5 atm of H<sub>2</sub>, LA conversion did not exceed 13% unless an acidic cocatalyst was used. As shown in Figure 2.8, at the same temperature (70 °C) albeit with 35 atm H<sub>2</sub>, the investigated multiphase system allowed a LA conversion over 90% with complete selectivity toward GVL after 4 h. This seems to indicate that the role of the *i*-octane phase was more than just to keep the three phases separate, but that it might also contribute to enhancing or preserving catalyst activity.

It was possible to use homogeneous RuCl<sub>3</sub> in place of heterogeneous Ru/C in the multiphase system. However, RuCl<sub>3</sub> acted as a catalyst precursor rather than a water-soluble metal complex: under H<sub>2</sub> pressure, TEM analyses proved that the metal salt was rapidly converted into Ru nanoparticles (Ru-NPs), which were efficiently confined in the IL phase (Figure 2.13). A very similar result was reported by our group in the investigation of the behaviour of homogeneous Pd and Rh-salts added to org/IL/aqueous multiphase systems.<sup>18a, 18d</sup>

Even more recently, the formation of metal nanoparticles was described and reviewed by several Authors.<sup>46</sup> They reported that organometallic complexes were the most common source to generate metal NPs in ILs and both molecular hydrogen and metal hydrides were the reducing agents. For example, iridium NPs of a monomodal size distribution (2.0 nm in diameter) were prepared by the reduction of [Ir(cod)Cl]<sub>2</sub> (cod = 1,5-cyclooctadiene) by molecular hydrogen (4 atm) in 1-*n*-butyl-3-methylimidazolium hexafluorophosphate IL ([BMI][PF<sub>6</sub>]), at 75 °C.<sup>17b</sup> In an analogous way, rhodium,<sup>47</sup> platinum,<sup>48</sup> ruthenium,<sup>49</sup> and palladium<sup>50</sup> NPs were obtained in different ILs. It was generally suggested that different factors affected the control of the size and shape of such metal NPs. These (factors) were related to the type of metal precursor, the nature of the reducing agent, the reaction conditions, and the IL structure. In particular, in the generation of NPs from RuCl<sub>3</sub>, **IL1** seemed to provide a template-like effect, that stabilized Ru-NPs on the basis of their ionic nature without the need of additional stabilizer/ligand, as shown in the example in Figure 2.19.<sup>51</sup>

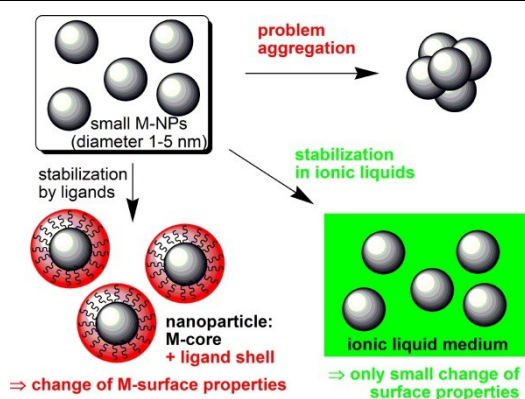


**Figure 2.19** Stabilization of metal nanoparticles (M-NP) through protective ligand stabilizers or in ionic liquids (IL).<sup>51</sup>

In addition to the reduction processes, other methods such as the thermal decomposition of the organometallic precursors,<sup>52</sup> the phase transfer of preformed NPs in water or organic solvents to the IL,<sup>53</sup> and the bombardment of bulk metal precursors with deposition on the ILs<sup>54</sup> were developed.

In the hydrogenation of LA investigated in this work, experiments demonstrated that Ru-NPs behaved as the active species and they could be easily recovered and recycled. In this case the best operative conditions were so identified: 150 °C, 35 atm H<sub>2</sub>, 16 h, Cat = RuCl<sub>3</sub> (20 mg, 0.0964 mmol; 1.22 mol %), LA (810  $\mu$ L, 7.875 mmol), water = iooctane = 4.4 mL, [N<sub>8,8,8,1</sub>][Cl] (486 mg). The use of [N<sub>8,8,8,1</sub>][Cl] as the IL phase was based on previous results<sup>18a</sup>: this ionic liquid was chosen notwithstanding that it was slightly partitioned in the aqueous phase (Table 2.3), mainly for its affinity with RuCl<sub>3</sub>. The performance of such a “homogeneous-multiphasic” system was evaluated as a function of the IL/Cat ratio. This showed the following: *i*) The LA conversion to GVL could not be further improved above a ratio IL/Cat (w/w) = 7. In particular, it (conversion) leveled off at around 65%. *ii*) The RuCl<sub>3</sub> based system appeared less active than the corresponding Ru/C-based system. However, a peculiar feature of this reaction was that the initial reaction mixture appeared biphasic with the RuCl<sub>3</sub> dispersed in the water–[N<sub>8,8,8,1</sub>][Cl] phase, whereas the final mixture was again perfectly separated in three distinct phases (Figure 2.11). Deeper understanding of the reaction as well as positive feedback on the homogeneous system came from the recycling experiments. As shown in Figure 2.12, when the IL-catalyst ensemble was recovered and reused, the second cycle showed a substantially quantitative conversion of LA to GVL. This indicated that a very active catalytic species could form after an induction period in the system. Moreover, once formed, it was able to promote the reaction for at least 6 cycles without loss of activity. The most plausible explanation for such a behavior was the presence of Ru-nanoparticles stabilized by the IL-phase.

Finally, we wish to note that, although during the first catalytic run  $[N_{8,8,8,1}][Cl]$  was slightly partitioned in the aqueous phase (2–3%) as seen earlier (in the Best IL section), once the catalytic Ru nanoparticles were formed, no trace of  $[N_{8,8,8,1}][Cl]$  was detected in water any longer. The reasons for this are still largely obscure.

*The multiphasic LA-hydrogenation in the presence of formic acid.* As was mentioned in the introduction to this chapter, the output of LA production from the hydrolytic treatment of cellulose is in a mixture of levulinic acid and formic acid. This reason stimulated our efforts to consider the applicability of multiphasic conditions for the direct hydrogenation of LA to GVL in different aq. LA/FA solutions. The experiments provided evidence that the investigated triphasic systems were not suitable for the conversion of LA to GVL using formic acid (FA) as an *in-situ* hydrogen source in the presence of Ru/C. Under such conditions (aq. LA/FA mixtures), not even an additional pressure of molecular hydrogen (up to 35 bar) or the introduction of organic bases allowed a satisfactory progress of the reaction. At 150 °C with Ru/C, the LA conversion was of only 9% after 32 hours, and it slightly improved up to 21% in the presence of trioctylamine (Table 1.4). It should be noted that the presence of FA was detrimental for the hydrogenation of LA not only in the multiphasic org/IL/aq.-systems, but also in simpler aqueous solutions: at 150 °C and 35 bar ( $H_2$ ) with Ru/C, the reaction of an aq. LA/FA (1:1 mol/mol) showed an LA conversion of 77% after 16 hours; while, over the same catalyst, the hydrogenation of aq. LA was quantitative in less than 1 h at 100 °C and 35 bar ( $H_2$ ).

Among possible reasons, a first hypothesis for this behavior was the change of acidity due to FA. Formic acid ( $pK_a = 3.77^{55}$ ) is stronger than levulinic acid ( $pK_a = 4.6^{1e}$ ), meaning that multiphasic experiments in aq. LA/FA mixtures were performed at a lower pH (1.6) than those in aq. LA solutions (pH=2.2). Literature studies on aqueous phase hydrogenations of organic substrates such as benzene on different supported metal catalysts, reported that an increased acidity of the reaction environment could induce both a leaching of the metal from the support and a catalyst poisoning, thus causing a drop of the catalytic activity.<sup>56</sup> This offered a support for the evidence of low LA hydrogenation rates in plain aqueous LA/FA solutions. However, the total catalytic inhibition observed for multiphasic tests run on LA/FA mixtures (Figure 2.16) as well as the drop of the LA conversion observed after the addition of NaOH (Table 2.4) still remained unclear. Under multiphasic conditions, since the catalyst appeared perfectly confined in the IL phase, the overall reaction was likely to take place at the aq-IL interphase. Then, due to mutual immiscibility, the acidity of the aq. solutions was not expected to be transferred in the IL phase which should act as a metal protective environment. This was even truer for formic acid

which was more hydrophilic than LA. Indeed, the complete lack of any (multiphasic) reaction suggested the occurrence of complex interphase phenomena. This interpretation was also supported by different aspects and observations: *i*) the LA hydrogenation was held back by the simple addition of *i*-octane (without any IL) to an aq. LA/FA solution (Table 1.4); *ii*) the tendency of FA to form H-bond networks<sup>57</sup>(plausibly involving LA) which might limit the availability of LA at the aq.-IL interphase; *iii*) minor changes of density and viscosity of the aq. phase that could be determined by the addition of FA. A detailed analysis of such points will be the object of future investigations.

It should finally be noted that the presence of FA had no detrimental effects on the stability of the product GVL in aqueous solutions. Although this compound could undergo both acid and basic hydrolysis,<sup>58</sup> it was demonstrated that a good yield (up to 77%) of GVL could be achieved in the hydrogenation of aq. LA/FA mixtures (Figure 1.15). The investigated acidic conditions were apparently not sufficient to allow the hydrolytic cleavage of the lactone. This was confirmed by an additional experiment where an equimolar aq. mixture of GVL and FA (7.875 mmol; total volume 4.4 mL) was set to react at 150 °C, under 35 bar of H<sub>2</sub>, in the presence of 5% Ru/C (0.0124 mmol). After 16 hours, GVL was recovered unaltered.

## 2.4 Conclusions

This investigation demonstrated that multiphasic systems formed by the mutual immiscibility of three liquid phases such as water, *i*-octane, and an ionic liquid were efficient arrangements to run catalytic hydrogenation reactions of LA and, most of all, to simply recover and recycle Ru-based catalysts. Other advantages of multiphasic systems were the easy experimental setup and the high versatility that allowed the use of both heterogeneous catalysts and homogeneous metal precursors.

The hydrogenation reaction took place with both organic reagent and product (LA and GVL, respectively) solubilised in the water phase, while the metal catalyst was segregated in the IL. Different mechanisms were however, responsible for the segregation of heterogeneous and homogeneous catalysts: in the case of Ru/C, a plausible reason was the high affinity of the charcoal support for onium salts, while for RuCl<sub>3</sub>, the formation of metal nanoparticles accounted for the catalyst stabilization in the IL phase.

Although the presence of the hydrocarbon solvent (*i*-octane) appeared at first sight inconsequential, it was instead functional to good phase separation for the recovery of products and the recycle of the catalyst.

In all cases, experiments demonstrated that the architecture of triphasic systems preserved the catalytic performance unaltered over several (at least eight) recycles during which the GVL product was easily recovered by phase separation and isolated in yields up to 99% after each reaction. This represents a major advantage over most procedures reported for the conversion of LA to GVL, where the reuse of the catalyst (especially from water-based matrices) was hardly efficient, if practicable at all.

A limitation of our system has been found in its application to mixtures of LA/FA, meaning that the multiphasic procedure could not be extended to the upgrade of crude LA/FA streams from the hydrolysis of cellulose. The presence of FA was detrimental for the hydrogenation of LA not only in the multiphasic org/IL/aq.-systems, but also in simpler aqueous solutions. Several hypotheses based on the pH effect, the change of physical properties (viscosity or density) of the water phase, and the formation of a H-bond network were proposed to explain the effect of FA on the system. None of these suggestions have been able to be confirmed.

Nonetheless, the multiphasic method here described represents an inventive application of ionic liquid phases and a genuine advance in the design of chemical transformations that are intrinsically greener, notwithstanding that some of the issue addressed above still need to be fully understood.

Results described in this chapter led to the publication of three scientific paper.

## 2.5 Experimental section

### 2.5.1 Materials and chemicals

All chemicals are reagent ACS grade and used without further purification. Unless otherwise specified, they were purchased from Sigma-Adrich. 5% Ru/C was from BASF. H<sub>2</sub> was purchased from SIAD. Tri-*n*-octylphosphine (TOP) was from Strem Chemicals. Tri-*n*-octylamine (TOA) was from Fluka. Deionized (milli-Q) water was used in all experiments.

<sup>1</sup>H and <sup>13</sup>C NMR spectra were acquired on a Varian Unity 400 MHz spectrometer. In the case of the ionic liquids used in this Thesis, also HMBC, HMQC and INADEQUATE experiments were used to assign the corresponding structures.

GC/MS spectra were acquired on a Hewlett Packard 5890 gas-chromatograph equipped with a HP-FFAP capillary column (30m, Ø 0.25 mm; coating thickness 0.25 µm).

The analysis GC/MS were conducted by diluting the samples in diethylether, while the  $^1\text{H}$  and  $^{13}\text{C}$  NMR spectra were acquired in deuteratedchloroform ( $\text{CDCl}_3$ ) using TMS as the internal reference.

### 2.5.2 Synthesis of ionic liquids

The synthesis of all ionic liquids **IL1-IL5** involved two steps: (i) the reaction of dimethyl carbonate ( $\text{MeOCO}_2\text{Me}$ , DMC) with trioctylamine and trioctylphosphine, to yield the corresponding methyl- ammonium and phosphoniummethylcarbonate salts and (ii) the anion exchange reaction, to yield the desired IL <sup>37</sup>. In particular, methyltrioctyl ammonium chloride ( $[\text{N}_{8,8,8,1}]\text{Cl}$  **IL1**), methyltrioctyl ammonium bistriflamide ( $[\text{N}_{8,8,8,1}]\text{NTf}_2$ , **IL2**), and methyltrioctyl ammonium trifluoroacetate ( $[\text{N}_{8,8,8,1}]\text{CF}_3\text{COO}$ , **IL4**) were prepared starting from methyltrioctyl ammonium methylcarbonate ( $[\text{N}_{8,8,8,1}]\text{CH}_3\text{OCO}_2$ , **1a**). While, methyltrioctylphosphoniumbistriflamide ( $[\text{P}_{8,8,8,1}]\text{NTf}_2$ , **IL3**) and methyltrioctylphosphonium nitrate ( $[\text{P}_{8,8,8,1}]\text{NO}_3$ , **IL5**) were prepared starting from methyltrioctylphosphoniummethylcarbonate ( $[\text{P}_{8,8,8,1}]\text{CH}_3\text{OCO}_2$ , **1b**).

*Synthesis of methyltrioctyl- ammonium and phosphoniummethylcarbonate salts* ( $[\text{N}_{8,8,8,1}]\text{CH}_3\text{OCO}_2$  **IL6** and  $[\text{P}_{8,8,8,1}]\text{CH}_3\text{OCO}_2$  **IL7**). In a typical procedure, a sealed 200 mL steel autoclave fitted with a pressure gauge and a thermocouple for temperature control was charged with a trioctylamine (24.5 mL, 19.8 g, 0.056 mol) or a trioctylphosphine (25.0 mL, 20.8 g, 0.056 mol), dimethyl carbonate (30.0 mL, 32.1 g, 356 mmol) and methanol (30 mL). Three freeze–pump–thaw cycles were performed to ensure complete degassing of the mixture and air removal. The empty volume was then filled with nitrogen. The autoclave was heated for 24 h at 140 °C with magnetic stirring. Then, the reactor was cooled to rt and vented. Methanol and the residual DMC were removed from the mixture by rotary evaporation. A small amount (<1 equiv) of methanol could remain incorporated in the sample even after a prolonged high vacuum was applied. Isolated yields were 99-100%: **IL6** (20.0 g) and **IL7** (27.5 g).

*Anion exchange reaction of methylcarbonate salts. General procedure.* A 50 mL round bottomed flask was charged with an equimolar mixture of methyltrioctylammonium or phosphoniummethylcarbonate (6 mmol: **IL6**, 2.65 g; **IL7**, 2.95 g) and of a Brønsted acid ( $\text{H-A}$ :  $\text{A} = \text{Cl}$ ,  $\text{NO}_3$ ,  $\text{CF}_3\text{COO}$ ).  $\text{HCl}$  (0.50 mL) and  $\text{HNO}_3$  (0.39 mL) were used in aqueous commercial solutions (37% and 69% respectively), while pure TFAA (0.69 g) was added drop wise over 5 min. The mixture was kept under magnetic stirring for 1 h at 40 °C. Then, water, methanol and



unreacted acid were removed in vacuum obtaining the desired products **IL1**, **IL4** and **IL5** in quantitative yields.

*Synthesis of methyltrioctyl- ammonium and phosphoniumbis(trifluoromethane)sulfonimide salts (IL2 and IL3).* In a 250 mL round bottomed flask, the selected methyltrioctyl ammonium or phosphoniummethylcarbonate (8.12 mmol: **IL6**, 3.86 g; **IL7**, 4.0 g) were dissolved in water (70 mL). An aqueous solution of LiNTf<sub>2</sub> (2.33 g, 8.13 mmol in 50 mL) was then added and the resulting mixture was stirred at 70 °C for 2 h. The resulting white precipitate was extracted with CH<sub>2</sub>Cl<sub>2</sub> to afford pure bis(trifluoromethane)sulfonimide salts **IL2** (2.95 g, 4.85 mmol, 60%) and **IL3** (3.05 g, 4.87 mmol, 60%) as clear colourless liquids.

All onium salts were fully characterized as such, by <sup>1</sup>H and <sup>13</sup>C NMR, and used without further purifications.

### **The reactor (autoclave) for hydrogenation reactions under pressure**

Hydrogenation tests performed in this Thesis work were all performed under H<sub>2</sub> or inert (N<sub>2</sub>) pressure. To the scope, a 250 mL stainless steel autoclave (D = 35 mm, L = 150 mm) was used (Figure 2.20). The reactor was equipped with: i) a thermocouple for the constant monitoring of temperature ii) a manometer for the constant monitoring of pressure; iii) two needle valves which were used for inlet and purging of gases (H<sub>2</sub> or N<sub>2</sub>) at the beginning and at the end of experiments, respectively; iv) a flat-bottom cylindrical glass tube (D = xx mm, L = yy mm) fitted with a holed cover and a magnetic stirring bar, which was used to charge the reacting mixture. The glass tube was sized to be perfectly inserted in the autoclave. In the range of temperature up to 150 °C, the autoclave was heated by an external circulating glycol bath. For higher temperatures (up to 180 °C), silicone oil was used. The autoclave was placed on a magnetic stirrer plate, which ensured a vigorous stirring of reacting mixtures.

*SAFETY WARNING.* Operators of high pressure equipments should take proper precautions to minimize the risks of personal injury (P. G. Jessop, T. Ikariya and R. Noyori, J. Am. Chem. Soc., 1996, 118, 344–355).



Figure 2.20

### 2.5.3 The Ru/C-catalyzed hydrogenation of LA in organic solvents

In a typical procedure, a mixture of 5% Ru/C (25 mg; 0.0124 mmol of Ru), dioxane (4.4 mL), and levulinic acid (810  $\mu$ L, 7.875 mmol) was added to the above described glass tubular reactor and placed in the above described autoclave. The latter was pressurized with H<sub>2</sub> (from 20 and 60 bar), and heated at due temperature (from 80 and 150 °C) for the due time (from 4 and 16 hours) with vigorous stirring (details on pressure/temperatures/times are given in the Results section). At the end of the experiment, the autoclave was cooled to room temperature, and the residual gases were vented. The reaction mixture was then filtered and dioxane was removed by rotary evaporation. Reagent conversion and product distribution were determined by <sup>1</sup>H NMR analyses.

### 2.5.4 The Ru/C-catalyzed hydrogenation of LA in triphasic systems

In a typical procedure, a mixture of 5% Ru/C (25 mg, 0.0124 mmol), [P<sub>8,8,8,1</sub>][NTf<sub>2</sub>] (0.9–1.0 mmol), H<sub>2</sub>O (4.4 mL), and isooctane (4.4 mL) was added to the above described glass tubular reactor and stirred until complete dissolution of the catalyst in the IL phase. Levulinic acid (810  $\mu$ L, 7.875 mmol) was then added to the system. The tube was placed in the in the above described autoclave which was then pressurized with H<sub>2</sub> (35 bar), heated at due temperature (from 30 and 100 °C), for the due time (from 0.5 and 4 hours), with vigorous stirring (details on temperatures/times are given in the Results section). The autoclave was then cooled to room temperature, and the residual gases were vented. At the end of the reaction, the supported metal catalyst was still completely segregated in the IL phase. An aliquot (~50  $\mu$ L) of the clear water solution was separated and extracted with CDCl<sub>3</sub> (~0.8 mL). <sup>1</sup>H NMR analyses of extracts in CDCl<sub>3</sub> allowed the determination of the reaction conversion and the product distribution.

### 2.5.5 The triphasic hydrogenation of LA in the presence of $\text{RuCl}_3$

In a typical procedure, a mixture of  $\text{RuCl}_3$  (20 mg, 0.0964 mmol),  $[\text{N}_{8,8,8,1}][\text{Cl}]$  (0.9–1.0 mmol),  $\text{H}_2\text{O}$  (4.4 mL), and isooctane (4.4 mL) was added to the above described glass tubular reactor and stirred. The catalyst completely dissolved in the water phase, giving a brownish aq. solution. Levulinic acid (810  $\mu\text{L}$ , 7.875 mmol) was then added to the system. The tube was placed in the in the above described autoclave which was then pressurized up to 35 atm with  $\text{H}_2$ , and heated at 150  $^\circ\text{C}$  for 16 h, with vigorous stirring. The autoclave was then cooled to room temperature, and the residual gases were vented. At the end of the reaction, the catalyst appeared completely segregated in the IL phase, which showed a yellow-brown color. An aliquot ( $\sim 50\mu\text{L}$ ) of the clear water solution was separated and extracted with  $\text{CDCl}_3$  ( $\sim 0.8$  mL).  $^1\text{H}$  NMR analyses of extracts in  $\text{CDCl}_3$  allowed the determination of the reaction conversion and the product distribution.

### 2.5.6 The Ru/C-catalyzed hydrogenation of LA in the presence of formic acid

*Reactions in water.* In a typical procedure, a mixture of 5% Ru/C (25 mg, 0.0124 mmol of Ru), levulinic acid (810  $\mu\text{L}$ , 7.875 mmol), formic acid (300  $\mu\text{L}$ , 7.875 mmol)  $\text{H}_2\text{O}$  (4.4 mL) was added to the above described glass tubular reactor, which was then placed in the autoclave. This was subsequently was pressurized with  $\text{H}_2$  (typically at 35 bar), and heated at 150  $^\circ\text{C}$  for the due time (typically for 16 h), with vigorous stirring. The autoclave was then cooled to room temperature, and the residual gases were vented. An aliquot ( $\sim 50$   $\mu\text{L}$ ) of the water solution was extracted with  $\text{CDCl}_3$  ( $\sim 0.8$  mL).  $^1\text{H}$  NMR analyses of extracts in  $\text{CDCl}_3$  allowed the determination of the reaction conversion and the product distribution.

*Triphasic reaction.* The same procedure was used for reactions run in the presence of  $[\text{P}_{8,8,8,1}][\text{NTf}_2]$  (0.9–1.0 mmol), isooctane (4.4 mL), and 5% Ru/C (25 mg, 0.0124 mmol of Ru) or  $\text{RuCl}_3$  (20 mg, 0.0964 mmol).

### 2.5.7 Analysis of the reaction mixtures

As was mentioned above, once LA hydrogenations were complete, an aliquot of the aqueous solution ( $\sim 0.1$  mL) was withdrawn and extracted with  $\text{CDCl}_3$  ( $\sim 0.8$  mL). The  $\text{CDCl}_3$  solution was placed in a NMR tube and the corresponding  $^1\text{H}$  NMR spectrum was acquired on a Varian Unity NMR spectrometer at 400 MHz. LA conversion and GVL selectivity were evaluated from integrals in the  $^1\text{H}$  NMR spectrum. Figure 2.21 reports a typical  $^1\text{H}$  NMR spectrum of the reaction mixture recovered at the end of the multiphasic LA hydrogenation

performed under the conditions of Figure 2.7 **black dots**, [reaction conditions: 1 h, 100°C,  $p[\text{H}_2]$  = 35 atm, LA 810  $\mu\text{L}$  (7.875 mmol), Ru/C 25 mg (0.0124 mmol of Ru), water = *i*-octane = 4.4 mL, **IL3** (366 mg, **IL3**:cat = 14.6)]. Such an experiment, yielded an LA conversion of 80% and 100% selectivity towards the product GVL.

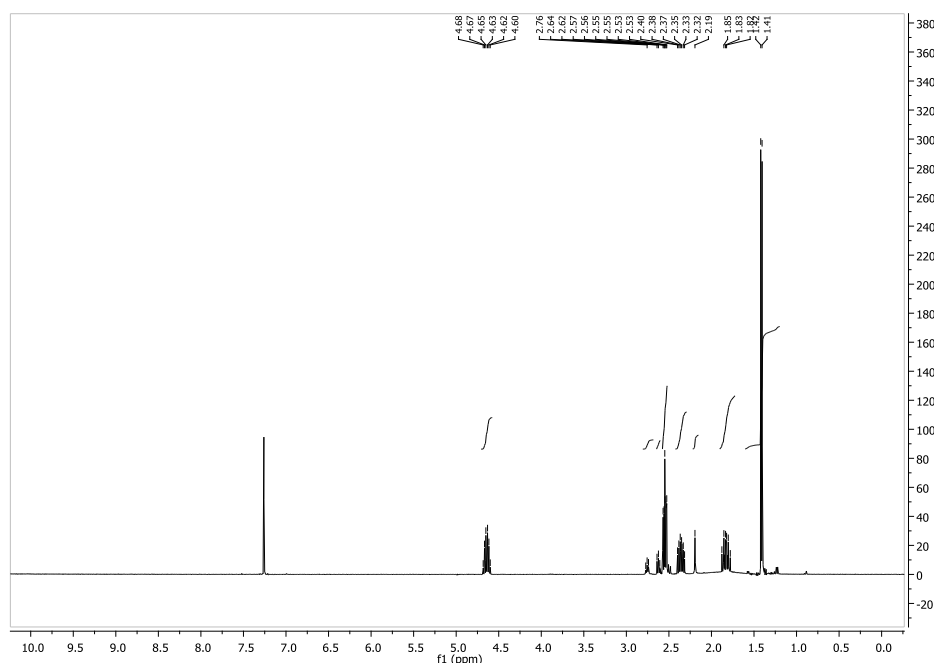


**Figure 2.21**  $^1\text{H}$  NMR spectrum after the multiphasic LA hydrogenation performed under the following conditions: 1 h, 100°C,  $p[\text{H}_2]$  = 35 atm, LA 810  $\mu\text{L}$  (7.875 mmol), Ru/C 25mg (0.0124 mmol of Ru), water = *i*-octane = 4.4mL, **IL3** (366 mg **IL3**:cat = 14.6).

Both reactant (LA) and product (GVL) were clearly identified by their  $^1\text{H}$  NMR signals. In particular:

**LA**: ( $\text{CDCl}_3$ , 400 MHz)  $\delta$  2.20 (s, 3H), 2.60-2.65 (m, 2H), 2.73-2.78 (m, 2H).

**GVL**: ( $\text{CDCl}_3$ , 400 MHz)  $\delta$  1.40-1.43 (d, 3H), 1.77-1.88 (m, 1H), 2.31-2.41 (m, 1H), 2.51-2.59 (m, 2H), 4.59-4.69 (m, 1H) ppm.

Chemical shifts ( $\delta$ ) were reported in parts per million (ppm) downfield from TMS. They were in full agreement with those reported in the literature,<sup>59</sup> and those of commercial authentic samples.

## 2.5.8 Isolation of the product GVL

A typical procedure is described for the reaction performed under the conditions of entry 3, Table 2.3: 4 h, 100°C,  $p[\text{H}_2]$  = 35 atm, LA (810  $\mu\text{L}$ , 7.875 mmol), Ru/C (25 mg,

0.0124 mmol of Ru), water = *i*-octane = 4.4 mL, **IL3** (266 mg, **IL3**:cat = 10). Such an experiment yielded a substantially quantitative LA conversion with 100% selectivity towards the product GVL. The final aqueous mixture was extracted with ethyl acetate (3x15 mL), and combined organic fractions were dried over Na<sub>2</sub>SO<sub>4</sub>. After filtration and removal of ethyl acetate by rotary evaporation, crude GVL was obtained as a colourless liquid (785 mg, 99%).

Figure 2.22 reports the <sup>1</sup>H NMR spectrum of crude GVL.

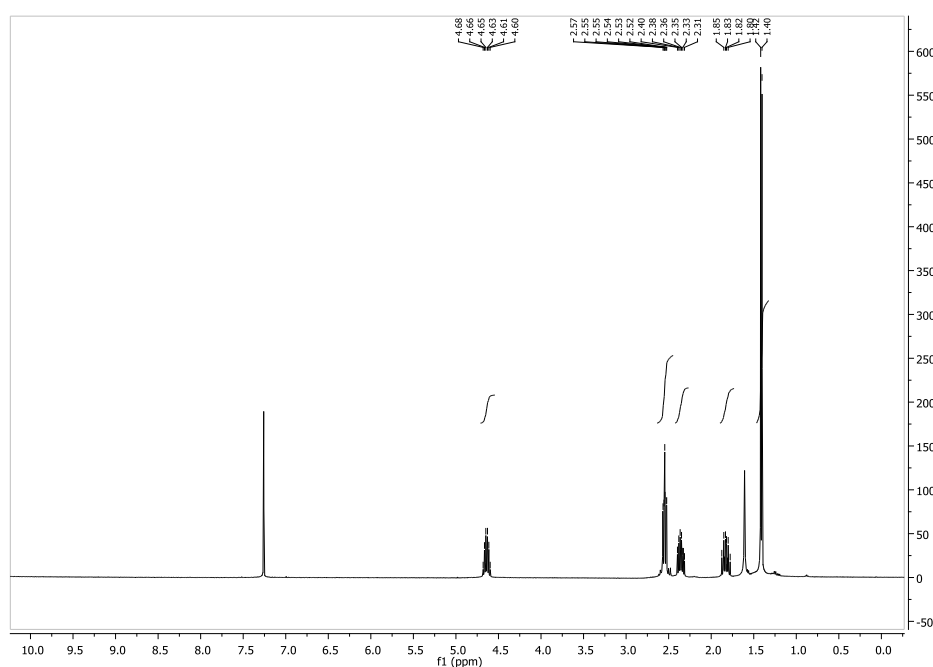


**Figure 2.22** <sup>1</sup>H NMR spectrum of crude GVL extracted after multiphasic LA hydrogenation in the presence of **IL3**.

### 2.5.9 Characterization of IL1-7

<sup>1</sup>H and <sup>13</sup>C NMR spectra of all ionic liquids were collected either neat at 60 °C on a Varian Unity 400 MHz spectrometer by locking the sample on DMSO-*d*<sub>6</sub> placed in a sealed capillary blocked in a coaxial position by means of a Teflon insert in the NMR tube. Chemical shifts were reported in  $\delta$  values downfield from TMS. INADEQUATE experiments were used to assign all the <sup>13</sup>C-NMR signals in P<sub>8,8,8,1</sub>[CH<sub>3</sub>OCOO] and N<sub>8,8,8,1</sub>[CH<sub>3</sub>OCOO], HMBC experiments were used to assign the peak of residual MeOH in the same samples, and HMQC to assign all <sup>1</sup>H peaks based on the correlation with the <sup>13</sup>C signals. The <sup>13</sup>C satellites were used, where possible, as internal standards to calculate the amount of impurities<sup>60</sup>. Since however the <sup>1</sup>H NMR spectra were acquired in the neat phase, the vast majority of all the resonance bands was rather broad, making integration very tricky and subject to a large error. The absence of other signals

indicates, conservatively, that the purity of the onium salts was greater than 95%. Characterization data ( $^1\text{H}$  and  $^{13}\text{C}$  NMR) were in full agreement with those previously reported.<sup>37</sup>

**Tri-*n*-octylmethylammonium chloride**  $[(\text{C}_8\text{H}_{17})_3\text{NCH}_3]^+\text{Cl}^-$  ( $[\text{N}_{8,8,8,1}]\text{Cl}$ ) **IL1**  $^1\text{H}$  NMR (400 MHz,  $\text{CDCl}_3$ )  $\delta$  3.48 – 3.35 (m, 1H), 3.31 (s, 1H), 1.65 (s, 1H), 1.29 (dd, 5H,  $J = 22.7, 14.9$  Hz), 0.85 (t, 1H,  $J = 6.8$  Hz).  $^{13}\text{C}$  NMR (101 MHz,  $\text{CDCl}_3$ )  $\delta$  61.5 (3C,  $\text{C}_1$ ), 48.9 (1C,  $\text{N-CH}_3$ ), 31.6 (3C,  $\text{C}_6$ ), 29.07 (3C,  $\text{C}_5$ ), 28.94 (3C,  $\text{C}_4$ ), 26.30 (3C,  $\text{C}_3$ ), 22.49 (3C,  $\text{C}_7$ ), 22.40 (3C,  $\text{C}_2$ ), 13.95 (3C,  $\text{C}_8$ ).

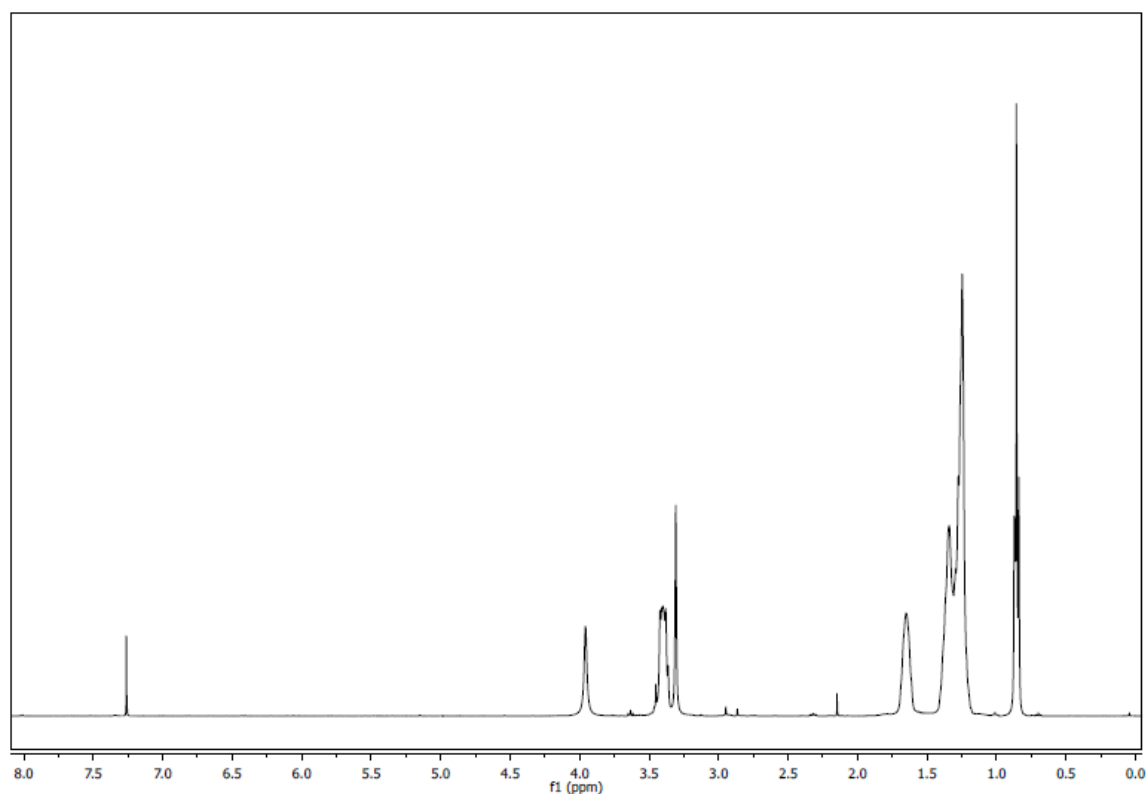


**Figure 2.23**  $^1\text{H}$ -NMR ( $\text{CDCl}_3$ , 400MHz) spectrum of compound **IL1**.

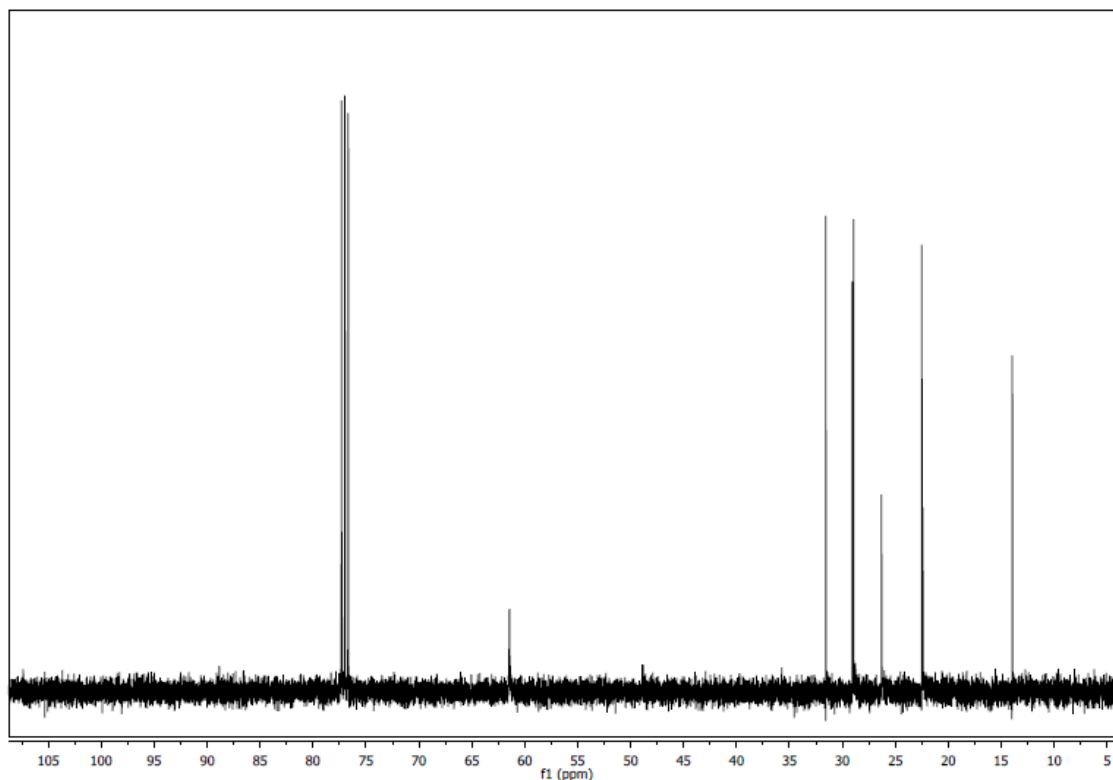


**Figure 2.24**  $^{13}\text{C}$ -NMR ( $\text{CDCl}_3$ , 100MHz) spectrum of compound **IL1**.

**Tri-*n*-octylmethylammoniumbis(trifluoromethane)sulfonimide**

$[(\text{C}_8\text{H}_{17})_3\text{NCH}_3]^+[\text{NTf}_2]^-$  ( $[\text{N}_{8,8,8,1}][\text{NTf}_2]$ ) **IL2**.  $^1\text{H}$ -NMR (neat, 60 °C, 400 MHz)  $\delta$  (ppm relative to TMS,  $\text{dmsO-d}_6$ ): 2.98 (b, 6H, N- $\text{CH}_2$ ), 2.73 (3H, N- $\text{CH}_3$ ), 1.45 (b, 6H), 1.12 (b, 6H), 1.07 (b, 24H), 0.67 (t, 9H,  $J = 7.2$  Hz);  $^{13}\text{C}\{^1\text{H}\}$  NMR (neat, 60 °C, 100 MHz)  $\delta$  (ppm relative to TMS,  $\text{dmsO-d}_6$ ): 119.1 (q, 1C,  $J_{\text{F-C}} = 322$  Hz,  $\text{CF}_3$ ), 60.8 (3C,  $\text{C}_1$ ), 46.9 (1C, N- $\text{CH}_3$ ), 30.5 (3C,  $\text{C}_6$ ), 27.8 (6C,  $\text{C}_5\text{-C}_4$ ), 25.0 (3C,  $\text{C}_3$ ), 21.4 (3C,  $\text{C}_7$ ), 21.0 (3C,  $\text{C}_2$ ), 12.6 (3C,  $\text{C}_8$ ) IR  $\nu_{\text{max}}$  neat/ $\text{cm}^{-1}$  2929, 2859, 1469, 1378, 1353.

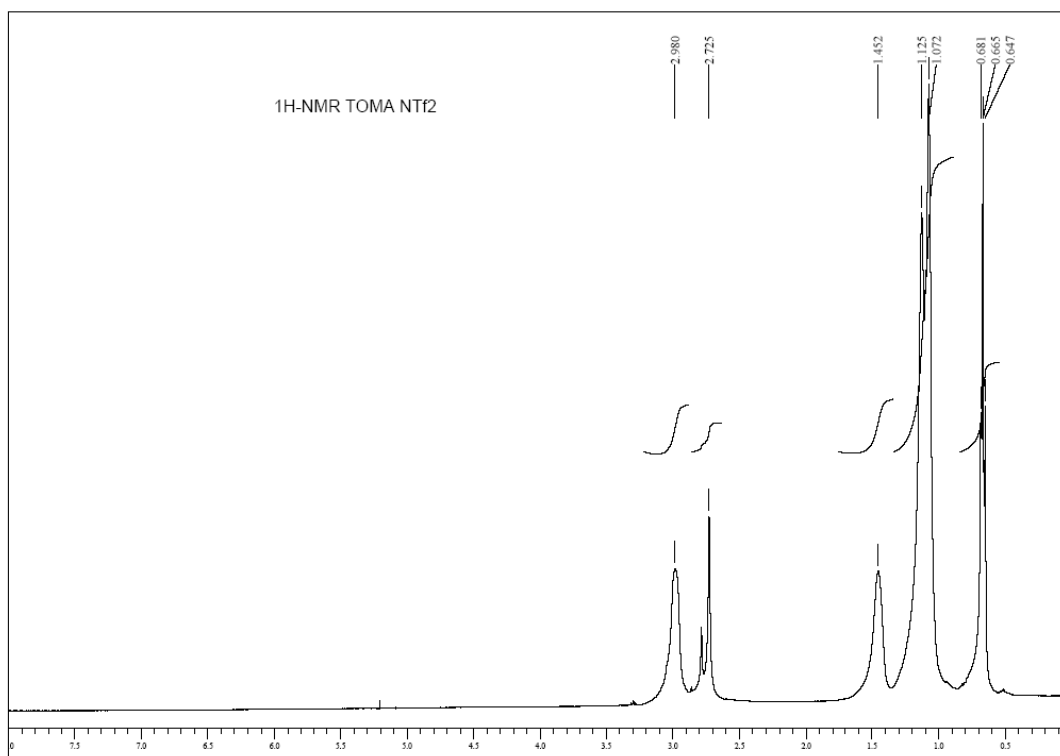


Figure 2.25 Neat  $^1\text{H-NMR}$  spectrum of compound **IL2**.

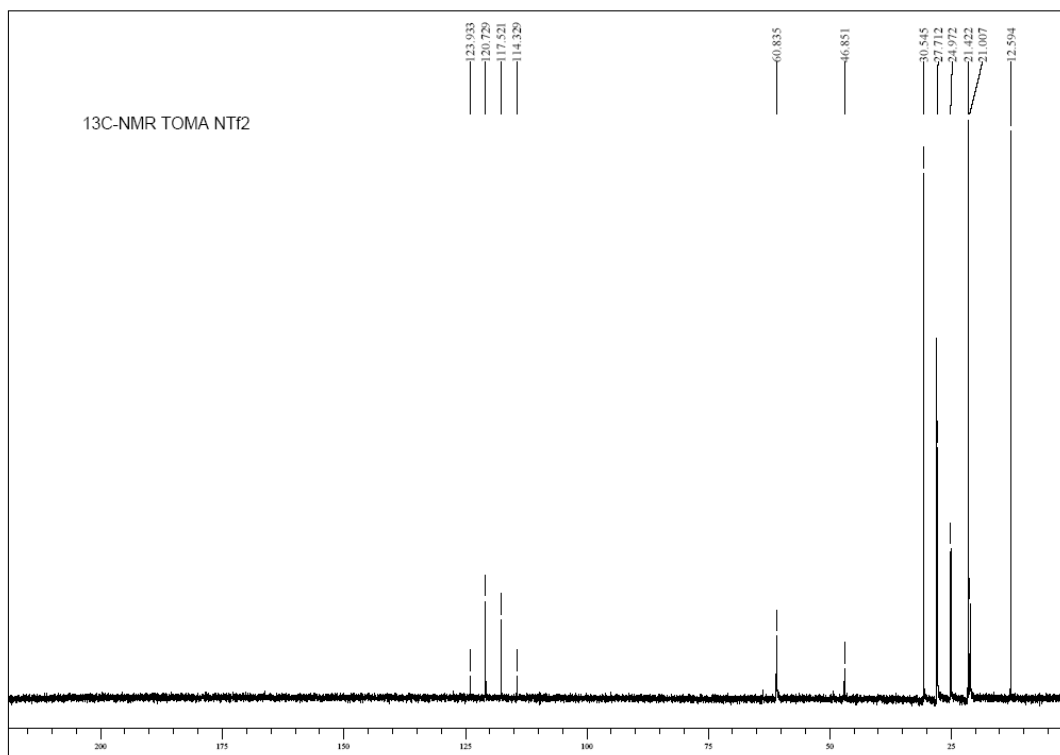
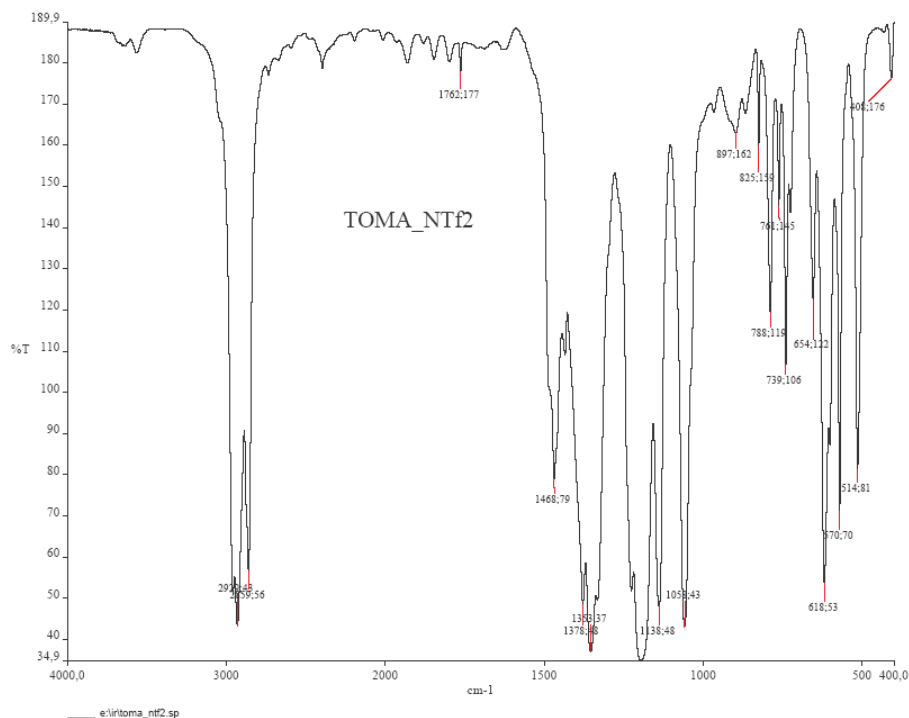


Figure 2.26 Neat  $^{13}\text{C-NMR}$  spectrum of compound **IL2**.





**Figure 2.27** IR spectrum of compound **IL2**.

**Tri-*n*-octylmethylphosphoniumbis(trifluoromethane)sulfonimide**

$[(C_8H_{17})_3PCH_3]^+[NTf_2]^-$  ( $[P_{8,8,8,1}][NTf_2]$ ) **IL3**.  $^1H$ -NMR (neat, 60 °C, 400 MHz)  $\delta$  (ppm relative to TMS, dms $o$ - $d_6$ ): 1.96 (b, 6H, P- $\underline{C}H_2$ ), 1.55 (d, 3H,  $J_{P-H} = 13$  Hz, P- $\underline{C}H_3$ ), 1.34 (b, 6H), 1.24 (b, 6H), 1.09 (b, 24H), 0.68 (bt, 9H);  $^{13}C\{^1H\}$  NMR (neat, 60 °C, 100 MHz)  $\delta$  (ppm relative to TMS, dms $o$ - $d_6$ ): 119.1 (q, 2C,  $J_{F-C} = 321$  Hz,  $\underline{C}F_3$ ), 30.6 (3C,  $C_6$ ), 29.3 (d, 3C,  $J_{P-C} = 15$  Hz,  $C_3$ ), 27.8 (3C,  $C_5$ ), 27.5 (3C,  $C_4$ ), 21.4 (3C,  $C_7$ ), 20.2 (d, 3C,  $J_{P-C} = 5$  Hz,  $C_2$ ), 19.0 (d, 3C,  $J_{P-C} = 48$  Hz,  $C_1$ ), 12.6 (C3,  $C_8$ ), 2.3 (d, 3C,  $J_{P-C} = 52$  Hz, P- $\underline{C}H_3$ ). IR  $\nu_{max}$  neat/ $cm^{-1}$  2930, 2859, 1468, 1352.

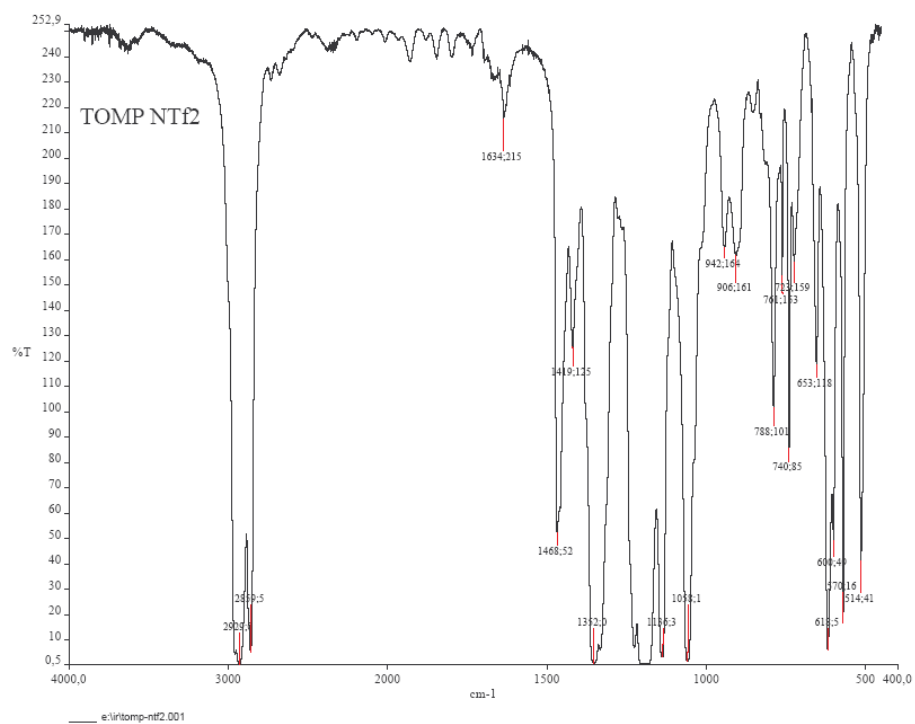


Figure 2.28 IR spectrum of compound IL3.

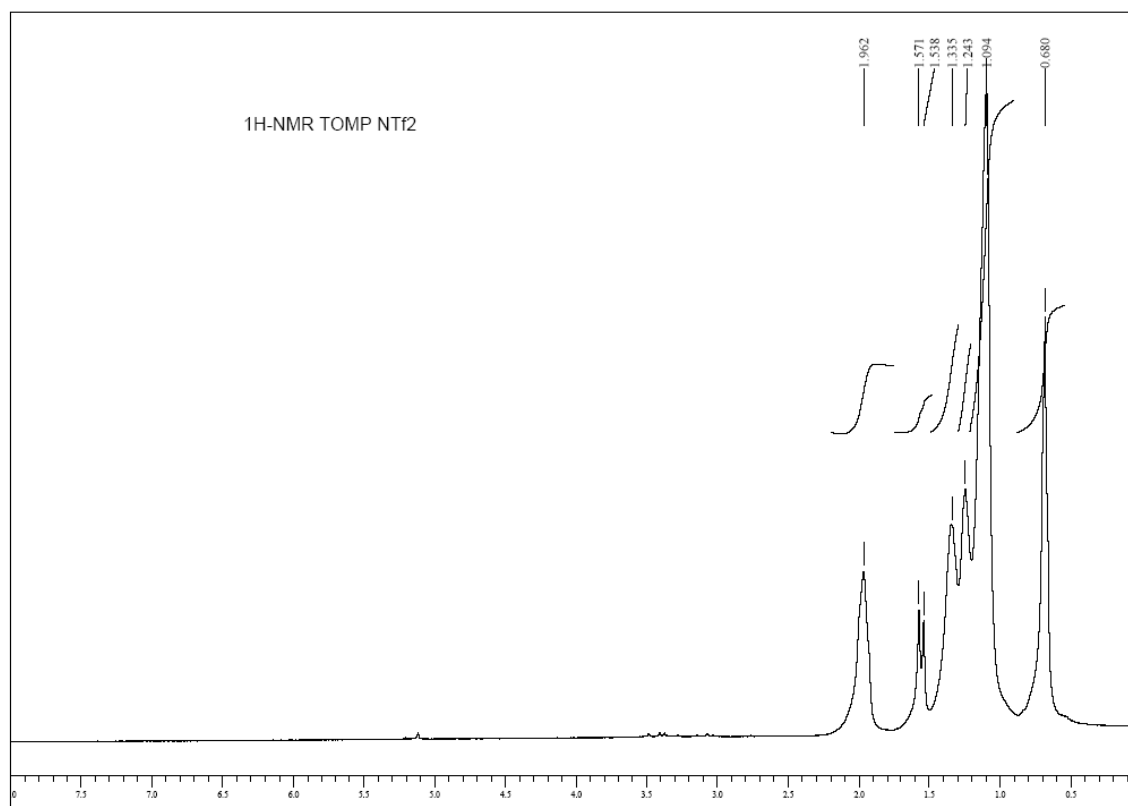


Figure 2.29 Neat <sup>1</sup>H-NMR spectrum of compound IL3.

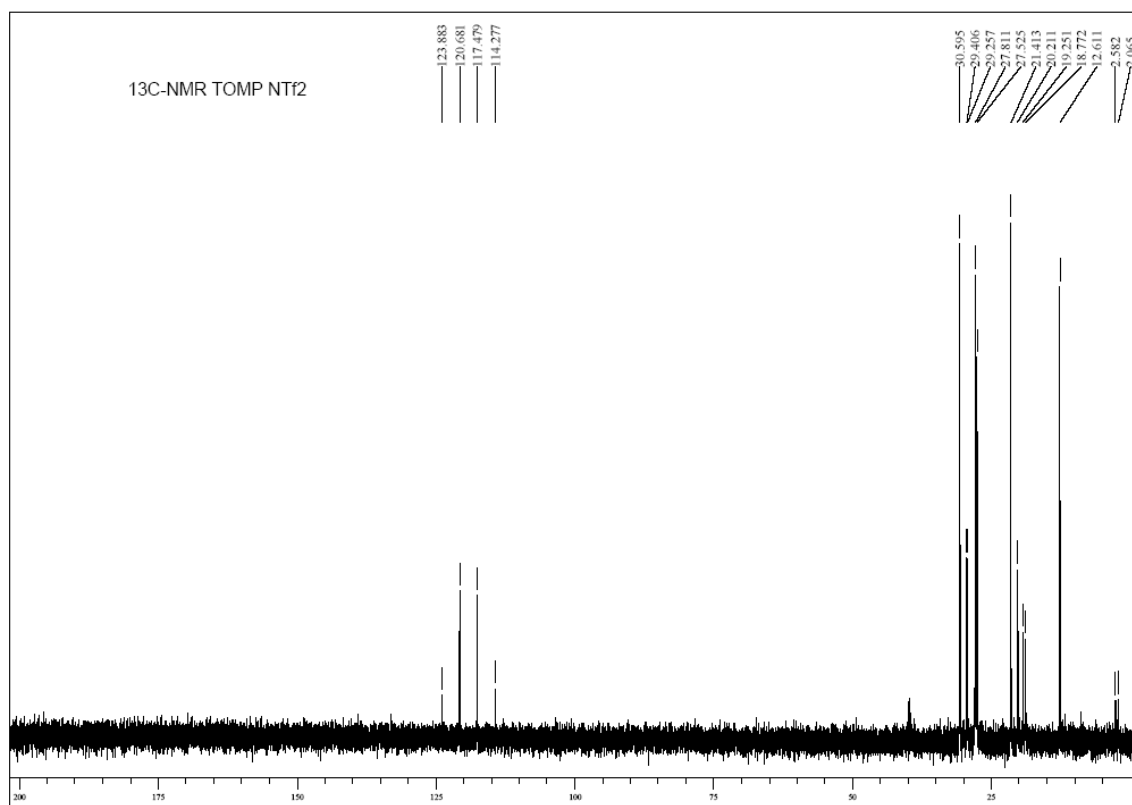


Figure 2.30 Neat  $^{13}\text{C}$ -NMR spectrum of compound IL3.

**Tri-*n*-octylmethylammoniumtrifluoroacetate**  $[(\text{C}_8\text{H}_{17})_3\text{NCH}_3]^+[\text{CF}_3\text{COO}]^-$   
**( $\text{N}_{8,8,8,1}[\text{CF}_3\text{COO}]$ ) ( $[\text{N}_{8,8,8,1}][\text{TFA}]$ ) IL4.**  $^1\text{H}$ -NMR (neat, 60 °C, 400 MHz)  $\delta$  (ppm relative to TMS, dms $o$ - $d_6$ ): 3.21 (b, 6H, N- $\text{CH}_2$ ), 3.00 (3H, N- $\text{CH}_3$ ), 1.51 (b, 6H), 1.14 (b, 6H), 1.09 (b, 24H), 0.68 (bt, 9H);  $^{13}\text{C}\{^1\text{H}\}$  NMR (neat, 60 °C, 100 MHz)  $\delta$  (ppm relative to TMS, dms $o$ - $d_6$ ): 158.2 (q, 1C,  $J_{\text{F-C}} = 31$  Hz,  $\text{C}=\text{O}$ ), 116.9 (q, 1C,  $J_{\text{F-C}} = 299$  Hz,  $\text{CF}_3$ ), 60.2 (3C,  $\text{C}_1$ ), 47.0 (1C, N- $\text{CH}_3$ ), 30.7 (3C,  $\text{C}_6$ ), 28.0 (3C,  $\text{C}_5$ ), 27.9 (3C,  $\text{C}_4$ ), 25.3 (3C,  $\text{C}_3$ ), 21.5 (3C,  $\text{C}_7$ ), 21.1 (3C,  $\text{C}_2$ ), 12.7 (3C,  $\text{C}_8$ ). IR  $\nu_{\text{max}}$  neat/ $\text{cm}^{-1}$  2900, 2858, 1688, 1378, 1199, 1170, 1125.

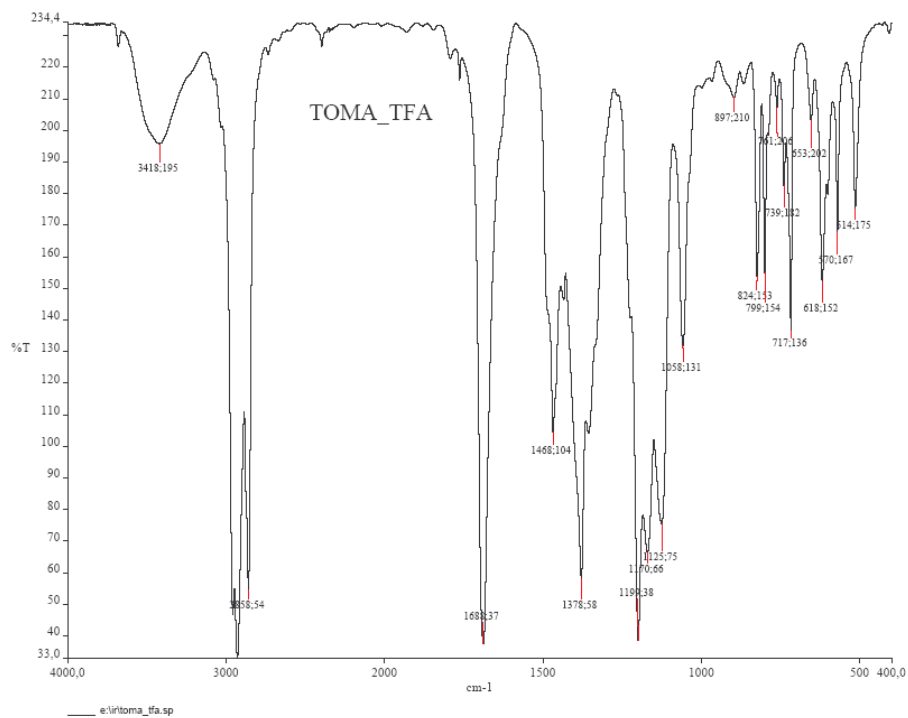


Figure 2.31 IR spectrum of compound IL4.

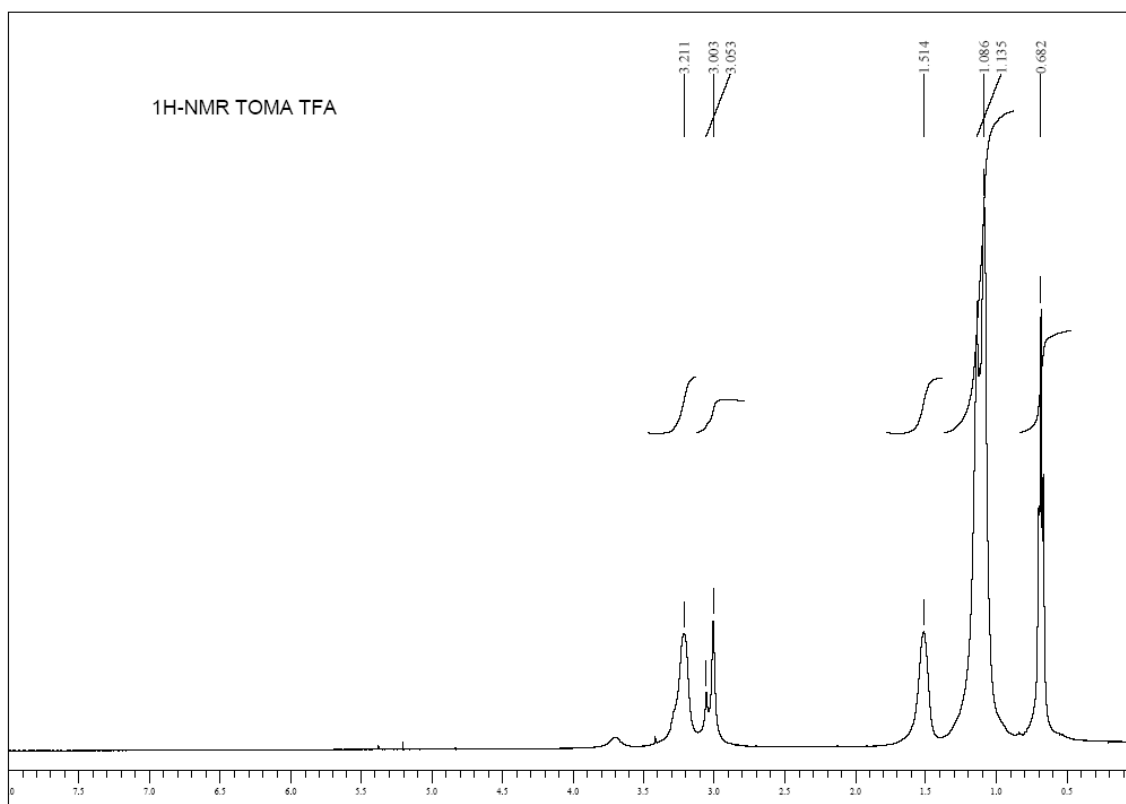


Figure 2.32 Neat <sup>1</sup>H-NMR spectrum of compound IL4.

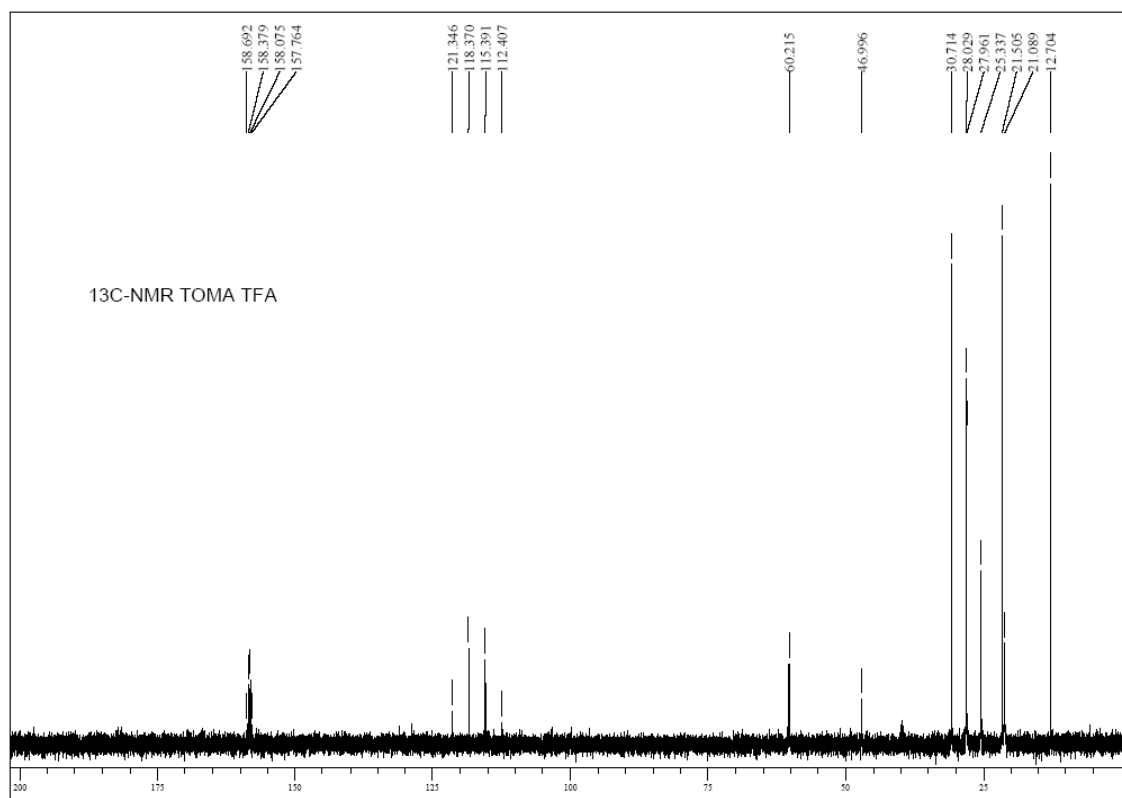


Figure 2.33 Neat  $^{13}\text{C}$ -NMR spectrum of compound IL4

**Tri-*n*-octylmethylphosphonium nitrate**  $[(\text{C}_8\text{H}_{17})_3\text{PCH}_3]^+[\text{NO}_3]^-$  ( $[\text{P}_{8,8,8,1}][\text{NO}_3]$ ) **IL5**.  
 $^1\text{H}$ -NMR (neat, 60 °C, 400 MHz)  $\delta$  (ppm relative to TMS, dms $\text{O-d}_6$ ): 2.25 (b, 6H; P- $\text{CH}_2$ ), 1.79 (d, 3H,  $J_{\text{P-H}} = 13$  Hz; P- $\text{CH}_3$ ), 1.43 (b, 6H), 1.26 (b, 6H), 1.11 (b, 24H), 0.70 (bt, 9H);  $^{13}\text{C}\{^1\text{H}\}$  NMR (neat, 60 °C, 100 MHz)  $\delta$  (ppm relative to TMS, dms $\text{O-d}_6$ ): 30.9 (3C,  $\text{C}_6$ ), 29.8 (d, 3C,  $J_{\text{P-C}} = 15$  Hz,  $\text{C}_3$ ), 28.1 (3C,  $\text{C}_5$ ), 28.0 (3C,  $\text{C}_4$ ), 21.7 (3C,  $\text{C}_7$ ), 20.5 (3C,  $\text{C}_2$ ), 19.0 (d, 3C,  $J_{\text{P-C}} = 49$  Hz,  $\text{C}_1$ ), 13.0 ( $\text{C}_3$ ,  $\text{C}_8$ ), 2.5 (d, 1C,  $J_{\text{P-C}} = 51$  Hz, P- $\text{CH}_3$ ). IR  $\nu_{\text{max}}$  neat/ $\text{cm}^{-1}$  2930, 2856, 1467, 1340.

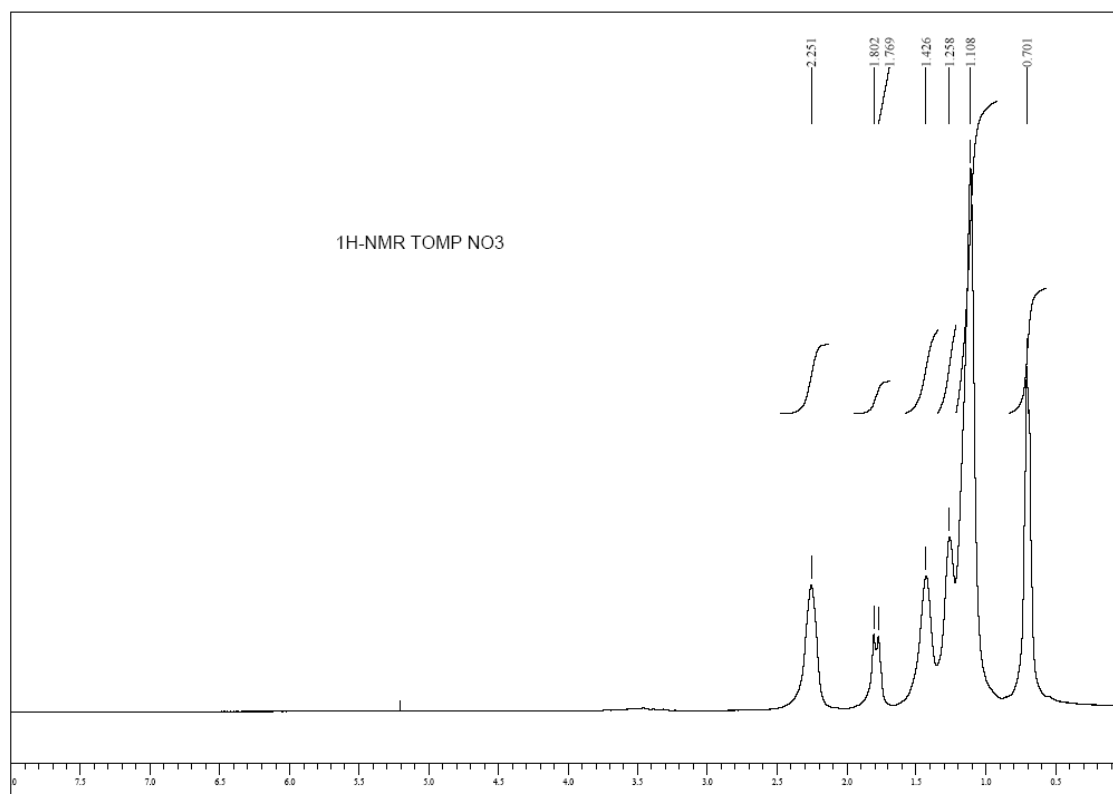


Figure 2.34 Neat  $^1\text{H-NMR}$  spectrum of compound IL5.

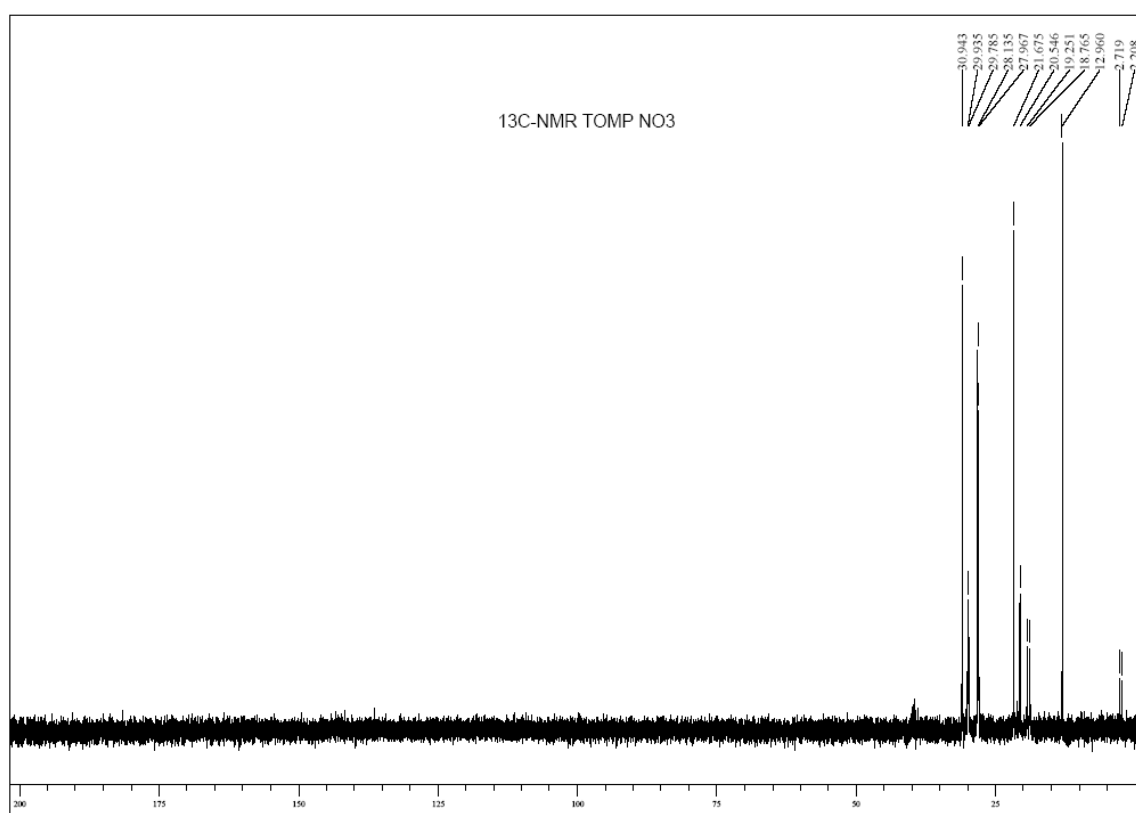
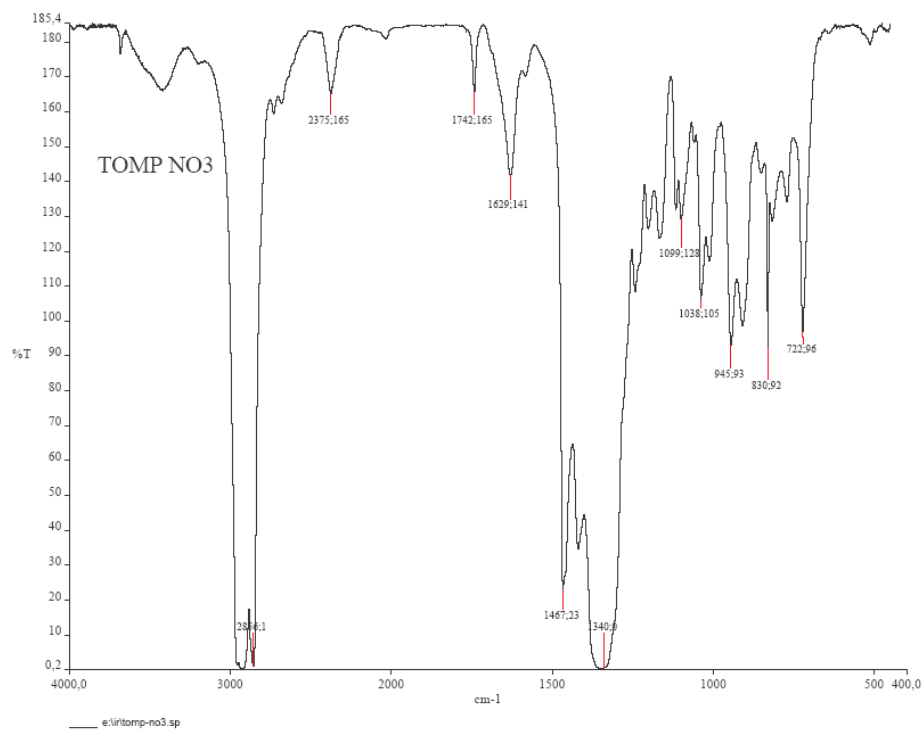


Figure 2.35 Neat  $^{13}\text{C-NMR}$  spectrum of compound IL5.



**Figure 2.36** IR spectrum of compound **IL5**.

**Tri-*n*-octylmethylammoniummethylcarbonate**  $[(C_8H_{17})_3NCH_3]^+[CH_3OCOO]^-$   
**([N<sub>8,8,8,1</sub>][CH<sub>3</sub>OCOO]) IL6.** (viscous clear yellow liquid)  $^1H$  NMR (neat, 60 °C, 400 MHz)  
 ( $\delta$ /ppm relative to TMS, dms<sub>o</sub>-d<sub>6</sub>): 3.36 (6H, N-CH<sub>2</sub>), 3.11 (6H, N-CH<sub>3</sub> and CH<sub>3</sub>O), 1.54 (b, 6H),  
 1.08 (b, 30H), 0.67 (9H);  $^{13}C\{^1H\}$  NMR (neat, 60 °C, 100 MHz):  $\delta$  (ppm relative to TMS,  
 dms<sub>o</sub>-d<sub>6</sub>, CH<sub>2</sub>'s assigned by 2D inadequate) 155.5 (1C, C=O), 59.9 (3C, C<sub>1</sub>), 50.0 (1C, CH<sub>3</sub>O),  
 46.8 (1C, N-CH<sub>3</sub>), 30.9 (3C, C<sub>6</sub>), 28.2 (6C, C<sub>5</sub>-C<sub>4</sub>), 25.7 (3C, C<sub>3</sub>), 21.6 (3C, C<sub>7</sub>), 21.3 (3C, C<sub>2</sub>),  
 12.8 (3C, C<sub>8</sub>). IR  $\nu_{max}$  neat/cm<sup>-1</sup> 2900, 2857, 1669.

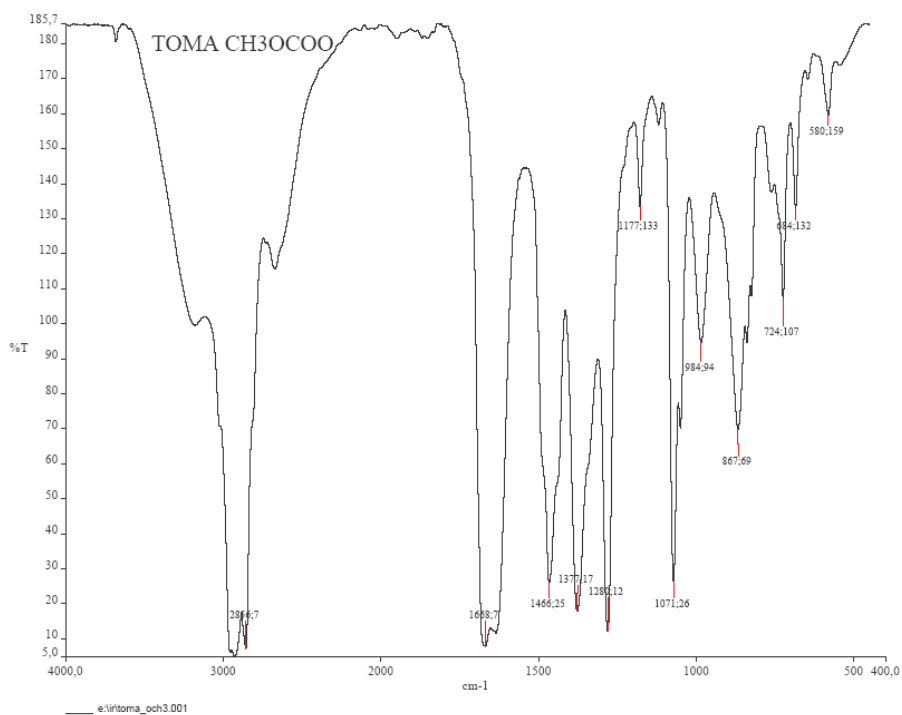


Figure 2.37 IR spectrum of compound IL6.

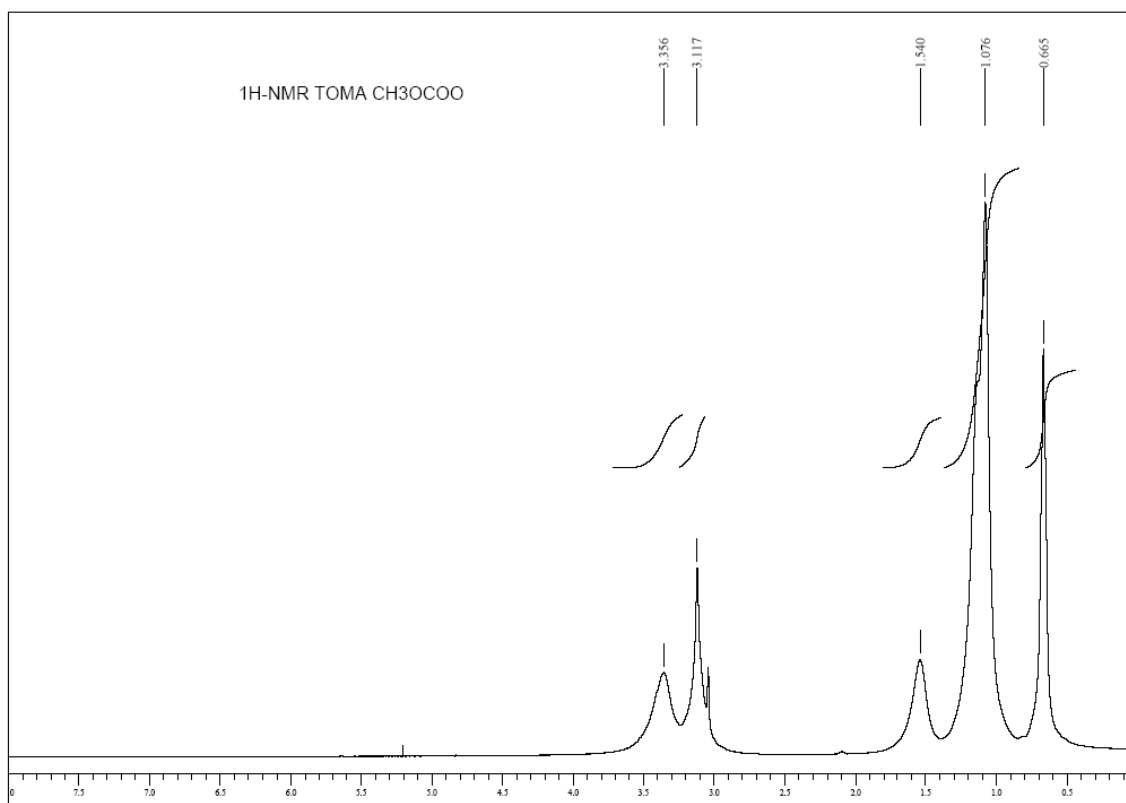


Figure 2.38 Neat <sup>1</sup>H-NMR spectrum of compound IL6.



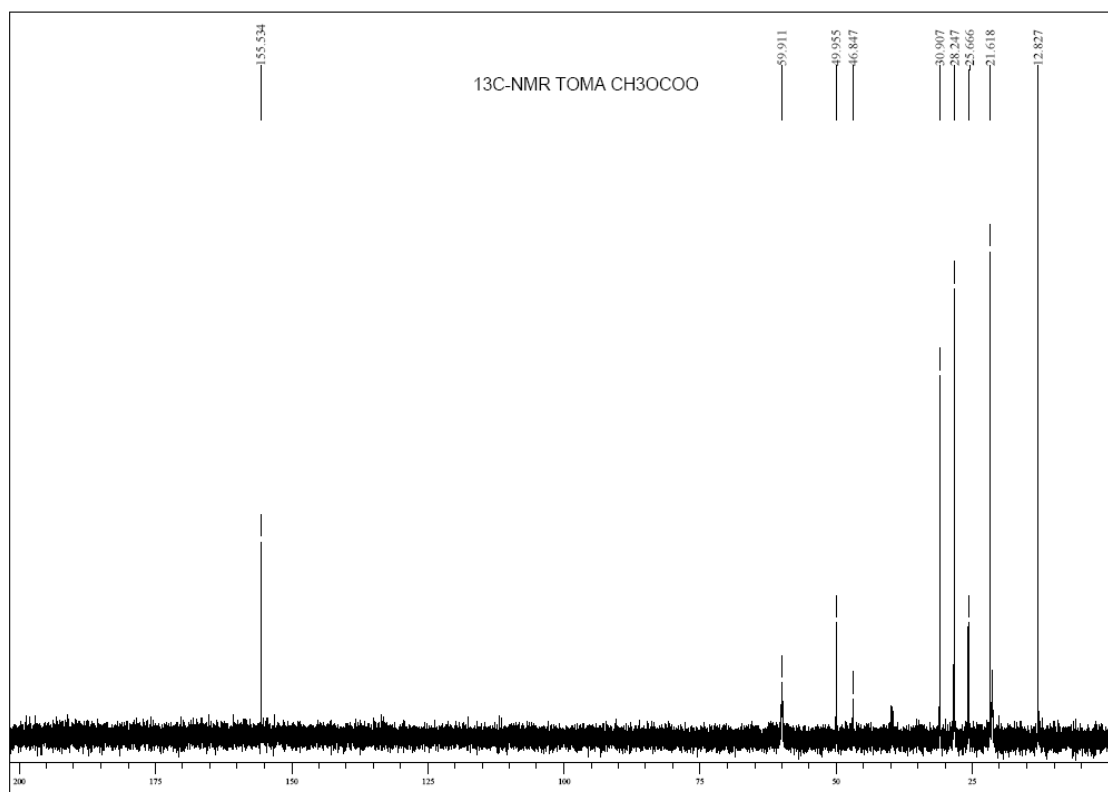


Figure 2.39 Neat  $^{13}\text{C}$ -NMR spectrum of compound IL6.

**Tri-*n*-octylmethylphosphoniummethylcarbonate**  $[(\text{C}_8\text{H}_{17})_3\text{PCH}_3]^+[\text{CH}_3\text{OCOO}]^-$   
**( $[\text{P}_{8,8,8,1}][\text{CH}_3\text{OCOO}]$ ) IL7.** (viscous clear colourless liquid)  $^1\text{H}$ -NMR (neat, 60 °C, 400 MHz)  $\delta$  (ppm relative to TMS,  $\text{dms}\text{-d}_6$ ): 3.15 (s, 3H,  $\text{CH}_3\text{OCOO}$ ), 2.33 (bt, 6H, P- $\text{CH}_2$ ), 1.88 (d, 3H,  $J_{\text{P-H}} = 14$  Hz, P- $\text{CH}_3$ ), 1.42 (b, 6H), 1.27 (b, 6H), 1.11 (b, 24H), 0.70 (bt, 9H);  $^{13}\text{C}\{^1\text{H}\}$  NMR (neat, 60 °C, 100 MHz) ( $\delta$ /ppm relative to TMS,  $\text{dms}\text{-d}_6$ ,  $\text{CH}_2$ 's assigned by 2D inadequate): 155.8 (1C,  $\text{C}=\text{O}$ ), 50.0 (1C,  $\text{CH}_3\text{O}$ ), 30.9 (3C,  $\text{C}_6$ ), 29.9 (d, 3C,  $J_{\text{P-C}} = 15$  Hz,  $\text{C}_3$ ), 28.2 (3C,  $\text{C}_5$ ), 28.0 (3C,  $\text{C}_4$ ), 21.6 (3C,  $\text{C}_7$ ), 20.7 (d, 3C,  $J_{\text{P-C}} = 4$  Hz,  $\text{C}_2$ ), 19.0 (d, 3C,  $J_{\text{P-C}} = 48$  Hz,  $\text{C}_1$ ), 12.8 (3C,  $\text{C}_8$ ), 2.6 (d, 3C,  $J_{\text{P-C}} = 53$  Hz, P- $\text{CH}_3$ ). IR  $\nu_{\text{max}}$  neat/ $\text{cm}^{-1}$  2900, 2856, 1669.

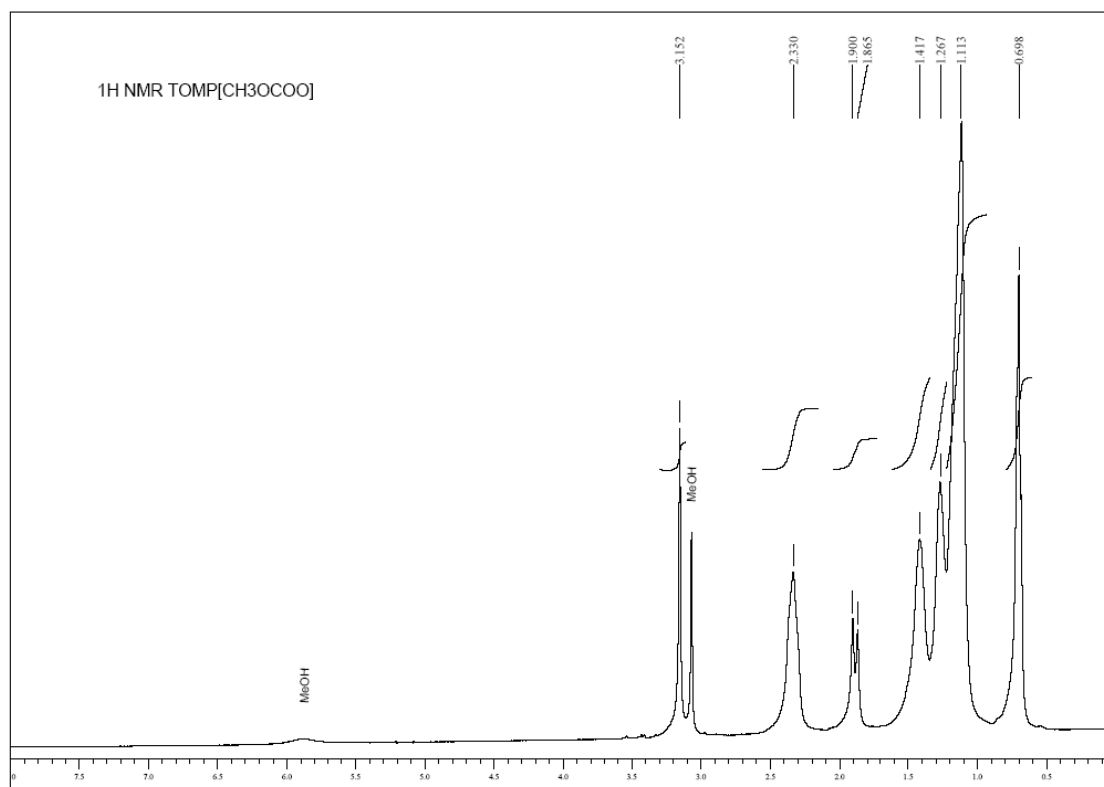


Figure 2.40 Neat  $^1\text{H}$ -NMR spectrum of compound **IL7**.

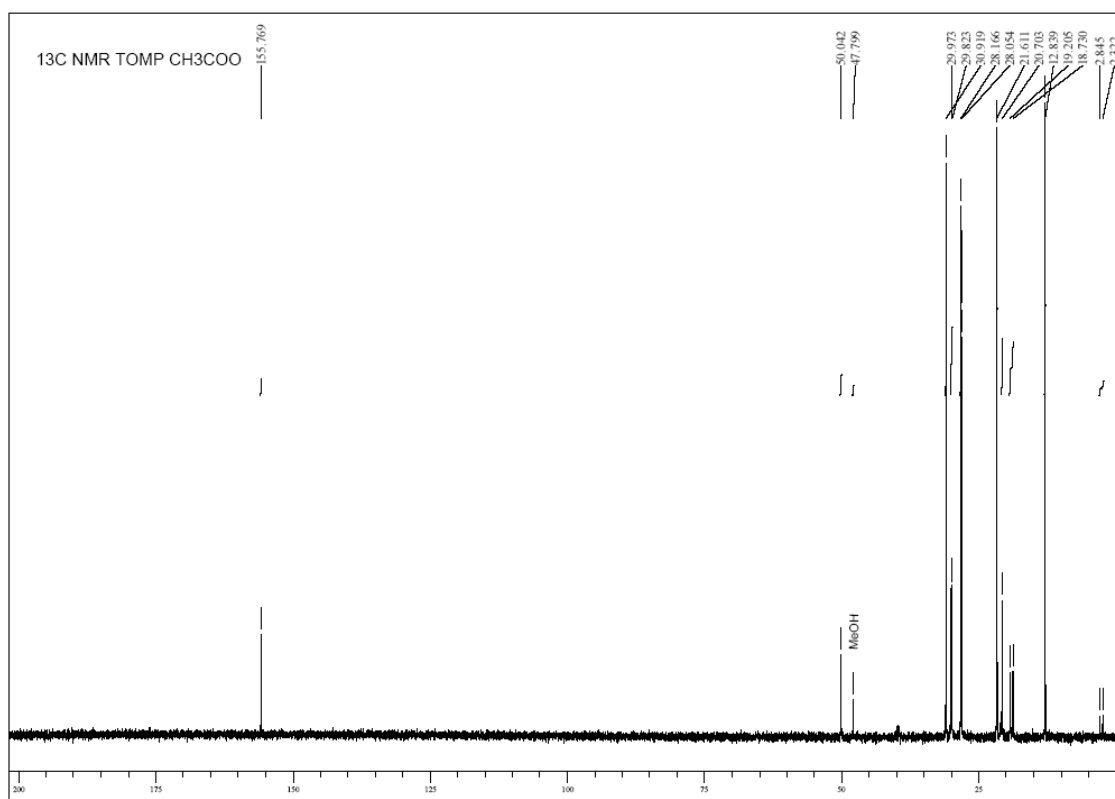


Figure 2.41 Neat  $^{13}\text{C}$ -NMR spectrum of compound **IL7**.

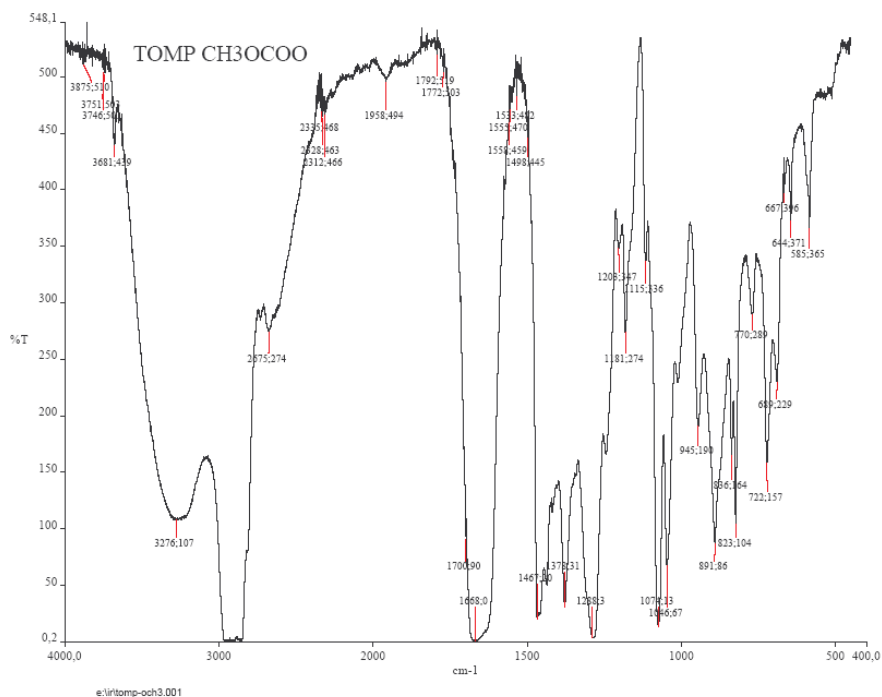


Figure 2.42 IR spectrum of compound IL7.

### 2.5.10 Preparation of Ru metallic mirrors

A mixture of RuCl<sub>3</sub> (4 mg, 0.019 mmol), [N<sub>8,8,8,1</sub>][NTf<sub>2</sub>] (850 mg, 1.358 mmol), H<sub>2</sub>O (4.4 mL), isooctane (4.4 mL) and levulinic acid (810  $\mu$ L, 7.875 mmol) was added to the above described glass tubular reactor and stirred. The tube was placed in the above described autoclave which was then pressurized up to 35 atm with H<sub>2</sub>, and heated at 150 °C for 16 h, with vigorous stirring. The autoclave was then cooled to room temperature, and the residual gases were vented. At the end of the reaction, the inner walls of the reactor are covered by a layer of ruthenium mirror in correspondence to the portion of the wall which has been wetted by the fluid during the reaction. The structure of Ru mirror after the reaction was examined by transmission electron microscopy.

### 2.5.11 Characterization of Ru-nanoparticles and Ru mirror

The structure of Ru catalyst after the reaction in the multiphase system using [N<sub>8,8,8,1</sub>]Cl and the structure of Ru mirror were examined by transmission electron microscopy (TEM). TEM measurements were performed using a JEM 3010 (JEOL) electron microscope operating at 300 kV; the lens parameters were Cs = 0.6 mm, Cc = 1.3 mm, giving a point resolution of 0.17 nm at

Scherzer defocus. TEM samples of Ru-NPs adsorbed in [N<sub>8,8,8,1</sub>]Cl were prepared by sonicating a drop of the ionic liquid phase containing the catalyst for 5 min in order to disrupt possible agglomerates, transferring a 5  $\mu$ L droplet of suspension onto an amorphous carbon film, coating a 200 mesh copper grid, drying at room temperature, and then placing into the microscope.

The samples of Ru mirror were prepared by scraping off from the surface of the glass reactor a portion of the solid, transferring it onto an amorphous carbon film, coating a 200 mesh copper grid, and then placing into the microscope.

## 2.6 References

- (a) Schuette, H. A.; Thomas, R. W., *J. Am. Chem. Soc.* **1930**, *52*, 3010-3012; (b) Christian, R. V.; Brown, H. D.; Hixon, R. M., *J. Am. Chem. Soc.* **1947**, *69*, 1961-1963; (c) Leonard, R. H., *Ind. Eng. Chem.* **1956**, *48*, 1330-1341; (d) Broadbent, H. S.; Campbell, G. C.; Bartley, W. J.; Johnson, J. H., *J. Org. Chem.* **1959**, *24*, 1847-1854; (e) V. Timokhin, B.; A. Baransky, V.; D. Eliseeva, G., *Russ. Chem. Rev.* **1999**, *68*, 73-84.
- Manzer, L. E., *Appl. Cat. A: Gen.* **2004**, *272*, 249-256.
- (a) Manzer, L. E. US6617464, 2003; (b) Manzer, L. E.; Hutchenson, W. W. US6946563 2005; (c) Bourne, R. A.; Stevens, J. G.; Ke, J.; Poliakoff, M., *Chem. Commun.* **2007**, *0*, 4632-4634.
- Yan, Z.-p.; Lin, L.; Liu, S., *Energy Fuels* **2009**, *23*, 3853-3858.
- Deng, L.; Li, J.; Lai, D.-M.; Fu, Y.; Guo, Q.-X., *Angew. Chem. Int. Ed.* **2009**, *48*, 6529-6532.
- Geilen, F. M. A.; Engendahl, B.; Harwardt, A.; Marquardt, W.; Klankermayer, J.; Leitner, W., *Angew. Chem. Int. Ed.* **2010**, *49*, 5510-5514.
- (a) Mehdi, H.; Fábos, V.; Tuba, R.; Bodor, A.; Mika, L.; Horváth, I., *Top. Catal.* **2008**, *48*, 49-54; (b) Horvath, I. T.; Mehdi, H.; Fabos, V.; Boda, L.; Mika, L. T., *Green Chem.* **2008**, *10*, 238-242.
- Galletti, A. M. R.; Antonetti, C.; De Luise, V.; Martinelli, M., *Green Chem.* **2012**, *14*, 688-694.
- Hückel, H., *Chem. Ber.* **1958**, *91*, XIX-LXVI.
- Plechkova, N. V.; Seddon, K. R., *Chem. Soc. Rev.* **2008**, *37*, 123-150.
- Welton, T., *Chem. Rev.* **1999**, *99*, 2071-2084.
- Earle, M. J. E.; J. M. S. S.; Gilea, M.A.; Lopes, J.N.C.; Rebelo, L.P.N., Magee, J.W.; Seddon, K.R., *Nature* **2006**, *439*.
- Gordon, C. M.; Muldoon, M. J., "Ionic Liquids in Synthesis" in *Ionic Liquids in Synthesis*, Wiley-VCH Verlag, 2008.
- Seddon, K. R., *Journal of Chemical Technology & Biotechnology* **1997**, *68*, 351-356.
- (a) López-Martin, I.; Burello, E.; Davey, P. N.; Seddon, K. R.; Rothenberg, G., *ChemPhysChem* **2007**, *8*, 690-695; (b) Seddon, K. R., *Kinet. Catal.* **1996**, *37*.
- (a) Abdul-Sada, A. a. K.; Greenway, A. M.; Hitchcock, P. B.; Mohammed, T. J.; Seddon, K. R.; Zora, J. A., *J. Chem. Soc., Chem. Commun.* **1986**, *0*, 1753-1754; (b) Fannin, A. A. K., L.A.; Levisky, J.A.; Wilkes, J.S., *J. Phys. Chem.* **1984**, *88*; (c) Avent, A. G.; Chaloner, P. A.; Day, M. P.; Seddon, K. R.; Welton, T., *J. Chem. Soc., Dalton Trans.* **1994**, *0*, 3405-3413; (d) van den Berg, J.-A.; Seddon, K. R., *Cryst. Growth Des.* **2003**, *3*, 643-661; (e) B. Aakeroy, C.; A. Evans, T.; R. Seddon, K.; Palinko, I., *New J. Chem.* **1999**, *23*, 145-152.
- (a) Favre, F.; Olivier-Bourbigou, H.; Commereuc, D.; Saussine, L., *Chem. Commun.* **2001**, *0*, 1360-1361; (b) Dupont, J.; Fonseca, G. S.; Umpierre, A. P.; Fichtner, P. F. P.; Teixeira, S. R., *J. Am. Chem. Soc.* **2002**, *124*, 4228-4229; (c) Dyson, P. J.; Geldbach, T. J., *Metal Catalysed Reactions in Ionic Liquids*. Springer 2005; (d) Tundo, P.; Perosa, A., *Chem. Soc. Rev.* **2007**, *36*, 532-550.
- (a) Perosa, A.; Tundo, P.; Selva, M.; Canton, P., *Chem. Commun.* **2006**, *0*, 4480-4482; (b) Cornils, B., *Multiphase Homogenous Catalysis*. Wiley-VCH: 2005; (c) Perosa, A.; Tundo, P.; Selva, M.; Zinovyev, S.; Testa, A., *Org. Biomol. Chem.* **2004**, *2*, 2249-2252; (d) Paganelli, S.; Perosa, A.; Selva, M., *Adv. Synth. Catal.* **2007**, *349*, 1858-1862; (e) Perosa, A.; Tundo, P.; Selva, M., *J. Mol. Catal. A: Chem.* **2002**, *180*, 169-175.
- (a) Marques, C. A.; Selva, M.; Tundo, P., *J. Org. Chem.* **1993**, *58*, 5256-5260; (b) Marques, C. A.; Selva, M.; Tundo, P., *J. Chem. Soc., Perkin Trans. 1* **1993**, *0*, 529-533; (c)

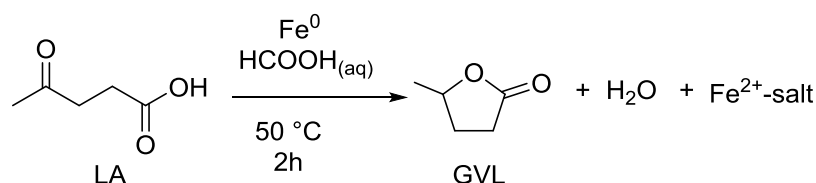
- Marques, C. A.; Selva, M.; Tundo, P., *J. Org. Chem.* **1994**, *59*, 3830-3837; (d) Tundo, P.; Perosa, A.; Selva, M.; Zinovyev, S. S., *Appl. Cat. B: Environ.* **2001**, *32*, L1-L7.
20. (a) Marques, C. A.; Selva, M.; Tundo, P., *J. Org. Chem.* **1995**, *60*, 2430-2435; (b) Marques, C. A.; Rogozhnikova, O.; Selva, M.; Tundo, P., *J. Mol. Catal. A: Chem.* **1995**, *96*, 301-309; (c) Bomben, A.; Marques, C. A.; Selva, M.; Tundo, P., *Synthesis* **1996**, *1996*, 1109-1114; (d) Selva, M.; Tundo, P.; Perosa, A., *J. Org. Chem.* **1998**, *63*, 3266-3271.
21. (a) Youn, D. H.; Bae, G.; Ham, D. J.; Lee, J. S., *Appl. Cat. A: Gen.* **2011**, *393*, 309-316; (b) Jessop, P. G.; Joó, F.; Tai, C.-C., *Coord. Chem. Rev.* **2004**, *248*, 2425-2442; (c) Hao, C.; Wang, S.; Li, M.; Kang, L.; Ma, X., *Catal. Today* **2011**, *160*, 184-190.
22. Joó, F., *ChemSusChem* **2008**, *1*, 805-808.
23. (a) Hyde, J. R.; Poliakoff, M., *Chem. Commun.* **2004**, *0*, 1482-1483; (b) Zhang, J.; Blazeczka, P. G.; Bruendl, M. M.; Huang, Y., *J. Org. Chem.* **2008**, *74*, 1411-1414.
24. Zhou, X.; Huang, Y.; Xing, W.; Liu, C.; Liao, J.; Lu, T., *Chem. Commun.* **2008**, *0*, 3540-3542.
25. (a) Loges, B.; Boddien, A.; Junge, H.; Beller, M., *Angew. Chem. Int. Ed.* **2008**, *47*, 3962-3965; (b) Junge, H.; Boddien, A.; Capitta, F.; Loges, B.; Noyes, J. R.; Gladiali, S.; Beller, M., *Tetrahedron Lett.* **2009**, *50*, 1603-1606; (c) Fellay, C.; Dyson, P. J.; Laurenczy, G., *Angew. Chem. Int. Ed.* **2008**, *47*, 3966-3968; (d) Gan, W.; Dyson, P.; Laurenczy, G., *React. Kinet. Catal. Lett.* **2009**, *98*, 205-213; (e) Himeda, Y., *Green Chem.* **2009**, *11*, 2018-2022.
26. Fellay, C.; Yan, N.; Dyson, P. J.; Laurenczy, G., *Chem. Eur. J.* **2009**, *15*, 3752-3760.
27. (a) Fukuzumi, S.; Kobayashi, T.; Suenobu, T., *ChemSusChem* **2008**, *1*, 827-834; (b) Morris, D. J.; Clarkson, G. J.; Wills, M., *Organometallics* **2009**, *28*, 4133-4140.
28. Haan, R. J.; Lange, J. P.; Petrus, L. WO2007099111, 2007.
29. Ogo, S.; Abura, T.; Watanabe, Y., *Organometallics* **2002**, *21*, 2964-2969.
30. Fegyverneki, D.; Orha, L.; Láng, G.; Horváth, I. T., *Tetrahedron* **2010**, *66*, 1078-1081.
31. Heeres, H.; Handana, R.; Chunai, D.; Borromeus Rasrendra, C.; Girisuta, B.; Jan Heeres, H., *Green Chem.* **2009**, *11*, 1247-1255.
32. Deng, L.; Zhao, Y.; Li, J.; Fu, Y.; Liao, B.; Guo, Q.-X., *ChemSusChem* **2010**, *3*, 1172-1175.
33. (a) Serrano-Ruiz, J. C.; Braden, D. J.; West, R. M.; Dumesic, J. A., *Appl. Cat. B: Environ.* **2010**, *100*, 184-189; (b) Upare, P. P.; Lee, J.-M.; Hwang, D. W.; Halligudi, S. B.; Hwang, Y. K.; Chang, J.-S., *J. Ind. Eng. Chem.* **2011**, *17*, 287-292.
34. Dunlop, A. P. M., J. W. US2786852 (A), 1957.
35. March, J., *Advanced organic chemistry: reactions, mechanisms, and structure*. Wiley: 1992.
36. Serrano-Ruiz, J. C.; Wang, D.; Dumesic, J. A., *Green Chem.* **2010**, *12*, 574-577.
37. Fabris, M.; Lucchini, V.; Noè, M.; Perosa, A.; Selva, M., *Chem. Eur. J.* **2009**, *15*, 12273-12282.
38. Kim, Y. J.; Varma, R. S., *J. Org. Chem.* **2005**, *70*, 7882-7891.
39. (a) Blake, P. G.; Davies, H. H.; Jackson, G. E., *J. Chem. Soc. B* **1971**, *0*, 1923-1925; (b) Bjerre, A. B.; Soerensen, E., *Ind. Eng. Chem. Res.* **1992**, *31*, 1574-1577; (c) Saito, K.; Kakumoto, T.; Kuroda, H.; Torii, S.; Imamura, A., *J. Chem. Phys.* **1984**, *80*, 4989-4996.
40. Prasad, K.; Jiang, X.; Slade, J. S.; Clemens, J.; Repič, O.; Blacklock, T. J., *Adv. Synth. Catal.* **2005**, *347*, 1769-1773.
41. (a) Perosa, A.; Tundo, P.; Zinovyev, S., *Green Chem.* **2002**, *4*, 492-494; (b) Tundo, P.; Perosa, A.; Zinovyev, S., *J. Mol. Catal. A: Chem.* **2003**, *204-205*, 747-754; (c) Tundo, P.; Perosa, A., *React. Funct. Polym.* **2003**, *54*, 95-101; (d) Zinovyev, S. S.; Perosa, A.; Tundo, P., *J. Catal.* **2004**, *226*, 9-15.
42. Selva, M.; Tundo, P., *Tetrahedron Lett.* **2003**, *44*, 8139-8142.
43. Gattow, G.; Behrendt, W., *Angew. Chem., Int. Ed. Engl.* **1972**, *11*, 534-535.

44. (a) Foropoulos, J.; DesMarteau, D. D., *Inorg. Chem.* **1984**, *23*, 3720-3723; (b) DesMarteau, D. D.; Lu, C., *J. Fluorine Chem.* **2007**, *128*, 1326-1334; (c) Pitula, S.; Mudring, A.-V., *Chem. Eur. J.* **2010**, *16*, 3355-3365.
45. Zinovyev, S.; Perosa, A.; Yufit, S.; Tundo, P., *J. Catal.* **2002**, *211*, 347-354.
46. Anastas, P. T. P., A.; Selva M., *Handbook of Green Chemistry, Volume 8, Green Processes, Green Nanoscience*. Wiley-VCH Weinheim, 2012; Vol. Volume 8.
47. Fonseca, G. S.; Umpierre, A. P.; Fichtner, P. F. P.; Teixeira, S. R.; Dupont, J., *Chem. Eur. J.* **2003**, *9*, 3263-3269.
48. Scheeren, C. W.; Domingos, J. B.; Machado, G.; Dupont, J., *The Journal of Physical Chemistry C* **2008**, *112*, 16463-16469.
49. Rossi, L.; Machado, G.; Fichtner, P. P.; Teixeira, S.; Dupont, J., *Catal. Lett.* **2004**, *92*, 149-155.
50. Umpierre, A. P.; Machado, G.; Fecher, G. H.; Morais, J.; Dupont, J., *Adv. Synth. Catal.* **2005**, *347*, 1404-1412.
51. Vollmer, C.; Janiak, C., *Coord. Chem. Rev.* **2011**, *255*, 2039-2057.
52. (a) Scheeren, C. W.; Machado, G.; Dupont, J.; Fichtner, P. F. P.; Teixeira, S. R., *Inorg. Chem.* **2003**, *42*, 4738-4742; (b) Silveira, E. T.; Umpierre, A. P.; Rossi, L. M.; Machado, G.; Morais, J.; Soares, G. V.; Baumvol, I. J. R.; Teixeira, S. R.; Fichtner, P. F. P.; Dupont, J., *Chem. Eur. J.* **2004**, *10*, 3734-3740.
53. (a) Itoh, H.; Naka, K.; Chujo, Y., *J. Am. Chem. Soc.* **2004**, *126*, 3026-3027; (b) Zhao, D.; Fei, Z.; Ang, W. H.; Dyson, P. J., *Small* **2006**, *2*, 879-883.
54. Bell, W. C.; Myrick, M. L., *J. Colloid Interface Sci.* **2001**, *242*, 300-305.
55. Braude, E. A.; Nachod, F. C.; Zuckerman, J. J., *Determination of Organic Structures by Physical Methods*. Academic Press: 1955.
56. (a) Daguinet, C.; Dyson, P. J., *Catal. Commun.* **2003**, *4*, 153-157; (b) Dorfling, C.; Akdogan, G.; Bradshaw, S. M.; Eksteen, J. J., *Hydrometallurgy* **2013**, *138*, 21-32; (c) Yuan, G.; Keane, M. A., *Appl. Cat. B: Environ.* **2004**, *52*, 301-314.
57. (a) Hartnig, C.; Griminger, J.; Spohr, E., *J. Electroanal. Chem.* **2007**, *607*, 133-139; (b) Hu, C.; Ting, S.-W.; Chan, K.-Y.; Huang, W., *Int. J. Hydrogen Energy* **2012**, *37*, 15956-15965.
58. (a) Gómez-Bombarelli, R.; Calle, E.; Casado, J., *J. Org. Chem.* **2013**, *78*, 6868-6879; (b) Gómez-Bombarelli, R.; Calle, E.; Casado, J., *J. Org. Chem.* **2013**, *78*, 6880-6889.
59. (a) Omari, K. W.; Besaw, J. E.; Kerton, F. M., *Green Chem.* **2012**, *14*, 1480-1487; (b) Mitsudome, T.; Noujima, A.; Mizugaki, T.; Jitsukawa, K.; Kaneda, K., *Green Chem.* **2009**, *11*, 793-797.
60. Cassol, C. C.; Ebeling, G.; Ferrera, B.; Dupont, J., *Adv. Synth. Catal.* **2006**, *348*, 243-248.

### 3 The Bio-Inspired Reduction of Cyclohexanone and Levulinic Acid using an Iron/Acid System Coupled to the Electrocatalytic Regeneration of Active Iron Species

#### 3.1 Foreword

Fabos and coworkers<sup>1</sup> have recently demonstrated that several aldehydes and ketones could be hydrogenated to the corresponding alcohols by using metallic iron in aqueous acidic solutions, mostly containing formic or sulfuric acid. A remarkable example was the reaction of levulinic acid that proceeded with conversions of 38% and 12% in the presence of  $\text{H}_2\text{SO}_4$  and  $\text{HCOOH}$ , respectively (Scheme 3.1).

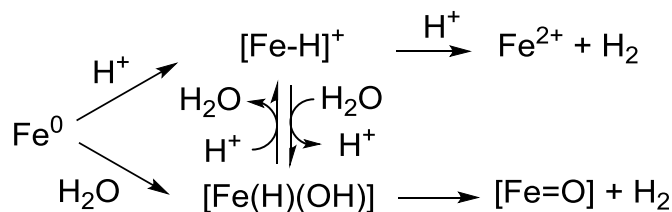


**Scheme 3.1** Example of hydrogenation reaction using an acidic aqueous solution in the presence of metallic iron

The contact of formic acid with metallic iron produced some gaseous hydrogen, interestingly; though, the exact mechanism of this process is still uncertain.

In the absence of organic substrates, previous investigations of the behavior of  $\text{Fe}^0$  in aqueous acidic solutions suggest the initial formation of iron-hydrides from which the subsequent generation of hydrogen takes place (Scheme 3.2). The same iron-hydrides were, therefore, considered as potential hydrogenating agents for the reduction of ketones such as cyclohexanone or LA: in other words, it was postulated that molecular hydrogen was not necessarily liberated before the reaction of the organic acid, but that the hydride could be an active species in the reduction of organics. Whatever the mechanism, iron, formic acid and water must be present in equimolar amounts, meaning that the process needs a stoichiometric quantity of iron. Under such conditions, the overall procedure is not only difficult to apply, but it is also not economically viable.<sup>1</sup>





**Scheme 3.2** Proposed mechanism for the formation of transient reducing iron-hydride species.<sup>1a</sup>

However, if a simple way for the reduction of  $\text{Fe}^{2+}$  (produced during the hydrogenation reaction) back to  $\text{Fe}^0$  could be devised, the use of the metal would be switched from stoichiometric to catalytic with great benefits, not only on the exploitation of starting materials and minimization of wastes, but also from the perspective of the possible implementation on a larger scale.

The general idea of this recovery and re-use of oxidised metal ions is bio-inspired as per the mechanism of action of metalloenzymes in nature. Consider for example, the remarkable case of hemoglobin devoted to oxygen transportation in the human blood: the global efficiency of such a metalloprotein relies on inorganic co-factors where  $\text{Fe}^{2+}/\text{Fe}^{3+}$  ions coordinated to porphyrin rings, are able to rapidly interconvert into each other.<sup>2</sup> The acidity of the environment plays a crucial role in maintaining the metal in the proper oxidation state (Bohr effect).<sup>3</sup>

With the same reasoning, the formic acid- $\text{Fe}^0$  redox couple employed for LA hydrogenation could become a natural mimic system, just by considering  $\text{Fe}^0$  as a co-factor that needs to be in this oxidation state to perform its function. In this study, the determining parameter that governs the regeneration of the active iron state is the electric potential, i.e. we aim to continuously regenerate the co-factor by electrochemical means.

## 3.2 Introduction

### 3.2.1 Iron

Iron is one of the most common and cheapest metals on earth.<sup>4</sup> The pure metal, however, is almost never found as such; most of the naturally occurring iron is present in minerals from which it is extracted by oxidation-reduction treatments carried out in a blast furnace.

Iron readily dissolves in dilute acids; it may exist in aqueous solution either in the divalent, ferrous, or the trivalent, ferric, state. In oxygenated water, ferrous iron is oxidized to ferric iron. The rate of this oxidation has been shown to be primarily dependent upon the pH and the

temperature of the solution. Soluble ferrous iron occurs mainly in the form of the following complex ions:  $[\text{Fe}(\text{H}_2\text{O})_6]^{2+}$ ,  $[\text{Fe}(\text{H}_2\text{O})_5(\text{OH})]^+$  and  $[\text{Fe}(\text{H}_2\text{O})_3(\text{OH})_3]^-$ .<sup>5</sup>

For the behavior of metals in aqueous solutions, one of the most important contributions found in the literature is the potential-pH Pourbaix diagram (Figure 3.1). This is a graphical representation of thermodynamic and electrochemical equilibria between a metal and water, illustrating the simultaneous influence of pH and electrons on the equilibria of aqueous iron.<sup>6</sup>

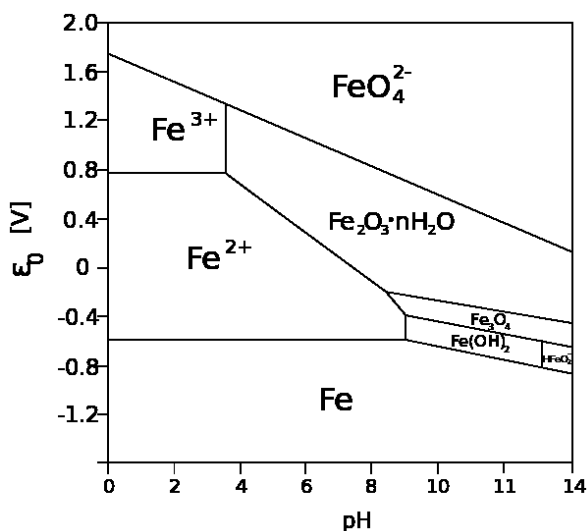


Figure 3.1 Potential-pH equilibrium Pourbaix diagram for the system iron-water at 25°C<sup>6</sup>

### 3.2.2 Electrochemical studies

The preliminary investigation on the electrochemical behavior of a system is usually carried out by experiments that sweep the potential with time, recording directly the current-potential curve. The potential is often varied linearly with time using conventional electrodes that allow voltage ramps ranging from 10 mV/s to about 1000 mV/s. Under such conditions, the current as a function of potential is obviously equivalent to the current versus time: therefore, the formal name of this experimental method is *linear potential sweep chronoamperometry*, also known as *linear sweep voltammetry* (LSV). One of the most used voltammetric techniques is the reverse technique *cyclic voltammetry* (CV), which takes the experiment a step further than linear sweep voltammetry, which ends the potential ramp when it reaches a set potential. When linear sweep voltammetry reaches a set potential, the potential scan of the working electrode is inverted. This inversion can happen multiple times during a single experiment. The technique of CV has become popular for initial electrochemical studies of new systems and has proven to be very valuable in obtaining information about electrode reactions.

Overall, investigations and results achieved by the potential sweep methods turn out to be useful to plan and develop experiments of *bulk electrolysis*(BE), *i.e.* exhaustive electrolysis. Unlike LSV and CV techniques that may be both carried out over long time periods without appreciable changes of the concentrations of the analytes, the bulk electrolysis considerably alters the composition of the solution. BE, in fact, is generally characterized by a large electrode area to solution volume ratio to allow effective mass-transfer conditions, large currents and time scales in the order of minutes or hours. During a controlled-potential (potenziostatic) bulk electrolysis (CPE) experiment, the working electrode potential is maintained constant with respect to reference electrode and the current is monitored. The auxiliary electrode has to be stable, carefully placed to provide a fairly uniform current distribution across the surface of the working electrode, and to minimize uncompensated resistance effects. For that reason, the auxiliary electrode is often positioned in a separate compartment isolated from the working compartment by a separator (a sintered-glass disk, ion exchange membrane, etc.).<sup>7</sup> These details will be clarified later this chapter.

### 3.2.3 Aim of the research

The purpose of this study has been the recovery and re-use of iron in the aqueous phase by electrolytical methods able to set up a clean and economically viable reduction of the  $\text{Fe}^{2+}$  (produced during the hydrogenation of organics) to recover the iron promoter (or co-factor)  $\text{Fe}^0$  and to make the reaction into an overall (electro)catalytic transformation. The reaction investigated has been the simple cathodic deposition:  $\text{Fe}^{2+} + 2\text{e}^- \rightarrow \text{Fe}^0$  (Standard Electrode Potentials in Aqueous Solutions at 25°C vs. NHE,  $E^0 = -0.44 \text{ V}$ ).<sup>7</sup>

For this analysis, the aforementioned techniques cyclic voltammetry, linear sweep – anodic stripping voltammetry and bulk electrolysis have been utilized.

Figure 3.2 reports a schematic representation of the hypothetical electrochemical(E)-chemical(C) process, where iron recovery process, occurring by bulk electrolysis, makes the reaction into an overall electrocatalytic transformation.

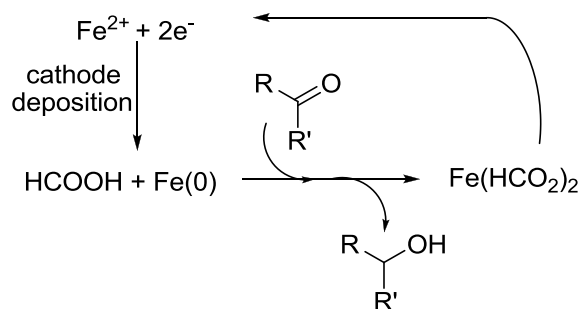


**Figure 3.2**  $\text{Fe}^0$ -promoted hydrogenation of levulinic acid and cyclohexanone in aqueous  $\text{FeSO}_4/\text{HCOOH}$  solution

In the *results and discussion* section, theoretical concepts associated with the interpretation of the data obtained are examined according to each of the techniques employed.

### 3.3 Cyclic voltammetric studies

The main byproducts of the reaction of  $\text{Fe}^0$  with sulfuric or formic acid during the hydrogenation reaction of ketones and aldehydes are iron sulfate and iron formate, respectively.<sup>1</sup> Therefore, in order to investigate the electrochemical recovery of iron in the exhausted hydrogenation mixture, two model systems (A and B) were prepared by dissolving iron sulfate in acidic aqueous solution of both formic and sulfuric acids. Iron sulfate was chosen for two reasons: *i*) iron was predominantly present in the form of bivalent cations ( $\text{Fe}^{2+}$  in ferrous sulfate); *ii*) it was more stable than iron formate in acidic solutions. In particular, 1-100 mM iron sulfate aqueous solutions were 1-100 mM and 1-10 mM with respect to formic and sulfuric acid, respectively. All the samples were prepared with 0.1 M  $\text{Na}_2\text{SO}_4$  as supporting electrolyte.

The supporting electrolyte (SE) is a substance added to the electrochemical cell that dissociates into charged particles and allows the transfer of the charge throughout the solution. The main factors that dictate the choice of the suitable supporting electrolyte include: *i*) solubility (it should be soluble in the solvent of choice at reasonable high concentration  $\sim 0.1$  M), *ii*) electrochemical inertness in the potential window exploited (it must be inert, i.e. not reactive with any component of the electrochemical cell including the solvent, the analyte or the electrodes), and *iii*) high conductivity. The ionic strength of the supporting electrolyte solution is generally two order of magnitude larger than the concentration of the analyte and, in the case of CV, the migration of the analyte to the electrodes is diffusion controlled.<sup>7</sup> Other effects of the presence of SE are the decrease of the cell resistance and of the matrix effects.

#### 3.3.1 Cyclic voltammetry experiments

As mentioned above, cyclic voltammetry (CV) is a simple, rapid, and powerful method to characterize analytes that can be electrochemically oxidized or reduced.<sup>8</sup> For this reason, CV was chosen for the initial screening to determine the characteristic potentials of the two investigated iron systems (A and B: aq.  $\text{FeSO}_4/\text{H}_2\text{SO}_4$  and aq.  $\text{FeSO}_4/\text{HCOOH}$ , respectively).<sup>9</sup> In particular, the experiments were aimed at the evaluation of the deposition potential and the onset of the hydrogen reduction reaction in the cathodic window.

### 3.3.1.1 Preliminary experiments

#### Hydrogen evolution at glassy carbon electrode

In the presence of glassy carbon electrodes, CV investigations of aqueous solutions may produce  $H_2$  or  $O_2$  due to water electrolysis (Scheme 3.3).<sup>10</sup>



**Scheme 3.3** Water electrolysis reactions

The cathodic reaction is the proton reduction to hydrogen and the anodic one is the water oxidation to oxygen.

In order to distinguish the hydrogen evolution from iron deposition at vitreous carbon, a set of blank CV experiments was performed in the absence of the ferrous salt. For example, in a 1 mM formic acid solution, the hydrogen evolution reaction occurred at about -1400 mV (Figure 3.3 left); while, in a 1 mM sulfuric acid solution, the same process took place at about -1800 mV (Figure 3.3 left). These tests established the onset of the hydrogen evolution reaction. Accordingly, the potential range of the solvent cathodic window was found for the present system.

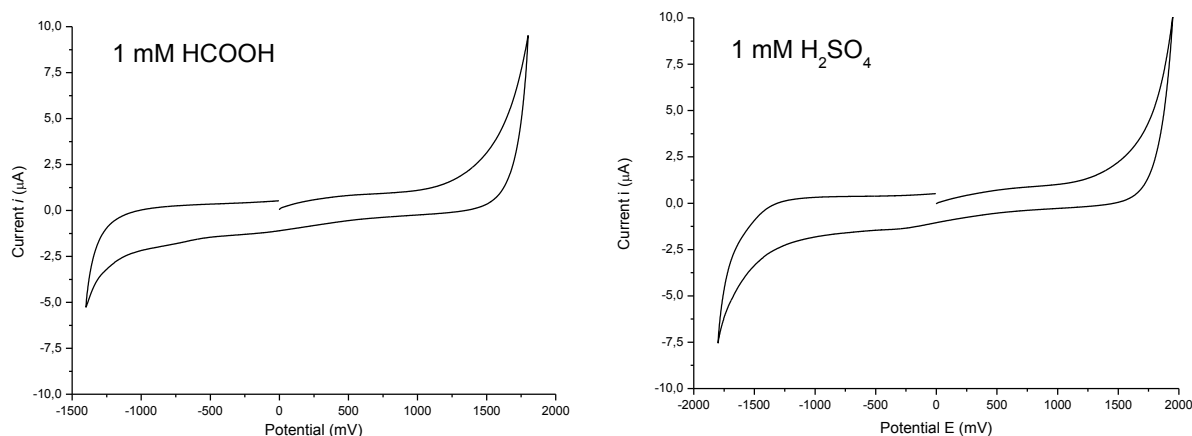
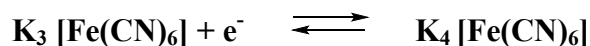


**Figure 3.3 (left)** CV of 1 mM formic acid/100mM sodium sulfate (blank); **(right)** CV of 1 mM sulfuric acid/100mM sodium sulfate (blank).

#### Measurements of the Electroactive Area

In order to characterize the  $Fe^{2+/3+}$  electron transfer process, the diffusion coefficient ( $D$ ) of the analyte must be determined. This, in turn, requires that the electrode surface area is known.

The surface area of the electrode was determined by the mass transfer method<sup>11</sup> using the following reaction:



Experiments were carried out in a solution of 1 mM potassium ferricyanide as the probe analyte, which D value is known, and 0.1 M potassium chloride as the supporting electrolyte. Deionized water was the solvent. Cyclic voltammograms were recorded from -1000 to 1300 mV (vs Ag/AgCl) by varying the scan rate. The cathodic currents were recorded in the forward sweep and corrected for the background current by the BASinc software. The anodic currents in the reverse sweep were not used, because the correction for the background current was not reliable. The square root of the scan rates was plotted against the peak cathodic currents and linearly fitted. The surface area was calculated using the slope of the plot and the Randles-Sevcik equation (1).

The *Randles-Sevcik* equation describes the effect of scan rate on the peak current at room temperature:<sup>7, 12</sup>

$$i_p = 2.69 \times 10^5 z^{3/2} A D^{1/2} C v^{1/2} \quad (1)$$

In the Randles-Sevcik equation,  $i_{\text{peak}}$  is the peak cathodic current in the voltammogram,  $z$  the number of moles of electrons transferred per mole of analyte (one for the  $[\text{Fe}(\text{CN})_6]^{3-/4-}$  couple),  $F$  the Faraday constant ( $\text{C} \times \text{mol}^{-1}$ ),  $A$  the surface area of the electrode ( $\text{cm}^2$ ),  $C$  the concentration of the analyte ( $\text{mol} \times \text{cm}^{-3}$ ),  $v$  the sweep rate ( $\text{V} \times \text{s}^{-1}$ ),  $D$  the diffusion coefficient of the analyte (taken as  $7.26 \times 10^{-6} \text{ cm}^2 \times \text{s}^{-1}$  for the  $[\text{Fe}(\text{CN})_6]^{3-}/[\text{Fe}(\text{CN})_6]^{4-}$  couple in aqueous KCl media at room temperature,<sup>13</sup>  $R$  the universal gas constant ( $\text{J} \times \text{mol}^{-1} \times \text{K}^{-1}$ ), and  $T$  the temperature (K).

Figure 3.4 left illustrates the cyclic voltammograms recorded at different scan rates (50, 100, 250, 500, 1000 mV/s). The related plot of the forward peak current as a function of the square root of the scan rate is presented in Figure 3.4 right.

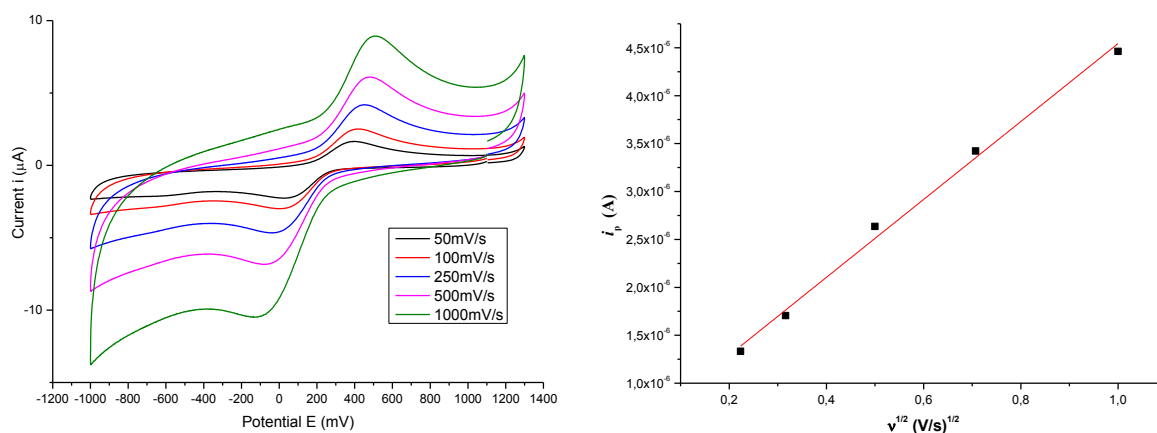


**Figure 3.4 (left)** CVs of  $[\text{Fe}(\text{CN})_6]^{3-}/[\text{Fe}(\text{CN})_6]^{4-}$  system with different scan rates. **(right)** The dependence of the reduction peak current of the  $[\text{Fe}(\text{CN})_6]^{3-}/[\text{Fe}(\text{CN})_6]^{4-}$  couple on the square root of the scan rate for the iron species.

The slope of the linear fit of  $i_p$  vs  $v^{1/2}$  was equal to  $2.69 \times 10^5 n^{3/2} AD^{1/2} C$ . This allowed the calculation of an electrode area ( $A_{\text{exp}}$ ) for the glassy carbon electrode of:

$$A_{\text{exp}} = B / (2.69 \times 10^5 z^{3/2} (7.26 \times 10^{-6})^{1/2} C v^{1/2}) = 0.01 \text{ cm}^2$$

#### Determination of the Diffusion Coefficient for the $[\text{Fe}(\text{OH}_2)_6]^{2-}/[\text{Fe}(\text{OH}_2)_6]^{3-}$ couple

The effect of the scan rate on the peak current for the redox reaction  $[\text{Fe}(\text{OH}_2)_6]^{2+} \rightleftharpoons [\text{Fe}(\text{OH}_2)_6]^{3+} + e^-$  at glassy carbon electrode was investigated for both aq.  $\text{FeSO}_4/\text{H}_2\text{SO}_4$  and aq.  $\text{FeSO}_4/\text{HCOOH}$  systems. The anodic peak at about 900 mV and a cathodic peak at about 100 mV were assigned to the redox couple  $\text{Fe}^{2+}/\text{Fe}^{3+}$ . This process is present in every CV experiment of iron sulfate systems here studied at almost constant values of potential; however it is of secondary importance for the investigation of iron deposition, so it is exploited only at this point for the determination of the diffusion coefficient.

Figure 3.5 left and Figure 3.6 left illustrates the cyclic voltammograms recorded at different scan rates (50, 100, 250, 500, 1000 mV/s). The related plot of the forward peak current as a function of the square root of the scan rate is presented in Figure 3.5 right and Figure 3.6 right.



### A. Formic acid system (1 mM):

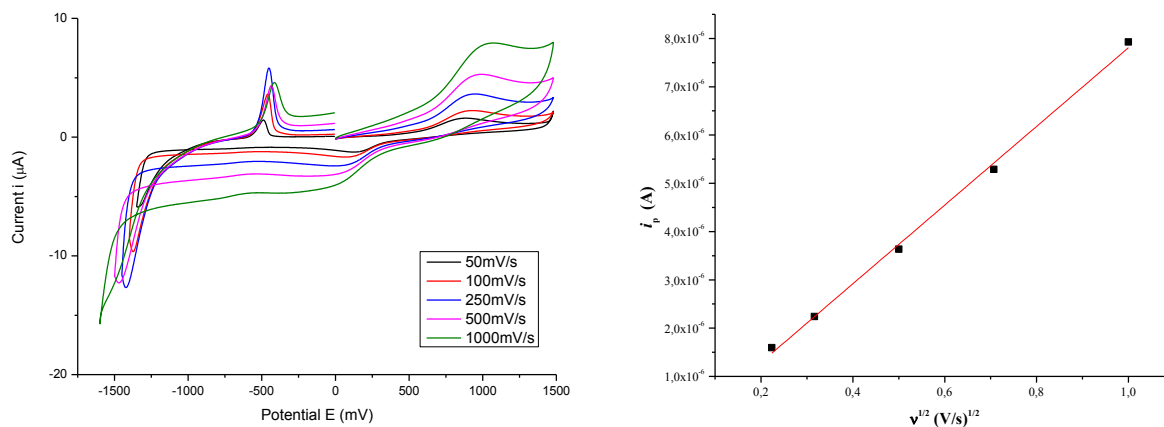


**Figure 3.5 (left)** CVs of  $\text{Fe}^{3+}/\text{Fe}^{2+}$  in aq.  $\text{HCOOH}$  recorded at different scan rates; **(right)** The dependence of the reduction peak current of the  $\text{Fe}^{2+}/\text{Fe}^{3+}$  couple on the square root of the scan rate for the iron species.

From the Randles-Sevcik equation, the diffusion coefficient was calculated as:

$$D = (B / (2.69 \times 10^5 z^{3/2} A_{\text{exp}} C))^2 = 9.18 \times 10^{-6} \text{ cm}^2/\text{s}$$

### B. Sulfuric acid system (1 mM)

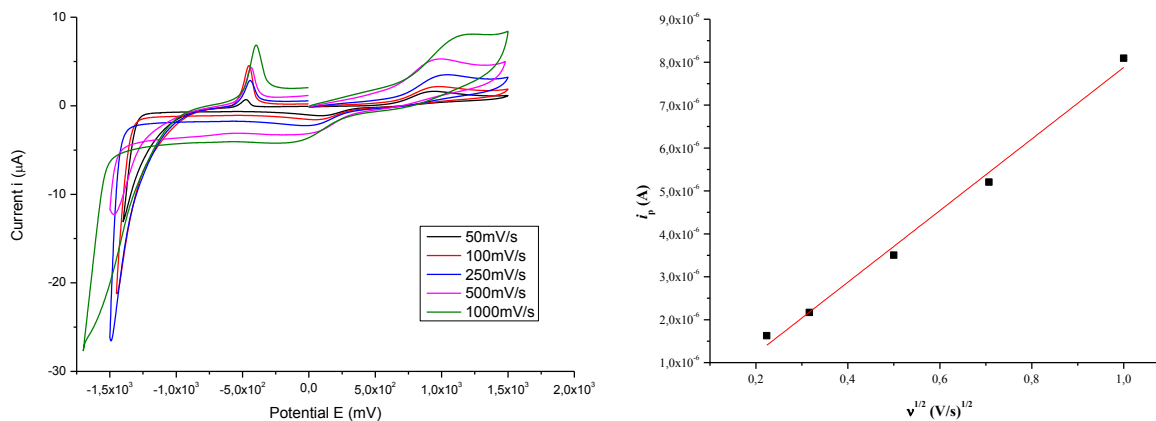


**Figure 3.6 (left)** CVs of  $\text{Fe}^{3+}/\text{Fe}^{2+}$  in aq.  $\text{H}_2\text{SO}_4$  recorded at different scan rates; **(right)** The dependence of the peak current of the  $\text{Fe}^{2+}/\text{Fe}^{3+}$  couple on the square root of the scan rate for the  $\text{FeSO}_4$  species.

From the Randles-Sevcik equation, the diffusion coefficient was:

$$D = 9.61 \times 10^{-6} \text{ cm}^2/\text{s}$$

### 3.3.1.2 Electrochemical characterization of $\text{FeSO}_4$ systems

Experiments for the initial characterization of  $\text{FeSO}_4$  systems were aimed at investigating whether iron deposition was possible, and if so, at which potential the deposition occurred. Different aqueous solutions containing  $\text{FeSO}_4 \cdot 7\text{H}_2\text{O}$  and formic acid or  $\text{H}_2\text{SO}_4$  were prepared. The concentration of both the ferrous salt and the acid were varied in the range of 1 to 100 mM.

Table 3.1 summarizes the composition/concentration of the investigated systems and temperatures at which CVs were recorded.

**Table 3.1**  
Summary of experimental conditions for the initial electrochemical experiments using different aqueous solutions of  $\text{FeSO}_4$ /acid

Entry	System	$\text{Fe}^{2+}$ conc. (mM)	Acid conc. (mM)	$\text{Na}_2\text{SO}_4$ (mM)	T ( $^\circ\text{C}$ ) <sup>a</sup>
1	$\text{FeSO}_4/\text{HCOOH}$	1	none	100	rt
2			1		rt
3			10		50
4			100		rt
6			1		rt
7			10		rt
8			100		rt
9			$\text{FeSO}_4/\text{H}_2\text{SO}_4$		1
10	1	rt			
11	10	50			
12	100	rt			
13	1	rt			
14	10	rt			

<sup>a</sup>Temperature at which CV were recorded.

#### A. aq. $\text{FeSO}_4/\text{HCOOH}$ system

Figure 3.7 (left) compares the CV recorded at room temperature (rt), for a 1 mM  $\text{FeSO}_4$  solution in the presence of formic acid (1 mM) (blue line) with the blank (1 mM formic acid/0.1 M  $\text{Na}_2\text{SO}_4$ , red line). For this system, blank experiments showed that the potential window for the solvent is  $-1400 < E < 1700$  mV. The onset of the desired cathodic iron deposition ( $[\text{Fe}(\text{OH}_2)_6]^{2+} + 2e^- \rightleftharpoons \text{Fe}^0 + 6\text{H}_2\text{O}$ ) is at about -1370 mV. The anodic stripping peak ( $\text{Fe}^0 + 6\text{H}_2\text{O} \rightarrow [\text{Fe}(\text{H}_2\text{O})_6]^{2+} + 2e^-$ ) is observed at about -470 mV.

The same iron redox potentials were observed with different acid concentrations (no acid, 10mM and 100 mM expressed by red line, blue line and pink line, respectively), but the magnitude of the current associated with the cathodic iron deposition was different for each system (Figure 3.7, right); it appeared to increase with the increase of the acid concentration, *i.e.* with decreasing pH. Moreover, the iron-stripping peak shifted from -560 mV in the absence of

acid (black line), to a less negative potential of -290 mV at higher acid concentrations (pink line).

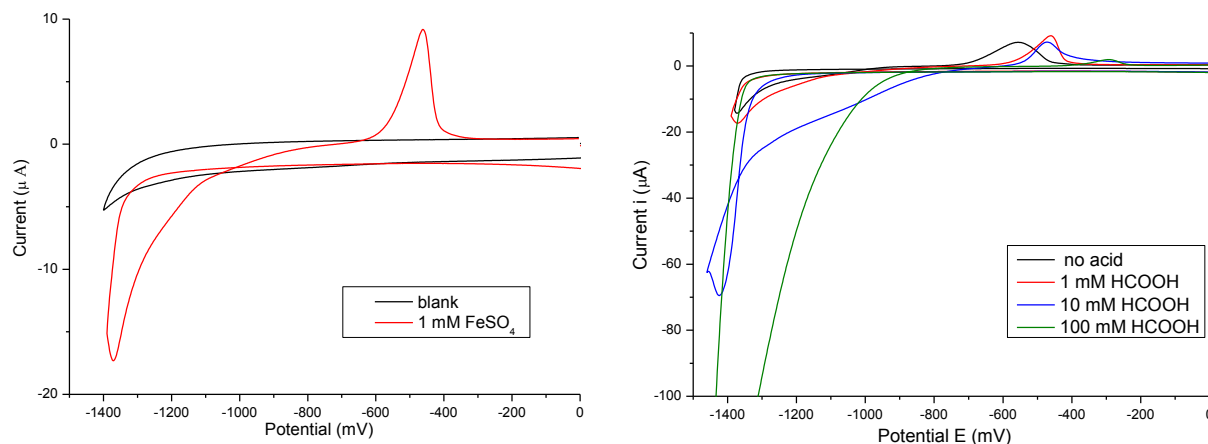


**Figure 3.7** (left) CV of iron sulfate (1 mM) in a 1 mM HCOOH solution compared with the blank (1 mM formic acid/0.1 M sodium sulfate); (right) CVs of iron sulfate (1 mM) in solutions at different HCOOH concentration (1-100 mM). Na<sub>2</sub>SO<sub>4</sub> (0.1 M) was present in all cases.

The electrochemical behavior of FeSO<sub>4</sub> (1 mM) at the lowest HCOOH concentration (1 mM) was investigated at the typical temperature used for hydrogenation experiments, *i.e.* at 50°C, by CV experiments. Under such conditions, the iron deposition potential shifted to a more positive value (about -1300 mV), while the stripping peak shifted to a more negative potential (-560 mV). The current magnitude of the iron deposition process was doubled (Figure 3.8).

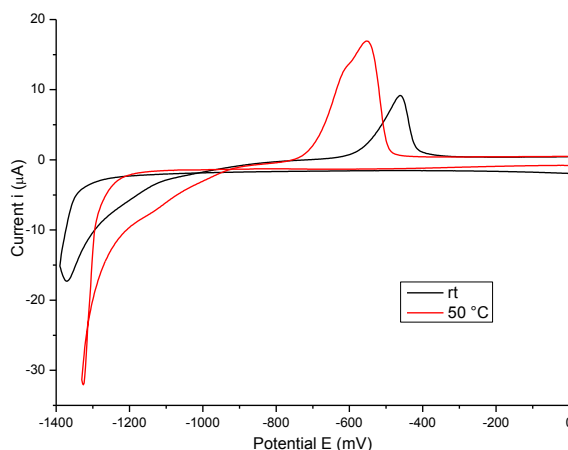


**Figure 3.8** CVs of FeSO<sub>4</sub> (1 mM) in a 1 mM solution of HCOOH. Experiments at different temperatures. Na<sub>2</sub>SO<sub>4</sub> (0.1M) was also present.

Possible effects due to the increase of the amount of Fe<sup>2+</sup> were explored. CVs were recorded at room temperature for two samples of FeSO<sub>4</sub> prepared at 10 and 100 mM concentration, respectively. In both cases, the concentrations of HCOOH and Na<sub>2</sub>SO<sub>4</sub> were 1 mM and 0.1 M, respectively. Relevant cyclic voltammograms are reported in Figure 3.9. The

potential at which iron deposition started was not greatly affected by the increase of the  $\text{Fe}^{2+}$  concentration. The reaction (deposition) occurred at about -1300 mV and -1250mV with 10 mM and 100mM of  $\text{Fe}^{2+}$ , respectively. However, the cathodic current value increased linearly with the increase of the iron concentration.

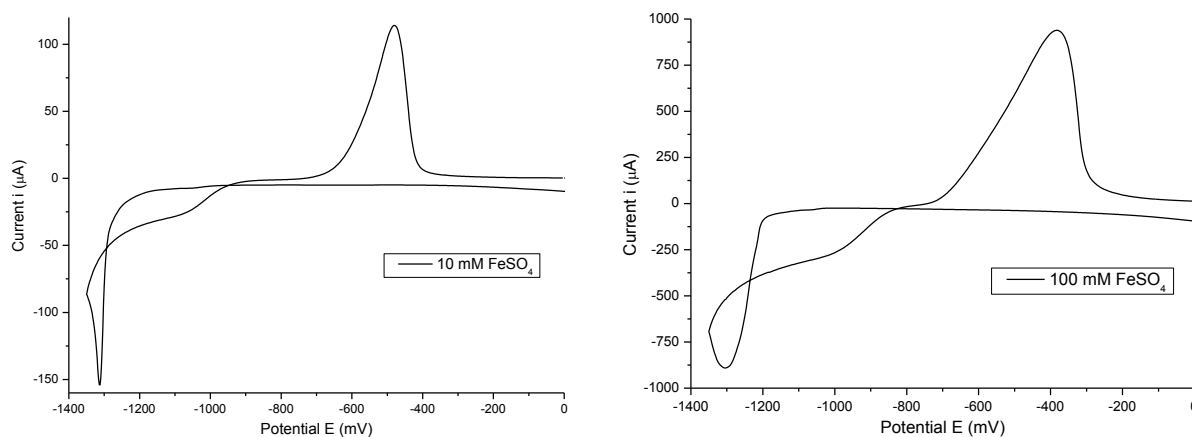


**Figure 3.9** CVs of aqueous solutions of:(left)  $\text{FeSO}_4$ ,  $\text{HCOOH}$ , and  $\text{Na}_2\text{SO}_4$  at 10 mM, 1 mM, and 0.1 M concentration, respectively; (right)  $\text{FeSO}_4$ ,  $\text{HCOOH}$ , and  $\text{Na}_2\text{SO}_4$  at 0.1 M, 1 mM, and 0.1 M concentration, respectively.

### B. aq. $\text{FeSO}_4/\text{H}_2\text{SO}_4$ system

Figure 3.10 left compares the CVs recorded at rt, for a 1 mM  $\text{FeSO}_4$  solution in the presence of sulfuric acid (1 mM) (blue line) with the blank (no  $\text{FeSO}_4$ , red line). Blank experiments showed that the potential window for the solvent is  $-1600 < E < 1800$  mV. The onset of the desired cathodic iron deposition is at about -1340 mV. The anodic stripping peak is observed at about -470mV.

The same iron redox potentials values were observed with different acid concentrations, but the intensity of the cathodic current relevant to the iron deposition was different for each system, in agreement with what was observed for formic acid. The peak current increases when decreasing the pH (Figure 3.7, right: compare black, red and blue curves). Unlike the deposition onset potential, which remained constant, the iron stripping peak shifted from -560 mV with no acid (black line) to a less negative potential of -420 mV at increasing the acid concentration (blue line).

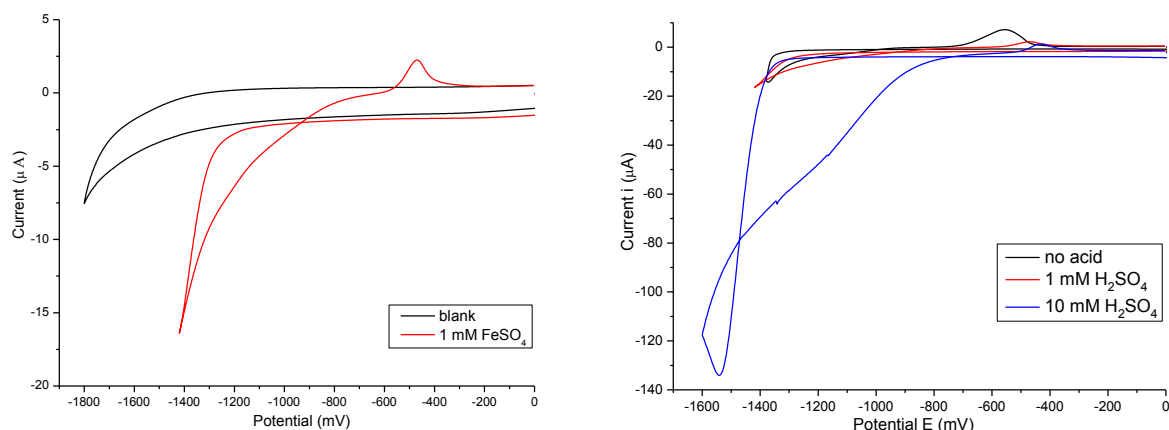


**Figure 3.10** (left) CV of iron sulfate (1 mM) in a 1 mM H<sub>2</sub>SO<sub>4</sub> solution compared with the blank (1 mM H<sub>2</sub>SO<sub>4</sub>/0.1 M sodium sulfate); (right) CVs of iron sulfate (1 mM) in solutions at different H<sub>2</sub>SO<sub>4</sub> concentration (1-100 mM). Na<sub>2</sub>SO<sub>4</sub> (0.1 M) was present in all cases.

The electrochemical behavior of FeSO<sub>4</sub> (1 mM) at the lowest H<sub>2</sub>SO<sub>4</sub> concentration (1 mM) was also investigated at 50°C. Figure 3.11 shows the cyclic voltammograms recorded at room temperature (black line) and at 50 °C (red line). The analysis of these voltammograms indicates that the increase of the temperature causes a shift of the cathodic peak to less negative value (about -1260 mV), while the stripping peak potential shifted to a more negative potential (-550 mV).

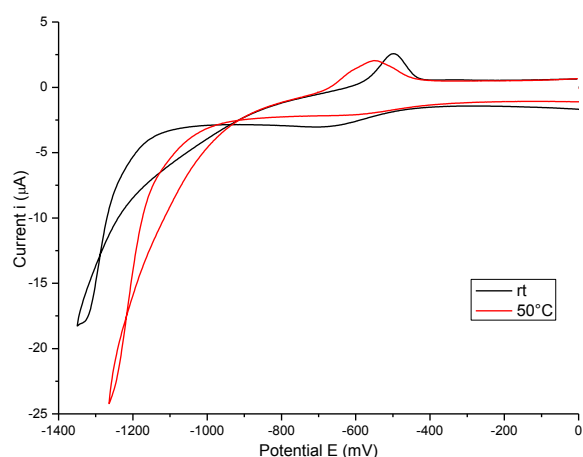


**Figure 3.11** CVs of iron sulfate (1 mM) in aqueous solution of H<sub>2</sub>SO<sub>4</sub> (1 mM) at different temperatures. Na<sub>2</sub>SO<sub>4</sub> (0.1 M) was also present.

Possible effects of the Fe<sup>2+</sup> concentration were also studied for sulfuric acid-based systems. CVs were recorded at room temperature for two samples of FeSO<sub>4</sub> prepared at 10 and 100 mM concentrations. In both cases, H<sub>2</sub>SO<sub>4</sub> and Na<sub>2</sub>SO<sub>4</sub> concentrations were 1 mM and 0.1 M, respectively.

Relevant cyclic voltammograms are reported in Figure 3.12. The potential at which iron deposition started was about -1310 mV and -1220mV with 10 mM and 100 mM  $\text{Fe}^{2+}$ , respectively. As was observed with HCOOH, in the presence of  $\text{H}_2\text{SO}_4$ , the cathodic current value also increased proportionally with the increase in the iron concentration.

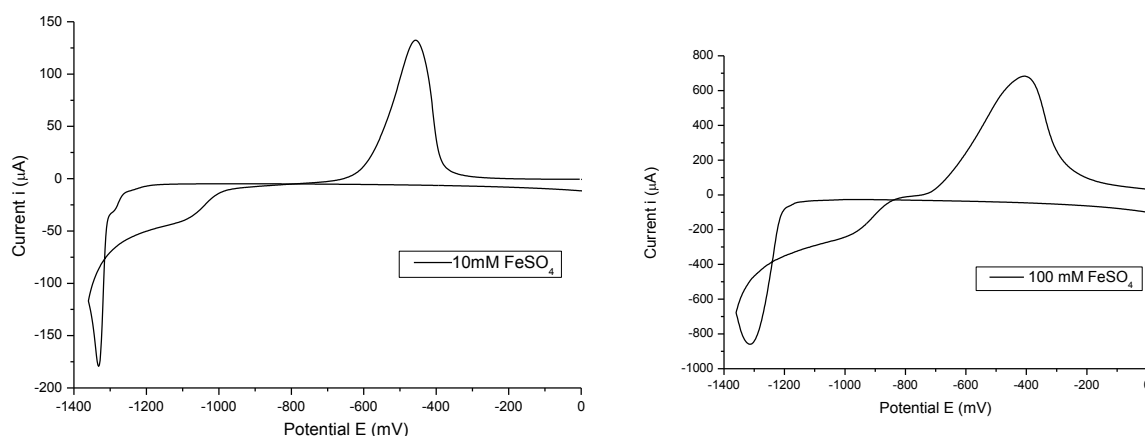


**Figure 3.12** CVs of aqueous solutions of: **(left)**  $\text{FeSO}_4$ ,  $\text{H}_2\text{SO}_4$ , and  $\text{Na}_2\text{SO}_4$  at 10 mM, 1 mM, and 0.1 M concentration, respectively; **(right)**  $\text{FeSO}_4$ ,  $\text{H}_2\text{SO}_4$ , and  $\text{Na}_2\text{SO}_4$  at 0.1 M, 1 mM, and 0.1 M concentration, respectively.

To conclude this section, the CV of  $\text{FeSO}_4$  (1mM) in HCOOH (1mM,  $\text{pK}_a = 3.77$ ) was compared to that of  $\text{FeSO}_4$  (1mM) in  $\text{H}_2\text{SO}_4$  (1 mM,  $\text{pK}_a = -3$ ) (Figure 3.13). The iron deposition clearly took place at a more positive potential in the presence of the stronger acid ( $\text{H}_2\text{SO}_4$ ), while the stripping peak potential was slightly affected by the type of acid.

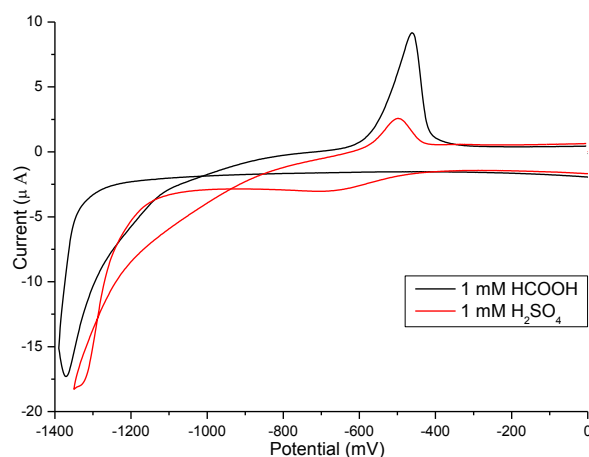


**Figure 3.13** Black profile: CV of  $\text{FeSO}_4$  (1 mM) in formic acid (1mM); red profile: CV of  $\text{FeSO}_4$  (1 mM) in sulfuric acid (1mM). In both cases,  $\text{Na}_2\text{SO}_4$  (0.1 M) was present.

## The addition of different organic substrates

The study continued by exploring whether the presence of organic substrates has any effect on the potential of the iron redox processes. Initial experiments were carried out using levulinic acid (LA) that is the organic substrate to be hydrogenated, which is not electroactive over the potential window studied. This behavior is evidenced by the absence of any faradic peak in the CV voltamogram. (see Figure 3.33 in appendix). Therefore, LA was added to the  $\text{Fe}^{2+}$  sulfate systems with both  $\text{HCOOH}$  and  $\text{H}_2\text{SO}_4$ . The potential window was the same exploited for the systems previously investigated in the absence of LA (Figure 3.7 left).

### A. LA in formic and sulfuric acid (1 mM) systems

CV experiments were recorded in aqueous solutions of  $\text{FeSO}_4$  (1 mM) and  $\text{HCOOH}$  or  $\text{H}_2\text{SO}_4$  acid (1 mM) to which LA was added at different concentrations (1, 10, and 100 mM, respectively). Figure 3.14 shows the results. The cathodic iron deposition peak was slightly affected by LA amount: the reaction was observed at about -1340 and -1330 mV in the presence of  $\text{HCOOH}$  and  $\text{H}_2\text{SO}_4$ , respectively. However, the anodic stripping peak was strongly modified by the increase of the LA concentration: *i*) for  $\text{HCOOH}$ -based systems, the corresponding potential shifted from -540 mV to -480 mV at 1 mM and 10 mM LA concentration; *ii*) for  $\text{H}_2\text{SO}_4$ -based systems, the corresponding potential was rather constant at -490 mV. Notably, for both systems, the associated current decreased at higher LA amounts, at the point that it was no longer measurable when the LA concentration was 100 mM (i.e., LA was present in large excess relative to the starting  $[\text{Fe}^{2+}]$ ).

A similar behaviour was observed during CV experiments carried out at 50°C (not shown here; for details, see Figure 3.34 in appendix).

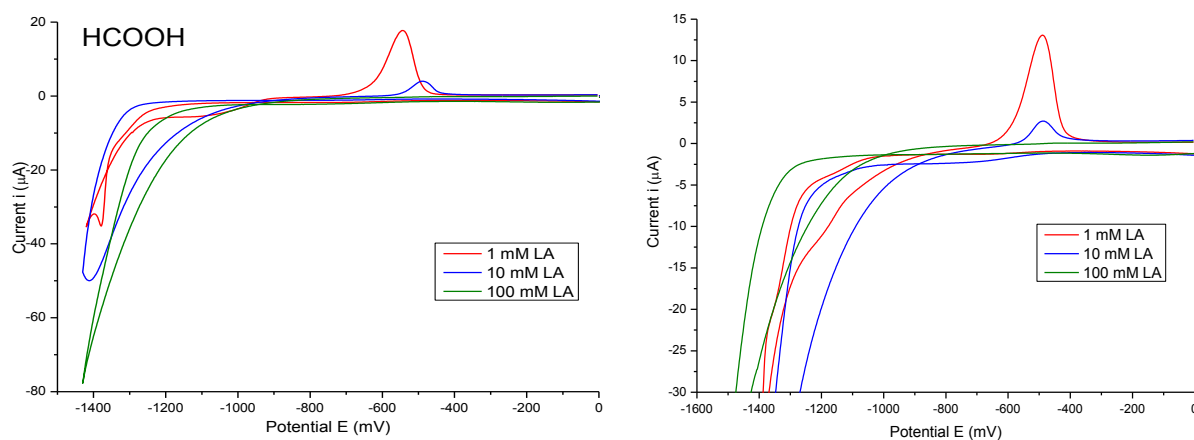


**Figure 3.14** CVs of aqueous solutions of: (left)  $\text{FeSO}_4$  (1 mM),  $\text{HCOOH}$  (1 mM), and LA (1-100 mM); (right)  $\text{FeSO}_4$  (1 mM),  $\text{H}_2\text{SO}_4$  (1 mM), and LA (1-100 mM).  $\text{Na}_2\text{SO}_4$  (0.1 M) was always present. Experiments were run at room temperature.

Further experiments were carried out to investigate the decrease of the iron-stripping peak observed at increasing LA concentration. Under such conditions, one hypothesis is that iron sulfate could undergo the cathodic deposition to produce iron, which, at the same time, could be readily re-oxidized by the onset of the LA hydrogenation in an electrochemical-chemical (E-C) process.<sup>7</sup> To verify this hypothesis, five different systems (B-E) were considered. They were composed by: i) aqueous solutions of  $\text{FeSO}_4$  and LA without any additional  $\text{HCOOH}$  or  $\text{H}_2\text{SO}_4$ , and ii) aqueous solutions of  $\text{FeSO}_4$ ,  $\text{HCOOH}$  or  $\text{H}_2\text{SO}_4$ , and an organic substrate chosen from 2-pentanone,  $\gamma$ -valerolactone (GVL), and ethyl levulinate. 2-Pentanone is a non-acid model compound, which, similarly to LA, could be easily hydrogenated and is water soluble. The knowledge of the electrochemical behavior of  $\gamma$ -valerolactone appeared necessary since this compound is the hydrogenation product of LA. Ethyl levulinate is a further convenient example: its structure is very similar to LA, but the acid function was protected.

### B. LA in aqueous solution (no acid)

CV experiments were recorded at rt, on aqueous solutions of  $\text{FeSO}_4$  (1 mM) to which LA was added at different concentrations (1, 10, and 100 mM, respectively). Relevant cyclic voltammograms are reported in Figure 3.15. The iron deposition onset was observed at about -1350 mV for all systems, while, the stripping peak shifted from -550 mV at the lower LA (1 mM), to a less negative potential of -470 mV at the higher LA concentration (100 mM). Also, the associated current decreased with increasing of the LA amount (compare black, red and blue voltammograms corresponding to LA concentration of 1, 10, and 100 mM, respectively).

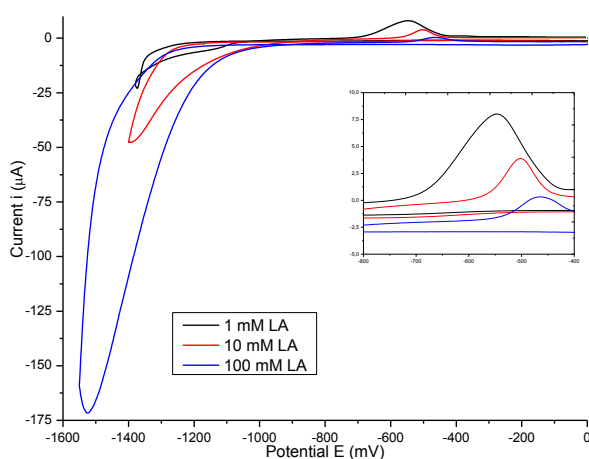
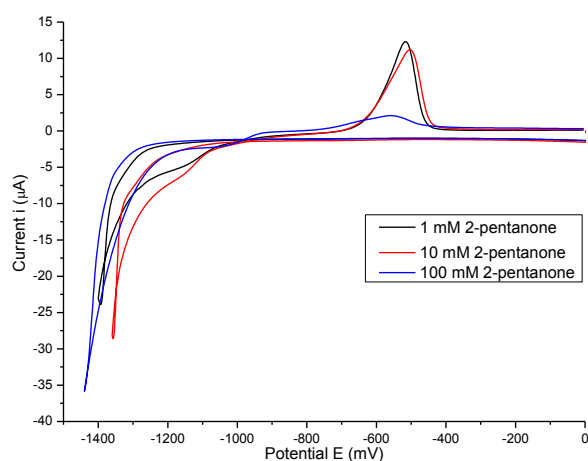


Figure 3.15. CVs of aqueous solutions of  $\text{FeSO}_4$  (1 mM), and LA (1-100 mM).



### C. 2-Pentanone in aqueous formic acid

CV experiments were recorded at rt, on aqueous solutions of  $\text{FeSO}_4$  (1 mM) and  $\text{HCOOH}$  (1 mM) to which 2-pentanone was added at different concentrations (1, 10, and 100 mM, respectively). Relevant cyclic voltammograms are reported in Figure 3.16. The cathodic iron deposition was analogous to that observed in the presence of LA: the corresponding peak potential was at about -1350 mV. The increase of the 2-pentanone concentration did not affect the position of the anodic stripping peak, which was observed at about -510 mV, although the corresponding current maximum remarkably dropped as the amount of 2-pentanone was increased up to 100 mM.



**Figure 3.16** CVs of aqueous solutions of  $\text{FeSO}_4$  (1 mM),  $\text{HCOOH}$  (1 mM) and 2-pentanone (1-100 mM).  $\text{Na}_2\text{SO}_4$  (0.1 M) was present.

### D. GVL in aqueous formic or sulfuric acid

CV experiments were recorded at rt, on aqueous solutions of  $\text{FeSO}_4$  (1 mM) and  $\text{HCOOH}$  or  $\text{H}_2\text{SO}_4$  (1 mM) to which  $\gamma$ -valerolactone (GVL) was added at different concentrations (1, 10, and 100 mM, respectively). A reference experiment was performed also in the absence of GVL. The corresponding voltammograms are reported in Figure 3.17. The iron deposition peak was observed at about -1400 mV and -1330 mV in the presence of  $\text{HCOOH}$  and  $\text{H}_2\text{SO}_4$ , respectively. The anodic stripping showed an unexpected pattern: *i*) for  $\text{HCOOH}$ -based systems (**left**) at the lower GVL concentration (1 mM, red curves), two partially overlapped peaks were observed at about -540 mV and -470 mV; the stripping peaks were broad and not well defined when the amount of GVL was increased to 10 mM and 100 mM, respectively (left and right: blue and fuchsia curves); *ii*) for  $\text{H}_2\text{SO}_4$ -based systems (**right**) at the lower GVL concentration (1 mM, red curves), similarly two partially overlapped peaks were observed at about -620 mV and -470

mV; the stripping peaks observed at -510 mV were well defined when the amount of GVL was increased to 10 mM and 100 mM, respectively.

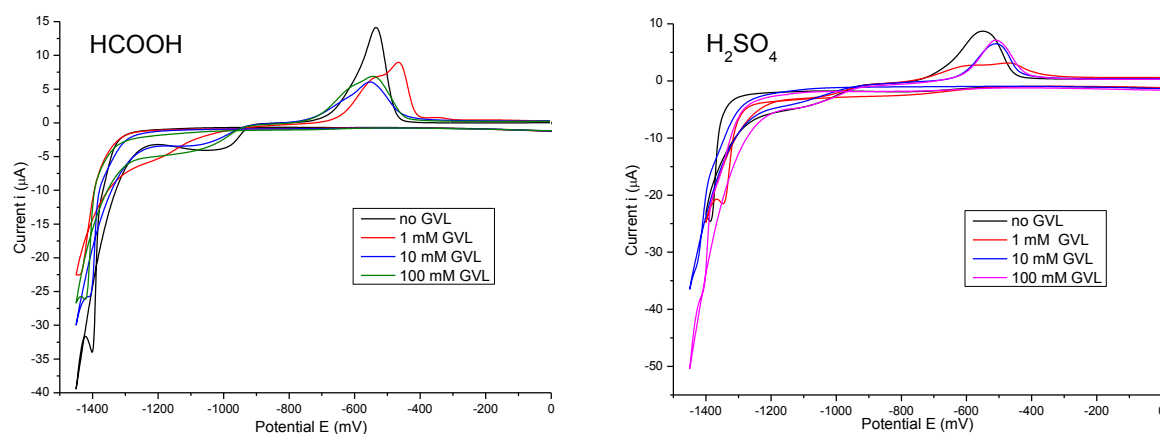


**Figure 3.17** CVs of aqueous solutions of: **left**) FeSO<sub>4</sub> (1 mM), HCOOH (1 mM) and GVL (1-100 mM); **right**) FeSO<sub>4</sub> (1 mM), H<sub>2</sub>SO<sub>4</sub> (1 mM) and GVL (1-100 mM). Na<sub>2</sub>SO<sub>4</sub> (0.1 M) was always present.

An additional CV (not shown here) was also recorded in the absence of iron: no peaks were detected confirming that GVL is not electrochemically active in this potential window.

### E. GVL in aqueous solutions (no acid)

CV experiments were recorded at rt, on aqueous solutions of FeSO<sub>4</sub> (1 mM) to which GVL was added at different concentrations (1, 10, and 100 mM, respectively). Relevant cyclic voltammograms are reported in Figure 3.18. The shape of CVs did not greatly differ from those previously observed in the presence of HCOOH or H<sub>2</sub>SO<sub>4</sub>. The onset of cathodic iron deposition was observed at about -1340 mV, while anodic stripping peaks were partially overlapped with their maximum centered at about -600 mV and -450 mV (blue and fuchsia curves).

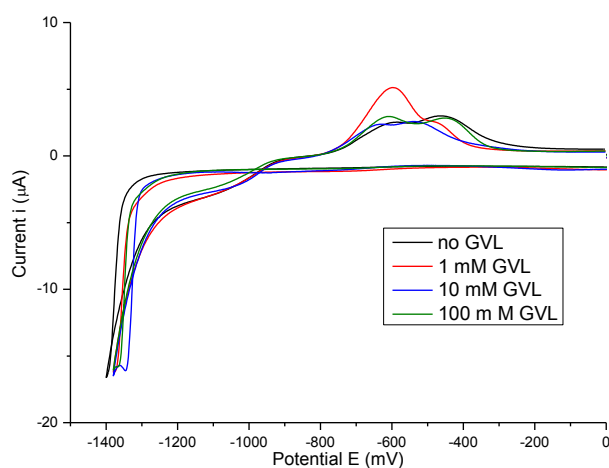


**Figure 3.18** CVs of aqueous solutions of FeSO<sub>4</sub> (1 mM) and GVL (1-100 mM).

Overall, the electrochemical behavior of GVL-containing solutions suggested that two different oxidation reactions could take place, the kinetics of which depended on the GVL concentration. The onset of these redox reactions was not affected by the nature/presence of either HCOOH or H<sub>2</sub>SO<sub>4</sub>. This investigation however, was not further detailed since it was beyond the scope of this work.

#### F. Ethyl levulinate (EL) in aqueous solutions (no acid)

CV experiments were recorded at rt, on aqueous solutions of FeSO<sub>4</sub> (1 mM) and EL (1 mM). Relevant cyclic voltamograms are reported in Figure 3.19. The onset of iron deposition took place at about -1340 mV. The shape of the relevant stripping peaks was dependent on the potential at which the scan was reversed. In particular, if *i*) the scan was reversed at a potential of -1350 mV, then the stripping peak was observed at about -550 mV (black curve); *ii*) the scan was reversed at a more negative potential of -1380 mV, then two partially overlapped anodic peaks were observed at about -600 mV and -500 mV (red curve).

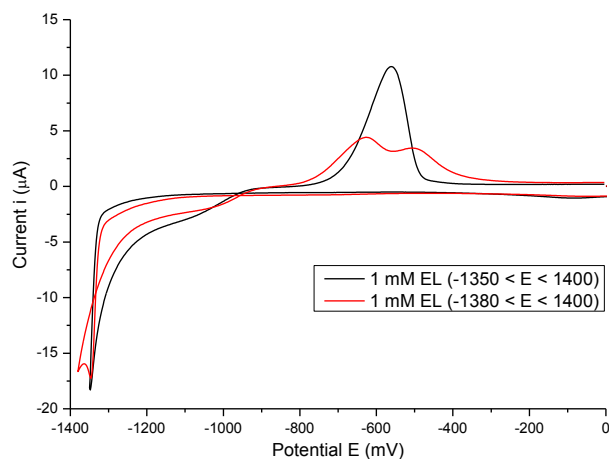


**Figure 3.19** CVs of aqueous solutions of FeSO<sub>4</sub> (1 mM) and EL (1 mM). Na<sub>2</sub>SO<sub>4</sub> (0.1 M) was present.

### 3.4 Linear sweep - anodic stripping voltammetric studies

The experiments described above led to the hypothesis that the double anodic peak observed for both GVL- and EL-containing solutions, could be due to different morphological species of Fe<sup>0</sup>. If so, regardless of the presence of GVL or EL, the double peak would have been obtained by applying an appropriate potential to aqueous solutions of FeSO<sub>4</sub>. To prove this, linear sweep - anodic stripping voltammetry (LS-ASV) was chosen<sup>8c</sup>. The general strategy of LS-ASV experiments is composed of two steps: *i*) in the first one, a constant negative potential (equal to the deposition potential of iron) was applied for a defined time to a working electrode

in aqueous solutions of  $\text{FeSO}_4$ , and *ii*) the potential was anodically scanned on LSV at a scan rate of 100 mV/s.

### A. Formic acid system

LS-ASV experiments were recorded in aqueous solution of  $\text{FeSO}_4$  (1 mM) and formic acid (1 mM). Initial LS-ASV voltammograms were recorded starting from different deposition potentials (-1100 to -1440 mV) at a constant deposition time of 5 seconds. The relevant cyclic voltammograms, reported in Figure 3.20, show that the deposition potential affected not only the position of the stripping peak, but also its shape and the corresponding current. The potentials for the anodic process ranged from -630 to 180 mV. In some cases, a single broad signal was observed, while in some others, two partially overlapped peaks were present.

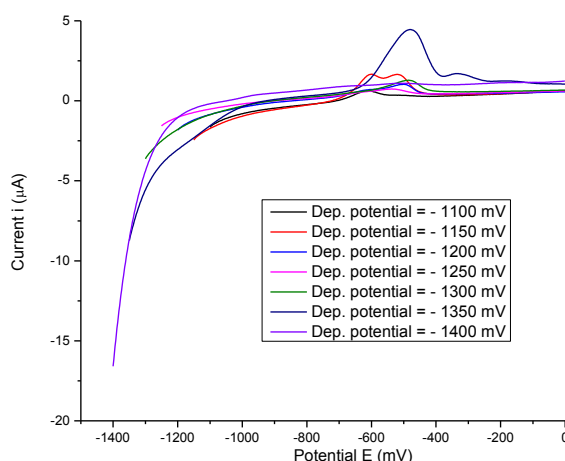


**Figure 3.20** LS-ASV of an aqueous solution of  $\text{FeSO}_4$  (1 mM) and formic acid (1 mM) recorded at different deposition potentials (deposition time: 5 sec).

Further LS-ASVs were recorded by varying the deposition time (from 5 to 60 sec) at two constant deposition potentials of -1100 mV and -1150 mV, respectively. Relevant cyclic voltammograms are reported in Figure 3.21. Experiments showed that the change of the deposition time did not substantially modify the potential at which the anodic stripping occurred (peak on the left and on the right: at about -600 and -520 mV, respectively); however, the shape of the stripping peaks was altered. In particular, two partially overlapped peaks were observed. As the deposition time was increased, these peaks progressively grew up inhomogeneously: in Figure 3.21 left, with a deposition potential of -1100 mV, the peak on the left (-600 mV) rose more quickly; while in Figure 3.21 right, with a deposition potential of -1150 mV, the peak on the right (-520 mV) grew faster.

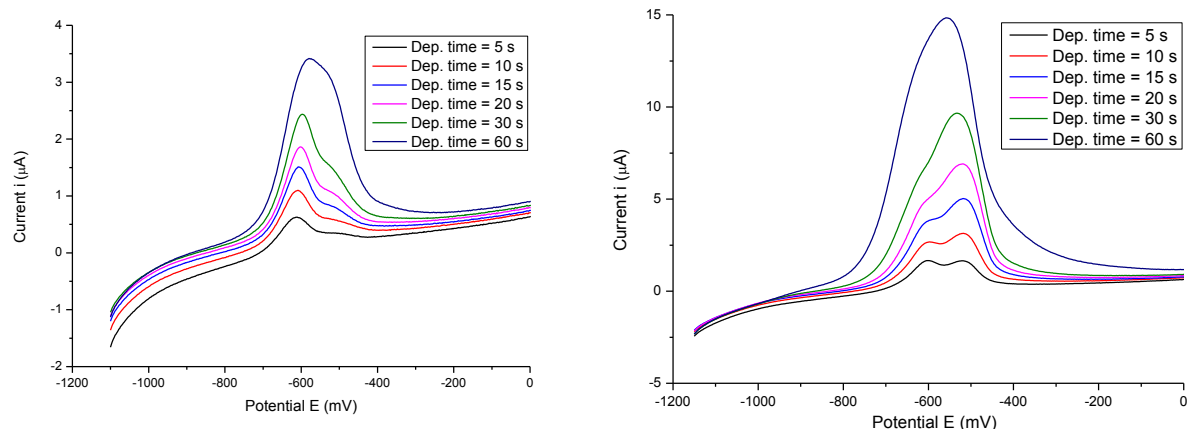


**Figure 3.21** LS-ASV of an aqueous solution of  $\text{FeSO}_4$  (1 mM) and formic acid (1 mM) at different deposition times (5-60 sec): **(left)** starting deposition potential was -1100 mV; **(right)** starting deposition potential was -1150 mV

### B. Sulfuric acid system

LS-ASV experiments analogous to those described above were carried out on an aqueous solution of  $\text{FeSO}_4$  (1 mM) and  $\text{H}_2\text{SO}_4$  (1 mM). Figure 3.22 reports LS-ASV curves recorded by applying starting deposition potentials from -1150 mV to -1400 mV at a constant deposition time of 5 sec. Figure 3.23 shows LS-ASV curves acquired by changing the deposition time (from 5 to 60 sec) at two constant deposition potentials of -1150 mV and -1200 mV, respectively.

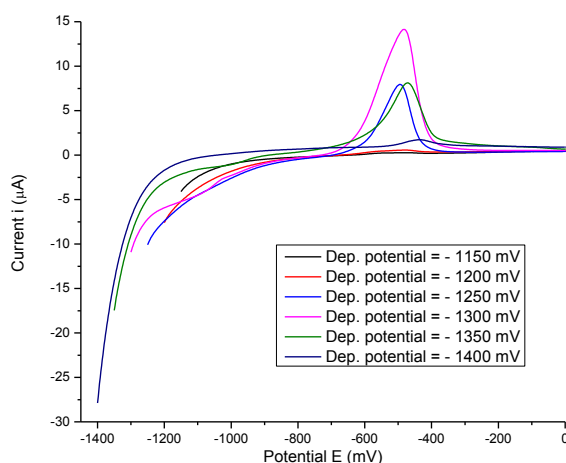


**Figure 3.22** LS-ASV of an aqueous solution of  $\text{FeSO}_4$  (1 mM) and  $\text{H}_2\text{SO}_4$  (1 mM) recorded at different deposition potentials (deposition time: 5 sec).

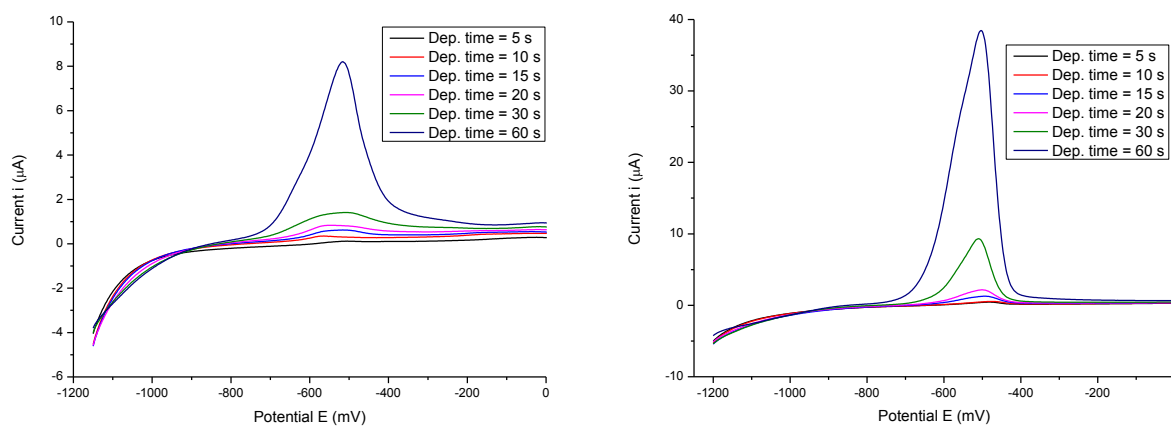


**Figure 3.23** LS-ASV of an aqueous solution of  $\text{FeSO}_4$  (1 mM) and  $\text{H}_2\text{SO}_4$  (1 mM) at different deposition times (5-60 sec): **(left)** starting deposition potential was -1150 mV; **(right)** starting deposition potential was -1200 mV.

The results led to similar conclusions as for the  $\text{FeSO}_4/\text{HCOOH}$  system described above. The position and the shape of the stripping peaks were affected by both the starting deposition potential and the deposition time. (**Figure 3.23 left and right**: stripping peak at about -520 and -500 mV, respectively). Also, the corresponding currents were modified: they showed a remarkable enhancement by increasing the deposition time.

### 3.5 Discussion

It is known from the literature that the cathodic deposition of iron in aqueous solutions always takes place along with a simultaneous evolution of hydrogen.<sup>10</sup> In general, the current efficiency of the deposition reaction is less than 100% and practical methods to improve such a process are based on the use of moderate acidic solutions at pH ranging from 3 to 6.<sup>9a, 10</sup> This simple expedient allows a small  $\text{H}^+$  reduction current density compared to the effective iron cathodic current density, and it rules out the precipitation of the metal hydroxide ( $\text{FeSO}_4 + 2 \text{OH}^- \rightarrow \text{Fe}(\text{OH})_2 + \text{SO}_4^{2-}$ ). A further measure to increase the current efficiency is the use of vitreous carbon electrodes, the surface of which is known to inhibit the evolution of hydrogen even at highly negative potentials.<sup>14</sup>

In the light of these considerations, experiments carried out in this work to investigate the electrochemical behavior of aqueous  $\text{FeSO}_4$  exploited two different acidic environments, that are aqueous formic and sulfuric acid solutions.

*i) Formic acid systems.* The cyclic voltammetric response observed for  $\text{Fe}^{2+}$  at a glassy carbon electrode in formic acid aqueous solutions was recorded over the potential range of the solvent window (from -1400 mV to 1700 mV) and it consisted of two well-defined processes

(Figure 3.5 left - Figure 3.7). The process at  $E_{1/2} = 750$  mV is ascribed to the  $\text{Fe}^{2+/3+}$  redox couple. The diffusion coefficient ( $D$ ) for this couple was determined by preliminary experiments through the application of the Randles-Sevcik equation;  $D$  was  $9.18 \times 10^{-6}$   $\text{cm}^2/\text{s}$ . The process observed at  $-1370$  mV was the reduction reaction of  $\text{Fe}^{2+}$  to  $\text{Fe}^0$ . The occurrence of this reaction was confirmed by the presence of the typical anodic stripping peak recorded when the potential was reversed towards positive values, in the last segment of the cyclic voltammogram (left to right). The iron deposition potential was slightly affected by the change of the acid concentration over the range from 0 to 100 mM, although the current magnitude increased at lower pH. Since this enhancement was observed for samples at a constant concentration of  $\text{FeSO}_4$  (1 mM), it could hardly be attributed to an effect induced by iron. Instead, the current increase was plausibly due to the reduction of hydrogen ions,  $2\text{H}^+ + 2\text{e}^- \rightleftharpoons \text{H}_{2\text{ads}}$ , the extent of which was plausibly increased by higher amounts of formic acid (lower pH). This was further corroborated by the visual observation of  $\text{H}_2$  microbubbles over the cathode surface during CV experiments. In general, this behavior confirmed the above-mentioned literature results, which show a drop of the current efficiency for iron deposition at  $\text{pH} < 3$ . Moreover, the iron-stripping peak shifted from about  $-0.56$  V to a less negative potential ( $-0.29$  V) with the increase of the acid concentration. As the pH was progressively decreased, a greater formation of  $\text{H}_2$  bubbles at the electrode surface was expected. The variation in the gas evolution plausibly caused two effects: *i*) the deposition of iron crystals with different morphologies which were oxidized at different potentials, and *ii*) a partial (mechanical) detachment of the iron deposition from the electrode surface that accounted for the observed decrease of the current intensity.<sup>15</sup>

Beyond the concentration of formic acid, the increase of the temperature from rt to  $50$  °C also caused two major consequences (Figure 3.8): *i*) the current magnitude for both the deposition and stripping reactions was almost doubled, and *ii*) the peak-to-peak separation of the reduction and oxidation potentials decreased, *i.e.* the iron deposition shifted to a less negative potential while the iron oxidation to a more negative one. This behavior was likely due to both thermodynamic and kinetic factors. The temperature affected both *i*) the redox potential of a process ( $E$ ), as indicated by the Nernst equation ( $E = E^0 + [(RT/nF) \times \ln(C_O/C_R)]$ ), and *ii*) the peak current magnitude ( $i_{\text{peak}}$ ), as indicated by Randles-Sevcik equation (Section 3.3.1.1), since the diffusion coefficient of the analyte depends on the temperature.<sup>16</sup>

The cathodic current magnitude was also increased by an increase of the iron ( $\text{Fe}^{2+}$ ) concentration (Figure 3.9): as was expected, the iron deposition took place to a large extent when

a larger amount of  $\text{Fe}^{2+}$  ions was available in the solution. Again, the Randles-Sevcik equation accounted for this behavior since the peak current is a function of the analyte concentration.

*ii) Sulfuric acid systems.* The cyclic voltammetric response of iron in sulfuric acid solutions was recorded over the potential range of the solvent window (from -1.6 V to 1.8 V) and it was analogous to that observed in formic acid solutions. **Figure 3.6 left - Figure 3.10** shows at  $E_{1/2} = 810$  mV a well-defined process ascribed to the  $\text{Fe}^{2+/3+}$  redox couple, with a diffusion coefficient of  $9.61 \times 10^{-6} \text{ cm}^2/\text{s}$ ; and at  $E = -1340$  mV the reduction reaction of  $\text{Fe}^{2+}$  to  $\text{Fe}^0$ . The investigation of the effect of the acid concentration, the temperature and the iron concentration gave results similar to those observed for formic acid systems. In particular: *i)* the iron deposition potential was almost unaffected by the change of the acid concentration, though the current magnitude for the cathodic reaction increased with the decreasing of pH; *ii)* the increase of sulfuric acid concentration also caused the iron stripping peak to shift to more positive potentials, but the associated current was not influenced at all; *iii)* at 50 °C, the peak-to-peak separation of the reduction and oxidation potentials decreased with respect to that at rt; *iv)* the increase of the current magnitude for the cathodic deposition was linearly to the increase of iron concentration.

Once the behavior of iron (1 mM) in the two different aqueous acidic environments was investigated, the addition of organic substrates was considered. Levulinic acid had minor, if any, effects on iron deposition, but its presence affected the anodic reaction: the stripping peak shifted to more positive potentials and disappeared when the LA concentration went up to 100 mM (Figure 3.14). This result led to the several hypotheses. Since ferric/ferrous ions are known to form stable complexes with organic acids<sup>17</sup>, the presence of a LA- $\text{Fe}^{2+}$  species was considered. However, this was hardly compatible with the evidence of the cathodic deposition that required free  $\text{Fe}^{2+}$  ions in aqueous solution. The formation of an adduct LA- $\text{Fe}^0$  at the electrode surface was then hypothesized: although no references were found on such species of iron in the presence of small organic acids. If the sequestration of the metal took place, then the passivation of the electrode and the subsequent prevention of the anodic oxidation would have occurred. This eventuality was checked via multicycle voltammetry experiments carried out in aqueous solutions containing LA (100mM). These tests (not shown here, see Figure 3.35 in appendix), showed that after the first iron deposition, a second and third cycle could be performed during which the electrode surface was still active to promote both the anodic reaction ( $\text{Fe}^{2+} \rightarrow \text{Fe}^{3+}$ ) and the cathodic reductions ( $\text{Fe}^{3+} \rightarrow \text{Fe}^{2+}$  and  $\text{Fe}^{2+} \rightarrow \text{Fe}^0$ ), respectively. Although the stripping peak was not detected, electrode passivation was clearly not taking place.



One final hypothesis was based on the consumption of electrodeposited  $\text{Fe}^0$  through the direct hydrogenation of LA (to GVL) promoted by the presence of both formic and sulfuric acids (see Scheme 3.1). Two consequences of this hypothesis are: *i*) the  $\text{Fe}^0$  stripping peak must be evident if no formic or sulfuric acids were used, and *ii*)  $\text{Fe}^0$  must also be consumed by different organic substrates that similarly to LA, could be hydrogenated. The first condition *i*) was verified by performing CV experiments of  $\text{Fe}^{2+}$  (1 mM) in acid-free solutions (without HCOOH or  $\text{H}_2\text{SO}_4$ , Figure 3.15): the iron stripping peak was observed even at the highest LA concentration (100 mM), meaning that the electrochemical oxidation  $\text{Fe}^0 \rightarrow \text{Fe}^{2+}$  was occurring. The second condition *ii*) was verified when LA was replaced with 2-pentanone (Figure 3.16) in a 1 mM  $\text{Fe}^{2+}$  acidic system. In these experiments the iron-stripping peak almost disappeared as the concentration of 2-pentanone was increased up to 100 mM. Overall, these results corroborated the assumption that the simultaneous presence of substrates able to be hydrogenated and aqueous acids consumes electrodeposited  $\text{Fe}^0$ .

A different situation emerged in the presence of GVL (Figure 3.17). CVs in both formic and sulfuric acid solutions showed that the iron deposition process was not affected by GVL, whilst the shape of the iron stripping peak suggested that two different oxidation reactions of  $\text{Fe}^0$  could occur. In particular, oxidation processes that could involve: *i*) GVL in association with  $\text{Fe}^0$  and/or *ii*) two types of  $\text{Fe}^0$ , the physical characteristics and morphologies of which were differentiated by the presence of GVL in the aqueous solution. The second hypothesis seemed to be also substantiated by CV experiments carried out with the addition of ethyl levulinate (EL), which showed how the anodic reaction ( $\text{Fe}^0 \rightarrow \text{Fe}^{2+}$ ) was expressed by a single peak or by two partially overlapped peaks if the potential was reversed at -1350 mV or at 1380 mV, respectively (Figure 3.19). The nature of the organic compound (GVL or EL) added to the  $\text{Fe}^{2+}$  system as well as the applied potential could plausibly affect the morphology of the iron crystals so that their oxidations occurred at slightly different voltages. This behavior was further confirmed by ASV experiments (Figure 3.20 and Figure 3.22). In this case, different shapes of the stripping peaks were observed when the reduction potential ranged between -1100 and -1400 mV (without GVL). The prolonged time (5-60 sec) of these tests was plausibly sufficient to allow the formation of two morphological types (at least) of iron crystals that were re-oxidized at different potentials.

### 3.6 Controlled potential bulk electrolysis

The short time-frame results of the potential sweep methods provided a basis for longer time scale experiments of *bulk electrolysis* (BE), *i.e.* exhaustive electrolysis.

Controlled potential electrolysis (CPE) is an electrochemical technique in which the analyte is fully reduced (or oxidized). The current is measured as a function of time, at a constant potential difference applied between two electrodes. The two important outcomes of CPE are: *i*) the calculation of the number of electrons required for the reduction (or oxidation) per unit of analyte (Faraday's law), and *ii*) the preparation of the reduced (or oxidized) product in a sufficiently large amount to allow its further characterization.

Similarly to voltammetry, CPE involves the use of a three electrode system, but the cell design is different. For an efficient, fast, and complete electrolysis, the working and counter electrodes are constructed to have large surface areas. In addition, because these two electrodes allow two opposite half reactions, the electrodes must be placed in separated compartments that communicate with each other via a glass frit (or a porous semi-permeable material). This expedient avoids any possible interference during the operation of the cell. Also, a stable and reliable reference electrode must be employed so as to specify the electrolysis potential. It should be noted that when cyclic voltammetric techniques are used to choose the electrolysis potential, the working potential of the CPE experiment is set to a slightly more negative value ( $\sim 200$  mV) than that of the reduction process (or to a slightly positive value than that of the oxidation reaction) measured CV peak potentials of the half processes considered. Care should also be taken to ensure that other electrochemical processes do not occur within the range of the chosen potential.

In order to increase the mass transport rate, the aqueous solution of the analyte must be stirred throughout the electrolysis experiment. The results are described by plotting the current against time. By definition, since the current  $i = dQ/dt$ , the plot of current versus time is used to calculate the total charge consumed  $Q = \int_0^t i dt$ , which also corresponds to the area below the CPE curve obtained by plotting the current ( $i$ ) vs. time ( $i$ - $t$  curves). The overall process is complete when the current is 1% of the starting current. The net charge consumed by a defined quantity of the analyte is obtained through the Faraday's law equation  $Q = zNF$ , where  $F$  is the Faraday constant,  $N$  is the number of moles of the analyte, and  $z$  is the number of electrons transferred per unit of analyte.

### 3.6.1 Results

The purpose of this part of the work was to verify whether the iron deposition observed during CV experiments in acidic aqueous solutions could also be obtained by exhaustive bulk electrolysis experiments carried out under controlled potential conditions over a large surface area glassy carbon working electrode.

#### 3.6.1.1 The setup of the bulk electrolysis cell

Preliminary CPE experiments were necessary to verify the correct operation of the bulk electrolysis cell. Tests were performed at rt, using an aqueous solution (10 mL) of potassiumferricyanide (1 mM) and potassium chloride (0.1 M) as supporting electrolyte. The peak potentials of the half redox processes for the  $\text{Fe}^{3+}/\text{Fe}^{2+}$  couple ( $E_R$  and  $E_O$ ) were determined in Section 3.3.1.1 by preliminary CV experiments (Figure 3.4). Figure 3.24 and Figure 3.25 report the results of the CPE experiments of reduction and oxidation of the couple  $[\text{Fe}(\text{CN})_6]^{3-/4-}$ , respectively.

#### A. Reduction of ferricyanide to ferrocyanide $[\text{Fe}(\text{CN})_6]^{3-} + e^- \rightarrow [\text{Fe}(\text{CN})_6]^{4-}$

A potential  $E_R = 0 \text{ V}$  was used to investigate the reduction reaction.

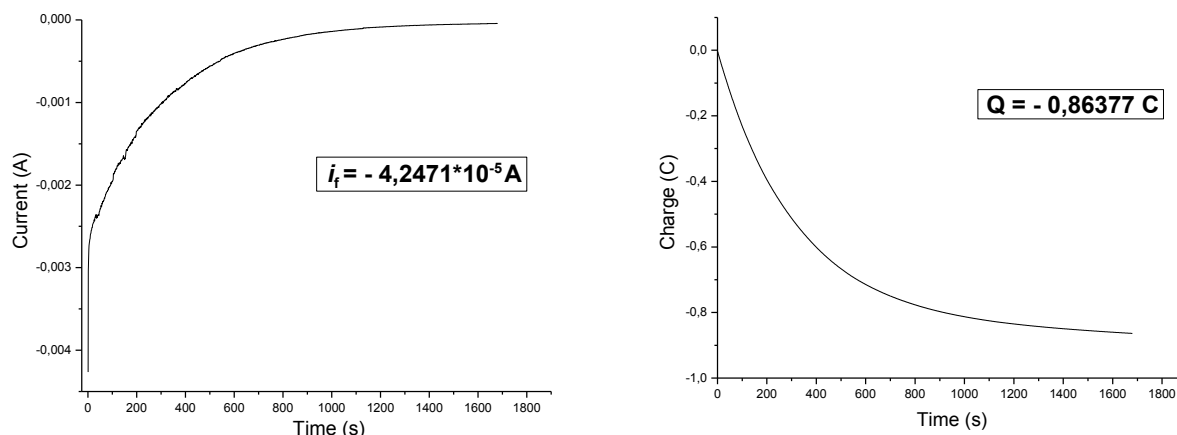


**Figure 3.24** Bulk electrolysis of an aqueous solution (10 mL) of  $\text{K}_3[\text{Fe}(\text{CN})_6]$  (1 mM) and  $\text{KCl}$  (0.1 M). The dependence of the current (A; **left**) and the charge (C; **right**) with time during the reduction process  $[\text{Fe}(\text{CN})_6]^{3-} + e^- \rightarrow [\text{Fe}(\text{CN})_6]^{4-}$

The use of an end to start current ratio of 1% enabled a net charge  $Q$  of  $-0.86377 \text{ C}$  to be calculated. From Faraday's law, the number of moles of electrons transferred during the reduction of  $1 \times 10^{-2} \text{ mmole}$  of  $\text{Fe}^{3+}$  to  $\text{Fe}^{2+}$  were:

$$N = Q/(zF) = 0.009 \text{ mmol}$$

This corresponded to 2.9 mg of reduced analyte meaning that  $\text{Fe}^{3+}$  was quantitatively consumed.

### B. Oxidation of ferrocyanide to ferricyanide $[\text{Fe}(\text{CN})_6]^{4-} \rightarrow [\text{Fe}(\text{CN})_6]^{3-} + \text{e}^-$

A potential  $E_{\text{O}} = +0.3 \text{ V}$  was used to investigate the oxidation reaction.

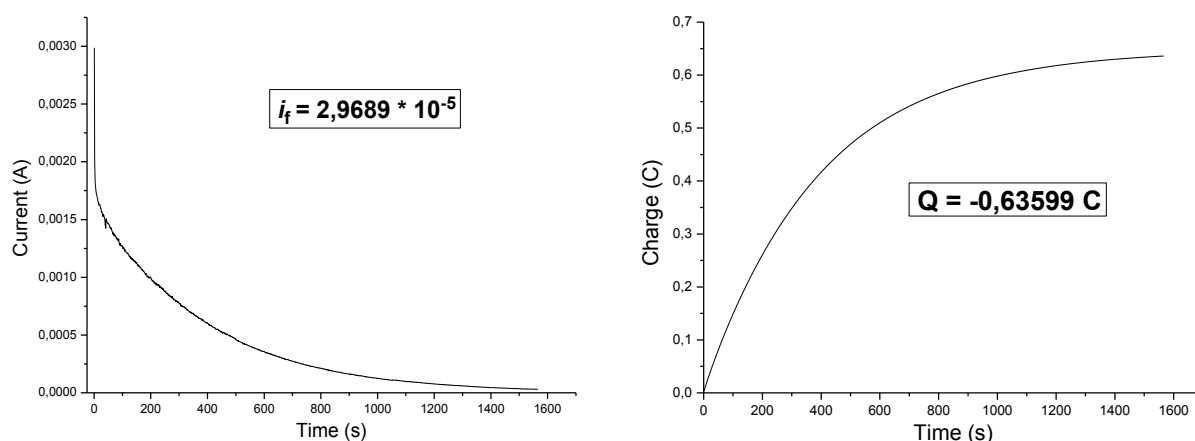


**Figure 3.25** Bulk electrolysis of an aqueous solution (10 ml) of  $\text{K}_3[\text{Fe}(\text{CN})_6]$  (1 mM) and  $\text{KCl}$  (0.1 M). The dependence of the current (A; **left**) and the charge (C; **right**) with time during the back-oxidation process  $[\text{Fe}(\text{CN})_6]^{4-} \rightarrow [\text{Fe}(\text{CN})_6]^{3-} + \text{e}^-$ .

In this case, the net charge  $Q$  was  $-0.63599 \text{ C}$ . From Faraday's law, the number of moles of electrons transferred during the oxidation of  $\text{Fe}^{2+}$  to  $\text{Fe}^{3+}$ , was  $N = 0.007 \text{ mmol}$  which corresponded to 2.5 mg of re-oxidized species.

These results confirmed that the bulk electrolysis cell was working properly with good conversions for the relevant redox reactions; in particular, starting from 0.01 mmol of the analyte in solution, the conversion was 90% and 77% for the reduction and the oxidation process, respectively.

#### 3.6.1.2 Single-step CPE

Initial  $\text{Fe}^{2+}$  reduction (deposition) experiments were carried out at rt, using a single-step technique: a constant potential was applied to the aqueous solution of the analyte and kept for the entire duration of the test. The potential was set in a range between  $-1.42 \text{ V}$  and  $-1.20 \text{ V}$  for the electrolysis of 1-10 mM  $\text{FeSO}_4$  solutions. Sulfuric acid was used at concentrations between 1 and 10 mM.

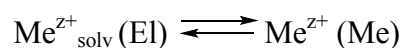


**Figure 3.26** Yellow-green precipitate inside the CPE cell obtained by single-step CPE experiment on a aqueous solution of FeSO<sub>4</sub> (10 mM) and H<sub>2</sub>SO<sub>4</sub> (1 mM)

All experiments resulted in the formation of a yellow-green precipitate/suspension, the visual observation of which suggested that iron hydroxide<sup>10</sup> or hydroxy sulfate green rust<sup>18</sup> were obtained. **Figure 3.26** shows an image of this yellow-green precipitate inside the CPE cell obtained through a model single-step CPE performed on an aqueous solution of FeSO<sub>4</sub> (10 mM) and sulfuric acid (1 mM). Although the product was not isolated and identified, the hypothesis is that iron zero did not deposited on the glassy carbon surface in these experiments, i.e. a single step approach was not suitable. A multi-step technique was therefore used to continue the investigation.

### 3.6.1.3 Multistep CPE

The electrochemical deposition and the dissolution of metals are interrelated by the following equilibrium:<sup>19</sup>



Where  $\text{Me}^{z+}_{\text{solv}}(\text{El})$  represents the metal ions in the electrolyte phase (El) and  $\text{Me}^{z+}(\text{Me})$  denotes the metal ions in the metal bulk phase (Me), which are coupled to the electrons  $e^-$  (Me) in the Me-crystals lattice ( $\text{Me}^{z+}(\text{Me}) + ze^-(\text{Me}) = (\text{Me})$ ). At the Nernst potential  $E_{\text{Me}/\text{Me}^{z+}}$ , identical amounts of  $\text{Me}^{z+}_{\text{solv}}(\text{El})$  and  $\text{Me}^{z+}(\text{Me})$  are obtained. The corresponding electrochemical potentials are also the same ( $\mu_{\text{Me}^{z+}_{\text{solv}}(\text{El})} = \mu_{\text{Me}^{z+}(\text{Me})}$ ). The deviation from equilibrium  $\Delta\mu = \mu_{\text{Me}^{z+}_{\text{solv}}(\text{El})} - \mu_{\text{Me}^{z+}(\text{Me})}$  is given by:

$$\Delta\mu = -zF(E - E_{\text{Me}/\text{Me}^{z+}}) = -zF\eta$$

where E and  $\eta$  are the actual electrode potential and the overpotential, respectively. If the kinetics of metal deposition and dissolution are not controlled by charge transfer, ion transport or additional chemical reaction steps,  $\eta$  represents the so-called crystallization overpotential. In this case, the foregoing equation defines the thermodynamic driving forces of the phase formation

and dissolution processes, *i.e.*, supersaturation ( $\Delta\mu > 0$  for  $\eta < 0$ ) and undersaturation ( $\Delta\mu < 0$  for  $\eta > 0$ ).

The mechanism of metal electrodeposition on foreign substrates (S, *i.e.* the glassy carbon surface in this study) strongly depends on the Me-S interaction. A weak Me-S interaction (weak adhesion) means that metal deposition starts at supersaturation conditions in the so-called overpotential deposition (OPD) range  $E < E_{\text{Me}/\text{Me}^{z+}}$ . In the case of strong Me-S interactions (strong adhesion) the deposition process starts even at undersaturation conditions in the so-called underpotential deposition (UPD) range  $E > E_{\text{Me}/\text{Me}^{z+}}$ .<sup>19-20</sup>

In this work, when the iron deposition was investigated by CV experiments on glassy carbon, at Monash University in Melbourne (Figure 3.27), the occurrence of an additional cathodic peak was noted when the potential was reversed after the onset of the  $\text{Fe}^0$  deposition process<sup>1</sup>. This peak, at a less negative potential of -1.25 V, was plausibly due to the deposition of iron on the iron crystals directly stuck on the C-surface. Me-Me interactions were therefore stronger than Me-C ones.

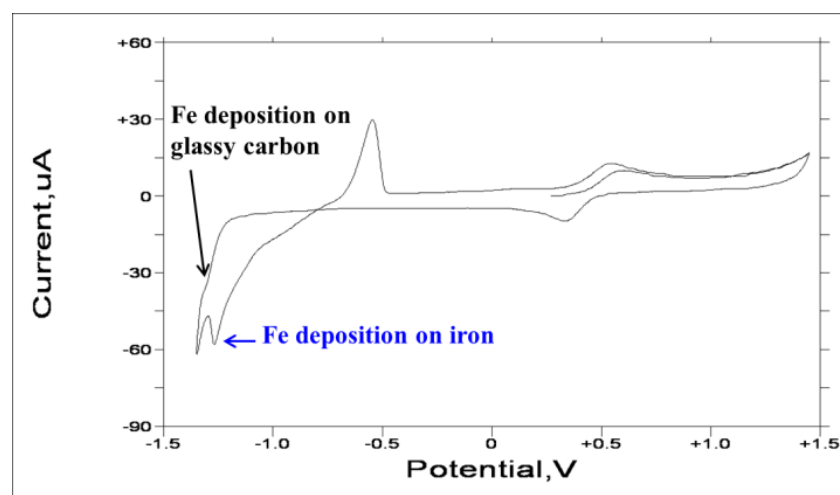


**Figure 3.27** CV of iron in sulfate system prepared with 1mM  $\text{H}_2\text{SO}_4$  solutions. Conditions: 1 mM  $\text{FeSO}_4$  + 0.1 M  $\text{Na}_2\text{SO}_4$ , scan rate 100mV/s

Overall, the deposition of iron could be explained via two phenomena: *i*) the nucleation in which first crystals formed on the surface of the electrode at a certain potential, and *ii*) the subsequent growth of the iron crystals, which required a less negative potential. Accordingly, a multistep approach to the Coulometry has been used. At rt, deposition experiments were carried out using two potentials (V1 and V2), which were differentiated from each other by  $\approx 0.1$  V. These potentials were chosen on the basis of the results obtained from CV experiments. In the

<sup>1</sup>It should be noted that the additional peak was not clearly observed during CV tests carried out at the University of Sydney. This could be due to the different surface of the glassy carbon working electrodes used in the two laboratories.

case of bulk electrolysis of aq. solutions of  $\text{FeSO}_4$  (100 mM) and sulfuric acid (1 mM), V1 and V2 were set to -1.30 and -1.15 V and they were applied for 60 s (V1) and 940 s (V2), respectively (total time = 1000 s). In the case of aq. solutions of  $\text{FeSO}_4$  (100 mM) and formic acid (10 mM), V1 and V2 were set to -1.25 and -1.15 V and they were applied for 60 s (V1) and 940 s (V2), respectively. The total time of CPE experiments was chosen arbitrarily to equal 1000 s. In these experiments, the charge that passed through the cell per minute would never be less than 1% of the charge passed in the first minute of the process, because of the continuous occurrence of the hydrogen evolution.

The choice of pH was crucial. In general, the iron deposition potential was always more negative than that of the  $\text{H}_2$  evolution, and the difference became larger for acidic solutions. As mentioned previously,<sup>10</sup> the pH had to be sufficiently high to allow a small  $\text{H}^+$  diffusion current density (compared to the effective cathodic current density), but at the same time, it could not be over 6 otherwise the precipitation of the metal hydroxide occurred. For this reason, multistep CPE experiments were carried out at pH = 3, which was achieved by using sulfuric acid and formic acid at 1 mM and 10 mM concentrations, respectively.

The relatively high concentration of  $\text{FeSO}_4$  (100 mM) was necessary to allow the visual observation of the iron deposit, i.e. to establish that this had taken place.

Under such conditions, solid particles of  $\text{Fe}^0$  were obtained in the cathodic reaction. A simple confirmation of the composition of such particles came from the fact that they were attracted by a magnetic stir bar (Figure 3.28 left). Figure 3.28 right show an image of the cylindrical working electrode on which iron was deposited during CPE experiments on an aqueous  $\text{FeSO}_4$ /sulfuric acid solution. Iron crystals were partially stuck to the working electrode surface and partially precipitated in the water phase.

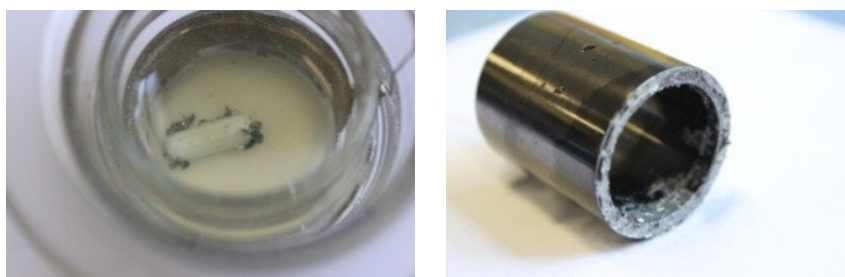


**Figure 3.28**  $\text{Fe}^0$  attracted by a magnetic stir bar inside the CPE cell (**left**) and iron deposits on cylindrical glassy carbon electrode (**right**) obtained by multi-step CPE experiment on an aqueous solution of  $\text{FeSO}_4$  (100 mM) and  $\text{H}_2\text{SO}_4$  (1 mM).

The iron deposition however, appeared to be affected by the nature of the acid, sulfuric or formic, present in the aqueous solution. In fact, in the case of the  $\text{FeSO}_4$ /formic acid solution, iron crystals from CPE experiments adhered firmly to the electrode surface and it was difficult to scratch them out (

**Figure 3.29).**

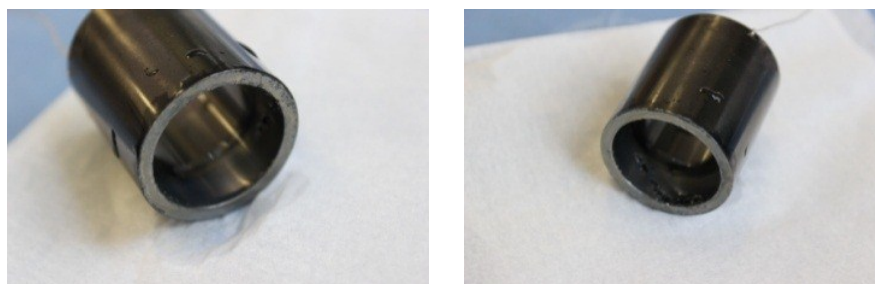


**Figure 3.29** Iron deposits on cylindrical glassy carbon electrode obtained by multi-step CPE experiment on a aqueous solution of  $\text{FeSO}_4$  (100 mM) and  $\text{HCOOH}$ (10 mM).

A SEM investigation was therefore performed to observe the morphological aspects of such depositions. Figure 3.30 compares the SEM images of  $\text{Fe}^0$  obtained from a 1 mM sulfuric acid solution and a 10 mM formic acid solution, respectively (both solutions at pH 3).

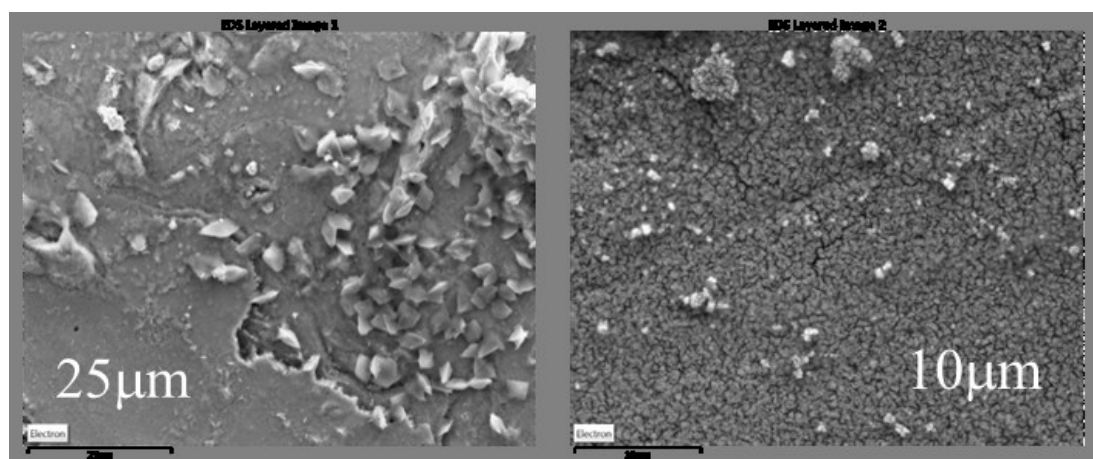


**Figure 3.30** SEM images of iron depositions obtained by CPE experiments: **(left)** aqueous solution of  $\text{FeSO}_4$  (100 mM) and  $\text{H}_2\text{SO}_4$  (1 mM), and **(right)** aqueous solution of  $\text{FeSO}_4$  (100 mM) and  $\text{HCOOH}$  (10 mM).

In the case of formic acid solutions (Figure 3.30 **right**), a thin and compact homogeneous iron layer was observed. On the contrary, in the case of sulfuric acid (Figure 3.30 **left**) the iron deposit appeared somewhat disordered as if it was composed by several layers.

Four final experiments were set up as preparatory tests to the investigation of the CPE technique in the presence of organic substrates that could be subjected to hydrogenation



reactions. The bulk electrolysis was investigated at both 25 and 50 °C by using the same potentials described for the previous tests, *i.e.* -1.30 and -1.15 V for sulfuric acid (1 mM) solutions and -1.25 and -1.15 V for formic acid (10 mM) solutions. The concentration of FeSO<sub>4</sub> was 100 mM. Iron depositions were obtained in all cases. The processes, however, were accompanied by a significant evolution of hydrogen at the cathode, which plausibly limited the efficiency of the metal reduction.

In order to quantify the progress of such reactions, the iron deposits obtained in each CPE experiment were washed with water, acetone and dried under a nitrogen stream, and then weighed (since a rapid oxidation of metallic iron could take place, the overall procedure had to be done very quickly to minimize experimental errors). This allowed the real molar amount of metal produced in each reduction test to be calculated. Moreover, from the net Q charge measured during the reactions, the Faraday's law equation ( $N = Q/zF$ ) also gave the determination of the theoretical molar amount of reduced iron. The ratio between such experimental and theoretical quantities led to the Faradic efficiency percentage ( $f$ ) which offered an estimate of the BE effectiveness. Results are reported in Table 3.2, where deposit weight, net charge (Q) and Faradic efficiency ( $f$ ) of BE experiments performed with H<sub>2</sub>SO<sub>4</sub> or HCOOH, are indicated at both 25 and 50 °C. Faradic efficiency values higher than 80% in each system confirmed that the investigated method was successful for the recovery of the iron.

**Table 3.2**  
Multi-step iron deposition CPE experiments on an acidic aqueous solution (pH 3) of FeSO<sub>4</sub> (100 mM) at rt and 50 °C.

	Acid	Temp (°C)	Q (C)	Fe <sup>0</sup> dep. (mmol)	$f$ (%)
1	H <sub>2</sub> SO <sub>4</sub>	25	40.320	0.208	99.4
2	H <sub>2</sub> SO <sub>4</sub>	50	34.830	0.161	89.3
3	HCOOH	25	42.220	0.238	108.9*
4	HCOOH	50	50.120	0.210	80.7

\* A faradic efficiency over 100% was ascribed to an error in gravimetric determinations due to the spontaneous oxidation of iron.

#### 3.6.1.4 Multistep CPE in the presence of organic substrates

CPE experiments were performed by adding organic substrates to acidic aqueous solutions of FeSO<sub>4</sub>. This investigation was aimed at demonstrating that the iron deposition at the electrode surface in the bulk electrolysis cell could act as a hydrogenation promoter for organic derivatives (Scheme 3.1). Previous CV and LS-ASV experiments suggested that this type of (hydrogenation)

reaction was plausible (see Section 3.5); if successful, CPE tests would establish that the electrochemical restoration of  $\text{Fe}^0$  was a convenient method to allow large-scale hydrogenation processes in aqueous solutions.

Two organic compounds were used: *i*) levulinic acid (LA) which was the target molecule of this study, and *ii*) cyclohexanone (CyCO) which was chosen as a model because its hydrogenation to the corresponding alcohol was already known to proceed over iron catalysts in dilute acidic solutions.<sup>1</sup> It should be noted that cyclohexanone is sparingly soluble in water (8.6 g/100 mL<sup>21</sup>). For this reason, cyclohexanone was not used for CV and ASV experiments, during which solutions were not stirred.

CPE tests were carried out using a molar ratio  $[\text{Fe}^0]/[\text{organic substrate}] = 2.5$ . This corresponded to a 40 mM concentration of both LA and CyCO. In order to minimize the cathode  $\text{H}_2$  evolution, the pH was set to 3, the concentrations of sulfuric and formic acid were 1 and 10 mM, respectively. The corresponding molar ratios  $[\text{acid}]/[\text{organic substrate}]$  were 0.25 and 0.025, in formic and sulfuric acid solutions, respectively. Potentials were set to the values previously used (-1.30 and -1.15 V for the 1 mM sulfuric acid solution, and -1.25 and -1.15 V for the 10 mM formic acid solution).

The weight of iron deposits, the net Q charge, and the Faradic efficiencies were evaluated in all cases. Moreover, after the bulk electrolysis experiments, reaction mixtures were isolated and the organic components analysed by GC/MS. This analysis confirmed that both CyCO and LA were selectively hydrogenated to the corresponding cyclohexanol and  $\gamma$ -valerolactone. Results are reported in Table 3.3, where Faradic efficiencies can be compared to substrate conversions as determined by GC/MS.

The bulk electrolysis showed that iron deposition occurred in the presence of LA or CyCO. However, faradic efficiencies were quite different. With respect to the results obtained in the absence of any organic compound (Table 3.2),  $f$  was about the same or slightly lower when CyCO was used; while  $f$  remarkably dropped in the presence of LA. In particular,  $f$  was in the range of 75-100 % and of 4-22 % with CyCO and LA, respectively.

GC-MS analysis of reaction mixtures showed that the maximum conversion of CyCO (16%) were achieved in the presence of HCOOH at 50 °C (entry 4). The reaction of LA was instead more problematic. The onset of the LA hydrogenation was suggested by two facts: *i*) the occurrence/consumption of iron deposits at the cathode surface during CPE tests; *ii*) the presence of the expected product,  $\gamma$ -valerolactone, detected by GC/MS in aqueous solutions. Nonetheless, results gathered so far are still preliminary and do not allow certain conclusions on both the reaction conversion and the product distribution (selectivity) of the process.

These results however, were not further optimized due to time limitations and availability of the electrolysis cell.

**Table 3.3**

Multi-step iron deposition CPE experiments on an acidic aqueous solution (pH 3) of FeSO<sub>4</sub> (100 mM) at rt and 50 °C in the presence of CyCO or LA (40 mM).

	Acid	Temp (°C)	Q (C)	Fe <sup>0</sup> dep. (mmol)	Faradic efficiency ( <i>f</i> , %) <sup>a</sup>	Substrate conversion % <sup>b</sup>
CyCO	H <sub>2</sub> SO <sub>4</sub>	25	52.87	0.258	94.1	2.5
	H <sub>2</sub> SO <sub>4</sub>	50	56.06	0.292	100.5*	9.9
	HCOOH	25	29.58	0.122	79.4	7.4
	HCOOH	50	40.84	0.158	74.5	16.6
	H <sub>2</sub> SO <sub>4</sub>	25	23.30	0.027	22.3	n.d.
	H <sub>2</sub> SO <sub>4</sub>	50	21.11	0.007	6.5	n.d.
LA	HCOOH	25	27.59	0.021	15.0	n.d.
	HCOOH	50	23.95	0.005	4.3	n.d.

<sup>a</sup>*f* was calculated as previously indicated in Table 3.2. <sup>b</sup> The conversion of CyCO was determined by GC/MS. No conversion data were gathered in the case of LA: the acid was very soluble in water solutions, and due to its limited amount, it could not be quantitatively extracted and analyzed by GC/MS.

### 3.6.2 Discussion

The term electrocrystallisation is used to describe electrode processes that involve the formation of a solid phase by reduction of ions in solution, such as in the case of metal deposition. The first step of the growth of metals on inert substrates like carbon involves the formation of nuclei of a new phase. These nuclei act as growth centers which expand and coalesce to form a monolayer of the metal deposit; after that, the further enlargement of the deposition requires the nucleation of new centers on the freshly generated metallic surface.<sup>16</sup>

According to this model, the iron deposition during the above described CPE experiments can be plausibly explained by a two-step process involving *i*) the initial formation of an iron crystal monolayer, which occurred on the glassy carbon electrode surface, followed by *ii*) the further growth of subsequent metal layers stuck on the top of the first coating of the electrode. This sequence also clarifies why only a multistep CPE technique was successful to achieve the iron electrodeposition. In particular, when two different potentials were applied to an acidic aqueous solution of FeSO<sub>4</sub>, the first nucleation of the metal occurred at -1.30/-1.25 V (for 60 s), while the further growth of the iron layers took place at -1.15 V (for 940 s). The rationale for

these potential values was that the growth of iron crystals on existing nuclei of iron was always less energy demanding than the birth of iron nuclei on the glassy carbon surface of the electrode. In other words, the iron growth potential was always less negative than the nucleation one.<sup>19</sup>

A further aspect was the time of CPE experiments. It should be noted that the duration of a typical exhaustive electrolysis usually corresponds to the time after which the charge that passes through the cell per minute becomes less than 1% of the charge passed in the first minute of the process. In the present system however, the simultaneous occurrence of two cathodic reactions had to be considered: the iron deposition and the proton reduction to molecular hydrogen. The latter transformation implied an increase of pH that, if not controlled, brought about the precipitation of iron hydroxide and the consequent inhibition of  $\text{Fe}^0$  formation. For this reason, the total time (1000 s) for these CPE trials was chosen as a compromise to allow a satisfactory deposition of iron crystals and, at the same time, to rule out any significant increase of pH of aqueous solutions.

Preliminary SEM analysis showed that the geometry of iron deposits seemed to be sensitive to the composition/nature of the system. In particular, a thin and compact homogeneous iron layer was obtained using formic acid solutions, while a relatively disordered morphology of  $\text{Fe}^0$  depositions was observed from sulfuric acid solutions. The properties of the two acid solutions, particularly their density and viscosity ( $d$  and  $\eta$ , respectively) could offer a hypothesis to account for the result. Both  $d$  and  $\eta$  directly affected mass transport phenomena occurring at the electrode to-and-from the solutions. Consequently, they could also control the residence time of gas bubbles over the electrode surface and the transport/growth of the metal particles during the electrodeposition.<sup>15, 22</sup>

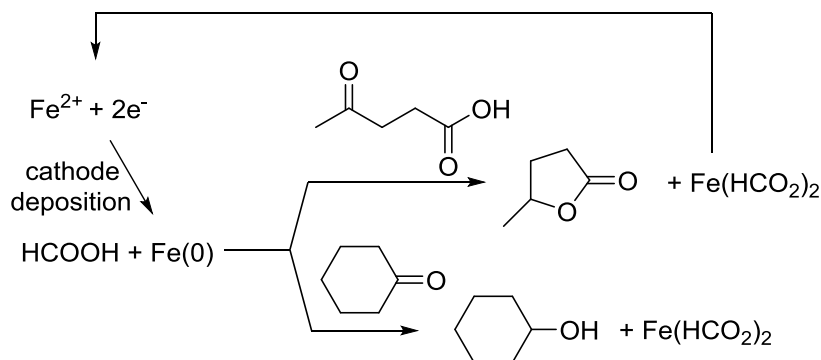
Moreover, the quantitative analysis of iron deposits showed that BE experiments performed with  $\text{H}_2\text{SO}_4$  or  $\text{HCOOH}$ , at 25-50 °C had a Faradic efficiency in the range of 80-100 %. Such a good efficiency was not appreciably altered by the addition of CyCO to the system. On the contrary,  $f$  remarkably dropped to 4-22 % in the presence of LA. GC-MS analysis of the reaction mixtures confirmed that both CyCO and LA were partially hydrogenated to the corresponding hydrogenated product cyclohexanol and GVL.

Although these results are not optimised, some hypotheses can be formulated.

In particular, in the presence of CyCO, the high Faradic efficiency and the partial conversion of the substrate (up to 17 %) suggested that  $\text{Fe}^0$ , deposited during the BE process, acted as promoter for the hydrogenation reaction without being consumed. The continuous current provided by the potentiostat through the working electrode plausibly protected the iron from re-oxidation. Under such conditions, iron was no longer a reagent, but rather a catalyst. The

conversion achieved was comparable to that previously reported in the original paper by Faboset *al.*<sup>1</sup> Although, the acid concentration investigated in this work, was by far lower.

By contrast the low Faradic efficiency calculated in the presence of LA suggested that that  $\text{Fe}^0$  was actually consumed by the onset of hydrogenation reactions, *i.e.* a chemical reaction took place where the metal was a reagent as shown in Scheme 3.4.



**Scheme 3.4.**  $\text{Fe}^0$ -promoted hydrogenation of levulinic acid and cyclohexanone in aqueous  $\text{FeSO}_4/\text{HCOOH}$  solution

The behavior of the system with LA was consistent with previous results of CV tests that showed how the addition of LA to acidic solutions of  $\text{FeSO}_4$  did not affect the potential of the iron deposition reaction, but it caused a decrease/disappearance of the stripping peak (at high LA concentrations).

In general, experiments showed that the hydrogenation of selected organic compounds on a moderate scale (up to 40 mM; ~50 mg) could be implemented through a CPE technique in the presence of iron. The role of the metal, however, seemed to depend also on the nature of the substrate:  $\text{Fe}^0$  was a catalyst in the hydrogenation of CyCO, while it was consumed as a reactant in the conversion of LA to GVL.

Although this result only partially meets the initial objective of this study, *i.e.* the achievement of a method for the electrochemical recovery of iron used in the reduction of LA, it represents a significant step towards that goal and clearly acts as a successful proof-of-principle and has been shown to work for another substrate - cyclohexanone. Therefore, there is strong experimental support for the idea underpinning the overall project and much scope to further continue on the investigation of the combination of the electrochemical reduction of  $\text{Fe}^{2+}$  (bulk electrolysis) with the chemical exploitation of  $\text{Fe}^0$  as a hydrogenation promoter.

### 3.7 Conclusions

The deposition of  $\text{Fe}^0$  on a glassy carbon surface was successfully obtained by electrochemical techniques developed for acidic aqueous solutions of  $\text{FeSO}_4$ . In particular, voltammetry and CPE experiments allowed the investigation of the influence on the metal deposition of major parameters such as the concentration of  $\text{Fe}^{2+}$ , the pH, the temperature and the co-presence of organic compounds (reagents or products of hydrogenation reactions). The most salient aspects of this study can be summarized as follows:

*i)* the current of the cathode reaction increased proportionally to the amounts of iron ions available in the aqueous solutions. This was expected from the Randles-Sevcik equation, which showed a linear relationship between the current magnitude and the analyte concentration.

*ii)* the control of pH of the solution was crucial. A compromise had to be chosen to limit two possible drawbacks such as the hydrogen evolution, which took place extensively in strongly acidic solutions, and the precipitation of iron hydroxide, which occurred in neutral-basic environments. An optimal value for pH was 3: this implied a careful check on both the nature of the acid ( $\text{pK}_a$ ) and its concentration. In the aqueous systems investigated, formic acid gave better performances than sulphuric acid. CPE experiments, in fact, showed that more uniform metal layers were obtained during the cathode deposition process in the presence of the organic acid. It is perhaps pertinent to note that formic acid could be a good option also from a more general standpoint: since bioderived LA is often available as crude aqueous LA–formic acid mixtures, the perspective of using formic acid as a H-donor for the upgrade of levulinic acid sounds very attractive (see introduction and chapter 2). Although this aspect was explored only at a preliminary stage during this electrochemical investigation, it certainly represents a key issue for the optimization/exploitation of the  $\text{Fe}^0$ -based reduction of LA.

*iii)* increasing the temperature from ambient to 50 °C affected the current magnitude and the potentials of both the deposition and the stripping reactions observed during CV experiments. Once again, the Nernst equation and the Randles-Sevcik equation accounted for these results.

*iv)* CV and ASV experiments suggested that the iron oxidation was not simply an electrochemical process when organic compounds that could be subjected to hydrogenation reactions were added to the  $\text{Fe}^{2+}$  aqueous acidic solutions. In particular, a decrease/disappearance of the anodic stripping peak in the presence of model derivatives including LA and 2-pentanone was observed. This was confirmed by CPE tests: once  $\text{Fe}^0$  was deposited at the cathode surface, iron was consumed as a promoter for the hydrogenation of LA to the corresponding  $\gamma$ -valerolactone. A similar behaviour was observed in the case of CyCO, where iron promoted the

partial conversion of the substrate (3-17 %) definitely. This behaviour did not result in a consumption of metallic iron deposited during BE process: Faradic efficiency values were always close to those obtained in the system without substrate, however faradic efficiency is a soft number and errors might account for the lack of correlation between CyCO conversion and observed faradic efficiency.

v) Under CPE conditions, the reaction took place on a scale up to 40 mM (~50 mg) of the organic reactant. CV and ASV experiments carried out in the presence of hydrogenated products (*e.g.*  $\gamma$ -valerolactone) showed that two different oxidation reactions could occur. In particular, at least two morphological types of iron crystals were obtained and these were oxidized at different potentials. The formation of such different iron crystals was also hypothesized to account for the results of the multi-step controlled potential bulk electrolysis that was investigated in this work.

vi) Under CPE conditions, experiments were successful only when a sequence of two potentials was applied to an acidic aqueous solution of  $\text{FeSO}_4$ ; this behaviour was plausibly due to the occurrence of an initial process of nucleation of iron crystals at -1.3 / -1.25 V, followed by a massive growth of the metal crystals at -1.15 V.

Although the present study is far from offering an exhaustive explanation of the electrochemical behaviour of acidic aqueous solutions of  $\text{FeSO}_4$  and organic compounds, tests for the recovery and re-use of iron by electrochemical methods were encouraging and they confirmed that the hydrogenation of carbonyl derivatives, including the biochemical target LA, was directly feasible in the aqueous solvent under mild and clean conditions. Overall, results gathered so far were an excellent starting point to optimize the investigated systems and, once optimised, to explore the economic viability of the whole process.

## 3.8 Experimental section

### 3.8.1 Preparation of aqueous solutions for CV and ASV experiments

$\text{Na}_2\text{SO}_4$  and distilled deionised water were used to prepare a 0.1 M stock supporting electrolyte solution. To aliquots of this standard solution, weighed amounts of acid ( $\text{HCOOH}$  or  $\text{H}_2\text{SO}_4$ ),  $\text{FeSO}_4 \cdot 7\text{H}_2\text{O}$  and other compounds (levulinic acid: LA;  $\gamma$ -valerolactone: GVL; 2-pentanone, and ethyl levulinate) were added to obtain the desired concentration of organic substrate and acid species. In particular, the procedure for the preparation of two typical solutions was:

- i) To a 500-mL flask charged with HCOOH (19 mL, 0.5 mmol) and FeSO<sub>4</sub>\*7H<sub>2</sub>O (139 mg, 0.5mmol), a 0.1 M aq. solution of Na<sub>2</sub>SO<sub>4</sub> as a supporting electrolyte, was added to a volume of 100 mL. The final concentration of both the acid and salt were 1 mM and 1mM, respectively. This aq. solution was used to carry out the CV experiments described in Figure 3.7 left, blue line.
- ii) To a 500-mL flask charged with HCOOH (19 mL, 0.5 mmol), FeSO<sub>4</sub>\*7H<sub>2</sub>O (139 mg, 0.5 mmol), and levulinic acid (507 mL, 5 mmol), a 0.1 M aq. solution of Na<sub>2</sub>SO<sub>4</sub> as a supporting electrolyte, was added to a volume of 100 mL. The final concentration of formic acid, the ferrous salt, and LA were 1mM, 1mM, and 10mM, respectively. This aq. solution was used to carry out the CV experiments described in Figure 3.14 left, blue line.

Solutions containing analyte species were used immediately when prepared. Prior to any experiment, air was removed in the electrochemical cell by a gentle flow of nitrogen for a few minutes. Unless otherwise specified, electrochemical experiments were performed at 20°C. The temperature of solutions used in this work was verified by a thermometer.

### 3.8.2 Instrumentation and procedures for voltammetry

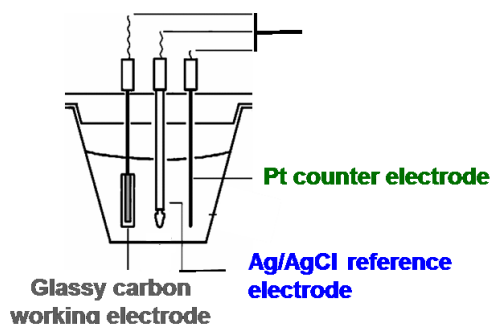


Figure 3.31. Schematic representation of the standard three-electrode cell

Cyclic voltammetry (CV) and Anodic Stripping - Linear Sweep voltammetry (ASV) experiments were conducted in a standard three-electrode cell (Figure 3.31) fitted with a glassy-carbon electrode (3mm in diameter, BAS inc) as a working electrode, platinum coated tungsten wire as a counter electrode and Ag/AgCl/aqueous AgCl<sub>sat</sub> + KCl 3 mol L<sup>-1</sup> as a reference electrode closed with a vycor frit, and connected to a potentiostat 466 System (Model ER466), EDAQ. Prior to use, the working electrode was polished on an MD-Nap polishing pad with a 1  $\mu$ m alumina suspension (BAS; BAS inc guidelines were followed). The electrode was then sonicated briefly in deionised water to remove residual alumina particles and finally, it was dried with paper. This method of preparation provided a smooth surface that was important to ensure the electrochemical reproducibility of all experiments. The scan rate of 100 mV/s was the same



in all tests, except when otherwise indicated. Under the set of conditions (technique, temperature and solvent) used in this study, all potentials were calibrated and reported against the Ag/AgCl reference electrode.

All CV experiments were initiated at zero potential *vs* Ag/AgCl, through a scan to positive potentials followed by a reversal to negative potentials. Then, the scan was again reversed to positive potentials. The initial potential of zero (*vs* Ag/AgCl) was used to conclude the test.

In a typical CV experiment, the above described cell was charged with an aq. solution (2 mL) of Na<sub>2</sub>SO<sub>4</sub> (the supporting electrolyte, 100 mM), HCOOH (1 mM) and FeSO<sub>4</sub>\*7H<sub>2</sub>O (1 mM). Then, the CVs were initiated at a potential of zero (*vs* Ag/AgCl), scanning to 1550 mV, reversal of the scan until -1400 mV, then the scan was again reversed to positive potentials. The initial potential of zero (*vs* Ag/AgCl) was the terminal potential. The results of this CV experiments are illustrated in Figure 3.7 left, red line.

ASV experiments were carried out using the above described cell. In this case however, the working electrode was held at a constant potential (deposition potential) for a certain time (deposition time) and then a linearly increasing potential staircase ramp was applied to the electrode.

In a typical LSV experiment, the cell described above was charged with an aq. solution (2 mL) of Na<sub>2</sub>SO<sub>4</sub> (the supporting electrolyte, 100 mM) HCOOH (1 mM) and FeSO<sub>4</sub>\*7H<sub>2</sub>O (1 mM). Then, the working potential was set to -1100 mV for 30 s and then a linearly increasing potential staircase ramp until 0 mV was applied to the electrode. The results of the ASV experiment are illustrated in Figure 3.21 left.

### 3.8.3 Instrumentation and procedures for bulk electrolysis

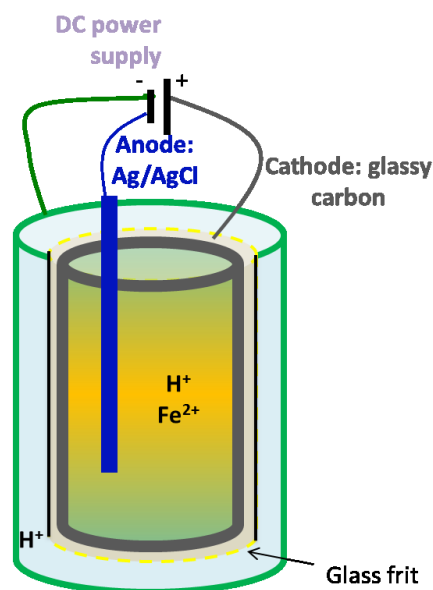


Figure 3.32. Schematic representation of the CPE cell

The bulk electrolysis experiments were carried out on an in-house built glassy carbon electrode cell (Figure 3.32). This looked like a beaker (total volume  $\sim 25$  mL; diameter  $\sim 5$  cm) into which a glass cylinder with a frit at the bottom was placed (total volume  $\sim 12$  mL). The working electrode (WE) was a cylindrical single piece of glassy carbon (DxL=  $\sim 3$  and  $\sim 5$  cm, respectively) and the counter electrode was a cylindrical large surface area platinum gauze basket design. The first (WE) was placed inside the glass cylinder equipped with the frit, along with the solvent, the electrolyte and the analyte of interest. The Ag/AgCl/aqueous  $\text{AgCl}_{\text{sat}} + \text{KCl}$   $3 \text{ mol L}^{-1}$  reference electrode closed with a vycor frit was also placed in the same compartment of the WE. The counter electrode was placed in the outer compartment, which was filled only with the solvent and the electrolyte mixture. The cover of the cell was fitted with five inlets/outlets to allow electrical contacts with the working, reference and counter electrodes. The cover was sealed with paraffin and the inlets with rubber septa. The cell was connected to a CHI700D/760D electrochemical workstation (CH Instruments, Austin, Texas, USA) for the recording and analysis of currents/potentials.

In a typical bulk electrolysis experiment, the inner compartment of the cell was charged with 10 mL of an aq. solution of  $\text{FeSO}_4$  (100mM) and  $\text{HCOOH}$  (10mM). During the electrolysis, the solutions in both compartments of the cell were vigorously stirred. The potentials V1 and V2 were set to -1.25 and -1.15 V and they were applied for 60 s (V1) and 940 s (V2), respectively (total time = 1000 s).

### 3.8.4 Characterization of Fe<sup>0</sup> deposits

The structure of iron deposits after the bulk electrolysis were examined by scanning electron microscopy (SEM). The field emission scanning electron micrographs were obtained on a JSM-6000F scanning microscope operating at 3.0 kV. The samples of iron deposit were prepared by scraping off from the surface of the glassy carbon electrode a portion of the solid, transferring it onto an amorphous carbon film, and then placing into the microscope.

## 3.9 Appendix

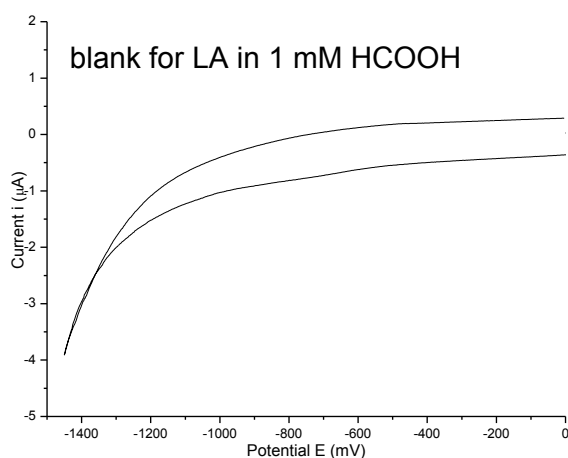


Figure 3.33 CV of aqueous solutions of (1mM) LA, (1 mM) HCOOH, and (0.1 M) Na<sub>2</sub>SO<sub>4</sub>.

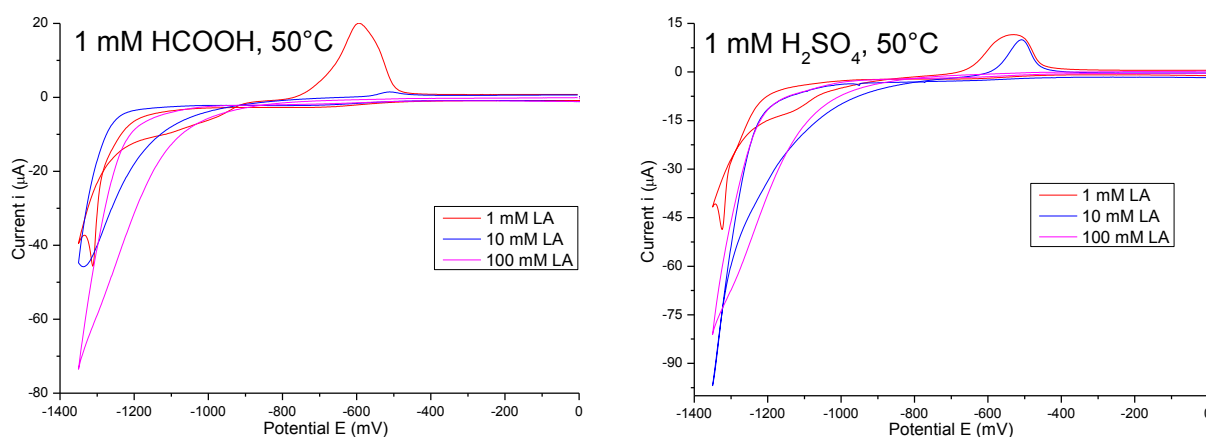
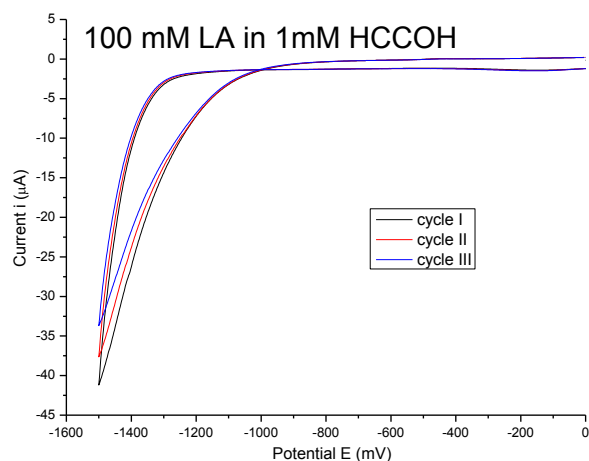
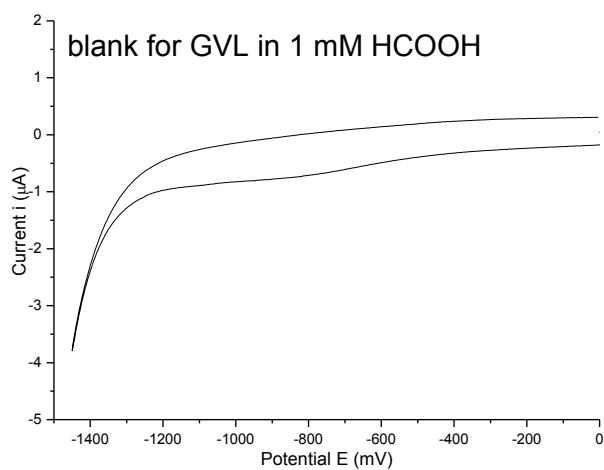


Figure 3.34 CVs of aqueous solutions of: **left**) FeSO<sub>4</sub> (1 mM), HCOOH (1 mM), and LA (1-100 mM); **right**) FeSO<sub>4</sub> (1 mM), H<sub>2</sub>SO<sub>4</sub> (1 mM), and LA (1-100 mM). Na<sub>2</sub>SO<sub>4</sub> (0.1 M) was the supporting electrolyte. Experiments were run at 50°C.



**Figure 3.35** Multicycle CV of aqueous solutions of (0.1 M) LA, (1 mM) HCOOH, and (0.1 M)  $\text{Na}_2\text{SO}_4$



**Figure 3.36** CV of aqueous solutions of (1mM) GVL, (1 mM) HCOOH, and (0.1 M)  $\text{Na}_2\text{SO}_4$

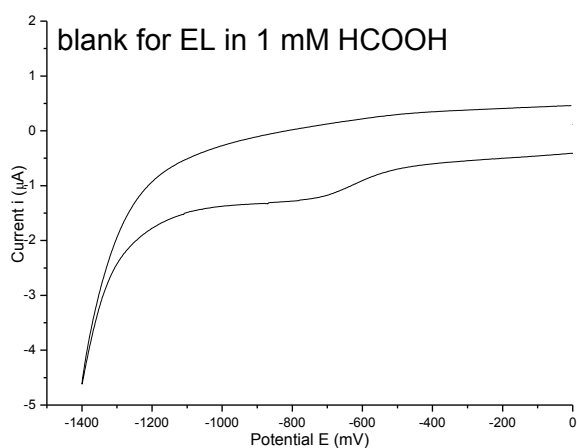


**Figure 3.37** CV of aqueous solutions of (1mM) EL, (1 mM) HCOOH, and (0.1 M)  $\text{Na}_2\text{SO}_4$

### 3.10 References

1. (a) Fábos, V.; Yuen, A. K. L.; Masters, A. F.; Maschmeyer, T., *Chem.–Asian J.* **2012**, *7*, 2629-2637; (b) Fábos, V.; Yuen, A. K. L.; Masters, A. F.; Maschmeyer, T., *Chem.–Asian J.* **2012**, *7*, 2638-2643.
2. (a) Que, L.; Tolman, J.; Tolman, W. B., *Nature* **2008**, *455*; (b) Andreini, C.; Bertini, I.; Cavallaro, G.; Holliday, G.; Thornton, J., *JBIC, J. Biol. Inorg. Chem.* **2008**, *13*, 1205-1218.
3. (a) Nelson, D. D. L.; Lehninger, A. L.; Cox, M. M., *Lehninger Principles of Biochemistry*. W.H. Freeman: 2013; (b) Stryer, L., *Biochemistry*. W.H. Freeman: 1995; (c) Fersht, A.; Bongarzone, C., *Struttura e meccanismi d'azione degli enzimi*. Zanichelli: 1989.
4. Remus, R.; Aguado Monsonet, M. A.; Roudier, S.; Delgado Sancho, L. *JRC reference report - Best available techniques (BAT) Reference document for iron and steel production Spain*, 2013.
5. Stumm, W.; Lee, G. F., *Schweizerische Zeitschrift für Hydrologie* **1960**, *22*, 295-319.
6. Beverskog, B.; Puigdomenech, I., *Corros. Sci.* **1996**, *38*, 2121-2135.
7. Bard, A. J.; Faulkner, L. R., *Electrochemical Methods: Fundamentals and Applications, 2nd Edition*. John Wiley & Sons, Inc: 2001.
8. (a) Kissinger, P. T.; Heineman, W. R., *J. Chem. Educ.* **1983**, *60*, 702; (b) Heinze, J., *Angew. Chem., Int. Ed. Engl.* **1984**, *23*, 831-847; (c) Bontempelli, G.; Toniolo, R., "Measurement Methods | Electrochemical: Linear Sweep and Cyclic Voltammetry" in *Encyclopedia of Electrochemical Power Sources*, Elsevier: Amsterdam, 2009; pp 643-654; (d) Millar, J.; Barnett, T. G., *J. Neurosci. Methods* **1988**, *25*, 91-95; (e) Nicholson, R. S., *Anal. Chem.* **1965**, *37*, 1351-1355.
9. (a) Grujicic, D.; Pesic, B., *Electrochim. Acta* **2005**, *50*, 4405-4418; (b) Gow, K. V.; Hutton, G. J., *Electrochim. Acta* **1972**, *17*, 1797-1802; (c) Heusler, K. E.; Knoedler, *Electrochim. Acta* **1970**, *15*, 243-250.
10. Dražić, D. M., "Iron and Its Electrochemistry in an Active State" in *Modern Aspects of Electrochemistry*, Springer US: 1989; Vol. 19, pp 69-192.
11. Trasatti, S.; Petrii, O. A., *Pure Appl. Chem.* **1991**, *63*.
12. Randles, J. E. B., *Trans. Faraday Soc.* **1948**, *44*, 327-338.
13. Konopka, S. J.; McDuffie, B., *Anal. Chem.* **1970**, *42*, 1741-1746.
14. Kinoshita, K., *Carbon: electrochemical and physicochemical properties*. Wiley: 1988.
15. Besra, L.; Uchikoshi, T.; Suzuki, T. S.; Sakka, Y., *J. Eur. Ceram. Soc.* **2009**, *29*, 1837-1845.
16. Pletcher, D., *Instrumental methods in electrochemistry*. Horwood Publishing Limited: 2001.
17. (a) Solov'ev, V.; Marcou, G.; Tsivadze, A.; Varnek, A., *Ind. Eng. Chem. Res.* **2012**, *51*, 13482-13489; (b) Kwan, C. Y.; Chu, W., *Chemosphere* **2007**, *67*, 1601-1611.
18. (a) Génin, J. M. R.; Olowe, A. A.; Refait, P.; Simon, L., *Corros. Sci.* **1996**, *38*, 1751-1762; (b) Génin, J.-M. R.; Refait, P. H.; Abdelmoula, M. *Hyperfine Interactions*, 2002, p. 119-131; (c) Ruby, C.; Gehin, A.; Aissa, R.; Ghanbaja, J.; Abdelmoula, M.; Génin, J. M. R., "Chemical stability of hydroxysulphate green rust synthesised in the presence of foreign anions: carbonate, phosphate and silicate" in *ICAME 2005*, Springer Berlin Heidelberg: 2007; pp 803-807; (d) Génin, J. M. R., "Fe(II–III) Hydroxysalt Green Rusts; from Corrosion to Mineralogy and Abiotic to Biotic Reactions by Mössbauer Spectroscopy" in *ICAME 2003*, Springer Netherlands: 2004; pp 471-485.
19. Krumm, R.; Guel, B.; Schmitz, C.; Staikov, G., *Electrochim. Acta* **2000**, *45*, 3255-3262.
20. (a) Oskam, G.; Searson, P. C., *Surf. Sci.* **2000**, *446*, 103-111; (b) Wang, H.; Qu, X.; Lu, J.; Bond, A. M.; Zhao, C., *CrystEngComm* **2011**, *13*, 4762-4769.

21. Kühne, R.; Ebert, R. U.; Kleint, F.; Schmidt, G.; Schüürmann, G., *Chemosphere* **1995**, *30*, 2061-2077.
22. Moravej, M.; Amira, S.; Prima, F.; Rahem, A.; Fiset, M.; Mantovani, D., *Materials Science and Engineering: B* **2011**, *176*, 1812-1822.

---

## 4 Concluding remarks

---

This Thesis work was aimed at the implementation of green procedures for the catalytic aqueous-phase hydrogenation of biomass-derived levulinic acid to  $\gamma$ -valerolactone. In particular, the research was focused on the development of innovative design for catalytic recycle and regeneration.

Results of Chapter 2 were obtained during the first part the activity carried out at the University of Ca' Foscari Venezia. An original design of multiphasic systems was set up by using Ru-based catalysts, both heterogeneous and homogeneous ones. After a screening of the most appropriate components of the multiphase arrangement, including solvents, catalysts, and ionic liquids, a highly selective hydrogenation of LA to  $\gamma$ -valerolactone was achieved using molecular hydrogen as a reducing agent, and either Ru/C or RuCl<sub>3</sub> as catalyst or catalytic precursors. Under such conditions, main advantages were the perfect confinement and stabilization of the catalytic system in the IL phase: this allowed not only an easy isolation of the product in quantitative yields, but also an *in situ* re-use of catalyst for at least eight recycles with unchanged performance. However, a limitation of these multiphasic systems was found in its application to mixture of LA/FA, where formic acid was expected to act as a hydrogen source. Under such conditions, no LA hydrogenation was observed, meaning that the multiphasic procedure could not be extended to upgrade crude LA/FA streams from the hydrolysis of cellulose.

Overall, the multiphasic method was an inventive application of ionic liquid phases and a genuine advance in the design of intrinsically greener chemical transformations.

Results of Chapter 3 were obtained during the second part the activity carried out at the University of Sydney (Australia). In this phase of the work, an investigation on electrochemical methods for the recovery and re-use of iron in acidic aqueous phases of FeSO<sub>4</sub> was carried out. The initial analysis was focused on the influence of major system parameters (including the concentration of Fe<sup>2+</sup>, pH, the temperature and the co-presence of organic compounds) on the

deposition of iron on glassy carbon electrodes. Then, the deposition of  $\text{Fe}^0$  by CPE experiments was explored through a multistep approach, in acidic aqueous solutions (pH 3) of  $\text{FeSO}_4$ .

The most interesting results of CPE experiments were considered to implement an iron-based technique for the hydrogenation of organic compounds on a practical laboratory scale (0.4 mmol, ~50 mg). Under such conditions,  $\text{Fe}^0$  acted as a promoter for the hydrogenation of the model reactants levulinic acid and cyclohexanone.

Overall, results gathered so far were encouraging and they confirmed that the hydrogenation of carbonyl derivatives including the biochemical target LA, was directly feasible in the aqueous solvent under mild and clean conditions.

Although the present study is still far from offering an exhaustive explanation of the electrochemical behaviour of acidic aqueous solutions of  $\text{FeSO}_4$  and organic compounds, it may be considered an original starting point to optimize the investigated systems with the aim of improving also the economic viability of the whole process.

#### 4.1 Paper originated from this thesis

Overall topics investigated during this PhD thesis led to the drafting of a scientific paper and communications:

##### SCIENTIFIC PAPERS:

- Selva, M.; Gottardo, M.; Perosa, A., “Upgrade of Biomass-Derived Levulinic Acid via Ru/C-Catalyzed Hydrogenation to  $\gamma$ -Valerolactone in Aqueous–Organic–Ionic Liquids Multiphase Systems”, *ACS Sustainable Chem. Eng.*, 2013, **1**, 180-189.
- Selva, M.; Noè, M.; Perosa, A.; Gottardo, M., “Carbonate, acetate and phenolate phosphonium salts as catalysts in transesterification reactions for the synthesis of non-symmetric dialkyl carbonates”, *Org. Biomol. Chem.*, 2012, **10**, 6569.
- Caretto, A.; Gottardo, M.; Fiorani, G.; Noè, M.; Perosa, A.; Selva, M., “Phosphonium ionic liquids (PILs) as organocatalysts for green reactions: nucleophilic electrophilic cooperative catalysis”, *Sciences at Ca’ Foscari*, 2012, **1**, 60-70.

##### COMMUNICATIONS TO CONFERENCE:

- Gottardo, M.; Perosa, A.; Selva, M.; “Upgrading of Biomass-derived Levulinic Acid via Ru/C-catalysed Hydrogenation to  $\gamma$ -Valerolactone in Aqueous-Organic-ILs Multiphase Systems”, *CSIRO Cutting Edge Symposium*, Melbourne (Australia), November 2012



- Gottardo, M.; Perosa, A.; Selva, M., “The Conversion of Platform Chemicals from Biomass: Multiphase Hydrogenation/Dehydrogenation of Levulinic Acid to  $\gamma$ -valerolactone (GVL)”, *8th International School of Organometallic Chemistry*, Camerino (Italia), August 2011
- Gottardo, M.; Perosa, A.; Selva, M., “The Conversion of Platform Chemicals from Biomass: Multiphase Hydrogenation/Dehydrogenation of Levulinic Acid to  $\gamma$ -valerolactone (GVL), *Chimica Verde, Chimica Sicura II edition*, Pavia (Italia), June 2011

## 4.2 Acknowledgements

I would like to express my gratitude to those who gave me the possibility to complete this thesis. A dutiful thank goes to "MIUR – progetto giovani borse aggiuntive" for founding my PhD scholarship and the "Australia Awards Endeavour Scholarships and Fellowships " for sponsoring six months of my Sydney stay.

A special appreciation goes to both my Italian and Australian supervisors: Prof. Maurizio Selva and Prof Thomas Maschmeyer. Prof. Selva was my supervisor at Ca' Foscari University; I thank him for being an encouraging and helpful teacher, for his criticisms and all the valuable professional advices. Prof Maschmeyer, my Australian supervisor, always encouraged me to work in an independent way, but, at the same time, was always ready to give me suggestion and assistance. His enthusiasm inspired and helped me to overcome all the difficulties. I thank both of them for giving me the possibility to perform part of my PhD in Sydney, as part of the cotutelle project, and to discover the world “down-under”. Another person who contributed strongly to the realisation of this work was Dr. Alvise Perosa a sort of third supervisor. I thank him for all his multiphasic support, for both the chemical and international issues. I thank Tony Masters. His experience and dedication to chemistry and his trust in me were precious during the time spent working at the School of Chemistry, in Sydney. A special thank goes to Prof. Alan Bond for his hospitality and supervision during my short term mission in Melbourne. He welcomed me at the Monash University and helped me to discover the wonderful world of electrochemistry. I want also to thank all the people of the Bond's laboratory who helped me, in particular Dr. Si-Xuan Guo and Dr Jie Zhang. Among the personnel of the Università Ca' Foscari di Venezia, I would like to cite Prof. Stefano Paganelli, for the enormous availability and for sharing his professional knowledge; and "Relazioni Internazionali" and “Segreteria didattica del dottorato” offices for the help in the bureaucracy.

Lab life is fun also because of the labmates met on the way. I wish to thank Dr. Marco Noè, “el vecio”, for his “wisdom of the old” and for our useful discussions, above all those inspired by a spritz; Alessio Caretto, adventures mate in Australia and New Zealand, for his inspiring creativity and efficiency and for the afternoon coffee breaks with Tim Tam at USyd; Giulia Fiorani, the nerdy, for her technological support and her lessons above all in English and diplomacy. I have to thank also all the people who worked in the lab in Venice during the last three years: Vanni Benedet, Sandro Guidi, Camilla Soragni, Manuela Facchin, Massimo Fabris, Marta Meneghello, Manuele Galvan, Andrea Loro. Thanks guys for all the patience that you had with me!! Thanks to all the labmates of Sydney who make my periods at USyd fruitful, formative and pleasant: Viktoria, Stephan, Ioan, Paul and Ilona, Ant, Max, Manuel Ghezzi, Cameron, Michael, Jess, Alex Yuen, Alex Keilar, Kapil. Thank for spending time with me, while working in the lab and getting drunk at the pub.

Thanks to my lovely Sydney family: Adam, Ali and Katie as wonderful housemates; Claudio as motivating gym buddy; Micol as personal wine and food guide in Sydney, Ignacia as business woman, Katie as my rescuer in the hostel, Enrico e Loris as country cousins; Sara, Nima, Hesam, Vivien, Eric and Lars.

I wish to thank all my friends. Martina my best friend, with her I do not need words, just a look. I thank Stefi, my favorite globetrotter; Eli Cod, determined and energetic woman; Alberto, my oldest friend; Betti, the mother of Achille; Dr. Giulio Bianchini; the "Sinforose" Angela, Marta and Silvia; Dr. Filippo Zanella.

I want to thank my parents Bianca and Giuseppe for their support during my studies, my aunties Donella and Mariagrazia and my grandma Oliva.

Last but not least, I thank Denis for his support and comprehension when I was tired and nervous, his contribution to this thesis was much more "crutial" than he could ever imagine. Thank to those who had the patience to read this long thesis and to those I forgot to mention.

Marina Gottardo

## Estratto per riassunto della tesi di dottorato

Studente: **Marina Gottardo**

matricola: **985839**

Dottorato: **Dottorato di ricerca in Scienze Chimiche**

Ciclo: **XXVI**

**Titolo della tesi: Green Procedures for the Selective Aqueous-Phase Hydrogenation of Biomass-Derived Levulinic Acid to  $\gamma$ -Valerolactone. Innovative Design for Catalytic Recycle and Regeneration**

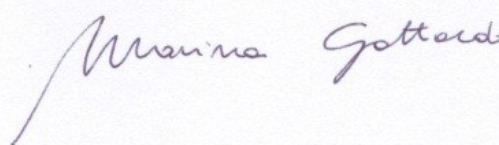
Estratto:

La tesi è stata focalizzata allo studio della trasformazione selettiva dell'acido levulinico (LA), uno dei più noti *platform chemicals* di origine rinnovabile, nel corrispondente derivato di idrogenazione/disidratazione, il  $\gamma$ -valerolattone (GVL). Obiettivo principale del lavoro è stato lo sviluppo di procedure per il recupero, la rigenerazione, e il riutilizzo di diversi tipi di catalizzatori e promotori sia eterogenei che omogenei, impiegati per la reazione. Il lavoro è stato svolto nell'ambito di un accordo di cotutela tra le Università Ca' Foscari Venezia e la Sydney University (Australia), articolando le attività di ricerca in due fasi.

La prima fase è stata condotta presso l'Università Ca' Foscari Venezia ed ha riguardato l'esame dell'idrogenazione catalitica del LA in condizioni multifasiche. Sono state messe a punto condizioni innovative di reazione nelle quali grazie all'uso di miscele ternarie costituite da coppie di solventi mutuamente immiscibili (acqua/idrocarburi) e da un liquido ionico della classe dei sali di ammonio e fosfonio, si è potuto segregare sia catalizzatori eterogenei che omogenei (rispettivamente Ru/C e RuCl<sub>3</sub>), nella fase di liquido ionico. In questo modo, non solo è stato possibile idrogenare efficacemente l'acido levulinico a GVL in soluzione acquosa, ma sono stati riutilizzati i catalizzatori impiegati per numerosi cicli senza perdita di attività e/o selettività. Lo studio ha evidenziato altri aspetti di interesse, tra i quali il confinamento di nanoparticelle metalliche (originate a partire dal precursore salino RuCl<sub>3</sub>) ad elevata attività catalitica, come pure la non praticabilità delle condizioni multifasiche per l'idrogenazione di miscele acquose di acido levulinico e formico originate dal trattamento idrolitico di carboidrati C5 provenienti da biomasse vegetali.

La seconda fase è stata condotta presso la Sydney University (Australia) e si è incentrata sullo studio dell'idrogenazione catalitica del LA in soluzione acquosa acida (per acido formico o solforico), in presenza di Fe come promotore. In tal caso, il Fe metallico viene ossidato stechiometricamente nel corso della reazione, a Fe<sup>2+</sup>: sebbene il meccanismo d'azione sia ancora incerto, si ritiene che il metallo permetta la generazione di H<sub>2</sub> che diviene l'effettivo riducente. Obiettivo del lavoro è stato trovare una procedura per il recupero del Fe<sup>2+</sup> che attraverso metodi elettrochimici ne consentisse il ripristino a Fe<sup>0</sup>. Sono stati perciò esaminati diversi sistemi acquosi a differenti concentrazioni di acido e di sali di Fe per studiare le condizioni migliori di riduzione catodica mediante voltammetria ciclica e elettrolisi a potenziale controllato (CPE). I risultati hanno evidenziato che l'idrogenazione di substrati modello quali il cicloesanone ed il LA sono possibili, ma al momento i dati seppure promettenti, non sono stati conclusivi sull'efficienza globale dei processi studiati.

Firma dello studente



## Abstract for the Summary of the PhD Thesis

Student: **Marina Gottardo**

matriculation number: **985839**

PhD: **PhD in Chemical Science**

Cycle: **XXVI**

Title of the Thesis: **Green Procedures for the Selective Aqueous-Phase Hydrogenation of Biomass-Derived Levulinic Acid to  $\gamma$ -Valerolactone. Innovative Design for Catalytic Recycle and Regeneration**

Abstract:

This Thesis work was aimed at studying the catalytic upgrading of an important biomass derived platform chemical such as levulinic acid (LA). In particular, the hydrogenation/dehydration of levulinic acid (LA) to  $\gamma$ -valerolactone (GVL) was considered with a major focus on the implementation of original methods for the recovery and recycle of catalysts, both heterogeneous and homogeneous ones. Research activities were carried out within a cotutelle agreement between the University of Ca' Foscari Venezia (Italy) and the University of Sydney (Australia).

In Venezia, a liquid triphase system made by an aqueous phase, an organic phase, and an ionic liquid was designed and applied for the conversion of LA to GVL. It was demonstrated that, operating at 100–150°C and 35 atm of H<sub>2</sub>, in the presence of either Ru/C or RuCl<sub>3</sub> as catalysts, the use of the triphase system designed to match the investigated reaction allowed: *i*) to obtain up to quantitative conversions and 100% selectivity toward the desired product; *ii*) to recover the product by simple phase separation; and *iii*) to preserve the catalyst activity for *in situ* recycles without any loss of metal. Overall, the study proved the concept that a multiphasic catalytic system could remarkably improve the global sustainability of the investigated hydrogenation reaction, where a key step was the catalyst segregation in an IL phase and its recycle.

In Sydney, the behavior of iron as a hydrogenation promoter of model organic compounds was explored. In particular, the recovery and recycle of iron was examined through electrochemical methods including both cyclic voltammetry and bulk electrolysis (BE). The deposition of Fe<sup>0</sup> was carried out in acidic aqueous solutions (pH ~3) of FeSO<sub>4</sub>. Under such conditions, at 25- 50°C, the aqueous phase hydrogenation of both cyclohexanone and LA could be performed selectively to produce the expected products (cyclohexanol and GVL, respectively) on a practical laboratory scale (0.4 mmol, ~50 mg). Though, conversions must be further optimized. Based on the gravimetric analyses of deposits of Fe and the measurement of the net Q charge involved in BE experiments, preliminary results suggested that Fe<sup>0</sup> plausibly acted as reactant/promoter for the hydrogenation of the levulinic acid, while it (Fe) was a catalyst in the reduction of cyclohexanone. Globally, although the investigation was far from being exhaustive, it was proved that the hydrogenation of carbonyl derivatives including the target of this study (*i.e.* LA), was feasible in aqueous solutions through a iron-based clean procedure.

Signature of the student

